Understanding the molecular functions of Neuronal Calcium Sensor-1 in *Neurospora crassa*

A

thesis submitted in partial fulfilment of the

requirements for the award of the degree of

DOCTOR OF PHILOSOPHY

by

DIBAKAR GOHAIN

Roll No. 136106009

Department of Biosciences and Bioengineering

Indian Institute of Technology Guwahati

Guwahati – 781039, Assam (India)

भारतीय प्रौद्योगिकी संस्थान गुवाहाटी
INDIAN INSTITUTE OF TECHNOLOGY GUWAHATI
Department of Biosciences and Bioengineering
Guwahati- 781 039

DECLARATION

I do hereby declare that the content embodied in this thesis entitled "**Understanding the molecular functions of Neuronal Calcium Sensor-1 in *Neurospora crassa***" is the result of investigations carried out by me in the Department of Biosciences and Bioengineering, Indian Institute of Technology Guwahati, for the award of degree of Doctor of Philosophy, under the supervisions of **Prof. Ranjan Tamuli** and **Dr. Ajaikumar B. Kunnumakkara**. The research presented in this thesis is original and has not been submitted in part or full for any degree or diploma to any other institute or university to the best of my knowledge and belief.

Dibakar Gohain

Guwahati
March, 2019

Dibakar Gohain
(Enrolment No. 136106009)

भारतीय प्रौद्योगिकी संस्थान गुवाहाटी
INDIAN INSTITUTE OF TECHNOLOGY GUWAHATI
Department of Biosciences and Bioengineering
Guwahati- 781 039

CERTIFICATE

This is to certify that the research work in this thesis entitled "**Understanding the molecular functions of Neuronal Calcium Sensor-1 in *Neurospora crassa***" by Dibakar Gohain (Roll No. 136106009) has been carried out at the Indian Institute of Technology Guwahati for the award of degree of Doctor of Philosophy in Biosciences and Bioengineering, under our supervision. The outcome of the research work presented in this thesis is original and has not been submitted in part or full for any degree or diploma to any other institute or university.

Guwahati
March, 2019

Thesis Supervisor: Prof. Ranjan Tamuli
Professor
Department of Biosciences & Bioengineering

Thesis Co-Supervisor: Dr. Ajaikumar B. Kunnumakkara
Associate Professor
Department of Biosciences & Bioengineering

Dedicated to my parents and all the martyrs of India

List of Figures

List of Tables

List of Abbreviations

ANOVA	analysis of variance
bp	base pair
BLAST	basic local alignment search tool
BOD	biological oxygen demand
°C	degree Celsius
CA	California
CDD	Conserved Domain Database
cDNA	complementary deoxyribonucleic acid
CHIP	chromatin immunoprecipitation
cm	centimetre
DIC	differential interference contrast
DNA	deoxyribonucleic acid
EMSA	electrophoretic mobility shift assay
ExPASy	Expert Protein Analysis System
FGS	fructose glucose sorbose
FGSC	Fungal Genetics Stock centre
g	gram
g	relative centrifugal force
GFP	green fluorescent protein

h	hour
hph	hygromycin B resistance gene
Jm^{-2}	joule per square metre
KV	kilovolt
kb	kilo base pair
kDa	kilo Dalton
LG	linkage group
m	metre
M	molar
mA	milliampere
MEGA	Molecular Evolutionary Genetic Analysis
µg	microgram
µl	microlitre
µm	micrometre
µM	micromolar
ml	millilitre
mm	millimetre
mM	millimolar
N	normal
NCBI	National Center for Biotechnology Information

NCU	*Neurospora crassa* unit
NEB	New England Biolab
ng	nanogram
nM	nanomolar
NMR	nuclear magnetic resonance
Ω	ohm
OD	optical density
ORF	open reading frame
p	probability
PAGE	polyacrylamide gel electrophoresis
PCR	polymerase chain reaction
pm	picometre
psi	pound-force per square inch
PVDF	polyvinylidene fluoride
qRT-PCR	quantitative real time polymerase chain reaction
RFP	red fluorescent protein
RIP	repeat induced point mutation
RNA	ribonucleic acid
rpm	revolution per minute
RT-PCR	reverse transcription polymerase chain reaction

s	second
SCM	synthetic crossing media
SDM	site directed mutagenesis
SOB	super optimal broth
SOC	super optimal broth with Catabolite repression
UCR	University of California Riverside
UK	United Kingdom
USA	United States of America
UV	ultra violet
VM	Vogel's minimal media
V	volt
w/v	weight/volume
w/w	weight/weight

Acknowledgements

"Equipped with his five senses, man explores the universe around him and calls the adventure Science." – *Edwin Powell Hubble*.

This thesis arose as the fruit of years of research that has been pursued since I joined the '*Neurospora* Research Group' and also marks the end of my journey in obtaining Ph.D. degree. During this remarkable journey, my work has been kept on track and it has seen the light of completion with the assistance and inspiration from numerous people, including my supervisors, teachers, colleagues, my friends, well-wishers and various institutions. So, I take the pleasure to express my gratitude to all those who have contributed in numerous ways to the successful completion of this thesis work and making it a cherished experience for me.

"It is the supreme art of the teacher to awaken joy in creative expression and knowledge."– *Albert Einstein*. First and foremost, I would like to offer my sincere gratitude to my supervisor Prof. Ranjan Tamuli for his keen guidance, mentorship from the inception of my Ph. D. work in the Indian Institute of Technology (IIT) Guwahati, and introducing me to the fascinating world of *Neurospora* genetics and cell signaling. I have fallen short of words to express my gratitude for his remarkable role in constantly mentoring not only my research work but also other important aspects of my professional life throughout my stay at IIT Guwahati. I am also grateful to him for patiently reviewing various versions of my thesis and critical suggestions. I also thank my co-supervisor Dr. Ajaikumar B. Kunnumakkara for the support and helpful suggestions throughout my research period at IIT Guwahati.

I would also like to express my sincere gratitude to all doctoral committee members Prof. Kannan Pakshirajan and Prof. Utpal Bora from the Department of Biosciences and Bioengineering, and Dr. Manabendra Sarma from the Department of Chemistry, IIT Guwahati

for their noble suggestions and constructive criticisms on my work that in the long run led to successful completion of my research work.

"Without laboratories men of science are soldiers without arms" –*Louis Pasteur*. I would like to thank the present and the previous Directors of IIT Guwahati, the present and the previous Heads of the Department of Biosciences and Bioengineering for providing all the necessary facilities and support. I also thank all the staff members of Department of Biosciences and Bioengineering for their help and support during my research work. I also like to acknowledge the analytical and laboratory facilities of Department of Biosciences and Bioengineering and Central Instrumentation Facility (CIF), Lakhminath Bezborua Central Library, IIT Guwahati, for the books and reading space and Guwahati Biotech Park for the Confocal Microscope Facility. I specially acknowledge the Ministry of Human Resource Development (MHRD), Government of India for my fellowship; Department of Science and Technology (DST), and Department of Biotechnology (DBT), Govt. of India for the research grants to my supervisor which were crucial for successful accomplishment of my research work. I also extend my gratitude to all the taxpayers of India for which all the government research funding and the fellowships have become possible.

I am indebted to the Fungal Genetics Stock Centre (FGSC), University of Missouri, Kansas City, USA, for providing *Neurospora* strains and generously waiving the charges for the same. I also thank Prof. Katherine A. Borkovich, Department of Plant Pathology and Microbiology, University of California, Riverside, USA, for providing some *Neurospora* strains which were essential for the research work. I also acknowledge Prof. Robert D. Burgoyne, Physiological laboratory, University of Liverpool, UK for providing the rat *ncs-1* cDNA as a kind gift.

The lab was like a family for me and I always enjoyed the warmth and support of my lab members during my Ph.D. life. I am extremely grateful to all the present lab members Dr. Anand Tiwari, Ajeet, Avishek, Christy, Darshana, Serena, Rahul, Shalini and Nayan; and also to the lab alumni Dr. Ananya Barman, Dr. Vijya Laxmi, Dr. Rekha Deka, Dr. Ravi Kumar, Pallavi and Manju for their continuous help and support. I would like to mention specially about Avishek, who was more of a younger brother to me than a colleague for his unfathomable help and support in various aspects of my life in IIT Guwahati.

"A friend is one that knows you as you are, understands where you have been, accepts what you have become, and still, gently allows you to grow." –*William Shakespeare*. I thank all my friends in IIT Guwahati as well as outside Shasanka, Rebakanta, Akash, Dhruva, Pankaj, Biplob, Madhurjya, Arif, Naba, Madhurya, Babul, Sharbani, Shaad, Reshmi, Kamalesh, Karukriti, Neha, Ankit, Amarendra, Ashish, Papori, Jon, Pulakeswar, Langtuk, Hasnahana, Debajyoti, Adhiraj, Tinka, Dharitri, Vimal, Manash, and Dr. Jintu Dutta who have always supported and cheered for me making my stay in IIT Guwahati a memorable one.

"Without a family, man, alone in the world, trembles with the cold." –*Andre Maurois*. I would like to pay my heartiest regards and love to my father, my mother, my younger sister and to all my cousin brothers and sisters for their sincere encouragement and belief throughout my research work.

"God is, or God is not. Reason cannot decide between the two alternatives." –*Blaise Pascal*. The belief in the God, the almighty has played an important role in my life. Praises and thanks to the God for his showers of blessings and motivation for the successful completion of the research work during my Ph.D. tenure.

Last but not least, I am also grateful to the internet giants Google, YouTube, Wikipedia, Google Scholar, Science Direct, and Research Gate for the valuable online resources without which research is almost impossible in this digital world.

March, 2019 Dibakar Gohain

Synopsis

In this thesis work, I investigated the molecular mechanism of the Neuronal calcium sensor-1 (NCS-1) mediated tolerance to Ca^{2+} stress in *Neurospora crassa*. I found that *ncs-1* transcription is upregulated in repose to high concentration of Ca^{2+} in the medium. Furthermore, the transcription factor calcineurin responsive zinc-finger-1 (CRZ-1) physically binds to the *ncs-1* promoter and upregulates its expression to cope up with the high Ca^{2+} concentration, suggesting that NCS-1 functions via the calcineurin-CRZ-1 signaling pathway for tolerance to Ca^{2+} stress. Further, a direct interaction between NCS-1 and plasma membrane localized MID-1 ion channel during high Ca^{2+} concentration was also established. Therefore, this study revealed that CRZ-1 upregulates the expression of NCS-1 that eventually binds to MID-1 ion channel to prevent the Ca^{2+} influx for survival under high concentration of Ca^{2+} by maintaining the Ca^{2+} homeostasis. In addition, the *Rattus norvegicus* NCS-1 ($NCS\text{-}1^{Rat}$) was expressed in *N. crassa* and the heterologous expression of $NCS\text{-}1^{Rat}$ complemented the phenotypes of *N. crassa* Δ*ncs-1* mutant, suggesting an interspecies functional conservation of NCS-1. Moreover, like *N. crassa* NCS-1, the glutamic acid at position 120 was also found to be essential for rat NCS-1 functions confirming the functional conservation of this key residue across species. Therefore, this study revealed calcineurin-CRZ-1 signaling pathway to upregulate NCS-1, which interacts with the MID-1 ion channel for its possible closure, and interspecies functional conservation of the NCS-1 orthologs.

Thesis title: "Understanding the molecular functions of Neuronal Calcium Sensor-1 in *Neurospora crassa*"

Objectives:

1. To study the cell functions of neuronal calcium sensor-1 (NCS-1) and associated proteins in tolerance to Ca^{2+} stress in *Neurospora crassa*.
2. To study the regulation of *ncs-1* transcription and the molecular mechanism of NCS-1 mediated pathway for tolerance to Ca^{2+} stress.
3. To study the critical amino acid residues important for the NCS-1 function and its interspecific complementation.

Chapters:

Chapter 1: Introduction

Chapter 2: Materials and Methods

Chapter 3: The *ncs-1* transcription is upregulated during Ca^{2+} stress and is controlled via the calcineurin -calcineurin responsive zinc-finger-1 (CRZ-1) pathway.

Chapter 4: CRZ-1 binds to a unique sequence in *ncs-1* promoter to induce NCS-1 expression which eventually interacts with the MID-1 ion channel for Ca^{2+} stress tolerance.

Chapter 5: *Neurospora crassa* and *Rattus norvegicus* orthologs of NCS-1 show functional conservation.

Conclusions and future perspectives

Appendix

Chapter 1: Introduction

Neurospora crassa is a filamentous fungus of the ascomycetes family which grows mainly on dead and burned vegetation in tropical and subtropical regions (Luque *et al.*, 2012). *N. crassa* has been well established as an excellent eukaryotic model organism model for understanding different facets of complex biological processes including calcium (Ca^{2+}) signaling. Chapter 1 briefly describes about the *N. crassa* history and life cycle with an overview of the importance and evolution of calcium ion (Ca^{2+}) as universal signaling molecule. In eukaryotic organisms, Ca^{2+} plays a versatile role in regulating a wide array of cellular processes and adaptive responses (Berridge *et al.*, 1998; Sanders *et al.*, 2002; Davies and Terhzaz, 2009). The cytosolic free Ca^{2+} concentration ($[Ca^{2+}]_c$) is maintained ~100 nM at resting level and transient rise to 1 μM or more to trigger Ca^{2+}-signaling (Chin and Means, 2000; Bootman *et al.*, 2001). In eukaryotes, including the filamentous fungus *N. crassa*, resting level of $[Ca^{2+}]_c$ is maintained via Ca^{2+} transport across the plasma membrane and buffering processes in the cellular organelles (Bowman *et al.*, 2011; Barman and Tamuli, 2015). In *N. crassa*, Ca^{2+}-signaling is associated with several biological processes such as growth, hyphal tip branching, ion transport, sexual development, circadian regulated conidiation, thermotolerance, stress tolerance, and ultraviolet (UV) survival (Tamuli *et al.*, 2011; Deka *et al.*, 2011; Kumar and Tamuli, 2014; Barman and Tamuli, 2015; Laxmi and Tamuli, 2015; Laxmi and Tamuli, 2017; Barman and Tamuli, 2017). The *N. crassa* Ca^{2+}-signaling machinery comprises of 48 Ca^{2+}-signaling proteins, comprising of three Ca^{2+} channel proteins, two Ca^{2+}/Na^{+} exchangers, six Ca^{2+}/H^{+} exchangers, nine Ca^{2+}/cation- ATPases, four phospholipase C-δ subtype (PLC- δ) proteins, one calmodulin (CaM), and 23 Ca^{2+} and/or CaM binding proteins, effectively coordinating an array of cellular responses (Galagan *et al.*, 2003; Borkovich *et al.*, 2004; Zelter *et al.*, 2004). Transient rise in the $[Ca^{2+}]_c$ activates Ca^{2+} sensors, including the neuronal calcium sensor-1 (NCS-1), a member of the NCS protein family (Pongs *et al.*, 1993; Bourne *et*

al., 2001). The NCS-1 is a Ca^{2+}-myristoyl-switch protein, containing a conserved N-terminal myristoylation domain and four Ca^{2+} binding EF-hand domains (Burgoyne *et al.*, 2004; Burgoyne, 2007). NCS-1 protein is conserved evolutionarily across the species, and its homologs have been identified in yeast, fungi, nematodes, *Drosophila*, fish, birds, rodents, and humans (Nef, 1996; Sánchez-Gracia *et al.* 2010; Tamuli *et al.*, 2011). Only three among the four EF hands are functional in NCS-1 as the first EF-hand of the N-terminal domain has a cysteine and a proline residues in the putative Ca^{2+}-binding loop preventing Ca^{2+} binding (Burgoyne *et al.*, 2004; Tamuli *et al.*, 2011). In mammals NCS-1 is a very important protein as it is associated with nerve terminal growth, synaptic transmission, learning and memory (Gomez *et al.*, 2001; Romero-Pozuelo *et al.*, 2007; Dason *et al.*, 2009; Saab *et al.*, 2009). In human, NCS-1 has great clinical significance for its association with various neurodegenerative disorders like bipolar disorder and schizophrenia (Koh *et al.*, 2003). In the fission yeast *Schizosaccharomyces pombe*, the NCS-1 homolog Ncs1p targets Ca^{2+} permeable channel Yam8p directly during Ca^{2+} stress (Hamasaki-Katagiri and Ames, 2010). In *N. crassa,* NCS-1 is associated with growth, Ca^{2+} dependent germlings fusion, Ca^{2+} and UV stress tolerance (Deka *et al.*, 2011; Palma-Guerrero *et al.*, 2013).

Calcineurin, another important Ca^{2+} signaling protein, plays a critical role in forming apical Ca^{2+} gradient, normal growth and development in *N. crassa* (Prokisch *et al.*, 1997; Kothe and Free, 1998; Tamuli *et al.*, 2016). In *N. crassa*, calcineurin is a heterodimer of a 63.9 kDa catalytic subunit calcineurin A (CNA-1) and a 19.8 kDa regulatory subunit calcineurin B (CNB-1), and these two subunits physically interact (Tamuli *et al.*, 2016). The transcription factor calcineurin responsive zinc finger 1 (Crz1) is a well-studied target of calcineurin that translocates into the nucleus on dephosphorylation by activated calcineurin and regulates target gene expression (Chen *et al.*, 2010). The *N. crassa* Crz1-homolog, encoded by the *crz-1* gene (NCU07952) contains two DNA binding C_2H_2 Zinc-finger domains (Virgilio *et al.*, 2017). In

S. pombe, calcineurin dephosphorylates the Crz1 homolog Prz1p causing its nuclear translocation and binding to the promoter of *ncs1* for transcriptional upregulation during Ca^{2+} stress, which is essential for closing the Yam8p channel to stop Ca^{2+} influx (Hirayama *et al.*, 2003; Hamasaki-Katagiri and Ames, 2010). In *S. cerevisiae*, *m*ating pheromone-*i*nduced *d*eath (Mid1) is a plasma membrane protein essential for mating and Ca^{2+} influx (Iida *et al.*, 1994). Similarly, in *S. pombe*, Yam8p, the MID-1 homolog, is essential for maintaining Ca^{2+} influx (Hamasaki-Katagiri and Ames, 2010). In *N. crassa*, the Mid1 or Yam8p homolog MID-1 is encoded by the *mid-1* gene (Lew *et al.*, 2008). In *N. crassa*, *mid-1* has role in growth, Ca^{2+} ion transport and homeostasis (Lew *et al.*, 2008). Moreover, the Δ*mid-1* mutant was able to rescue the Ca^{2+} sensitive phenotype of the Δ*ncs-1* mutant, indicating that reduced Ca^{2+} influx in the Δ*mid-1* mutant might provide protection against high extracellular Ca^{2+} (Deka and Tamuli, 2013). However, it was remained in oblivion whether NCS-1 directly interacts with MID-1 to regulate Ca^{2+} influx in response to high Ca^{2+} stress. Therefore, in this study, I investigated the molecular mechanism of NCS-1 mediated Ca^{2+} stress tolerance in *N. crassa* and also the physical interaction between NCS-1 and MID-1. Additionally, I studied the functional conservation of the *Neurospora crassa* and *Rattus norvegicus* orthologs of NCS-1 as they shared significant sequence similarity.

Chapter 2: Materials and methods

Chapter 2 describes materials and methods used in my thesis work. Growth, maintenance, and crosses of *N. crassa* strains were performed essentially as described previously (Westergaard and Mitchell, 1947; Davis and de Serres, 1970). The *N. crassa* strains primarily the wild type and various knockout mutant strains used in this study were obtained from the Fungal Genetics Stock Center (FGSC, Manhattan, KS). The other *N. crassa* strains were either generated in the lab of Prof. Katherine A. Borkovich (University of California Riverside, USA) or in our laboratory. Chemicals and reagents were purchased from the standard suppliers, and used after

being autoclaved or filter sterilized whenever required. Cloning, polymerase chain reaction (PCR), reverse Transcriptase PCR, quantitative real time PCR, chromatin immunoprecipitation (CHIP), electrophoretic mobility shift assay (EMSA), western blotting, and other molecular biology experiments were performed by using either the standard protocols (Sambrook and Russel, 2001) or according to manufacturer's instructions. Confocal microscopy was performed in the 'Bioprospecting Facility' of the Guwahati Biotech Park. All the statistical analyses of the experimental data and the graphs were plotted by using Microsoft Excel, SigmaPlot® and RStudio®.

<u>Chapter 3</u>: The transcription of *ncs-1* is upregulated during Ca^{2+} stress and is controlled via the calcineurin -calcineurin responsive zinc-finger-1 (CRZ-1) pathway

In this chapter, I described the role of NCS-1, calcineurin, and its target transcription factor calcineurin responsive zinc-finger-1 (CRZ-1) for survival under the Ca^{2+} stress in *N. crassa*. In this study, I observed a gradual increase in *ncs-1* transcription in response to increasing $CaCl_2$ concentration, suggesting that *ncs-1* transcription is induced by Ca^{2+} in *N. crassa*. In addition, I showed that NCS-1 overexpression, under the nitrogen-regulatable $P_{nit\text{-}6}$, was able to recover the Δ*ncs-1* Ca^{2+} sensitive phenotype, suggesting that NCS-1 is a key player in Ca^{2+} stress tolerance in *N. crassa*. A Ca^{2+} stress survival assay revealed that the Δ*crz-1* mutant was also sensitive to the Ca^{2+} stress like the Δ*ncs-1* mutant. Therefore, the transcription factor CRZ-1 is also involved in Ca^{2+} stress tolerance in *N. crassa*. The transcription level of *ncs-1* was reduced drastically in the Δ*crz-1* mutant, and it remained reduced even under the Ca^{2+} stress condition. This result suggested the involvement of CRZ-1 in the transcription of *ncs-1* in *N. crassa*. In *S. pombe*, calcineurin dephosphorylates the CRZ-1 homolog Prz1p and results its nuclear translocation (Hirayama *et al.*, 2003) and binds to a region of 130 bp in the *ncs1* promoter, which is upstream of the start codon (ATG), and upregulates *ncs-1* transcription (Hamasaki-Katagiri and Ames, 2010). Calcineurin is the only reported serine/threonine protein

phosphatase that is activated by Ca^{2+}/CaM (Klee *et al.*, 1979; Klee *et al.*, 1998). The other Ca^{2+} sensors CaM and the calcineurin subunit B (CNB) bind to the catalytic calcineurin subunit A (CNA) in response to the increased [$(Ca^{2+})_c$] (Klee *et al.*, 1979; Winkler *et al.*, 1984; Klee *et al.*, 1998; Rusnak and Mertz, 2000; Hogan *et al.*, 2003; Rumi-Masante *et al.*, 2012). In *N. crassa*, inhibition of the calcineurin by FK506 resulted reduction in the transcript level of *ncs-1* even under the Ca^{2+} stress. However, the transcript level of *crz-1* and *mid-1* was not significantly varied due to the calcineurin inhibition in Ca^{2+} stress, which showed no significant role of calcineurin in their transcription under the Ca^{2+} stress condition. In summary, under the Ca^{2+} stress, the transcription factor CRZ-1 upregulates NCS-1 expression, which could interact with the MID-1 ion channel in *N. crassa*. Therefore, this study showed that NCS-1 functions through the calcineurin-*crz-1* signaling pathway, possibly for interaction with the MID-1 channel to prevent Ca^{2+} influx for survival under the Ca^{2+} stress condition in *N. crassa*.

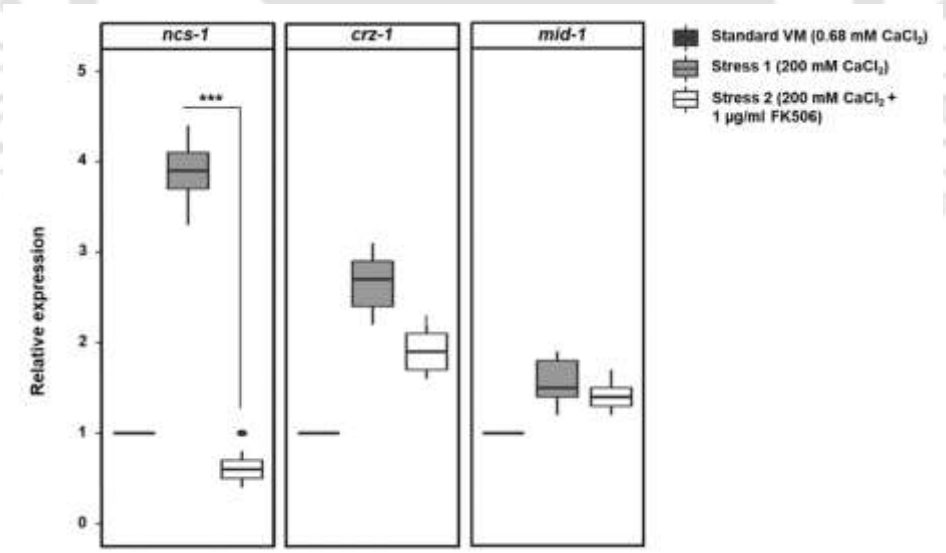

Fig.1: Relative expressions of *ncs-1*, *crz-1*, and *mid-1* under the Ca^{2+} stress with and without addition of the calcineurin inhibitor FK506. The relative expressions of *ncs-1*, *crz-1*, and *mid-1* were normalized to the *β*-tubulin expression and compared with the growth in standard VM that contains 0.68 mM $CaCl_2$.

Chapter 4: CRZ-1 binds to a unique sequence in the *ncs-1* promoter to induce NCS-1 expression which eventually interacts with the MID-1 ion channel for Ca^{2+} stress tolerance

In this chapter, I described the molecular mechanism of NCS-1 mediated Ca^{2+} stress tolerance in *N. crassa*. From the CHIP analysis it was clear that the transcription factor CRZ-1 binds to the *ncs-1* promoter to upregulate its expression under the Ca^{2+} stress condition. The binding of CRZ-1 to the *ncs-1* promoter was Ca^{2+} induced as the binding intensity increased with increasing Ca^{2+} level. In *S. cerevisiae*, calcineurin dephosphorylates the CRZ-1 homolog *TCN1/CRZ-1*, which is essential for its nuclear localization and which in turn regulates the transcription of the target genes (Stathopoulos and Cyert, 1997). From the EMSA, it was determined that CRZ-1 specifically binds to an 8 bp nucleotide sequence 5′-CCTTCACA-3′ in the *ncs-1* promoter, which is located 216 bp upstream of the start codon. Remarkably, unlike in the *S. cerevisiae*, the CRZ-1 binding site of the *ncs-1* promoter is not a CDRE sequence. The *N. crassa* CDRE sequence 5′-AGCCTC-3′ (Kumar *et al.*, 2006) was also absent in the *ncs-1* promoter. Similarly, in *S. pombe*, the Prz1p binding site sequence 5′-CAACT-3′ in the *ncs1* promoter is also different from the *S. cerevisiae* CDRE sequence (Hamasaki-Katagiri and Ames, 2010). To understand NCS-1 mediated Ca^{2+} stress tolerance pathway in *N. crassa*, I examined, if NCS-1 interacts with the ion channel protein MID-1 that might prevent Ca^{2+} entry to the cell. In *N. crassa*, there is three Ca^{2+} permeable channels (Tamuli *et al.*, 2013), including MID-1 which is the homolog of *S. pombe* Yam8p, necessary for Ca^{2+}-homeostasis (Lew *et al.*, 2008). Besides, both the Δ*mid-1* and Δ*ncs-1*; Δ*mid-1* mutants were able to recover the Ca^{2+} sensitive phenotype of the Δ*ncs-1* mutant, indicating a genetic interaction of *mid-1* and *ncs-1* during Ca^{2+} stress condition (Deka and Tamuli, 2013). Ca^{2+} induced closure of the MID-1 homolog Yam8p ion channel by Ncs1p was demonstrated in *S. pombe* (Hamasaki-Katagiri and Ames, 2010) and also evident in other higher eukaryotic NCS-1 homologs (ZuÈhlke *et al.*,

1999; Nakamura *et al.*, 2001). In the confocal microscopy study, it was observed that Ca^{2+} stress had resulted in NCS-1 localization to the plasma membrane, otherwise it mostly remained cytosolic. The in *vivo* and *in vitro* membrane pulldown assays revealed that NCS-1 was unable to bind to the membrane fraction that lacked MID-1, suggesting that NCS-1 specifically binds to MID-1 channel. The Co-IP assay established the physical interaction between NCS-1 and MID-1 which occurs only in the plasma membrane. In summary, under the Ca^{2+} stress, the transcription factor CRZ-1 binds to *ncs-1* promoter for inducing the expression of NCS-1, which in turn binds to the Ca^{2+}-permeable channel MID-1 in *N. crassa*. Therefore, from this study it can be suggested that the *N. crassa* NCS-1 functions via the calcineurin -CRZ-1 pathway for a possible closure of the MID-1 channel to prevent Ca^{2+} influx for survival under the Ca^{2+} stress condition.

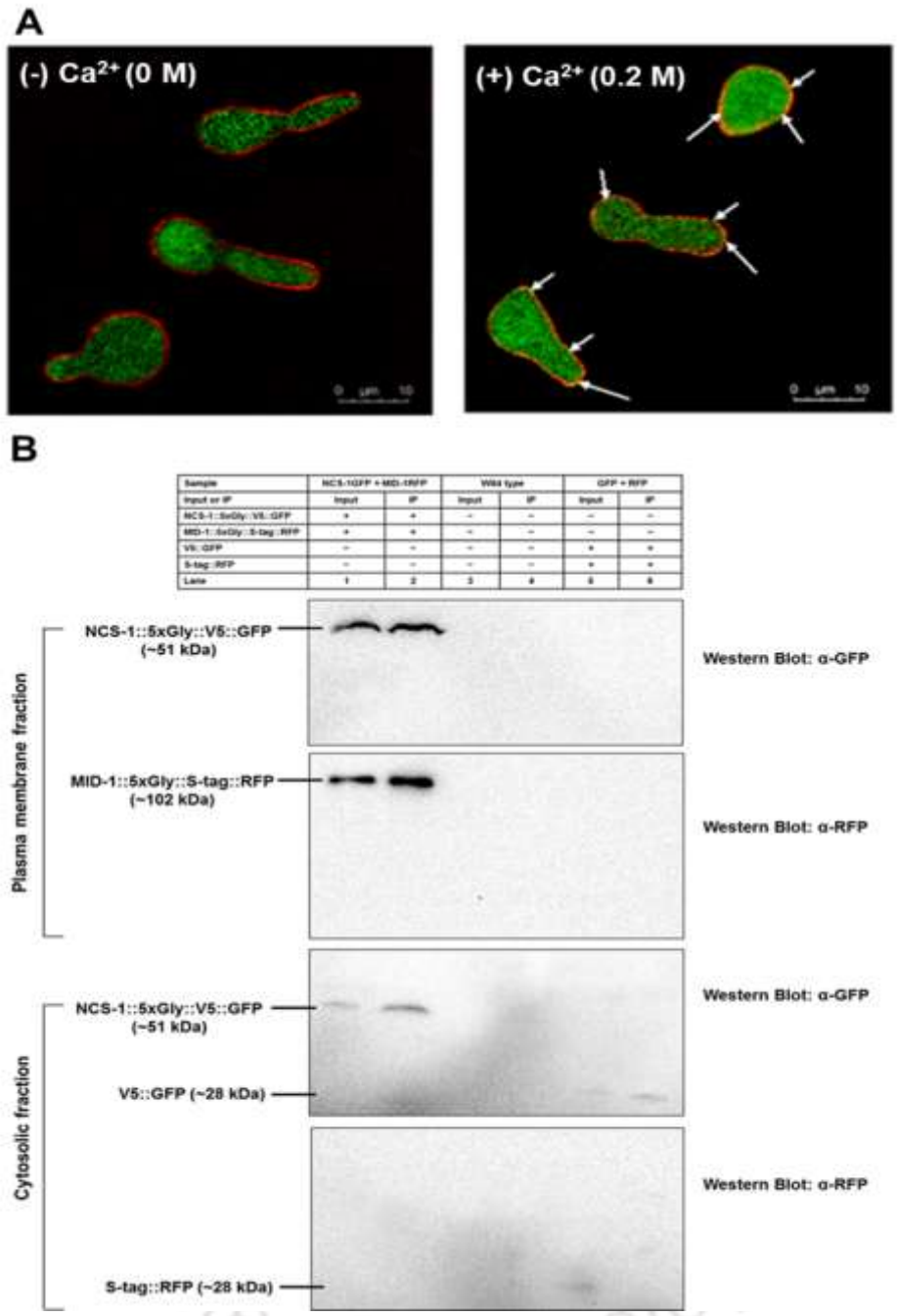

Fig. 2: NCS-1 directly binds to MID-1 during Ca^{2+} stress. A. Confocal microscopy showing localization of NCS-1 to plasma membrane during Ca^{2+} stress. B. Co-immunoprecipitation of NCS-1 and MID-1 proteins showing their interaction during Ca^{2+} stress.

Chapter 5: *Neurospora crassa* and *Rattus norvegicus* orthologs of NCS-1 show functional conservation

NCS-1 is a highly conserved protein with an N-terminal myristoylation site and four EF hand Ca^{2+}-binding domains. The human and rat NCS-1 are 100% identical and share about 66% identity with the *N. crassa* ortholog (Gohain *et al.*, 2016). Therefore, in this chapter, I tested if NCS-1 is also conserved functionally between *N. crassa* and rat or human, an interspecific complementation study was performed by expressing the rat NCS-1 ($NCS\text{-}1^{Rat}$) in *N. crassa*. The $NCS\text{-}1^{Rat}$ is identical to its human homolog. The $NCS\text{-}1^{Rat}$ tagged with GFP was expressed successfully in *N. crassa*, and complemented the slow growth, Ca^{2+} and UV stress sensitive phenotypes of the Δ*ncs-1* mutant. In the rat NCS-1, the glutamic acid at position 120 was changed to glutamine (E120Q) using the site-directed mutation (SDM) and the mutant construct was transformed into the *N. crassa* strain to study the effect of the mutation. The glutamic acid at position 120 is located in the third EF hand domain, which is an integral part of the 12 amino acid long Ca^{2+} binding loop present in EF hand domains found in NCS-1 (Gifford *et al.*, 2007; Deka *et al.*, 2011; Tamuli *et al.*, 2011; Gohain *et al.*, 2016). The *N. crassa* strains expressing rat $NCS\text{-}1^{E120Q}$ displayed slow growth, and sensitivity to Ca^{2+} and UV stresses similar to the Δ*ncs-1* mutant. The glutamic acid at position 120 was conserved in all NCS-1 proteins and was also found to be critical for NCS-1 functions in *N. crassa* (Gohain *et al.*, 2016). The E120Q mutation affected the functions of both rat NCS-1 and *N. crassa* NCS-1, thus, establishing glutamic acid at position 120 to be critical for the functions of the NCS-1 from lower to higher eukaryotes.

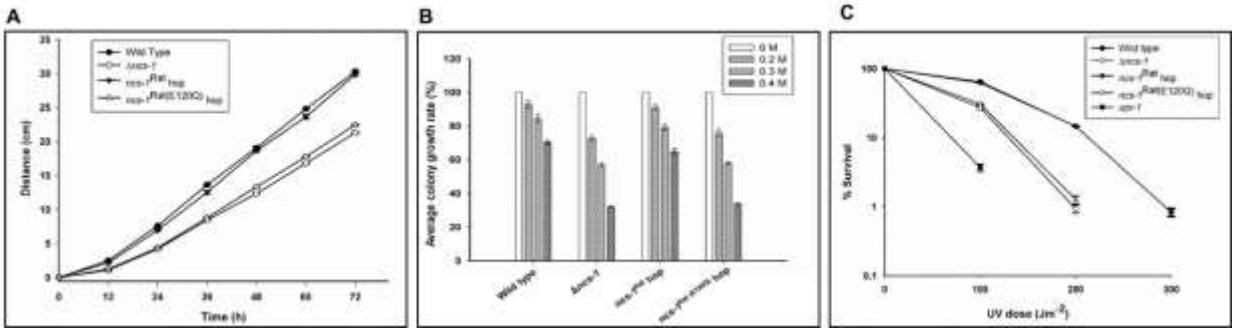

Fig. 3: Phenotypes of the *N. crassa* strains containing the *ncs-1*^{Rat} and *ncs-1*$^{Rat\ (E120Q)}$ transgenes. A. Apical growth study. B. Assay for tolerance to Ca^{2+} stress. C. Quantitative UV survival assay.

Conclusions and future prospects

This Chapter draws the conclusions of my entire research work. This section also includes the future prospects and directions of the current research work. In summary, it was well established from this study that NCS-1 plays an important role in Ca^{2+} stress tolerance in *N. crassa*. Under the high Ca^{2+} condition, the transcription factor CRZ-1 induces expression of NCS-1 that binds to the Ca^{2+}-permeable channel MID-1 in *N. crassa*. Therefore, this study showed that the *N. crassa* NCS-1 functions through calcineurin-CRZ-1 signaling pathway, and binds to MID-1 that might close the ion channel to prevent Ca^{2+} influx for survival under the Ca^{2+} stress condition. Furthermore, I found that the NCS-1 orthologs of *N. crassa* and rat were functionally conserved and the glutamic acid at position 120 was critical for the functions of NCS-1 from lower to higher eukaryotes.

Future perspectives of this research work:

Future directions will be: (i) to establish additional molecular details of the pathway involving calcineurin and the Ca^{2+} transporters for the mechanism of stress tolerance; (ii) to identify additional molecular targets of *N. crassa* NCS-1 for understanding its association with DNA damage repair pathway for its role in UV stress survival and (iii) to gain insight into the

structure-function relationship of *N. crassa* NCS-1 using either Nuclear Magnetic Resonance (NMR) and X-ray crystallography studies.

Appendix

The additional results of my thesis work have been described in appendix. I tried to evaluate the role of *ncs-1*, *crz-1* and *mid-1* genes on the regulation of *N. crassa* circadian clock under different temperature conditions. The *ncs-1* and *crz-1* mutants showed alteration in the period length with change in temperature and also temperature compensation was not observed. Further expression studies of the *frq* have revealed the role of *ncs-1* and *crz-1* in the circadian clock by modulating *frq* transcription. On the contrary, no alteration in period length as well as modulation in *frq* transcription was observed in case of the *mid-1* mutant with change in temperature. This preliminary finding established the role of the *ncs-1* and *crz-1* genes in regulation of the *N. crassa* circadian clock.

Chapter 1

An introduction to *Neurospora crassa* and calcium signaling

1.1 The biology of the model organism *Neurospora crassa*

Neurospora, meaning 'nerve spores' in Greek due to characteristic nerve like striations on its sexual spores, is a filamentous fungus (Fig. 1.1) extensively used as a model organism for understanding numerous facets of eukaryotic cell biology, biochemistry, genetics, and molecular biology (Perkins, 1992; Davis, 2000; Davis and Perkins, 2002; Galagan *et al.*, 2003). *Neurospora crassa* belongs to the phylum Ascomycota and was originally documented as the organism responsible for orange bread mould infestations in French bakeries and was first reported as *Oidium aurantiacum* (Payen, 1843) and *Penicillium sitophilum* (Montagne, 1843) independently. In the mid-1920s, *N. crassa* was identified as a heterothallic fungus with two mating types, *A* and *a* with eight asci by Shear and Dodge while Bernard Lodge and Carl Lindegren together demonstrated Mendelian inheritance in individual asci (Shear and Dodge, 1927; Dodge, 1939; Perkins, 1992). George Beadle and Edward Tatum discovered that the typical function of a gene was to control a particular enzyme synthesis using *N. crassa*, which eventually led to the famous 'one gene one enzyme' hypothesis using *N. crassa* (Beadle and Tatum, 1941) for which in 1958 they were awarded the Nobel Prize in "Physiology or Medicine". Thus, *N. crassa* emerged as an excellent eukaryotic model organism and contributed significantly in understanding various of biological processes like cellular differentiation and development, DNA methylation and repair, genome defence mechanisms, mitochondrial transport, and post-transcriptional gene silencing (Davis, 2000; Davis and Perkins, 2002; Galagan *et al.*, 2003). *N. crassa* is a multicellular, heterothallic, haploid organism with the fully sequenced genome of size 43 Mb comprising of 10,082 protein-coding genes distributed into seven linkage groups (LG I-VII) ranging in size from 4 to 10.3 Mb each (Davis and de Serres, 1970; Davis and Perkins, 2002; Galagan *et al.*, 2003). As a heterotroph, *N. crassa* can utilize a wide array of carbon and nitrogen sources, and only a few trace elements, simple salts, and a single vitamin- biotin are essential for its growth (Davis and de Serres, 1970;

Burnett, 1975; Perkins and Davis, 2000). *Neurospora* possesses a wide range of genome defence mechanisms that functions in different life cycle phases, a reversible post-transcriptional gene silencing (PTGS) mechanism known as 'quelling' (Romano and Macino, 1992) which occurs the vegetative phase, a transcriptional gene silencing (TGS) mechanism known as 'repeat-induced point mutation-RIP' (Cambareri *et al.*, 1989) unique to fungi and occurs after fertilization and before karyogamy, another PTGS mechanism known as 'meiotic silencing' which occurs during its sexual phase (Shiu *et al.*, 2001).

Fig.1.1: Morphology of *N. crassa*. Wild type strain of *N. crassa* (FGSC 987) was cultured in flask and Petri plates on Vogel's minimal agar medium. The deep orange pigmentation is due to the accumulation of carotenoid pigment called neurosporaxanthin in the conidia, hyphae and mycelium which makes the whole strain appear orange.

1.2 The life cycle of *N. crassa*

The multicellular fungus *N. crassa* has a complex life cycle compared to the unicellular yeasts which consists of both asexual (vegetative) and sexual phases (Raju, 1992; Springer, 1993). In the nutrient-rich environment, *N. crassa* enters the asexual phase and produces branched multinucleated filaments or vegetative hyphae that runs parallel to the surface of the solid medium (Springer, 1993). The vegetative hyphae are segmented by incomplete internal cross walls or septa that allows the movement of cellular organelles like mitochondria, and other inclusion bodies amongst cells. A hyphal network is also called mycelium. Under nutrient-deprived condition or in the presence of an air-water interface, specialized aerial hyphae develop from the mycelium and give rise to conidiophores which subsequently produce uninucleate asexual spores called microconidia or multinucleate macroconidia (Springer, 1993). Macroconidia are primarily used as vegetative culture inoculum and also as fertilizing male parent in a sexual cross. Submerged cultures of *N. crassa* normally maintain vegetative hyphae without conidiation, however, certain environmental stimuli such as nitrogen or carbon starvation and exposure to high temperatures also lead to the formation of conidiophores or conidia in submerged cultures (Cortat and Turian, 1974; That and Turian, 1978; Plesofsky-Vig *et al.*, 1983; Guignard *et al.*, 1984).

N. crassa is a heterothallic filamentous fungus that contains two non-switching mating types, '*A*' and '*a*' determined by alternative DNA sequence known as idiomorphs. Starvation of nitrogen, low temperature, and light initiate the sexual cycle by forming female reproductive structures known as protoperithecium (Raju, 1992). A specialized receptor hypha (trichogyne) originating from the protoperithecium that initiates chemotropic growth towards a male element of the opposite mating type that is typically a hyphal fragment, macroconidium, or microconidium. Fusion of the trichogyne with the conidium is followed by transport of the male nucleus to the protoperithecium and initiates the development of the multicellular sexual

apparatus known as perithecium (matured protoperithecium). The male and female nuclei coexist as a dikaryon after plasmogamy in a specialized structure called ascogenous hypha. The paired male and female nuclei undergo a series of synchronous mitosis at the tip of a specialized hook-shaped structure called the crozier. During karyogamy, nuclei of the opposite mating type fuse and form a diploid zygote which undergoes two immediate meiotic divisions and post-meiotic mitosis producing an octad of eight spindle-shaped sexual spores known as ascospores that are packed in a linear fashion in the narrow ascus. After maturation, the ascospores are ejected through a beak (ostiole) at the tip of the perithecium in the direction of blue light. In the presence of suitable temperature and nutrients, the ejected ascospores can germinate and produce their own vegetative hyphae (Fig. 1.2; Raju, 1980; 1992; Springer, 1993; Kim *et al.*, 2012).

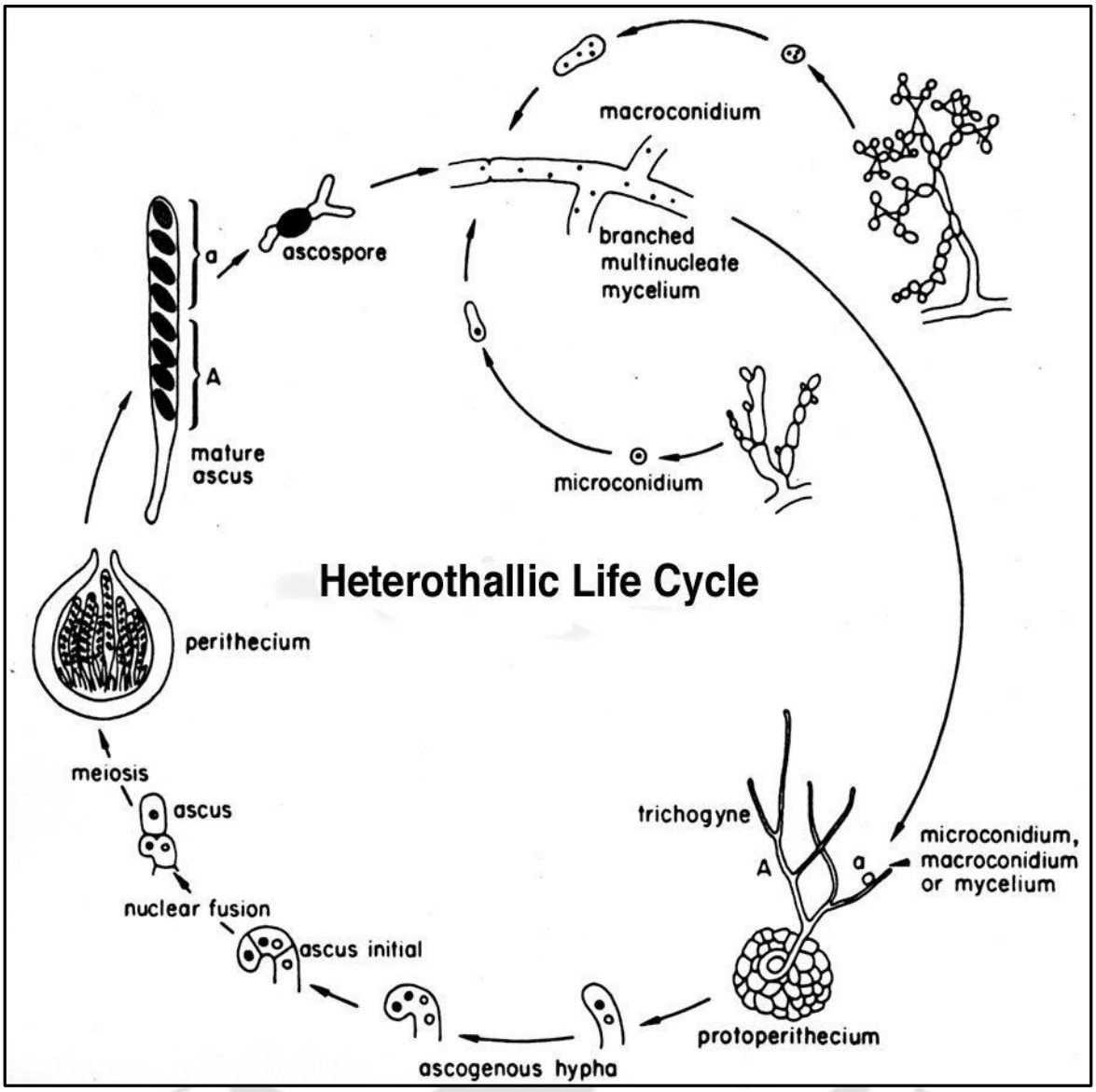

Fig. 1.2: The life cycle of *N. crassa*. During the asexual cycle, the multinucleate and branched vegetative mycelium develops into aerial hyphae and forms asexual spores, either multinucleate macroconidium or uninucleate microconidium that eventually germinate to form new mycelium. Sexual cycle is initiated with the formation of a female reproductive structure known as protoperithecium. It is fertilized by a conidium or mycelium of opposite mating type of a male parent and becomes matured perithecium which undergoes a series of mitosis and meiosis forming eight linearly ordered ascospores within an ascus. Once released, the mature pigmented multinucleate ascospores develops into new hyphae and forms the multicellular

mycelium to complete the asexual cycle or functions as male or a female parent to undergo another sexual cycle. Adapted from FGSC (http://www.fgsc.net/Neurospora/sectionB2.htm).

1.3 Role of calcium ion as a versatile and ubiquitous signaling molecule

Calcium ion (Ca^{2+}) is a universal second messenger and plays a versatile role in the regulation of various cellular processes and adaptive responses (Berridge *et al.*, 1998). Ca^{2+} is a versatile signaling molecule because of a cell's ability to precisely regulate the cellular concentrations of free and sequestered Ca^{2+} both in time and space (Campbell, 1983; Berridge *et al.*, 2000; Sanders *et al.*, 2002). One intriguing question is how only Ca^{2+} attained such versatility among various inorganic ions like H^+, Na^+, K^+, Mg^{2+}, Ba^{2+}, and Zn^{2+} etc. in the environment. Some of the first living cells appeared in the primitive ocean enriched with ions like Na^+, K^+, Cl^-, Ca^{2+} and Mg^{2+} from the salts of the earth's crust (Verkhratsky and Parpura, 2014). However, many palaeontologist theorise that the concentration of Ca^{2+} in the primeval ocean was very low, which was in the range of 100 nM, and therefore primitive living cells acquired low levels of Ca^{2+} and lived in a low Ca^{2+} environment which even today, some ancient organisms like the cyanobacteria exists which have a low Ca^{2+} requirement and are mostly alkalophilic (Gerloff and Fishbeck, 1969; Brock, 1973; Kazmierczak *et al.*, 2013). Due to various chemical and biological reactions during cooling of earth caused the rising of the levels of extracellular free Ca^{2+} in the environment (Jaiswal, 2001). The rise of Ca^{2+} in the environment exerted tremendous pressure on the cell as Ca^{2+} at high concentration is toxic as it causes precipitation of the phosphates necessary for the ATP based cellular energy transactions, organellar damage, aggregation of nucleic acids and proteins and disruption of lipid membranes (Jaiswal, 2001; Case *et al.*, 2007; Williams, 2007). Therefore, the increasing Ca^{2+} acted as a selective pressure for the need of a Ca^{2+} homeostatic system that led to the evolution of various Ca^{2+} pumps, exchangers and internal Ca^{2+} stores, so that cells could maintain their cytosolic free Ca^{2+} ($[Ca^{2+}]c$) within the tolerable range (Jaiswal, 2001; Verkhratsky and Parpura, 2014). The

presence of various Ca^{2+} pumps and intracellular Ca^{2+} stores like vacuoles, endoplasmic reticulum, and mitochondria could have contributed to the use of Ca^{2+} as a messenger molecule (Jaiswal, 2001). The versatility of Ca^{2+} as a messenger molecule rests in its chemistry involving its molecular structure, binding strength, balance state, ionization potential, and kinetic parameters in the biological reactions. The Ca^{2+} ion typically displays high co-ordination numbers (6-8) enabling to accommodate 4-12 oxygen atoms in its primary co-ordination sphere (Jaiswal, 2001). Due to its favourable ionic radius (100-120 pm) and its electronic structure the protein induced co-ordination geometry of Ca^{2+} is often irregular (Swain *et al.*, 1989; Carugo *et al.*, 1993; Jaiswal, 2001). In general, Ca^{2+} ion is coordinated by 6-7 oxygen atoms in a pentagonal bipyramidal, monocapped trigonal, or split-vertex octahedral manner (Fig.1.3.; Swain *et al*., 1989). Unlike other diavalent cations like Zn^{2+} and Mg^{2+} which have greater binding affinity for nitogen ligands, Ca^{2+} has maximum affinity for carboxylate oxygen, and interestingly, most proteins frequently contain acidic amino acids like aspartic acid and glutamic acid containing carboxylate oxygen (Jaiswal, 2001). The Ca^{2+} that enters the cytoplasm through Ca^{2+} channels, does not remain free and binds to a wide range of Ca^{2+} binding proteins through a characteristic Ca^{2+} binding helix-loop-helix structural motif known as EF-hand domain (Nakayama and Kretsinger, 1994; Clapham, 2007; Gifford *et al.*, 2007). In EF hand domain, the Ca^{2+} binding loop between the two α-helices contains 12 amino acids rich in acidic residues provide negatively charged oxygen atoms for Ca^{2+} co-ordination (Fig. 1.4 A) in a pentagonal bipyramidal geometry (Fig.1.4 B), which is the most preferable co-ordination chemistry for Ca^{2+} (Gifford *et al.*, 2007). The Ca^{2+} can bind and dissociate from a protein ~100-fold faster than Mg^{2+} due to its high rate of water exchange of metal aquo-complexes; which occurs at a rate of 10^8 s^{-1} for Ca^{2+} and 7×10^5 for Mg^{2+} at 25 °C (Ochiai, 1991; Jaiswal, 2001). All these factors have attributed to the evolution of Ca^{2+} as a ubiquitous second messenger.

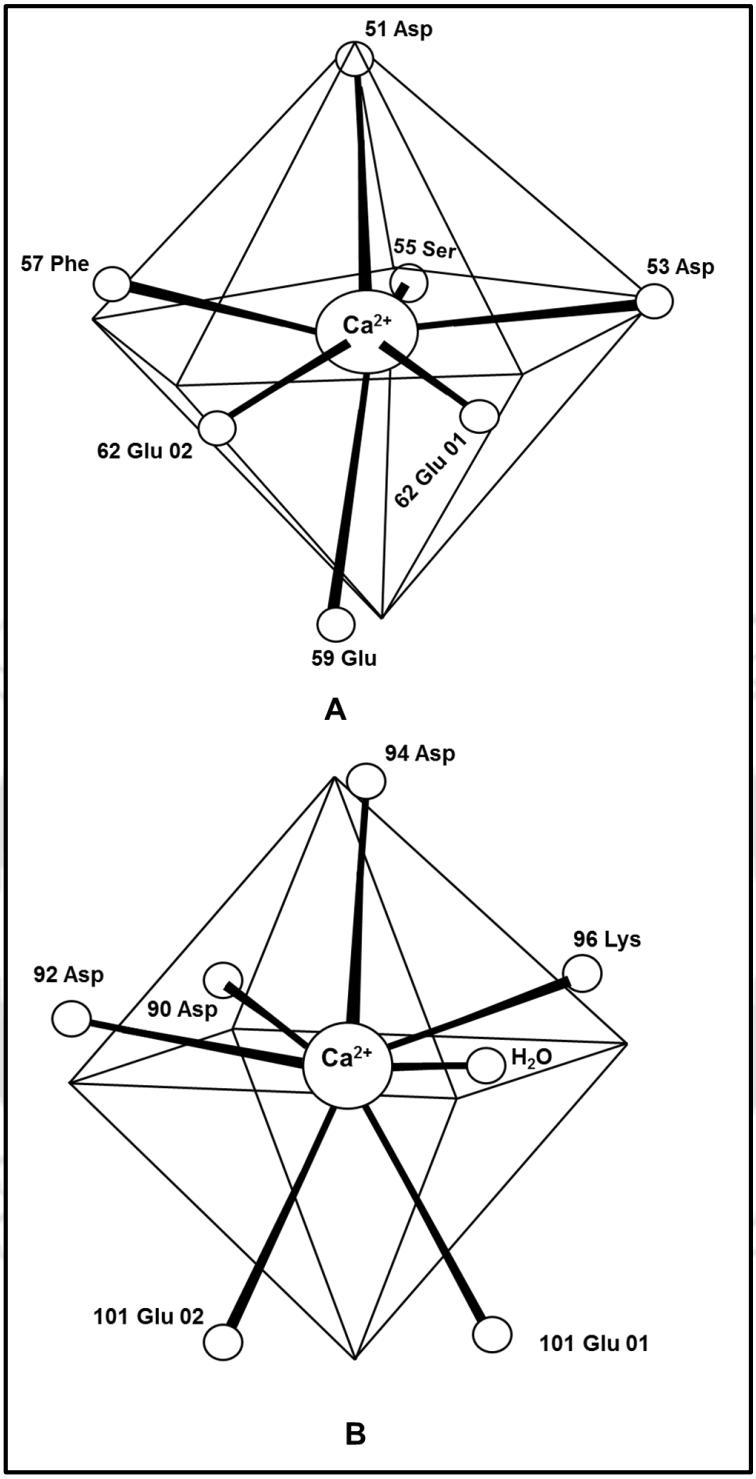

Fig. 1.3: Co-ordination geometry of Ca^{2+} ion in parvalbumin. Parvalbumin has six α helices starting from A to F and the loops between the helices C and D (CD site), E and F (EF site) bind to a Ca^{2+} ion (Kretsinger and Wasserman, 1980).

A. Pentagonal bipyramidal co-ordination geometry of Ca^{2+} in CD site of parvalbumin.

B. Monocapped trigonal prism or split-vertex octahedral co-ordination geometry of Ca^{2+} in EF site of parvalbumin. Adapted from Swain *et al.*, 1989.

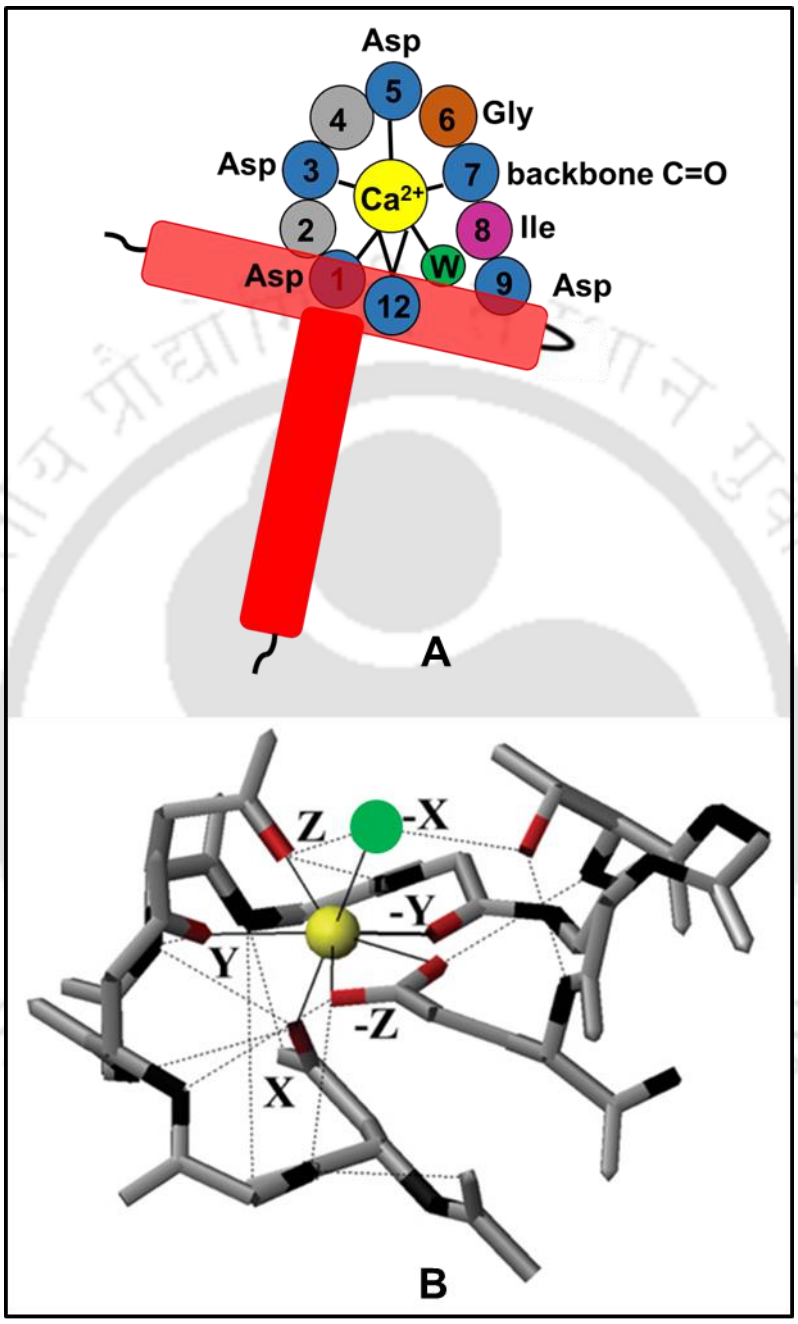

Fig. 1.4: The co-ordination sphere of the Ca^{2+} binding loop of EF hand.

A. Schematic diagram of the co-ordination sphere where the two α-helices are shown in red, the co-ordinating amino acid ligands are shown in blue and water molecule (W) in green. Conserved glycine (Gly) residues that provide the bend in the loop are shown in brown. The

conserved hydrophobic amino acid residue that forms a short β-sheet in the paired EF-hand is shown in purple.

B. Ca^{2+} co-ordination in the canonical EF-hand domain 1 (EF-1) of calmodulin (CaM) showing both pentagonal bipyramidal Ca^{2+} co-ordination (continuous lines) and hydrogen bonding (dotted lines). Adapted from Gifford *et al*., 2007.

1.4 Calcium signaling machinery in *N. crassa*

Ca^{2+} signaling regulates diverse biological processes in in living organisms (Norris *et al.*, 1996; Berridge *et al.*, 2003; Zelter *et al.*, 2004; Clapham, 2007; Kudla *et al.*, 2010). Ca^{2+} binding changes conformation and charge of protein thus regulating protein functions (Bootman *et al.*, 2001; Clapham, 2007). The resting level of cytosolic free Ca^{2+} ($[Ca^{2+}]_c$) is very low, usually 100-350 nM in fungi (Halachmi and Eilam, 1989; Iida *et al.*, 1990; Miller *et al.*, 1990), and 100-200 nM in plant and animal cells (Carafoli, 1987; Gilroy *et al.*, 1987; Johannes *et al.*, 1991). When $[Ca^{2+}]_c$ transiently increases to ~500-1000 nM either due to influx of extracellular Ca^{2+} or release of Ca^{2+} from the intracellular Ca^{2+} storage, Ca^{2+} signaling is triggered in order to maintain the resting level of $[Ca^{2+}]_c$ (Bootman *et al.*, 2001; Zelter *et al.*, 2004).

N. crassa possesses a complex Ca^{2+} signaling system (Fig.1.5) consisting of forty-eight Ca^{2+} signaling proteins (Table 1.1; Borkovich *et al*., 2004; Tamuli *et al*., 2013). The Ca^{2+} signaling in *N. crassa* is significantly unique from plant and animal cells in terms of the second messenger systems associated with the Ca^{2+} release from the internal stores (Galagan *et al.*, 2003; Borkovich *et al.*, 2004; Zelter *et al.*, 2004). *N. crassa* lacks inositol 1, 4, 5- trisphosphate (IP_3) receptors, ADP ribosyl cyclase and ryanodine receptors which are the key components of the mechanisms for Ca^{2+} release from internal stores in both plant and animal cells (Galagan *et al.*, 2003; Borkovich *et al.*, 2004). In addition, *N. crassa* also lacks extracellular Ca^{2+} sensing receptor proteins, as reported in animal cells for sensing changes in the extracellular Ca^{2+}

concentration (Brown *et al.*, 1993; Galagan *et al.*, 2003; Borkovich *et al.*, 2004). Interestingly *N. crassa* possesses both Ca^{2+}/Na^{+} and Ca^{2+}/H^{+} exchangers, while animals possess only Ca^{2+}/Na^{+} exchangers, and plants possess only Ca^{2+}/H^{+} exchangers,(Borkovich *et al.*, 2004). These notable differences suggest that *N. crassa* might possess novel intracellular Ca^{2+} release mechanisms yet to be identified.

[a] Table 1.1: Ca^{2+} signaling proteins in *N. crassa*

Sl. No.	**NCU No.**	**Gene name**	**Protein name**	**Protein type**	**Best overall[b] (e-value; organism; protein name; accession number)**
1	02762	*cch-1*	Cch-1	Ca^{2+} permeable channel	0; *Verticillium dahlia* (cch1); EGY18507.1
2	06703	*mid-1*	MID-1	Ca^{2+} permeable channel	2e-97; *Paracoccidioides brasiliensis* (MID1); EEH23338.1
3	11680[c]			Ca^{2+} permeable channel	0; *Ajellomyces dermatitidis* (Yvc1); EGE78766.1
4	03305	*nca-1*	NCA-1	Ca^{2+}-ATPase	0; *Trichophyton tonsurans* (SCA-1); EGD96734.1
5	04736	*nca-2*	NCA-2	Ca^{2+}-ATPase	0; *Magnaporthe oryzae* (Plasma membrane calcium transporting ATPase 3); EHA56671.1

6	05154	*nca-3*	NCA-3	Ca^{2+}-ATPase	0; *Glomerella graminicola* (Calcium translocating P-type ATPase); EFQ29373.1
7	03292	*pmr-1*	PMR-1	Ca^{2+}-ATPase	0; *Uncinocarpus reesii* (PMR1); XP_002541437.1
8	08147	*ph-7*	PH-7	Ca^{2+}-ATPase	0; *G. graminicola* (Potassium/sodium efflux Ptype ATPase); EFQ36596.1
9	04898	*trm-9*	TRM-9	Ca^{2+}-ATPase	0; *Cordyceps militaris* (Cation transporting ATPase 4); EGX91104.1
10	03818	*trm-10*	TRM-10	Ca^{2+}-ATPase	0; *V. dahlia* (Neo1p); EGY18069.1
11	07966	*trm-1*	TRM-1	Cation-ATPase	0; *T. tonsurans* (Cta3p); EGD97988.1
12	10143[d]	*atp-11*	ATP-11	Cation-ATPase	0; *C. militaris* (ATPase type 13A2); EGX92563.1
13	07075	*cax*	CAX	Ca^{2+}/H^{+} exchanger	0; *G. graminicola* (Calcium/proton exchanger); EFQ30300.1
14	00916	*trm-15*	TRM-15	Ca^{2+}/H^{+} exchanger	2e-176; *Aspergillus fumigatus* (membrane-bound cation transporter, XP_001481534.1)

15	00795	*trm-14*	TRM-14	Ca^{2+}/H^{+} exchanger	1e-149; *A. niger* (membrane-bound cation transporter, XP_001400827.2)
16	06366	*trm-18*	TRM-18	Ca^{2+}/H^{+} exchanger	0; *Sclerotinia sclerotiorum* (Ca^{2+}/H^{+} antiporter, XP_001589752.1)
17	07711	*trm-19*	TRM-19	Ca^{2+}/H^{+} exchanger	4e-160; *T. tonsurans* (vacuolar calcium ion transporter/H^{+} exchanger, EGD98067.1)
18	05360	*trm-17*	TRM-17	Ca^{2+}/H^{+} exchanger	0; *Metarhizium anisopliase* (calcium permease, EFY95914.1)
19	02826	*trm-16*	TRM-16	Ca^{2+}/Na^{+} exchanger	0; *Verticillium albo-atrum* (sodium/calcium exchanger protein, XP_003004985.1)
20	08490	*trm-20*	TRM-20	Ca^{2+}/Na^{+} exchanger	1e-83; *A. niger* (sodium/calcium transporter, XP_001397155.1)
21	01266	*plc-2*	PLC-2	Phospholipase C	0; *Sordaria macrospora* (phosphoinositide-specific phospholipase C, XP_003348116.1)
22	06245	*plc-1*	PLC-1	Phospholipase C	0; *G. graminicola* (phosphatidylinositol-

					specific phospholipase C, EFQ28596.1)
23	11415[e]	*inl-7*	INL-7	Phospholipase C	0; *G. graminicola* (Phosphatidylinositol-specific phospholipase C); EFQ31595.1
24	02175	*inl-15*	INL-15	Phospholipase C	3e-125; *Botryotinia fuckeliana* (BcPLC2); CCD34776.1
25	04120	*cmd*	CaM	Calmodulin	1e-103; *Gibberella zeae* (CaM); XP_382067.1
26	03804	*cna-1*	CNA-1	Ca^{2+} and/or CaM binding protein	0; *Sordaria macrospora* (Serine/threonine-protein phosphatase 2B catalytic subunit protein, XP_003352213.1)
27	03833	*cnb-1*	CNB-1	Ca^{2+} and/or CaM binding protein	2e-119; *Trichoderma reesei* (calcineurin, beta subunit, EGR44907.1)
28	09265	*cnx-1*	CNX-1	Ca^{2+} and/or CaM binding protein	0; *S. macrospora* (cnx1, XP_003347545.1)
29	05225[f]	*nde1*	NDE-1	Ca^{2+} and/or CaM binding protein	0; *M. oryzae* (mitochondrial NADH dehydrogenase, EHA47323.1)

30	02115			Ca^{2+} and/or CaM binding protein	0; *M. oryzae* (EF hand domain-containing protein, EHA48778.1)
31	01564	*mic-4*	MIC-4	Ca^{2+} and/or CaM binding protein	0; *M. oryzae* (calcium dependent mitochondrial carrier protein, EHA48778.1)
32	06948			Ca^{2+} and/or CaM binding protein	2e-54; *Mycosphaerella graminicola* (calcium ion binding, calmodulin, EGP88834.1)
33	04379	*ncs-1*	NCS-1	Ca^{2+} and/or CaM binding protein	4e-126; *Grosmannia clavigera* (neuronal calcium sensor 1, EFX03580.1)
34	02738	*pef-1*	PEF-1	Ca^{2+} and/or CaM binding protein	2e-130; *V. dahliae* (Peflin, EGY21808.1)
35	09871	*nup-34*	NUP-34	Ca^{2+} and/or CaM binding protein	4e-33; *V. dahliae* (Centrin-3,EGY16271.1)
36	01241	*mic-2*	MIC-2	Ca^{2+} and/or CaM binding protein	0; *T. reesei* (mitochondrial carrier protein, EGR44893.1)

37	06347	*ask-2*	ASK-2	Ca^{2+} and/or CaM binding protein	0; *S. macrospora* (actin cytoskeleton–regulatory complex protein, XP_003350109.1)
38	06617	*cdc4-2*	CDC4-2	Ca^{2+} and/or CaM binding protein	7e-93; *V. albo-atrum* (myosin regulatory light chain cdc4, XP_003009631.1)
39	03750	*cmd-2*	CMD-2	Ca^{2+} and/or CaM binding protein	8e-74; *B. fuckeliana* (calmodulin, XP_001560827.1)
40	08980	*nde-2*	NDE-2	Ca^{2+} and/or CaM binding protein	0; *G. clavigera* (alternative NADH-dehydrogenase, EFX03867.1)
41	02283	*camk-2*	CaMK-2	Ca^{2+} and/or CaM binding protein	0; *S. macrospora* (calcium/calmodulin-dependent protein kinase type I, XP_003344498.1)
42	09123	*camk-1*	CaMK-1	Ca^{2+} and/or CaM binding protein	0; *Sporothrix schenckii* (calcium/calmodulin-dependent kinase, AAV80434.1
43	09212	*camk-4*	CaMK-4	Ca^{2+} and/or CaM binding protein	0; *G. clavigera* (serine/threonine-protein kinase chk2, EFX01629.1)

44	02814	*prd-4*	PRD-4	Ca^{2+} and/or CaM binding protein	0; *V. dahliae* (serine/threonine-protein kinase srk1, EGY15110.1)
45	06650	*spp-3*	SPP-3	Ca^{2+} and/or CaM binding protein	3e-61; *Nectria haematococca* (phospholipase A2, XP_003042542.1)
46	02411			Ca^{2+} and/or CaM binding protein	0; *G. graminicola* (microtubule-associated protein, EFQ31793.1)
47	06177	*camk-3*	CaMK-3	Ca^{2+} and/or CaM binding protein	0; *M. grisea* (CMKK2, ACM41720.1)
48	04265	*inv*	INV	Ca^{2+} and/or CaM binding protein	7e-85; *Bacillus megaterium* (betafructosidase FruA, AEN90524.1)

[a]Adapted from Tamuli *et al*, 2013.

[b]BLASTp search was performed at NCBI (http://blast.ncbi.nlm.nih.gov/Blast.cgi; Altschul *et al.*, 1990; Altschul *et al.*, 1997; Altschul *et al.*, 2005) with default parameters for each of the 48 Ca^{2+} signaling proteins against the non-redundant protein sequence databases and the respective best overall match in other organisms with *e*-value has been indicated.

[c]Split from NCU07605.1

[d]Split from NCU01437.1

[e]Split from NCU0955.1

[f]NCU05225 was indicated as NCU08980.1 in Borkovich *et al.*, 2004.

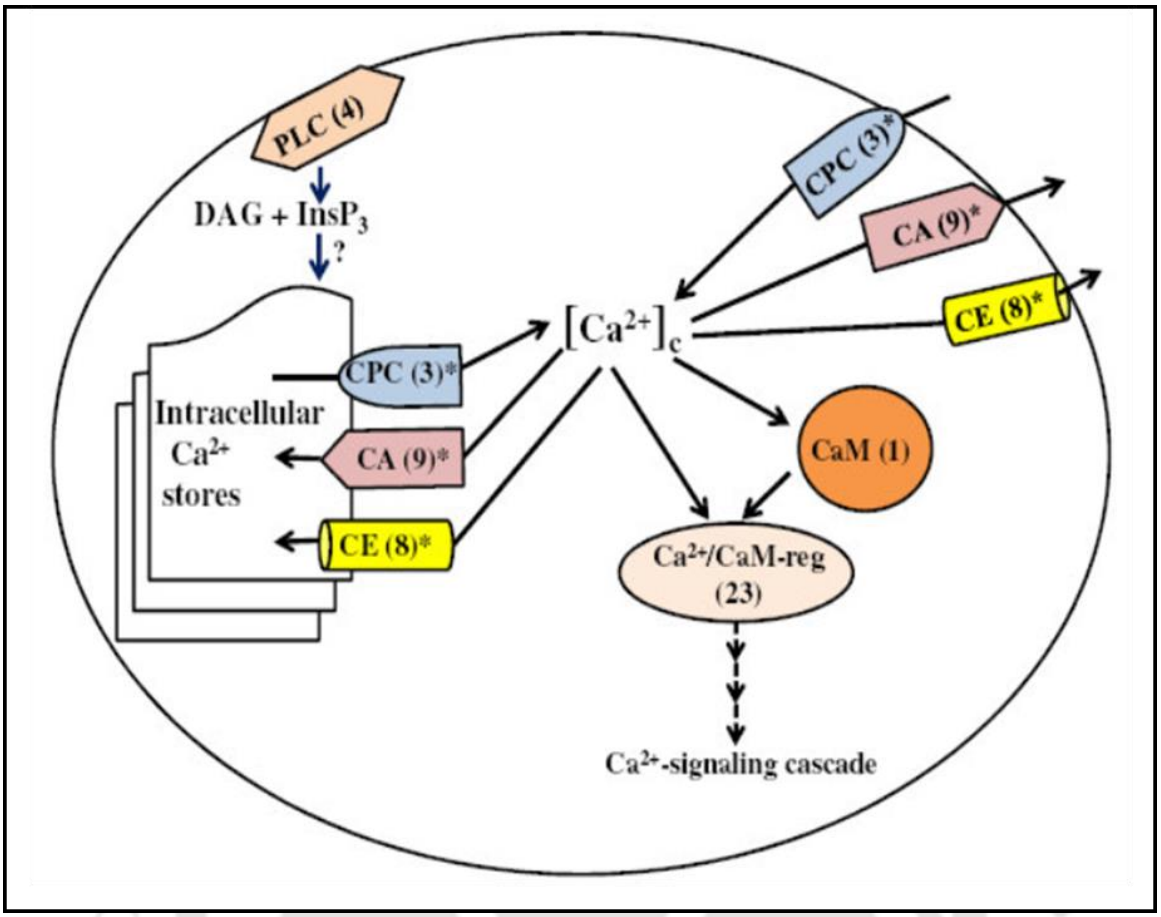

Fig. 1.5 Overview of calcium signaling system in *N. crassa*. The Ca^{2+} signaling proteins are CPC: Ca^{2+} permeable channel; CA: Ca^{2+}-and cation-ATPases; CT: Ca^{2+}/H^{+} and Ca^{2+}/Na^{+} exchanger; PLC: phospholipase C; CaM: Calmodulin; and Ca^{2+}/ CaM-reg: Ca^{2+} and/or calmodulin binding proteins. The intracellular second messengers are $InsP_3$: inositol 1,4,5-trisphosphate and DAG: 1,2-diacylglycerol. Numbers in parentheses indicate the number of identified genes in each class and the asterisk indicates the location of the membrane localized proteins. Adapted from Tamuli *et al*., 2013.

1.4.1 Ca^{2+}-permeable channels: Ca^{2+}-permeable channels are membrane localized channel proteins regulating passive Ca^{2+} flow across the membranes into the cytoplasm (Bootman *et al.*, 2001; Zelter *et al.*, 2004). In *N. crassa* NCU02762, NCU06703, and NCU11680 genes encodes three distinct Ca^{2+}-permeable channel proteins classified as group I, II, and III

respectively (Zelter *et al.*, 2004). The MID-1 (mating induced death-1) protein encoded by NCU06703 gene is a stretch activated mechanosensitive Ca^{2+}-permeable channel which has important role in ion transport regulation via Ca^{2+} homeostasis (Lew et al. 2008).

1.4.2 Ca^{2+} and cation-ATPases: Ca^{2+} and cation-ATPases are ATP driven membrane localized proteins which mediate Ca^{2+} efflux across biological membranes (Hao *et al.*, 1994; Møller *et al.*, 1996). *N. crassa* has a total of nine ATPases, amongst them seven are Ca^{2+} -ATPases and two are cation-ATPases. The Ca^{2+}-ATPases NCA-1, NCA-2, NCA-3, PMR-1, and PH-7 ATPases are encoded by NCU03305, NCU04736, NCU05154, NCU03292, and NCU08147 genes, respectively (Benito *et al.*, 2000). Strains lacking NCA-2 displays slow growth, Ca^{2+} sensitivity, higher intracellular Ca^{2+} accumulation and female sterility while lack of NCA-1 and NCA-3 does not show any significant defect in growth or Ca^{2+} distribution (Bowman *et al.*, 2011; Laxmi and Tamuli, 2015). Another *N. crassa* Ca^{2+}-ATPase TRM-9 encoded by NCU04898 plays important role in growth, Ca^{2+} sensitivity, and heat shock induced thermotolerance acquisition (Laxmi and Tamuli, 2015).

1.4.3 Ca^{2+}/H^{+} exchangers: Ca^{2+}/H^{+} exchangers are responsible for pumping Ca^{2+} ions out of the cell and also transporting Ca^{2+} into the organelles for intracellular Ca^{2+} storage to reduce high $[Ca^{2+}]_c$ essential for Ca^{2+} homeostasis (Zelter *et al.*, 2004). In *N. crassa*, two H^{+} ions are exchanged per Ca^{2+} ion transport across membranes (Miller *et al.*, 1990). Six Ca^{2+}/H^{+} exchangers encoded by the NCU07075, NCU00916, NCU00795, NCU06366, NCU07711, and NCU05360 genes had been identified in *N. crassa* (Galagan *et al.*, 2003; Borkovich *et al.*, 2004).

1.4.4 Ca^{2+}/Na^{+} exchangers: Ca^{2+}/Na^{+} exchangers remove Ca^{2+} from the cytoplasm and also allow Ca^{2+} entry into the cell (Lytton, 2007). Two Ca^{2+}/Na^{+} exchangers identified in *N. crassa* are encoded by the NCU02826 and NCU08490 genes.

1.4.5 Phospholipase C-δ subtype proteins: In *N. crassa*, four novel phospholipase C-δ subtype proteins (PLC-δ) encoded by the NCU01266, NCU02175, NCU06245, and NCU11415 genes were identified (Galagan *et al.*, 2003; Borkovich *et al.*, 2004). PLC-δ is a phosphoinositide-specific phospholipase which hydrolyses phospholipid phosphatidylinositol 4, 5-bisphosphate (PIP_2) in the plasma membrane to synthesize inositol 1,4,5-triphosphate (IP_3) and 1,2-diacylglycerol (DAG) which act as second messengers (Berridge, 1987; 1993). IP_3 induces Ca^{2+} release from intracellular Ca^{2+} storage vacuoles (Cornelius *et al.*, 1989). Interestingly, no recognizable IP_3 receptors is identified in *N. crassa* (Galagan *et al.*, 2003; Borkovich *et al.*, 2004). DAG activates protein kinase C (PKC), however both the *N. crassa* PKCs lack a C2 domain with Ca^{2+} binding sites (Schmitz and Heinisch, 2003; Borkovich *et al.*, 2004). PLC-1 encoded by the NCU06245 gene and the *plc-1* RIP mutant displayed 'spreading colonial' morphology with defects in hyphal size, and branching (Garnjobst and Tatum, 1967; Gavric *et al.*, 2007).

1.4.6 Calmodulin: In *N. crassa*, only one calmodulin (CaM), encoded by the NCU04120 gene, was reported (Galagan *et al.*, 2003; Borkovich *et al.*, 2004). CaM is essential for viability and it plays role in various biological processes including activation of chitin synthase and modulating DNA repair, circadian clock, DNA synthesis, and cell proliferation in both Chinese hamster ovary (CHO) and human cell lines (Chafouleas *et al.*, 1984; Chard, 1987; Pavelić, 1987; Capelli *et al.*, 1993; Mirzayans *et al.*, 1995; Sadakane and Nakashima, 1996; Suresh and Subramanyam, 1997; Galagan *et al.*, 2003; Borkovich *et al.*, 2004). Experiments in our lab indicated that the *Cmd* gene play role in vegetative growth, sexual development, UV survival, and survival in stress conditions (Laxmi and Tamuli 2015, 2016). In *N. crassa* calmodulin (*cmd)* is an essential gene and is associated with normal vegetative growth, ultraviolet survival, and sexual development (Laxmi and Tamuli, 2015; Laxmi and Tamuli, 2017).

1.4.7 Ca^{2+} and/or calmodulin binding proteins: In the *N. crassa* genome, 23 Ca^{2+} and/or calmodulin (CaM) binding proteins were identified (Galagan *et al.*, 2003; Borkovich *et al.*, 2004). The Ca^{2+} and/or CaM binding proteins are mostly involved in the regulation of $[Ca^{2+}]_c$ and they have several conserved domains like N-terminal catalytic domain, Ca^{2+} binding EF-hand domain, autoinhibitory, and overlapping CaM binding domain (Tamuli *et al.*, 2013). *N. crassa* has four Ca^{2+}/CaM dependent kinases including CaMK-1, CaMK-2, CaMK-3, and CaMK-4, encoded by the NCU09123, NCU02283, NCU06177, and NCU09212 genes respectively (Galagan *et al.*, 2003). Mutants lacking CaMK-1 show phase delay, light-induced phase shift in circadian conidiation rhythm, a small period lengthening, and slow growth phenotype (Yang *et al.*, 2001). The *N. crassa* Ca^{2+}/CaM dependent kinases are involved in growth, oxidative stress survival, thermotolerance, and sexual development (Kumar and Tamuli, 2014). In *N. crassa* the serine/threonine phosphatase calcineurin is a heterodimer of a calmodulin binding catalytic subunit calcineurin A (CNA-1), and a Ca^{2+} binding regulatory subunit calcineurin B (CNB-1), and these two subunits interact physically (Klee *et al.*, 1979; Winkler *et al.*, 1984; Tamuli *et al.*, 2016). Calcineurin, plays an important role in maintaining an apical Ca^{2+} gradient, growth, and development in *N. crassa* (Prokisch *et al.*, 1997; Kothe and Free, 1998; Tamuli *et al.*, 2016). The Ca^{2+} and/or CaM binding neuronal calcium sensor-1, NCS-1, encoded by the NCU04379 gene has a role in growth, Ca^{2+} stress tolerance, ultraviolet (UV) survival and germling fusion (Deka *et al.*, 2011; Palma-Guerrero *et al.*, 2013). Another Ca^{2+} and/or CaM binding protein NDE-1, encoded by the NCU08980 gene, is an external NADPH dehydrogenase of *N. crassa* mitochondria (Melo *et al.*, 1999; 2001; Borkovich *et al.*, 2004; Carneiro *et al.*, 2007). NDE-1 contains a Ca^{2+} binding motif and the NADPH oxidation activity of the NDE-1 protein is Ca^{2+}dependent (Melo *et al.*, 1999; 2001).

1.5 Neuronal Calcium sensor- 1 (NCS-1) - a calcium sensing protein

Neuronal calcium sensor-1 (NCS-1) is a 190 amino acids long protein that belongs to the neuronal calcium sensor family of proteins (Burgoyne *et al.*, 2004; Burgoyne, 2007) which are calcium-myristoyl-switch proteins with Ca^{2+} binding EF-hand domains (Bourne *et al.*, 2001). NCS-1 was first reported in *Drosophila* as frequenin that was found to modulate the synaptic transmission (Pongs *et al.*, 1993). NCS-1 has remained highly conserved throughout evolution, as the orthologs were identified in yeast, *Drosophila, Caenorhabditis elegans*, birds, rodents, and humans (Nef, 1996). NCS-1 is a globular protein consisting of ten alpha-helices and out of which four pairs of alpha-helices form four independent 12-amino-acid loops each containing a Ca^{2+} binding EF-hand domain (Bourne *et al.*, 2001; Burgoyne *et al.*, 2004). However, the most N-terminal EF hand in NCS-1 is non-functional and does not bind Ca^{2+} because of the presence of a cysteine and a proline in the putative Ca^{2+}-binding loop (Burgoyne *et al.*, 2004; Tamuli *et al.*, 2011). In addition, there is a myristoylation motif at the N-terminus that presumably allows association of NCS-1 with lipid membranes (Burgoyne *et al.*, 2004). Ca^{2+} Binding to the EF hands results in the conformational changes in NCS-1 leading to its activation (Ikura, 1996; Tamuli *et al.*, 2011). NCS-1 is a Ca^{2+} sensing protein which plays role in diverse cell functions in different eukaryotes (Table 1.2).

Table 1.2: Summary of the functions of NCS-1 in different organisms

Organisms	Protein	Function	Reference
Aspergillus fumigatus	NcsA	Sterol distribution, polar growth	Júnior *et al.*, 2008
Magnaporthe grisea	MG-NCS 1	Growth	Saitoh *et al.*, 2003

Neurospora crassa	NCS-1	Fungal communication, vegetative growth, Ca^{2+}-stress tolerance, UV survival	Deka *et al.*, 2011; Palma-Guerrero *et al.*, 2013.
Saccharomyces cerevisea	Frq 1	Cell growth, viability	Hendricks *et al.*, 1999.
Schizosaccharomyces pombe	Ncs1p	Calcium tolerance, sporulation regulation	Hamasaki-Katagiri *et al.*, 2004
Xenopus laevis	Xfreq	Synaptic development and neuronal plasticity.	Olafsson *et al.*, 1995
Caenorhabditis elegans	NCS-1	Learning and memory	Gomez *et al.*, 2001
Danio rerio	NCS-1	Internal ear development	Blasiole *et al.*, 2005
Drosophila melanogaster	Frq	Synaptic transmission, nerve terminal growth	Pongs *et al.*, 1993; Dason *et al.*, 2009
Homo sapiens	NCS-1	Synaptic transmission, nerve terminal growth	Hui *et al.*, 2007; Romero-Pozuelo *et al.*, 2007; Dason *et al.*, 2009

In animals, NCS-1, also known as frequenin, has been reported to be associated with the regulation of synaptic transmission and nerve terminal growth (Hui *et al.*, 2007; Romero-Pozuelo *et al.*, 2007; Dason *et al.*, 2009). In *Lymnaea stagnalis*, a fresh water snail, NCS-1 was reported to be modulating neurite extension and neuronal cell branching by regulating Ca^{2+} influx (Hui *et al.*, 2007). In *Drosophila*, deletion of the *frq1* gene which codes for frequenin results in locomotion defects, reduced neurotransmitter release, impaired Ca^{2+} entry, and nerve-

terminal overgrowth (Dason *et al.*, 2009). NCS-1 is associated with learning and memory development in *Caenorhabditis elegans* (Gomez *et al.*, 2001) and mammals (Saab *et al.*, 2009). NCS-1 mutation in *C. elegans* led to reduced acquisition and memory retention of isothermal recognition pattern while overexpression led to improved learning and memory (Gomez *et al.*, 2001). In mouse, overexpression of NCS-1 in the dentate gyrus region of the brain enhanced the exploratory and rearing behaviour, synaptic plasticity and spatial memory (Saab *et al.*, 2009). In human, NCS-1 has been reported to be associated with neurological disorders like bipolar disorder and some forms of schizophrenia (Koh *et al.*, 2003), and autism (Handley *et al.*, 2010). In bipolar disorder and schizophrenia patients significantly elevated level of NCS-1 protein expression was observed compared to a normal individual (Koh *et al.*, 2003). A point mutation R120Q was found in NCS-1 protein isolated from an autism spectrum disorder (ASD) patient suggesting its role in the autism as there was structural and functional deficit in NCS-1 due to the mutation (Handley *et al.*, 2010).

Orthologs of mammalian NCS-1 have been identified across many fungal species like *Saccharomyces cerevisiae*, *Schizosaccharomyces pombe*, *Magnaporthe grisea*, *Aspergillus fumigatus*, and *Neurospora crassa* (Tamuli *et al.*, 2011). The first fungal NCS-1 ortholog to be characterized was Frq1 in *S. cerevisiae* (Hendricks et al. 1999). Frq1 is essential for cell growth and viability as it is associated with the localization and regulation of the functions of phosphatidylinositol (PtdIns) 4-kinase (Pik1) essential for secretion in yeast cells (Garcia-Bustos *et al.*, 1994; Hama *et al.*, 1999; Walch-Solimena and Novick, 1999; Huttner *et al.*, 2003; Strahl *et al.*, 2005). In *S. pombe*, the NCS-1 ortholog Ncs1p was reported to be associated with starvation independent sexual development and Ca^{2+}-stress tolerance (Hamasaki-Katagiri *et al.*, 2004). In *M. grisea*, null mutants of a neuronal calcium sensor-1/frequenin like gene, *Mg-NCS-1* showed suppressed growth in high concentrations of Ca^{2+} and acidic conditions suggesting its role in Ca^{2+}-stress tolerance (Saitoh *et al.*, 2003). In *A. fumigatus*, the NCS-1

ortholog NcsA was found to be involved in the organization of membrane domains and polar growth as the Δ*ncsA* mutant showed sensitivity to sodium dodecyl sulphate (SDS), an anionic detergent (Júnior *et al.*, 2008). Moreover, reduced expression of ion pumps *pmcA* and *pmcB*, a P-type calcium ATPase and a Ca^{2+}-translocating P-type ATPase, respectively, was observed in the Δ*ncsA* mutant (Júnior *et al.*, 2008; Soriani *et al.*, 2008).

The *N. crassa* NCS-1 ortholog is encoded by the *ncs-1* gene (NCU04379) and it had been reported to be associated with vegetative growth, Ca^{2+}-stress tolerance, ultraviolet (UV) stress survival (Deka *et al.*, 2011) and fungal communication (Palma-Guerrero *et al.*, 2013). The Δ*ncs-1* mutants had slow growth rate, Ca^{2+}-stress and UV sensitive (Deka *et al.*, 2011) and defects in forming germling fusion (Palma-Guerrero *et al.*, 2013). The mammalian NCS-1, functions in response to Ca^{2+}-signaling during regulated exocytosis (Kapp-Barnea *et al.*, 2003)(Gromada *et al.*, 2005) and the yeast homolog Frq1p localizes to the Golgi membrane (Strahl *et al.*, 2005). The *N. crassa* NCS-1 was also found to be localized in the Golgi membrane as well as in cytoplasm (Palma-Guerrero *et al.*, 2013).

NCS-1 had been reported to be directly associated in activating two Ca^{2+}/CaM-dependent enzymes, 3'5'-cyclic nucleotide phosphodiesterase and protein phosphatase calcineurin in nerve cells (Schaad *et al.*, 1996). NCS-1 interacts with Dopamine Receptor D2, and therefore, it is also classified as dopamine receptor interacting protein (DRIP; Kabbani *et al.*, 2002; Bergson *et al.*, 2003). IL1-receptor accessory protein-like 1 (IL1RAPL1) which is associated with an inherited X-linked form of cognitive impairment (Carrié *et al.*, 1999) had been found to be directly interacting with NCS-1 in PC12 cell line (Gambino *et al.*, 2007). NCS-1 has also been reported to have direct interaction with other proteins like ADP-ribosylation Factor 1 (ARF1), and Phosphatidylinositol-4 Kinase-IIIβ (Haynes *et al.*, 2005; 2007), transient receptor potential channel (TRPC5; Hui *et al.*, 2006), guanine-exchange factor Ric8a (Romero-Pozuelo *et al.*, 2014), inositol 1, 4, 5-trisphosphate receptor ($InsP_3R$; Schlecker

et al., 2006). In *S. cerevisiae*, the NCS-1 homolog Frq 1 interacts with phosphatidylinositol-4-OH kinase 1 (Pik1) and binds to a conserved sequence motif in Pik1 outside Pik1's catalytic domain (Hendricks *et al.*, 1999). Pik1 is essential for secretion in yeast cells which in turn vital for the growth and survival (Huttner *et al.*, 2003; Strahl *et al.*, 2005). In *N. crassa*, a possibility of interaction between its NCS-1 with PIK-1 was suggested based on their roles in germling fusion (Palma-Guerrero *et al.*, 2013). In the fission yeast *S. pombe*, Ncs1p directly interacts with Ca^{2+} channel Yam8p during Ca^{2+} stress (Hamasaki-Katagiri and Ames, 2010). In *S. cerevisiae*, mating pheromone-induced death (Mid1) is a plasma membrane localized protein essential for Ca^{2+} influx and mating (Iida *et al.*, 1994) and in *S. pombe*, its homolog Yam8p is essential for maintaining Ca^{2+} influx (Hamasaki-Katagiri and Ames, 2010). In *N. crassa*, Mid1 or Yam8p homolog MID-1 is encoded by the *mid-1* gene (NCU06703) that has a role in growth, and Ca^{2+} ion transport and homeostasis (Lew *et al.*, 2008). Additionally, the Δ*mid-1* mutant rescued the Ca^{2+} sensitive phenotype of the Δ*ncs-1* mutant, signifying that the reduced Ca^{2+} influx in the Δ*mid-1* mutant might protect from the high extracellular Ca^{2+} (Deka and Tamuli, 2013). Therefore, it indicates a possible interaction of NCS-1 with MID-1 to regulate Ca^{2+} influx in response to high Ca^{2+} stress.

1.6 Objectives of this study

In animals, NCS-1 plays an important role in neuronal development and neurotransmission. In human, it has a lot of clinical significance as it has been associated with neurological disorders like autism, schizophrenia, bipolar disorder and X-linked mental diseases. Although the structure of mammalian NCS-1 has been determined, yet the mechanism by which it is associated with these diseases is still largely unknown. In fungi, NCS-1 orthologs are found to be important for growth and development. But, the structure and targets of NCS-1 of fungal origin have only been determined in *S. cerevisiae*. In case of filamentous fungi, structure and targets of NCS-1 are yet to be explored. In our lab, the functional importance of NCS-1 in *N.*

crassa was reported, but its target and molecular mechanism was remained unknown. Therefore, to understand the molecular mechanism of NCS-1 function in *N. crassa*, I decided to work on three broad objectives as given below.

Broad objectives of my thesis work were:

1. To study the cell functions of neuronal calcium sensor-1 (NCS-1) and associated proteins in tolerance to Ca^{2+} stress in *Neurospora crassa*.
2. To study the regulation of *ncs-1* transcription and the molecular mechanism of NCS-1 mediated pathway for tolerance to Ca^{2+} stress.
3. To study the critical amino acid residues important for the NCS-1 function and its interspecific complementation.

Chapter 2
Materials and Methods

2.1 Materials

2.1.1 Laboratory chemicals and other materials

Laboratory chemicals like acrylamide (C_3H_5NO), ammonium iron (II) sulfate hexahydrate [$Fe(NH_4)_2(SO_4)_2.6H_2O$], ammonium nitrate (NH_4NO_3), ammonium persulphate [APS, $(NH_4)_2S_2O_8$], arginine, biotin, boric acid (H_3BO_3), calcium chloride ($CaCl_2.H_2O$), calcium D-pantothenate ($C_{18}H_{32}CaN_2O_{10}$), cetyltrimethyl ammonium bromide (CTAB, $C19H_{42}BrN$), chloroform ($CHCl_3$), citric acid ($C_6H_8O_7.H_2O$), copper sulphate pentahydrate ($CuSO_4.5H_2O$), diethyl pyrocarbonate (DEPC, $C_6H_{10}O_5$), dimethyl sulphoxide (DMSO, C_2H_6OS), absolute ethanol (C_2H_5OH)), ethidium bromide (EtBr, $C_{21}H_{20}BrN_3$), ethylenediaminetetra acetic acid disodium salt dihydrate (EDTA, $C_{10}H_{14}N_2Na_2O_8.2H_2O$), ethylene glycol-bis (β-aminoethyl ether)-*N*,*N*,*N*′,*N*′-tetraacetic acid (EGTA, $C_{14}H_{24}N_2O_{10}$), ferrous sulphate heptahydrate ($FeSO_4.7H_2O$), formaldehyde (CH_2O), fructose($C_6H_{12}O_6$), glacial acetic acid (CH_3COOH), D-glucose ($C_6H_{12}O_6$), glutamine, glycerol ($C_3H_8O_3$), glycine, hydrochloric acid (HCL), 2-[4- (2-hydroxyethyl) piperazin-1-yl] ethanesulfonic acid (HEPES, $C_8H_{18}N_2O_4S$), isopropanol (C_3H_7OH), lithium chloride (LiCl), magnesium chloride ($MgCl_2$) magnesium sulphate heptahydrate ($MgSO_4.7H_2O$), manganous chloride tetrahydrate ($MnCl_2.4H_2O$), manganous sulphate ($MnSO_4.H_2O$), methanol (CH_3OH), *N*,*N*′-Methylenebisacrylamide ($C_7H_{10}N_2O_2$), (β-mercaptoethanol (C_2H_6OS), 3-Morpholinopropane-1-sulfonic acid (MOPS, $C_7H_{15}NO_4S$), NP-40, 1,4-Piperazinediethanesulfonic acid (PIPES, $C_8H_{18}N_2O_6S_2$), Phenol: Chloroform: Isoamyl mixture (25:24:1), phenylmethylsulphonyl fluoride (PMSF, $C_7H_7FO_2S$), potassium acetate (CH_3COOK), potassium hydroxide (KOH), potassium nitrate (KNO_3), potassium phosphate dibasic (K_2HPO_4), potassium phosphate monobasic (KH_2PO_4), silica gel (6-12 mesh), sodium bicarbonate ($NaHCO_3$), sodium chloride (NaCl), sodium citrate dihydrate ($Na_3C_6H_5O_7.2H_2O$), sodium deoxycholate ($C_{24}H_{40}O_4$), sodium dodecyl sulphate (SDS, $NaC_{12}H_{25}SO_4$), sodium hydroxide (NaOH), sodium molybdate ($Na_2MoO_4.2H_2O$), sodium nitrate ($NaNO_3$), D-sorbitol

($C_6H_{14}O_6$), sorbose ($C_6H_{12}O_6$), sucrose ($C_{12}H_{22}O_{11}$), tetramethylethylenediamine [TEMED, $(CH_3)_2NCH_2CH_2N(CH_3)_2$], Tris base ($C_4H_{11}NO_3$), triethanoleamine ($C_6H_{15}NO_3$), Triton X-100, Tween 20, Tween 80, and zinc sulphate heptahydrate ($ZnSO_4.7H_2O$) were procured from various manufacturers such as Himedia (Mumbai, India), Loba Chemie (Mumbai, India), Merck (Mumbai, India), and SRL (Mumbai, India). Bathocuproinedisulfonic acid disodium salt (BCS, $C_{26}H_{18}N_2Na_2O_6S_2$), dimethyl pimelimidate (DMP, $C_9H_{18}N_2O_2$), dithiothreitol (DTT, $C_4H_{10}O_2S_2$), fungal protease inhibitor cocktail (FPIC), and glufosinate ammonium ($C_5H_{15}N_2O_4P$) were procured from Sigma Aldrich (USA). Media for bacterial growth like Luria-Bertani (LB) agar and broth, Super Optimal broth (SOB), Super Optimal broth with Catabolite repression (SOC) and Tartoff-Hobbs Broth (Terrific Broth); skimmed milk powder; antibiotics like ampicillin and hygromycin B solution; bacto-agar, Prestained Protein ladder; Bradford Reagent; amido black and Coomassie Brilliant Blue G-250 (CBB) dye were obtained from Himedia (Mumbai, India). All the antibodies, agarose, EMSA kit, TRIzol™ reagent, SYBR Green Real-Time PCR Master Mix, Dynabeads® Protein A magnetic beads, plasma membrane dye FM™ 4-64, and nuclease-free water were purchased from Life Technologies (USA). All restriction enzymes, DNA size markers, Blue Gel Loading Dye (6X), Quick Ligation™ Kit, routine Taq DNA polymerase, Phusion® High-Fidelity DNA Polymerase and Q5® high-fidelity DNA Polymerase for PCRs were purchased from New England Biolabs (USA). Plasmid DNA isolation, Gel purification and PCR Clean-up kits were obtained from Qiagen (USA) as well as from GCC Biotech (Kolkata, India). Pancreatic RNAase A, proteinase K, and herring sperm DNA was purchased from Promega (USA). ECL™ western blotting detection kit and Hybond PVDF blotting membranes were obtained from GE Healthcare Life Sciences (USA). Verso cDNA synthesis kit was purchased from Thermo Fisher Scientific. Glassware was obtained from Borosil (Mumbai, India) and Jain scientific glass works (Ambala, India). Plasticware was procured from Tarsons (Kolkata, India) and

Genaxy (New Delhi, India). Rest of the chemicals were procured from local manufacturers and were of analytical grade.

2.1.2 *Neurospora crassa* strains

N. crassa strains were obtained from the Fungal Genetics Stock Centre and the University of California Riverside, and also generated in our laboratory.

1. **Strains acquired from the Fungal Genetics Stock Centre (FGSC):** *N. crassa* wild type, Δ*ncs-1*, Δ*cax*, Δ*mid-1*, Δ*crz-1* (heterokaryotic), and Δ*mus-52* knockout, and *his-3* mutant strains (Table 2.1) were obtained from the Fungal Genetics Stock Center (FGSC), University of Missouri, Kansas City, MO 64110 (McCluskey, 2003; McCluskey *et al.*, 2010).
2. **Strains obtained from University of California Riverside (UCR):** pccg-1_GFP, pccg-1_RFP, 45-23-crz, 559, and NCS-1-P2-HT 3 strains (Table 2.1) were generated and obtained from the laboratory of Prof. Katherine A. Borkovich (University of California Riverside, USA).
3. **Strains generated in our laboratory:** *his-3* Δ*ncs-1*A (11), *ncs-1*^{Rat} HT (RB10), *ncs-1*^{Rat} hop (RB10-7), *ncs-1*^{Rat} hop (RB10-14), *ncs-1*$^{Rat\ (E120Q)}$ HT (E5), *ncs-1*$^{Rat\ (E120Q)}$ hop (E5-28), *ncs-1*$^{Rat\ (E120Q)}$ hop (E5-3), Δ*crz-1* (145), Δ*crz-1* (122), P_{nit-6}::*ncs-1* (21), Δ*ncs-1*; Δ*mid-1*; P_{nit-6}::*ncs-1* (4) strains (Table 2.1) were generated in this study.

Table 2.1: List of strains used in the study

Sl. No.	Strains	Strain type or NCU no.	Genotype	Reference
1	74-OR23-1A	Wild type	Wild type; *mat A*	FGSC 987
2	74-OR8-1a	Wild type	Wild type; *mat a*	FGSC 988
3	11404	04379	Δ*ncs-1*::*hph*; *mat A*	FGSC 11404

4	11403	04379	Δ*ncs-1*::*hph*; *mat a*	FGSC 11403
5	11707	06703	Δ*mid-1*::*hph*; *mat a*	FGSC 11707
6	11708	06703	Δ*mid-1*::*hph*; *mat A*	FGSC 11708
7	52-4-9	00077	Δ*mus-52*::*nat*; *mat A*	FGSC 2479
8	51-IV-8	Homokaryotic	Δ*rid-1*::*nat*; Δ*mus-51*::*nat*; *mat a*	FGSC 23148
9	11249	07075	Δ*cax*::*hph*; *mat A*	FGSC 11249
10	11248	07075	Δ*cax*::*hph*; *mat a*	FGSC 11248
11	11494	07952 (Heterokaryotic)	Δ*crz-1*:: *hph*; *mat a*	FGSC 11494
12	6032	03139	*his-3*; *mat A*	FGSC 6032
13	*his-3* Δ*ncs-1*A (11)	Homokaryotic	*his-3*; Δ*ncs-1*::*hph*; *mat A*	Our laboratory (Gohain *et al.*, 2016)
14	*upr-1* (34-97-3a)	NCU01951	*upr-1*^{Rip}; *mat a*	Tamuli *et al.*, 2006
15	*ncs-1*^{Rat} HT (RB10)	Heterokaryotic	*ncs-1*^{Rat}::*gfp*; Δ*ncs-1*::*hph*; *mat A*	Our laboratory
16	*ncs-1*^{Rat} hop (RB10-7)	Homokaryotic	*ncs-1*^{Rat}::*gfp*; Δ*ncs-1*::*hph*; *mat A*	Our laboratory (Gohain *et al.*, 2016)
17	*ncs-1*^{Rat} hop (RB10-14)	Homokaryotic	*ncs-1*^{Rat}::*gfp*; Δ*ncs-1*::*hph*; *mat a*	Our laboratory (Gohain *et al.*, 2016)

18	*ncs-1*$^{\text{Rat (E120Q)}}$ HT (E5)	Heterokaryotic	*ncs-1*$^{\text{Rat (E120Q)}}$::*gfp*; Δ*ncs-1*::*hph*; *mat A*	Our laboratory
19	*ncs-1*$^{\text{Rat (E120Q)}}$ hop (E5-28)	Homokaryotic	*ncs-1*$^{\text{Rat (E120Q)}}$::*gfp*; Δ*ncs-1*::*hph*; *mat A*	Our laboratory (Gohain *et al.*, 2016)
20	*ncs-1*$^{\text{Rat (E120Q)}}$ hop (E5-3)	Homokaryotic	*ncs-1*$^{\text{Rat (E120Q)}}$::*gfp*; Δ*ncs-1*::*hph*; *mat a*	Our laboratory (Gohain *et al.*, 2016)
21	Δ*crz-1* (145)	Homokaryotic	Δ*crz-1*::*hph*; *mat A*	Our laboratory
22	Δ*crz-1* (122)	Homokaryotic	Δ*crz-1*::*hph*; *mat a*	Our laboratory
22	Δ*ncs-1*; Δ*mid-1* (2)	Homokaryotic double mutant	Δ*ncs-1*::*hph*; Δ*mid-1*::*hph*; *mat a*	Our laboratory (Deka and Tamuli, 2013)
23	pccg-1_GFP	Homokaryotic	Δ*pan-2*::P$_{ccg-1}$::*5xGly*::*V5*::*gfp*; *mat a*	Borkovich Lab (UCR, USA) (Ouyang *et al.*, 2015)
24	pccg-1_RFP	Homokaryotic	Δ*inl*::P$_{ccg-1}$::*5xGly*::*S-tag*::*rfp*; *mat a*	Borkovich Lab (Ouyang *et al.*, 2015)
25	45-23-*crz*	Heterokaryotic	Δ*pan-2*$^{-}$::P$_{tcu-1}$::*crz-1*::*5xGly*::*V5*::*gfp*; *mat A*	Borkovich Lab (UCR, USA)
26	559	Homokaryotic	Δ*crz-1*::*hph;* Δ*pan-2*$^{-}$::P$_{tcu-1}$::*crz-1*::*5xGly*::*V5*::*gfp*; *mat a*	Borkovich Lab (UCR, USA)

27	NCS-1-P2-HT 3	Heterokaryotic	Δ*ncs-1*:: *hph;* Δ*pan-2*::P_{nit-6}::*ncs-1*::*5xGly*::*V5*::*gfp*; *mat a*	Borkovich Lab (UCR, USA)
28	P_{nit-6}::*ncs-1* (21)	Homokaryotic	Δ*ncs-1*::*hph;* Δ*pan-2*::P_{nit-6}::*ncs-1*:: *5xGly*::*V5*::*gfp*; *mat A*	Our laboratory
29	Δ*ncs-1*; Δ*mid-1*; P_{nit-6}::*ncs-1* (4)	Homokaryotic	Δ*ncs-1*:: *hph;* Δ*mid-1*::*hph*; Δ*pan-2*::P_{nit-6}::*ncs-1*::*5xGly*::*V5*::*gfp*; *mat A*	Our laboratory
30	MID-1-17-HT 21	Heterokaryotic	Δ*inl*::P_{nit-6}::*mid-1*:: *5xGly*::*S-tag*::*rfp*; Δ*mid-1*:: *hph*; *mat A*	Our laboratory
31	P_{tcu-1}::*mid-1* (11)	Homokaryotic	Δ*inl*::P_{nit-6}::*mid-1*:: *5xGly*::*S-tag*::*rfp*; Δ*mid-1*:: *hph*; *mat A*	Our laboratory
32	NCS-1 GFP + MID-1 RFP	Heterokaryotic	Heterokaryon of strain P_{nit-6}::*ncs-1* (21) + strain P_{tcu-1}::*mid-1* (11)	Our laboratory
33	GFP + RFP	Heterokaryotic	Heterokaryon of strain pccg-1_GFP + strain pccg-1_RFP	Our laboratory

2.1.3 Bacterial strain

The *Escherichia coli DH5α* strain with genotype *SupE*44 Δ*lac*U169 (φ80*lacZ* ΔM15) *hsdR*17 *recA*1 *end A*1 *gyrA*96 *thi*-1 *relA*1 (Sambrook and Russel, 2001) was used for all routine

bacterial cloning and transformations, plasmid growth and isolation, and selection of recombinants. The *E. coli DH5 α* is a recombination deficient nonsense (amber) suppressing strain with the φ80 *lacZ* ΔM15 mutation which allows α-complementation with the *β*-galactosidase amino terminus encoded in pUC vectors (Sambrook and Russel, 2001).

2.1.4 Plasmid vectors

1. **pMF272:** The plasmid vector pMF272 (Fig. 2.1) of size 8.4 kb, contains the GFP variant gene (*sgfp*), *lacZ′* sequence including the SP6 and T7 promoters, ampicillin as bacterial selection marker, and a multiple cloning site (MCS) for translational fusion of *Neurospora* genes to *sgfp* (Freitag *et al.*, 2004). The *sgfp* gene encodes for a derivative of GFP with substitution of serine to threonine at position 65 (S65T) which increases the brightness, and shifts the codon bias closer to that of humans. This vector contains the *N. crassa ccg-1* promoter (P_{ccg-1}), which is strongly induced by stress or glucose deprivation (McNally and Free, 1988). The P_{ccg-1}::*sgfp* cassette was constructed using the pBM60 backbone, which allows *his-3* targeting of the transgene by gene replacement (Margolin *et al.*, 1997).

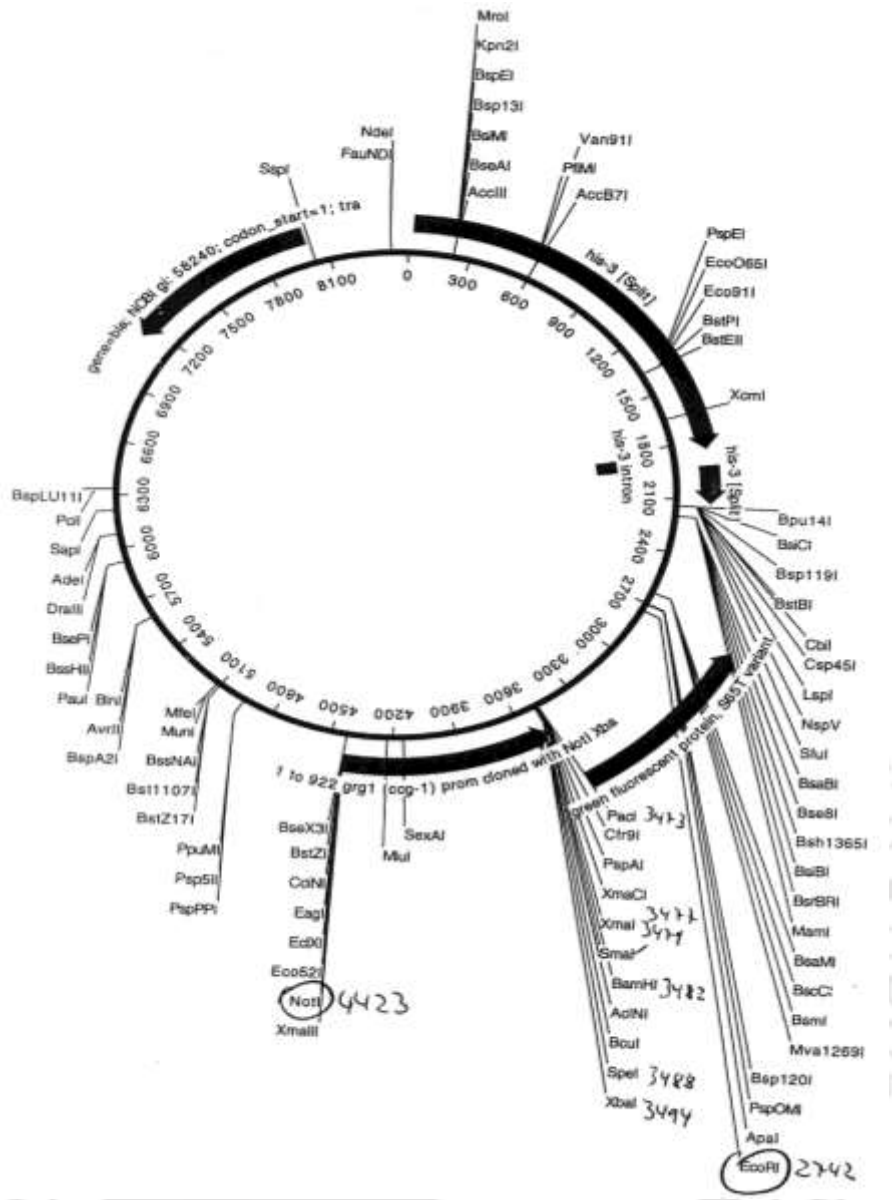

Fig. 2.1: Schematic of the pMF272 vector. The size of the pMF272 vector is 8.4 kb and it consists of a MCS region with unique restriction sites. The plasmid map is available at http://www.fgsc.net/plasmid/image/609.jpg.

2. **pRS426PVG/pnit-6_1.5 kb:** This vector consists of the backbone from the yeast/*E. coli* shuttle vector pRS426PVG (Ouyang *et al.*, 2015). The pRS426PVG/pnit-6_1.5 kb vector (Fig. 2.2) confer uracil prototrophy to *ura-3* yeast mutant (URA3) and ampicillin resistance (Ap^R) in *E. coli*. The pRS426PVG/pnit-6_1.5 kb vector contains the *N. crassa* nitrogen-controlled *nit-6* (NCU04720) promoter (P_{nit-6}), 5' and 3' flanking regions of the *N. crassa pan-2* (NCU10048) ORF surrounding P_{nit-6}, a multiple cloning site (MCS), a 5xGly linker,

a V5 peptide tag and the *gfp* gene. It also contains *bar* gene as the selection marker which confer resistance to Glufosinate ammonium commonly known as Basta® or Ignite®. P_{nit-6} is repressed by glutamine and induced by the addition of $NaNO_3$ in the medium as a nitrogen source (Exley *et al.*, 1993; Ouyang *et al.*, 2015).

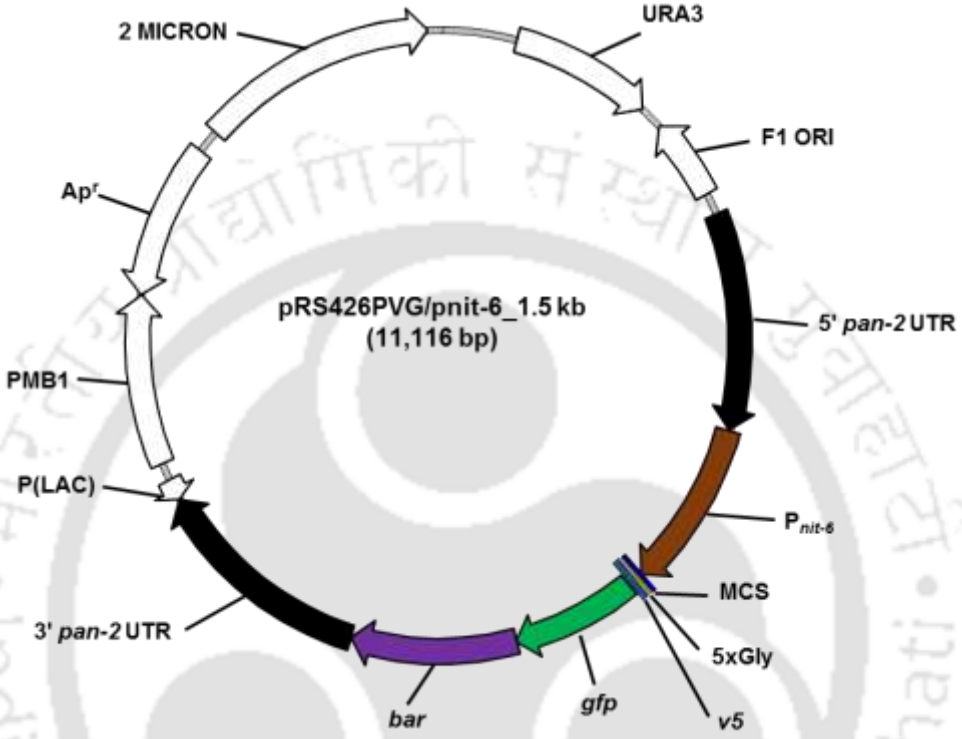

Fig. 2.2: Schematic of the pRS426PVG/pnit-6_1.5 kb. adapted from Ouyang *et al.*, 2015. The vector size is 11,116 bp.

3. **pRS426PVG/ptcu-1_1.5 kb:** This vector consists of the backbone from the yeast/*E. coli* shuttle vector pRS426PVG (Ouyang *et al.*, 2015). The pRS426PVG/ptcu-1_1.5 kb vector (Fig. 2.3) confer pantothenate auxotrophy in *N. crassa*, uracil prototrophy to *S. cerevisae ura-3* mutant (URA3) and ampicillin resistance (Ap^R) in *E. coli*. The pRS426PVG/ptcu-1_1.5 kb vector contains the 5' flanking region of the *N. crassa pan-2* (NCU10048) ORF followed by the *N. crassa* copper regulated *tcu-1* (NCU00830) promoter (P_{tcu-1}), a MCS, a 5xGly linker, a V5 peptide tag, the *gfp* gene, and 3' flanking region of the *N. crassa pan-2* (NCU10048) ORF. It also contains *bar* gene as the selection marker which confer resistance to Glufosinate ammonium commonly known as Basta® or Ignite®. P_{tcu-1} is

repressed by the addition of $CuSO_4$ and induced by the addition of BCS (Lamb *et al.*, 2013; Ouyang *et al.*, 2015).

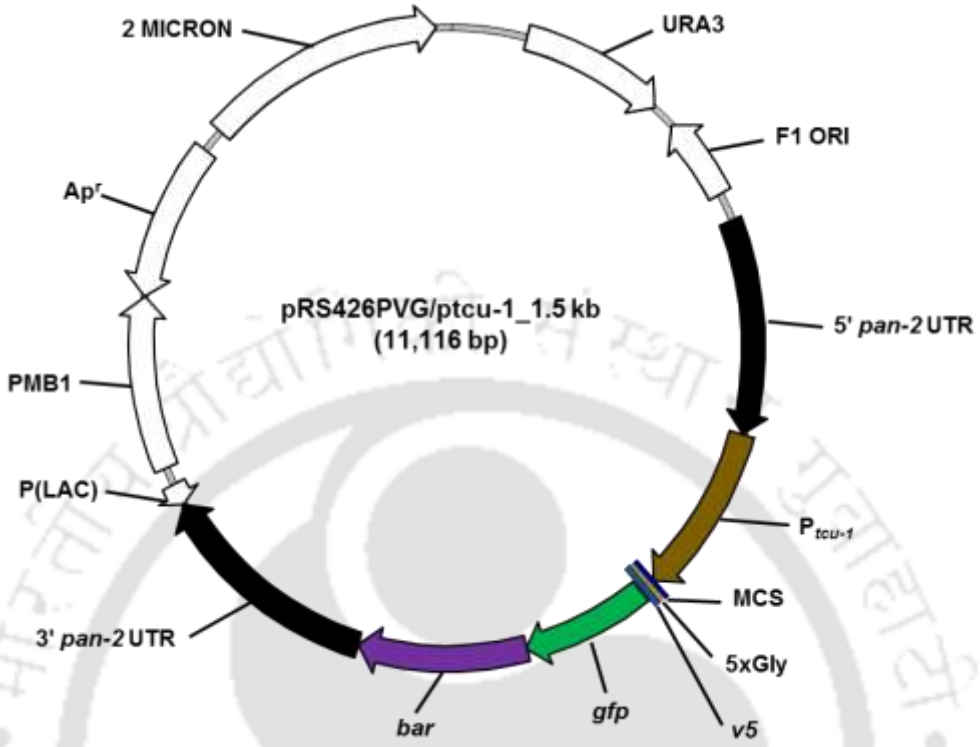

Fig. 2.3: Schematic of the pRS426PVG/ptcu-1_1.5 kb vector adapted from Ouyang *et al.*, 2015. The vector size is 11,116 bp.

4. **pRS426ISR/ptcu-1_1.5 kb:** This vector consists of the backbone from the yeast/*E. coli* shuttle vector pRS426PVG (Ouyang *et al.*, 2015). The pRS426ISR/ptcu-1_1.5 kb vector (Fig. 2.4) confer inositol auxotrophy in *N. crassa*, uracil prototrophy to *ura-3 S. cerevisiae* mutant (URA3) and ampicillin resistance (Ap^R) in *E. coli*. The pRS426ISR/ptcu-1_1.5 kb vector contains the *N. crassa* copper regulated *tcu-1* (NCU00830) promoter (P_{tcu-1}), 5' and 3' flanking regions of the *N. crassa inl* (NCU06666) ORF followed by *N. crassa* copper regulated P_{tcu-1}, a MCS, a 5xGly linker, *S-tag* and the red fluorescent protein (*rfp)* gene. It also contains *bar* gene as the selection marker which confer resistance to Glufosinate ammonium commonly known as Basta® or Ignite®. The 5' *inl* flank extends 1 kb upstream to the start codon ATG, whereas the 3' flank begins just beyond the stop codon extending upto 1 kb downstream.

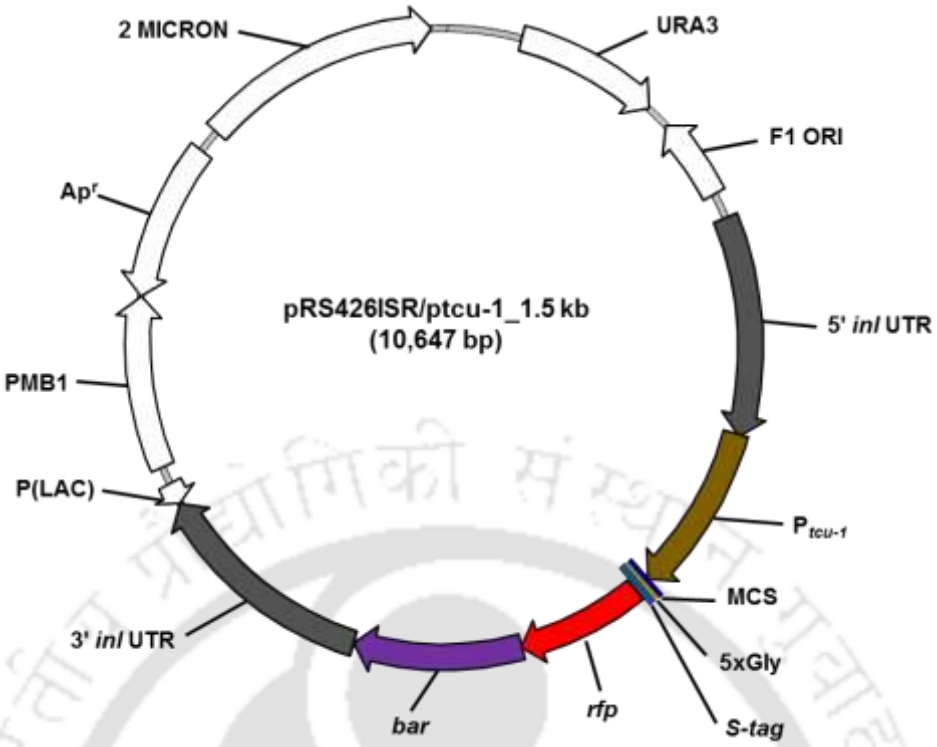

Fig.2.4: Schematic of pRS426ISR/ptcu-1_1.5 kb vector adapted from Ouyang *et al.*, 2015. The vector size is 10,647 bp.

2.1.5 Media for bacterial growth, antibiotics, and other commonly used reagents

1. **Bacterial media:** LB broth and agar, Terrific broth, SOB and SOC media were purchased from Himedia (Mumbai, India) and were prepared in distilled water as per the manufacturer's protocol. All the bacterial media were sterilized by autoclaving.
2. **Ampicillin:** A stock solution of ampicillin (100 mg/ml) was prepared by dissolving 200 mg ampicillin powder in 2 ml sterilized water and stored in 200 µl aliquots at minus 20 °C.
3. **Hygromycin B:** Hygromycin B was obtained from Himedia (Mumbai, India) as a ready-to-use solution with a concentration of 50 mg/ml.
4. **Glufosinate ammonium/Basta®:** Glufosinate ammonium also known as Basta® was purchased from Sigma Aldrich (USA). A stock solution of 100 mg/ml was prepared by dissolving 100 mg glufosinate ammonium in 1 ml sterile distilled water and stored as aliquots of 200 µl at minus 20°C.

5. **Pantothenate solution:** A stock solution of 1 mg/ml was prepared by dissolving 100 mg calcium D-pantothenate in 100 ml of distilled water and sterilized by autoclaving.
6. **Inositol solution:** A stock solution of 1 mg/ml was prepared by dissolving 100 mg inositol in 100 ml distilled water and sterilized by autoclaving.
7. **BCS solution:** 0.2 M stock solution was prepared by dissolving 113 mg BCS in 1 ml sterile distilled water.
8. **1 M sorbitol:** 18.21 g sorbitol was dissolved in 70 ml distilled water and the final volume was adjusted to 100 ml by adding distilled water and sterilized by autoclaving.
9. **8 M LiCl:** 33.9 g LiCl was dissolved in a final volume of 100 ml of DEPC treated sterile distilled water and sterilized by autoclaving.
10. **1 M glucose:** 16.02 g D-glucose was dissolved in 70 ml distilled water and volume was adjusted to 100 ml. The stock was stored by sterilized by filtering through a 0.45-µm syringe filter and stored at room temperature.
11. **3 M Na-acetate (pH 5.2):** 24.61 g Na-acetate was dissolved in 70 ml distilled water and pH was adjusted to 5.2 by adding glacial acetic acid. Volume was adjusted to 100 ml by adding water.
12. **5 M $CaCl_2$:** 73.5 g of $CaCl_2.2H_2O$ was dissolved in distilled water to a final volume of 100 ml. The solution was sterilized by autoclaving.
13. **10 N NaOH:** 40 g NaOH pellet was slowly dissolved in 80 ml of distilled water, stirring continuously in a glass beaker placed on ice, the volume was adjusted to 100 ml and stored at room temperature.
14. **2 M KCl:** 14.9 g of KCl was dissolved in 80 ml of distilled water, and the volume was adjusted to 100 ml and stored at room temperature.
15. **1 M glycine:** 7.5 g glycine was dissolved in 70 ml distilled water and volume was adjusted to 100 ml and stored at room temperature.

16. **EtBr:** A stock solution of EtBr (10 mg/ml) was prepared by dissolving 10 mg EtBr in 1 ml distilled water and stored at 4 °C.
17. **10% SDS:** 10 g SDS was dissolved in 90 ml distilled water and heated at 68 °C by stirring in a magnetic stirrer cum heater. The volume was adjusted to 100 ml and stored at room temperature.
18. **1 M Tris-HCl (pH 7.5):** 12.11 g Tris base was dissolved in 70 ml distilled water, adjusted pH to 7.5 by adding concentrated HCl, and adjusted the volume to 100 ml with distilled water and sterilized by autoclaving.
19. **1 M Tris-HCl (pH 8.0):** 12.11 g Tris base was dissolved in 70 ml of distilled water, adjusted pH to 8.0 by adding concentrated HCl, and adjusted the volume to 100 ml with distilled water and sterilized by autoclaving.
20. **1.5 M Tris-HCl (pH 8.8):** 18.17 g Tris base was dissolved in 70 ml distilled water, adjusted pH to 8.8 by adding concentrated HCl, and adjusted the volume to 100 ml with distilled water and sterilized by autoclaving.
21. **0.5 M Tris-HCl (pH 6.8**): 6.06 g Tris base was dissolved in 70 ml distilled water, adjusted pH to 8.8 by adding concentrated HCl, and adjusted the volume to 100 ml with distilled water and sterilized by autoclaving.
22. **0.5 M EDTA (pH 8.0):** 18.61g EDTA was dissolved in 70 ml distilled water, pH was adjusted to 8.0 by adding NaOH pellets, and volume was adjusted to 100 ml and sterilized by autoclaving.
23. **0.5 M EGTA (pH 8.0):** 19.017 g EGTA was dissolved in 60 ml sterile water and pH was adjusted to 8.0 by adding NaOH pellets. The final volume was adjusted to 100 ml and sterilized by autoclaving.
24. **1 M $MgCl_2$:** 20.33g $MgCl_2.6H_2O$ was dissolved in 80 ml distilled water, the volume was adjusted to 100 ml and sterilized by autoclaving.

25. **Proteinase K:** Proteinase K was dissolved at a concentration of 20 mg/ml in 50 mM Tris-HCl (pH 8.0), 10 mM $CaCl_2$, and stored at minus 20 °C.
26. **1X TE:** The solution was prepared by adding 10 mM Tris-HCl (pH 8.0) and 1 mM EDTA (pH 8.0) from their respective stocks and stored at 4 °C.
27. **50X TAE:** 1 L of the 50X TAE stock solution was prepared by adding 242 g Tris base, 57.1 ml of glacial acetic acid and 100 ml of 0.5 M EDTA (pH 8.0) and adjusting the volume to 1 L by adding distilled water. The solution was stored at 4 °C.
28. **10X MOPS buffer:** The stock solution of 10X MOPS for 100 ml contains 4.18 g of MOPS (0.2 M), 2 ml 1 M Na-acetate solution (20 mM), and 2 ml 0.5 M EDTA (10 mM). After dissolving, 4.18 g of MOPS in DEPC-treated water, added 3 M Na-acetate solution and 0.5 M EDTA in an indicated volume. The pH was adjusted to 7.0 with 10 N NaOH. Solution was sterilized by filtering through a 0.45 µm syringe filter and stored at room temperature protected from light.
29. **0.5 M PIPES buffer (pH 6.7):** 1.5 g PIPES was dissolved in 6 ml distilled water and pH was adjusted to 6.7 by adding 10 N NaOH solution and adjusted the volume to 10 ml. The solution was sterilized by filtering through a 0.45 µm syringe filter and stored at minus 20 °C.
30. **1 M HEPES buffer (pH 7.5):** 2.38 g HEPES was dissolved in 6 ml distilled water and pH was adjusted to 7.5 by adding 10 N NaOH solution and adjusted the volume to 10 ml. The solution was sterilized by filtering through a 0.45 µm syringe filter and stored at minus 20 °C.
31. **10X TBE buffer (pH 8.0):** 10.8 g Tris base and 5.5 g boric acid were dissolved in 50 ml distilled water. 4 ml 0.5 M EDTA (pH 8.0) was added and volume was adjusted to 100 ml by adding distilled water.

32. **0.5 M $NaHCO_3$:** 0.21 g $NaHCO_3$ was dissolved in 8 ml distilled water, the volume was adjusted to 10 ml and stored at room temperature.
33. **10% Na-deoxycholate:** 1 g Na-deoxycholate was dissolved in 8 ml distilled water. The volume was adjusted to 10 ml and stored at room temperature.
34. **100 mM DTT:** 0.15 g DTT was dissolved in 1 ml 100 mM HEPES buffer (pH 7.5) and stored at minus 20 °C protected from light.
35. **Alkaline lysis Solution I:** Alkaline lysis Solution I contains 50 mM glucose, 25 mM Tris-Cl (pH 8.0), and 10 mM EDTA (pH 8.0).
36. **Alkaline lysis Solution II:** Alkaline lysis Solution II contains 0.2 N NaOH and 1% SDS. The solution was freshly prepared just prior to use.
37. **Alkaline lysis Solution III:** For a volume of 100 ml solution, 60 ml of 5 M potassium acetate, 11.5 ml of glacial acetic acid, and 23.5 ml of distilled water were mixed together. The solution was sterilized by autoclaving and stored at 4 ºC.
38. **Inoue transformation buffer:** The Inoue transformation buffer contains 55 mM $MnCl_2$, 15 mM $CaCl_2$, 250 mM KCl and 10 mM PIPES buffer (pH 6.7).
39. **Lysis buffer for *N. crassa* genomic DNA isolation:** The lysis buffer contains 10 mM Tris HCl (pH 7.5), 0.5 M NaCl, 10 mM EDTA, 1% SDS, and 1% CTAB.
40. **Lysis buffer for *N. crassa* RNA isolation:** The lysis buffer contains 100 mM Tris HCl (pH 8.0), 0.6 M NaCl, 10 mM EDTA (pH 8.0), 4.5 % SDS, and 2 % β-mercaptoethanol.
41. ***N. crassa* native protein isolation buffer:** The protein isolation buffer contains 50 mM Tris-HCl (pH 7.5), 1 mM EDTA (pH 8.0), 6 mM $MgCl_2$, 2.5 mM PMSF and 0.1% fungal protease inhibitor cocktail (FPIC, Sigma Aldrich, USA).
42. ***N. crassa* plasma membrane fraction extraction buffer:** The extraction buffer contains 0.5 mM EDTA (pH 8.0), 1 M sorbitol, 1 mM DTT, 0.5 mM PMSF, and 10 mM HEPES (pH 7.5).

43. *N. crassa* plasma membrane fraction washing buffer: The washing buffer contains 50 mM Tris-C1 (pH 7.5), 1 mM DTT, 10% glycerol, and 0.5 mM PMSF.

2.1.6 Solutions for growth, maintenance and crossing of *N. crassa* strains

(i) Biotin solution: 5 mg biotin was dissolved in 100 ml 50% (v/v) ethanol, stored at 4 °C.

(ii) Trace element solution: Trace element solution was prepared by dissolving the following chemicals sequentially in 90 ml of distilled water with constant stirring.

$C_6H_8O_7.H_2O$	5.00 g
$ZnSO_4.7H_2O$	5.00 g
$Fe(NH_4)_2(SO_4)_2.6H_2O$	1.00 g
$CuSO_4.5H_2O$	0.25 g
$MnSO_4.1H_2O$	0.05 g
H_3BO_3	0.05 g
$Na_2MoO_4.2H_20$	0.05 g

The final volume was adjusted to 100 ml; 1 ml of chloroform was added as a preservative and stored at room temperature.

(iii) Vogel's Medium N (VGN): A 50X stock of Vogel's Medium N (Vogel, 1956; Vogel, 1964) was prepared by adding following chemicals sequentially in 75 ml distilled water with constant stirring.

$Na_3C_6H_5O_7.2H_2O$	12.5 g
KH_2PO_4	25 g
NH_4NO_3	10 g
$MgSO_4.7H_2O$	1 g
$CaCl_2.2H_2O$	0.5 g

(Pre-dissolved in 2 ml H_2O)

Biotin solution	500 µl
Trace element solution	500 µl
Chloroform	300 µl

The volume of the solution was adjusted to 100 ml and the chloroform was added as a preservative.

(iv) Vogel's minimal media (VM):

Vogel's Medium N	1X
Sucrose	2% (w/v)

(v) Vogel's minimal media (VM) agar:

Vogel's Medium N	1X
Sucrose	2% (w/v)
Agar	2% (w/v)

(vi) 4X Synthetic crossing medium (SCM): 4X strength synthetic crossing medium (SCM) was prepared by dissolving the following chemicals sequentially in 80 ml distilled water with constant stirring.

KNO_3	0.4 g
K_2HPO_4	0.28 g
KH_2PO_4	0.2 g
$MgSO_4.7H_2O$	0.2 g
$CaCl_2.2H_2O$	40 mg
NaCl	40 mg
Biotin solution	20 µl
Trace element solution	20 µl

The volume of the solution was adjusted to 100 ml and sterilized by autoclaving.

(vii) SCM agar:

SCM	1X
Glucose	1.5% (w/v)
Agar	2% (w/v)

(viii) 10X FGS (Fructose, glucose, and sorbose) stock: 10X FGS stock was prepared by dissolving the following chemicals in 80 ml distilled water.

Fructose	5% (w/v)
Glucose	5% (w/v)
Sorbose	20% (w/v)

The volume of the solution was adjusted to 100 ml and sterilized by autoclaving.

(ix) FGS agar:

FGS	1X
Vogel's Medium N	1X
Agar	2% (w/v)

(x) Top agar:

FGS	1X
Vogel's Medium N	1X
Agar	2.8% (w/v)

(xi) Media for circadian clock study:

Vogel's Medium N	1X
Glucose	0.1% (w/v)
Arginine	0.17% (w/v)

Biotin	50 ng/ml
Agar	1.5% (w/v)

2.1.7 Reagents for SDS-polyacrylamide gel electrophoresis

(i) Resolving gel (10 ml)

Acrylamide percentage	10%	12%
H_2O	3.8 ml	3.2 ml
Acrylamide/Bis-acrylamide (30%/0.8% w/v)	3.4 ml	4 ml
1.5 M Tris-HCl (pH 8.8)	2.6 ml	2.6 ml
10% w/v SDS	100 µl	100 µl
10% w/v APS	100 µl	100 µl
TEMED	10 µl	10 µl

(ii) Stacking gel (5 ml)

H_2O	2.975 ml
Acrylamide/Bis-acrylamide (30%/0.8% w/v)	0.67 ml
0.5 M Tris-HCl (pH 6.8)	1.25 ml
10% w/v SDS	50 µl
10% w/v APS	50 µl
TEMED	5 µl

(iii) 1X running buffer (1000 ml)

Glycine	15 g
1 M Tris-HCl (pH 8.0)	25 ml
10% w/v SDS	100 ml

H_2O	875 ml

(iv) 5X SDS-PAGE sample buffer (10 ml; Krystofova and Borkovich, 2005)

0.5 M Tris-HCl (pH 6.8)	1.25 ml
Bromophenol blue (1% w/v stock)	50 µl
10% w/v SDS	2 ml
β-mercaptoethanol	100 µl
H_2O	6.6 ml

(v) Staining solution (100 ml)

Coomassie Brilliant Blue	100 mg
Methanol	50 ml
Glacial acetic acid	10 ml
H_2O	40 ml

(vi) Destaining solution

Methanol	10 ml
Glacial acetic acid	7 ml
H_2O	83 ml

2.1.8 Reagents for western blotting

(i) Transfer buffer (100 ml)

Tris base	0.3 g
Glycine	1.41 g
Methanol	20 ml
H_2O	80 ml

(ii) 1X Tris buffered saline (TBS) pH 7.6 (1000 ml)

Tris base	2.42 g
NaCl	8 g

All the above chemicals were dissolved in 500 ml distilled water and pH was adjusted to 7.6 by adding concentrated HCl. Volume was made up to 1000 ml by adding distilled water.

(iii) TBST (100 ml)

Tris base	100 ml
Tween-20	50 µl

(iv) TBSTM (100 ml)

TBSTM	100 ml
Skimmed milk	5 g

(v) 0.1% amido black stain (100 ml)

Amido black	100 mg
Isopropanol	25 ml
Acetic acid	10 ml
H_2O	65 ml

2.1.9 Reagents for Chromatin Immunoprecipitation (CHIP)

(i) CHIP lysis buffer (10 ml)

1 M HEPES (pH 7.5)	500 µl
0.5 M EDTA (pH 8.0)	20 µl
5 M NaCl	180 µl
Triton X-100	100 µl
10% Na-deoxycholate	100 µl

100 mM PMSF	100 µl
FPIC	10 µl
H_2O	8.99 ml

(ii) RIPA buffer (10 ml)

1 M Tris-HCl (pH 8.0)	500 µl
0.5 M EDTA (pH 8.0)	40 µl
5 M NaCl	300 µl
10% w/v SDS	100 µl
10% w/v Na-deoxycholate	100 µl
NP-40	100 µl
H_2O	8.86 ml

(iii) Low salt wash buffer (10 ml)

1 M Tris-HCl (pH 8.0)	200 µl
0.5 M EDTA (pH 8.0)	40 µl
5 M NaCl	300 µl
10% w/v SDS	100 µl
Triton X-100	100 µl
H_2O	9.26 ml

(iv) High salt wash buffer

1 M Tris-HCl (pH 8.0)	200 µl
0.5 M EDTA (pH 8.0)	40 µl
5 M NaCl	300 µl
10% w/v SDS	100 µl
Triton X-100	100 µl

H_2O	9.26 ml

(v) LiCl wash buffer (10 ml)

1 M Tris-HCl (pH 8.0)	200 µl
0.5 M EDTA (pH 8.0)	40 µl
5 M NaCl	300 µl
10% w/v SDS	100 µl
Triton X-100	100 µl
H_2O	9.26 ml

(v) LiCl wash buffer (10 ml)

1 M Tris-HCl (pH 8.0)	100 µl
0.5 M EDTA (pH 8.0)	20 µl
3 M LiCl	100 µl
10% w/v Na-deoxycholate	2 ml
NP-40	100 µl
H_2O	7.68 ml

(vi) Elution buffer (10 ml)

10% w/v SDS	100 µl
0.5 M $NaHCO_3$	2 ml
H_2O	7.9 ml

2.1.10 Primers used in the study

Custom oligonucleotide primers were purchased from Bioserve (Hyderabad, India) India as well as from Integrated DNA Technologies (USA).

Table 2.2: List of primers used in the study

Sl. No.	Primer name	Sequence (5'→3')	Reference
1	Rat ncs-1 pMF272-F	CATTCTAGAATGGGGAAATCC	Our laboratory (Gohain *et al.*, 2016)
2	Rat ncs-1 pMF272-R	CATTTAATTAATACCAGCCCGT	Our laboratory (Gohain *et al.*, 2016)
$^{+}$3	Rat ncs-1 E120Q-F	TCACCAGAAAC**CAG**ATGCTGGAC	Our laboratory (Gohain *et al.*, 2016)
$^{+}$4	Rat ncs-1 E120Q-R	GTCCAGCAT**CTG**GTTTCTGGTGA	Our laboratory (Gohain *et al.*, 2016)
5	NCS-1-NIT-6-GFP-FOR	CAACTCTAGTCTTTCTGTCGTCAGCCAGC AATGGGCAAATCGTGAGTGACC	Borkovich Lab (UCR, USA)
6	NCS-1-NIT-6- GFP-REV	GTTAGGGATAGGCTTTCCGCCGCCTCCGC CGACGAGGCCATCGTACAAGGAG	Borkovich Lab (UCR, USA)
7	NCU07952-FOR	TTCGCACACACATCCCCAACCAACCATGG ACCAACAGTACACCGACGCCCG	Borkovich Lab (UCR, USA)
8	NCU07952-REV-gFP	GTTAGGGATAGGCTTTCCGCCGCCTCCGC CACGGCCGCCGTAG TCACTCGCAT	Borkovich Lab (UCR, USA)

9	HI-NCS-1-F	GTCTCAGCATGAAAGTCGTC	Our laboratory (Deka *et al.*, 2011)
10	5HPHR	ATCCACTTAACGTTACTGAAATC	Our laboratory (Deka *et al.*, 2011)
11	Pnit-6-Fw	CTAGTCTTTCTGTCGTCAGC	Our laboratory
12	P_{tcu}-CaM-RIP-FP-3	TTGAGAACGAATCCTTCATC	Our laboratory (Laxmi and Tamuli, 2017)
13	GFP-Rv	AACTTGTGGCCGTTTACGTC	Our laboratory
14	HI-*crz-1*F	CAGCCTGTTGCTTGCTTGTC	Our laboratory
15	HI-NCU06703-F	CCAAGGCTTATGCCGTCATC	Our laboratory (Deka and Tamuli, 2013)
16	RT-NCU04379-F	CAGTTCTTCCCCTTTGGCGA	Our laboratory
17	RT-NCU04379-R	CGAGCTTGTCCTCCATCTTG	Our laboratory
18	RT-NCU07952-F	GATGTCTCTTCGGTAGCCCA	Our laboratory
19	RT-NCU07952-R	CGTCCGACAGACTGAAGTTG	Our laboratory
20	RT-NCU06703-F	GCTCGCGGATCGATGAGTTT	Our laboratory

21	RT-NCU06703-R	ATTGAACCCCTTCTGGCCAG	Our laboratory
22	q-B-tub-FW	CCCAAGAACATGATGGCTGC	Our laboratory (Barman and Tamuli, 2017)
23	q-B-tub-RV	TTGTTCTGAACGTTGCGCATC	Our laboratory (Barman and Tamuli, 2017)
24	CHIP-1F	GCATTTTGCCCTGCCTCTCT	Our laboratory
25	CHIP-1R	GGACTTGGTCACTCACGATT	Our laboratory
26	CHIP-2F	CCAAACGTCCAGAACCCGAT	Our laboratory
27	CHIP-2R	GGTGTTGGGTTGTAATGGCA	Our laboratory
28	CHIP-3F	GGGCGAACGACTTCTCATTT	Our laboratory
29	CHIP-3R	CATTTGCAAAGAGGGGCAAC	Our laboratory
30	EMSA-1F	CCACCATACAAGGCTGCTTG	Our laboratory
31	EMSA-1R	TTGTCGTCGGCCGATAGGAT	Our laboratory
32	EMSA-2F	CTTTCGGCGCCAACCCCGT	Our laboratory
33	EMSA-2R	GTCGGAGGAGGGGTTCGGT	Our laboratory
34	Dup-1F	CAAGGCTGCTTGCTCCCATCGCTCGAGCAC	Our laboratory
35	Dup-1R	GTTCCGACGAACGAGGGTAGCGAGCTCGTG	Our laboratory
36	Dup-2F	CGTCTTGCCCTTCACACAGCGTCTCGTTAC	Our laboratory

37	Dup-2R	GCAGAACGGGAAGTGTGTCGCAGAGCAATG	Our laboratory
38	Dup-2MF	CGTCTTGCAAGGACAACAGCGTCTCGTTAC	Our laboratory
39	Dup-2MR	GCAGAGCGAACCTGTTGTCGCAGAGCAATG	Our laboratory

[+]The target codon in the sequence of the mutagenic primers for SDM is shown bold, and the mutated nucleotides are underlined.

2.2 Methods

2.2.1 Growth conditions

Growth and maintenance of the *N. crassa* strains were performed essentially as described previously (Davis and de Serres, 1970). Strains were cultured routinely on 1X Vogel's minimal medium N (VM) for vegetative growth (Vogel, 1956; Vogel, 1964), on 1X synthetic crossing medium (SCM) for crossing and sexual development (Westergaard and Mitchell, 1947) and FGS agar media for germination of ascospores (Davis and de Serres, 1970). Inositol and pantothenic acid stocks were prepared and added to the growth media at a concentration of 0.05 and 0.01 and mg/ml, respectively, for culturing respective auxotrophs (http://www.fgsc.net/methods/stanford.html; Murray and Perkins, 1963). For the selection of the *N. crassa* transformants, FGS agar media supplemented with Basta® or Ignite® (Pall, 1993) at a concentration of 400 µg/ml was used. For the selection of the *N. crassa* knockout mutants generated using the *hph* cassette, hygromycin was supplemented to the growth medium at a concentration of 220 µg/ml (Colot *et al.*, 2006).

2.2.2 Setting up crosses and harvesting ascospores

Crosses between *N. crassa* strains with opposite matting type were performed as described previously (Westergaard and Mitchell, 1947; Davis and de Serres, 1970). Crosses were performed by inoculating the agar plugs of the strains on SCM agar in 55 mm Petri dishes. The crosses were incubated at 22 °C in a BOD incubator for three to four weeks. Ascospores were harvested by washing the lids with 1 ml sterile water after 21-25 days. Ascospores were then plated on FGS agar plates, activated by heat shock at 65 °C for 30-60 min in a shaking water bath, and picked under dissection microscope by cutting out a small agar block containing the ascospore and transferred onto a slant with minimal or selective media followed by incubation at 30 °C for growth.

2.2.3 Maintenance of Stock

Silica stocks were prepared for long term storage of the *N. crassa* strains. Strains were grown in VM agar slants for 3 days in constant dark at 30 °C and then for 4 days at room-temperature under light. Silica (6-12 Mesh, Grade 40) was sterilized by autoclaving and dried at 60 °C and cooled to room temperature before use. Cryo tubes (4.5 ml) were filled with dried silica. For each strain, 1 ml of 5% autoclaved skimmed milk was added to the culture tube and vortexed vigorously. Spore suspension was drawn up by using a Pasteur pipette and dispensed into the pre-chilled silica gel in the cryo tubes placed in ice and vortexed vigorously for 5 min, to break up any clumps in the process. Tubes were regularly vortexed for 8-10 days and the tubes were stored at minus 20 °C until further use.

2.2.4 Conidial cell count

For quantification, conidia harvested from the agar surface with sterile distilled water was vortexed briefly for making conidial suspension. Conidial counting was performed using a

haemocytometer under a trinocular inverted microscope (AxioVert A1 FL, Carl Zeiss, Germany).

2.2.5 Growth rate

Growth was measured by placing mycelial plug in the centre of 90 mm Petri dishes containing VM agar and incubated at 30 °C. Colony growth was marked after 12 h from inoculation point with an interval of 3 h over a period of 24 h to obtain radial growth rate. The apical growth was measured by standard race tube assay (Fig. 2.5; Ryan *et al.*, 1943). Race tubes were partially filled with 13 ml of VM agar and inoculated with mycelial plug at one end and incubated at 30 °C for 3 days. The apical growth rate of *N. crassa* was calculated as mycelial extension rates at every 12 h interval in race tube. The distance of the hyphal growth front from the inoculation point was measured and plotted against time. Radial and apical growth rates were calculated as cm h^{-1}.

Fig. 2.5: Standard race tube assay (Top view). A race tube is hollow tube made of glass (~40 cm in length and 1.2-1.4 cm in diameter) with upward bends in both end.

2.2.6 Calcium stress tolerance assay

For determining the Ca^{2+} stress tolerance in the *N. crassa* strains, the agar plugs from 3 days old culture were inoculated in the centre of the 90 mm Petri dish containing VM agar supplemented with various concentrations of $CaCl_2$ (0, 0.2, 0.3 and 0.4 M) and incubated at 30 °C. Colony diameter (cm) was measured after 12 h at regular interval of 3 h over a period of 24 h. The average colony growth rate (cm h^{-1}) was calculated based on the data obtained from

three independent experiments for each strain. Average colony growth rate percentage (%) was calculated relative to the colony diameter of the strains in VM without $CaCl_2$ (0 M) considered as 100%

2.2.7 Ultraviolet sensitivity assay

For ultraviolet (UV) survival assay, conidia were grown in 250 ml flasks containing 50 ml VM agar for 4 days in constant dark at 30 °C and 1 day under light at room temperature. The conidia were harvested, washed with sterile water, and finally re-suspended in 1 ml sterile water. For the qualitative assay, a serial dilution (10^0, 10^{-1}, 10^{-2}, 10^{-3}, 10^{-4}, 10^{-5}, and 10^{-6}) was performed, then 5 µl conidial suspensions of each dilution were spotted on FGS agar plate and irradiated with UV doses of 0, 100, 200 and 300 J m^{-2} in a UV cross-linker (UVC 500, Hoefer, UK). After irradiation plates were quickly wrapped with aluminium foil to avoid light and stop photoreactivation, then incubated for 2 days at 30 °C. For quantitative assay, ~1000 conidia were plated on the FGS agar plate and irradiated with the same UV doses as in the qualitative assay. The plates were incubated overnight at 30 °C and number of viable colonies on each plate was counted. The survival percentage was calculated relative to the viable colonies on the control plate.

2.2.8 Scoring for antibiotic resistance in *N. Crassa*

To score antibiotic resistance conidia were streaked onto 1.5% VM agar plates supplemented with the antibiotic. The antibiotics used were hygromycin B (220 µg /ml from 100 mg/ml stock in water), and Basta® or Ignite® (400 µg/ml from 100 mg/ml stock in water).

2.2.9 Preparation of ultracompetent cells

Ultracompetent cells were prepared essentially as described previously (Inoue *et al.*, 1990). A single *E. coli DH5α* colony from a fresh LB agar plate was inoculated into 5 ml of LB broth and incubated at 37 °C at 200 rpm for 16 h. From this overnight culture, 1 ml was inoculated

into 100 ml of LB broth and incubated at 18 °C at 200 rpm, till the OD_{600} reached 0.55. The culture was chilled on ice and centrifuged for 15 min at 2,500 x *g* and 4 °C for pelleting the cells. The cells were suspended in 32 ml of ice cold Inoue transformation buffer and incubated on ice for 10 min. The cells were harvested by centrifugation for 15 min at 2,500 x *g* and 4 °C and finally suspended in 8 ml of ice cold Inoue transformation buffer containing 7% DMSO. The cell suspension was distributed into 100 µl aliquots, flash frozen in liquid nitrogen, and stored at minus 80 °C.

2.2.10 Restriction digestion of plasmids

Plasmid DNA was digested with specific restriction endonucleases (New England Biolabs, USA). An aliquot of ~1 µg plasmid DNA was digested with 1 µl of restriction endonuclease (~10 units) in a final volume of 50 µl. The reaction was carried out for 30 minutes using CutSmart® buffer (New England Biolabs, USA) and assay conditions as specified by the manufacturer's protocol. The digested DNA fragments were analysed by agarose gel electrophoresis. The New England Biolabs enzyme compatibility chart was referred before digesting with two enzymes.

2.2.11 Ligation of digested vectors and inserts

Ligation reactions were performed by using Quick Ligation™ Kit (Cat. no. M2200S, New England Biolabs, USA). The 20 µl ligation reaction volume contained ~50 ng of a linearized DNA vector, a 3-fold molar excess of insert, 10 µl of 2X ligation buffer, and 1 µl quick T4 DNA ligase enzyme. The ligation reaction was performed for 15-20 min at 25 °C in a circulating water bath (MRC Scientific Instruments, Israel).

2.2.12 Transformation of ultracompetent *E. coli DH5α* cells by heat shock

Ultracompetent cells taken out from the minus 80 °C freezer were thawed and placed on ice. Ligated DNA sample (~50-100 ng) was added to the ultracompetent cells and mixed by

swirling gently. The tubes were kept in ice for 30 min, followed by heat shock at 42 °C for 90 s in a circulating water bath (MRC Scientific Instruments, Israel). After heat shock, 800 µl of SOC was added to the cells and the tubes were incubated at 37 °C with 200 rpm shaking for 45 min. The transformed competent cells (~100-200 µl for 90 mm Petri dish) were plated on LB agar plates containing 100 mg/ml of ampicillin and incubated at 37 °C for 12-14 h.

2.2.13 Plasmid isolation by alkaline lysis method (Miniprep)

Small-scale preparation of plasmid (Miniprep) was done by alkaline lysis method (Sambrook and Russel, 2001). 5 ml of overnight bacterial culture was centrifuged in microfuge tube for 2 min at 12,000 x *g* and 4 °C. Pellet was suspended in 100 µl alkaline lysis solution I with vigorous vortexing. After mixing the contents, 200 µl of freshly prepared alkaline lysis solution II was added and mixed by inverting the tube 4-5 times. To the bacterial lysate, 150 ml alkaline lysis solution III was added, mixed by inverting the tube, and kept on ice for 3-5 min. The tube was centrifuged for 10 min at 12,000 x *g* and 4 °C. The supernatant was transferred to fresh microfuge tube and equal volume of phenol: chloroform: isoamyl alcohol (25:24:1) was added, again centrifuged for 10 min at 12,000 x *g* and 4 °C. The aqueous phase was transferred to a 1.5 ml microfuge tube and plasmid DNA was precipitated by adding 1 ml absolute ethanol. The tube was gently inverted few times and the DNA was pelleted by centrifuging the tube for 10 min at 12,000 x *g* and 4 °C. The pellet was washed with 70% ethanol by centrifuging for 2 min at 12,000 x *g* and 4 °C. DNA pellet was air dried at room temperature for 15 min to remove the ethanol. Finally, the pellet was dissolved in 30 µl of 1X TE buffer (pH 8.0) and stored at 4 ºC.

2.2.14 Isolation of *N. crassa* genomic DNA

The strain of interest was cultured in VM liquid at 30 °C for 3 days with shaking at 200 rpm. The mycelial mass harvested by filtration was lyophilized and were grinded with glass beads

(0.2 mm in diameter) to a fine powder using a mortar and a pestle. Approximately, 150 mg of the mycelia powder was taken in a 2 ml microfuge tube and 1 ml of lysis buffer was added. The tube was heated at 65 °C for 30 min, followed by centrifugation for 10 min at 12,000 x *g*. The supernatant was transferred to a 2 ml microfuge tube and added 500 µl of phenol: chloroform: isoamyl alcohol mixture (25:24:1). The tube was rotated for 15 min in a rotary mixer and centrifuged for 10 min at 12,000 x *g*. The aqueous phase was collected in a 1.5 ml tube and 600 µl of chloroform was added to remove last traces of phenol. The tube was centrifuged for 10 min at 12,000 x *g*. The aqueous phase was taken in a 1.5 ml microfuge tube and genomic DNA was precipitated by adding 1 ml absolute ethanol. The tube was gently inverted few times and the genomic DNA was pelleted by centrifuging at 12,000 x *g* for 10 min. The pellet was washed with 70% ethanol by centrifuging for 2 min at 12,000 x *g*. The genomic DNA pellet was air dried at room temperature for 15 min. Finally, the dried pellet was dissolved in 30 µl of 1X TE buffer (pH 8.0) and stored at 4 ºC. All centrifugation steps were performed at room temperature.

2.2.15 Transformation of *N. crassa* strain by electroporation

The transformation protocol was based on the method as described previously (Margolin *et al.*, 1997; Bhat *et al.*, 2004). The recipient strain was cultured in 250 ml conical flask containing 50 ml VM agar for a week at 30 °C. The conidia harvested in sterile water were made free from the mycelium by filtering through cheesecloth attached to a 250 ml conical flask. The conidial suspension was centrifuged for 10 min at 2000 x *g* and 4 °C. The conidial pellet was washed twice in 30 ml sterile water and finally suspended in 1 M sorbitol at a concentration of 3×10^9 spores/ml. About 40 µl conidial suspension was mixed with the DNA to be transformed and placed in a pre-chilled 0.2 cm gap sterile electroporation cuvette (BioRad Laboratories, USA). Electroporation was performed in a BioRad Gene Pulser apparatus (BioRad Laboratories, USA) using the parameters as- voltage: 1.5 KV, capacitance: 25 µF, and

resistance: 600 Ω. After the pulse, immediately 1 ml of chilled 1 M sorbitol was added and kept in ice for 5 min. The transformant conidial suspension was mixed with top agar, then plated on FGS agar plate and incubated at 30 °C. The transformants obtained were picked under a dissection microscope after 2-3 days. To eliminate the possibility of any contamination a control transformation was also performed without adding DNA

2.2.16 RNA isolation from *N. crassa* strains

RNA was isolated from *N. crassa* strains as described previously (http://www.fgsc.net/fgn37/sokol.html). For RNA the isolation, ~1 x 10^7 conidia of the strain of interest were inoculated in 10 ml of VM liquid medium, and incubated at 30 °C with constant 180 rpm shaking for 16 h. Mycelia harvested by filtration was crushed in a mortar and pestle to fine powder using liquid nitrogen. The mycelial powder (~25 mg) was immediately transferred into a 2 ml microfuge tube containing 300 µl TRIzol™ reagent (Cat. no. 15596026, Life Technologies, USA), and further added 750 µl RNA lysis buffer and 750 µl phenol: chloroform: isoamyl alcohol (25:24:1) mixture. The tube was rotated in a rotary mixer for 20 min and centrifuged for 10 min at 10,000 x *g*. The upper aqueous phase was taken in a 2 ml microfuge tube and 750 µl of 8 M LiCl was added. The mixture was stored at 4 °C for 16-20 h. The mixture was vortexed briefly and centrifuged for 10 min at 10,000 x *g*. The isolated pellet was suspended in 300 µl double distilled DEPC treated water, mixed with 30 µl of 3 M Na-acetate (pH 5.2) and 750 µl of absolute ethanol was added. The mixture was stored at minus 20 °C for 2 h and centrifuged for 10 min at 10,000 x *g*. The RNA pellet was washed with 70% ethanol. The RNA pellet was dried for 10-15 min at room temperature and finally dissolved in 30 µl RNAase free water. The RNA was stored at minus 80 °C. All centrifugation steps were carried out at room temperature.

2.2.17 Quantification of nucleic acids

The nucleic acid concentration was estimated by measuring the OD at 260 nm in a spectrophotometer (BioSpectrometer® Kinetic, Eppendorf, Germany). The following empirical relationships were used to calculate the concentrations. An OD_{260} of 1 corresponds to ~50 µg/ml of double stranded DNA, 40 µg/ml of single-stranded DNA and RNA, ~20 µg/ml of single-stranded oligonucleotides. The purity of nucleic acids was estimated by calculating the OD_{260}/OD_{280} ratio. Pure preparations of RNA and DNA have OD_{260}/OD_{280} values of 2.0 and 1.8 respectively.

2.2.18 Polymerase chain reaction (PCR)

The routine polymerase chain reaction (PCR) reaction was performed by using Taq DNA polymerase (Cat no. M0273S, New England Biolabs, USA) as per the manufacturer's protocol. For cloning purposes, Phusion® High-Fidelity DNA polymerase (Cat. no. M0530S, New England Biolabs, USA) was used as normal Taq DNA polymerase isolated from *Thermus aquaticus* lacked proofreading activity (3′-5′ exonuclease activity). The PCR conditions varied according to the size of the product and annealing temperature of the primers. All PCRs were performed with a thermal cycler (Arktik Thermal Cycler, Thermo Fisher Scientific, USA).

2.2.19 Reverse transcription PCR for cDNA synthesis

Reverse transcription PCR (RT-PCR) was used for cDNA synthesis for performing gene expression study. The cDNA synthesis was performed by using Verso cDNA synthesis kit (Cat. no. AB-1453/A, Thermo Fisher Scientific, USA). About 1 µg of total RNA was used in each 20 µl reaction. The cycling condition for cDNA synthesis was 50 °C for 45 min followed by 95 °C for 2 min for 1 cycle.

2.2.20 Real time quantitative PCR (qRT-PCR)

Total RNA isolated from *N. crassa* was used for real time quantitative PCR (qRT-PCR) for gene expression studies. qRT-PCR was performed in a real time PCR system (ABI 7500 Fast, Applied Biosystems, USA) using SYBR® select master mix (Cat. No. 4472903, Life Technologies, USA) in a final reaction volume of 15 µl. In general, 15 µl reaction mixture contained 7 µl of cDNA (~100 ng), 0.5 µl of forward primer, 0.5 µl of reverse primer, and 7 µl of SYBR® select master mix. The PCR reaction condition used was as follows: 95 °C for 10 min followed by 40 cycles of 95 °C for 15 s and 60 °C for 1 min. The relative expressions of the target genes were calculated by $2^{-\Delta\Delta C}{}_{T}$ method (Livak and Schmittgen, 2001), and the expression level of β-tubulin was used as the endogenous control.

2.2.21 Agarose gel electrophoresis

For loading 1 µl DNA sample was mixed with 1 µl of Blue Gel Loading Dye (6X) and 4 µl 1X TAE. The samples based on the size of the DNA to be resolve were loaded on 0.7% to 1.5% agarose gels prepared using 1X TAE containing 0.5 µg/ml ethidium bromide. Electrophoresis was performed in 1X TAE running buffer at 5 Vcm^{-1}. For estimation of DNA fragment sizes standard DNA size markers were run alongside the sample. The DNA samples stained with ethidium bromide were visualized in a gel documentation system (Bio print ST4, Vilber Lormat, France). RNA samples were resolved in 1.2% agarose gel containing 1X MOPS buffer, 2.2 M formaldehyde, and 0.5 µg/ml ethidium bromide.

2.2.22 DNA fragments purification from agarose gels

DNA to be used for cloning, sequencing, and transformation was amplified by PCR and then resolved on agarose gels. DNA bands to be eluted was excised by visualizing in a UV trans illuminator and transferred to a 1.5 ml microfuge tube. DNA from the gel slice was purified

from the agarose gel slices using gel extraction kit (Qiagen, USA or GCC Biotech, India) according to the manufacturer's protocol.

2.2.23 Sequence analysis

Basic local alignment search tool (BLAST) analysis (Altschul *et al.*, 1990; Altschul *et al.*, 1997; Altschul *et al.*, 2005) was performed using software tools available from NCBI. Conserved Domain Database (CDD; Marchler-Bauer and Bryant, 2004; Marchler-Bauer *et al.*, 2008) was used for identification of the conserved domains in the protein. Clustal X (Thompson *et al.*, 1997) was used to align the protein sequences, and then visualized with GeneDoc (Nicholas, 1997). These sequence alignments were used to generate phylogenetic trees (Felsenstein, 1985; Rzhetsky and Nei, 1992) using the software Molecular Evolutionary Genetic Analysis version 6 (MEGA 6; Tamura *et al.*, 2013).

2.2.24 Dynabeads® Protein A magnetic beads preparation

Dynabeads® Protein A magnetic beads (Cat. No. 10001D, Life Technologies, USA) were prepared as per the manufacture's protocol. To every 50 µl of beads (~1.5 mg), 10 µg of antibody was conjugated and cross-linked using DMP (Cat No. D8388-250MG, Sigma Aldrich, USA).

2.2.25 Chromatin immunoprecipitation (CHIP)

5 h old *N. crassa* germlings were used for performing chromatin immunoprecipitation (CHIP). Approximately 5 x 10^6 conidia/ml were inoculated in two 250 ml flasks one containing 50 ml standard VM liquid, another containing VM supplemented with 0.2 M $CaCl_2$, and cultured at 30 ºC and 180 rpm shaking for 5 h. Both the cultures were supplemented with 10 µg/ml pantothenic acid and 50 µM BCS. The germlings were harvested by centrifuging for 15 min at 4000 x *g* and 4 ºC. The harvested germlings were washed two times with 1X PBS (pH 7.4). Chemical crosslinking was performed by incubating the germlings in 1% formaldehyde

solution for 30 min at room temperature on a rotating platform. 125 mM glycine was added and incubated for 10 min at room temperature to quench the reaction. Germlings were harvested by centrifuging for 15 min at 4000 x *g* and 4 ºC. The harvested germlings were washed two times with 1X PBS and suspended in CHIP lysis buffer. Chromatin shearing was performed by sonicating the germlings in a sonicator (Vibra cell sonics, USA) on ice using the parameters as- amplitude: 33%, ON pulse: 8 s, OFF pulse: 10 s, cycles: 120, and time: 16 min. The sonicated samples were centrifuged for 10 min at 12,000 x *g* and 4 ºC to remove the cell debris, and DNA was quantified using a spectrophotometer (BioSpectrometer® Kinetic, USA). To precipitate CRZ-1::5xGly::V5::GFP bounded to the *ncs-1* promoter fragements, the sonicated chromatin was incubated with mouse anti-V5 monoclonal antibody (Cat. No. R960-25, Life Technologies, USA) using 1 µg antibody per 25 µg DNA. The samples treated with antibody and the input control (without antibody treatment) were incubated overnight with pre-blocked 50 µl Dynabeads® Protein A magnetic beads (Cat. No. 10001D, Life Technologies, USA) on a rocking platform in a cold-room. The beads were washed first with RIPA buffer and then the beads were sequentially given one high salt, one low salt and one LiCl wash. The chromatin bounded to the bead was eluted using elution buffer and incubated overnight at 65 ºC for de-crosslinking. After de-crosslinking, chromatin was treated with RNAse A (Cat. No. A7973, Promega, USA) for 1 h at 65 ºC and then proteinase K (Cat. No. V3021, Promega, USA) for 1 h at 45 ºC. PCR purification kit (Cat. No. 28104, Qiagen, Germany) was used to purify chromatin and was quantified using a spectrophotometer (BioSpectrometer® Kinetic, Eppendorf, Germany).

2.2.26 Protein isolation and purification

The NCS-1::5xGly::V5::GFP, CRZ-1::5xGly::V5::GFP, and 5xGly::V5::GFP proteins were isolated the $P_{nit\text{-}6}$::*ncs-1* (21), $P_{tcu\text{-}1}$::*crz-1* (559), and pccg-1_GFP strains (Table 2.1) respectively. The strains were cultured in VM liquid medium containing appropriate

supplements for 16 h at 30 °C and 180 rpm shaking. The mycelial mass was harvested from the culture by filtration and then crushed into a fine powder in a mortar and pestle using liquid nitrogen. Roughly 150 mg of mycelial powder from each sample was suspended in 500 µl native protein extraction buffer [50 mM Tris-HCl (pH 7.5), 1 mM EDTA, 6 mM $MgCl_2$, 2.5 mM phenylmethylsulphonyl fluoride (PMSF) and 0.1% fungal protease inhibitor cocktail (FPIC, Cat. No. P8215-1ML, Sigma Aldrich, USA) in 2 ml microfuge tube. The tubes were centrifuged for 15 min at 6000 x g at 4 ºC to isolate the crude proteins. 50 µg of the Dynabeads® Protein A magnetic beads (Cat. No. 10001D, Life Technologies, USA) conjugated and cross-linked with mouse anti-V5 monoclonal antibody (Cat. No. R960-25, Life Technologies, USA) was added to the crude protein samples and incubated overnight at 4 ºC on a rocking platform. 30 µl non-denaturing elution buffer [50 mM glycine (pH 2.8)] was added to the beads to elute the bounded protein and the acidic pH was neutralized by adding 5 µl of 1M Tris-HCl (pH 7.5). the purity was checked by resolving an aliquot of 5 µl eluted protein on a 10% SDS-PAGE gel and staining with Coomassie Brilliant Blue dye (Himedia, India). The Bradford assay was used for quantification of protein concentration.

2.2.27 Duplex DNA probe synthesis

30 bp duplex DNA probes were generated from the complementary primer pairs or nucleotide strands, Dup-1F and Dup-1R, Dup-2F and Dup-2R, and Dup-2MF and Dup-2MR (Table 2.2). The primer pairs were first denatured at 95 °C for 10 min, and then annealed at 25 °C for 30 min using a buffer [10 mM HEPES (pH 7.5), 0.1 mM EDTA, 0.1 M NaCl, and 5 mM $MgCl_2$], in a thermal cycler (Arktik, Thermo scientific, USA).

2.2.28 Electrophoretic mobility shift assay (EMSA)

Electrophoretic mobility shift assay (EMSA) was performed using a Molecular Probes™ EMSA Kit (Cat no. E33075, Life Technologies, USA) as per the manufacturer's protocol. The

individual DNA probes (5 µM) were incubated with the purified protein (50 µM) to test protein-DNA binding. To resolve protein-DNA complexes, non-denaturing polyacrylamide (30:1)/1 X TBE gels were used. Electrophoresis was performed at 200 volts for 1 h in 1X TBE running buffer. The gels were visualized in a gel documentation system (Bio-Print ST4, Vilber Lourmat, France).

2.2.29 SDS-polyacrylamide gel electrophoresis (SDS-PAGE)

Based on the protein size, 10-12% resolving gel was poured to the gap between the glass plates. The top was overlaid with isopropanol and the gel was allowed to polymerise for 45 min. The stacking gel was poured over the resolving gel after removing the isopropanol and the comb was placed. The gel was allowed to polymerise for 20-30 min. The comb was removed and the wells were rinsed with 1X running buffer to remove the unpolymerised acrylamide. The glass plates containing the gel was assembled in the electrophoresis apparatus. An aliquot of 8 µl of protein sample and 2 µl of 5X SDS-PAGE sample buffer were mixed in a micro centrifuge tube and was heated to 90 °C for 5 min. The samples were loaded into the gel contained in 1X running buffer and electrophoresis was performed at 70 mA current and 80 V voltage for the stacking gel, while 120 V voltage for the resolving gel. Staining was carried out for 2 hours with shaking at room temperature. Destaining was done by soaking the gel in destaining solution on a slowly rocking platform for 8-12 h.

2.2.30 Western blotting

First 50 µg of total protein for each sample was resolved in 10-12% acrylamide SDS gel as described above. Later the resolved proteins were transferred from the gel into PVDF membrane (Amersham Hybond^{TM}-LFP, GE Healthcare, USA) in a semi-dry blotter (Biotech R&D Laboratories, India). The blotting was done at 20 V voltage and 215 mA for 20 min. Before transfer, the PVDF membrane was activated first in methanol for 5 min followed by

transfer buffer for 5 min. Transferred membrane was washed three times with 1X TBS for 5 min each on a rocking platform. Washed membrane was blocked with 1X TBSTM for 1 h. and again washed three times with 1X TBS for 5 min each. The blocked membrane was first treated with rabbit anti-GFP antibody (Cat. No. A6455, Life Technologies, USA) dissolved in 1X TBSTM at dilution of 1:5000 overnight at 4 °C. Next day, the membrane was washed three times with 1X TBS for 5 min each and then treated with horseradish peroxidase (HRP) conjugated goat anti-rabbit secondary antibody (Cat. No. 656120, Life Technologies, USA) dissolved in 1X TBSTM at dilution of 1:20,000 for 1 h at room temperature. The membrane was again washed three times with 1X TBS for 5 min each. The blots were visualized in a ChemiDoc (ChemiDoc™XRS+ Imager, Bio-Rad, USA) using a western blotting chemiluminescent detection kit (Cat. No. RPN2232, Amersham ECL™ Prime, GE Healthcare, USA) as per manufacturer's protocol. After detection, the membranes were stained using 0.1% w/v amido black staining solution to indicate equal loading and transfer of proteins to the membranes.

2.2.31 Isolation of membrane fraction from *N. crassa*

To isolate membrane fractions, conidia from the *N. crassa* strains were cultured in 50 ml VM liquid without $CaCl_2$ and with 0.2 M $CaCl_2$ in 250 ml flasks at 30 ºC with 180 rpm shaking for 6 h. Mycelia were harvested by centrifuging for 15 min at 4000 x *g* and 4 ºC. To the mycelial pellets 20 ml ice-cold extraction buffer [0.5 mM EDTA (pH 8.0), 0.5 mM PMSF, 1 mM DTT, 1 M sorbitol, and 10 mM HEPES (pH 7.5)] was added. The cells were disrupted in a sonicator (Vibra cell sonics, USA). The whole suspension was centrifuged for 10 min at 1000 x *g* and 4 ºC. The collected supernatant was transferred into 30 ml high-speed oak ridge centrifuge tubes (Thermo Scientific, USA) and further centrifuged for 30 min at 15,000 x *g* and 4 ºC in a high-speed centrifuge (Sigma 3-30 K, Sigma, USA). The supernatant was collected and again centrifuged for 1 h at 46,000 x *g* at 4 ºC. The pellet obtained at this step contains the membrane

fraction. It was suspended in 5 ml ice-cold wash buffer [50 mM Tris-C1 (pH 7.5), 1 mM DTT, 10% glycerol, and 0.5 mM PMSF] and again centrifuged for 30 min at 46,000 x *g* and 4 ºC. This process was repeated once more to remove any unbounded protein. The washed pellet was finally suspended in 100 µl ice-cold wash buffer containing 1% Triton X-100.

2.2.32 Co-immunoprecipitation assay

For the co-immunoprecipitation (Co-IP) analysis was performed using forced heterokaryotic *N. crassa* strains. Two kinds of forced heterokaryons (Table 2.1) were produced by co-inoculating the individual strains in 250 ml flasks containing 50 ml VM agar and incubating at 30 °C in constant dark for 3 days and at room temperature for four days under constant light. The heterokaryon NCS-1 GFP + MID-1 RFP was used as the test strain while the heterokaryon GFP + RFP and wild type (FGSC 987) strains (Table 2.1) were used as the control strains. The conidia (~ 1 x 10^6 conidia/ml) from these two heterokaryons and wild type (FGSC 987) strain were inoculated in 50 ml VM liquid containing 0.2 M $CaCl_2$ in 250 ml flasks and incubated at 30 ºC with 180 rpm shaking for 6 h. The isolation of the membrane fractions was performed as described above. The cytosolic fractions were also collected during the isolation of the membrane fractions. Co-IP was performed in two sets, in one set the membrane fraction was used while the other set the cytosolic fraction was used. proteins were precipitated using Dynabeads® Protein A magnetic beads (Cat. No. 10001D, Life Technologies, USA) conjugated and cross-linked with rabbit anti-GFP antibody (Cat. No. A6455, Life Technologies, USA). Protein was eluted from the beads by the adding 30 µl non-denaturing elution buffer [50 mM glycine (pH 2.8)] and 5 µl of 1M Tris-HCl (pH 7.5)] to neutralize the acidic pH, essentially as per the manufacturer's protocol (Cat. No. 10001D, Life Technologies, USA). An aliquot of the 18 µl eluted protein was mixed with 2 µl of 5x SDS-PAGE sample buffer and heated at 90 °C for 5 minutes. The samples were centrifuged for 5 min at 500 x g and 4 °C and the supernatants were collected. The samples were run in SDS-PAGE (10%

acrylamide) gels. Two sets of western blots were done, one using rabbit anti-GFP antibody (Cat. No. A6455, Life Technologies, USA) and another using rabbit anti-RFP antibody (Cat. No. 710530, Life Technologies, USA) as described above.

2.2.33 Confocal microscopy

The $P_{nit\text{-}6}$::*ncs-1* (21) strain was cultured on the VM agar plates supplemented with pantothenic acid for 3 days at 30 ºC. The conidia were harvested in sterile water. Equal amount of conidial suspensions was inoculated in 20 ml VM liquid in two 100 ml flasks one without $CaCl_2$ and other containing 0.2 M $CaCl_2$ and incubated for 4 h at 30 ºC with 180 rpm shaking. FM™4-64 dye (Cat. No. T3166, Life Technologies, USA) was used for plasma membrane visualization as per the manufacturer's standard protocol. Microscopy was executed using a confocal microscope [Leica TCS SP8 (DMi8), Leica Microsystems CMS, GmbH, Germany]. Images were visualized with a 63x oil immersion objective, 4x zoom, 1024 x 1024 pixels resolution, and 400 Hz scan speed using the Hybrid Detection system (HyD) laser (Leica Microsystems CMS, GmbH, Germany). Images were acquired successively, plasma membrane images stained with FM™4-64 were acquired with excitation at 515 nm and emission from 600 -700 nm, and GFP images were acquired by excitation at 488 nm with emission from 500 - 535 nm. To observe the co-localization both images were merged. Image acquisition and analysis were performed using Leica Application Suite X (LAS X; Leica Microsystems CMS, GmbH, Germany).

2.2.34 Circadian regulated conidiation study

The *N. crassa* strains were inoculated at one end of the race tube containing ~13 ml of circadian agar media. The tubes were incubated at 25 °C for 24 h in constant light and the growth fronts were marked. The tubes were then incubated in constant darkness at 25 °C. The growth fronts were marked at regular interval of 24 h for 5 days under a red safe light. The period lengths were calculated by multiplying the distance between the conidial bands with the inverse of

slope. The slope is the distance/hour determined from plot of distance between growth fronts versus 24 hour days (http://www.fgsc.net/teaching/circad.htm).

2.3 Databases and software programs used

1. **Basic Local Alignment Search Tool (BLAST):** BLAST (Altschul *et al.*, 1990; Altschul *et al.*, 1997; Altschul *et al.*, 2005) was used to compare nucleotide or protein sequences to sequence databases. This is available at http://blast.ncbi.nlm.nih.gov/Blast.cgi.
2. **Clustal X:** Clustal X (Thompson *et al.*, 1997) software was used for multiple sequence alignment of DNA and protein sequences. Clustal X is available online at http://www.clustal.org/clustal2/#Webservers.
3. **ExPasy Translate tool:** The ExPasy Translate tool was used for translating DNA sequences to protein sequences. It is available at http://web.expasy.org/tools/DNA.
4. **Conserved Domain Database (CDD):** CDD (Marchler-Bauer and Bryant, 2004; Marchler-Bauer *et al.*, 2008) was used to identify conserved domains in the proteins. This is available at http://www.ncbi.nlm.nih.gov/Structure/cdd/wrpsb.cgi.
5. **GeneDoc:** GeneDoc software (Nicholas, 1997) was used for finding conserved domains among aligned sequences of DNA or protein. It is available at http://www.nrbsc.org/gfx/genedoc/.
6. **RestrictionMapper:** This was used for restriction mapping of DNA sequences. It is available at http://www.restrictionmapper.org/.
7. **Molecular Evolutionary Genetic Analysis Version 6 (MEGA 6):** The MEGA software (Tamura *et al.*, 2013) was used to depict the evolutionary relationship among the organisms or gene sequences. It is available at http://www.megasoftware.net/.
8. ***Neurospora crassa* genome databases:** Genome resource for *Neurospora* is available at http://fungidb.org. The web site for Fungal Genetics Stock Center is http://www.fgsc.net/.

9. **NCBI:** NCBI at http://www.ncbi.nlm.nih.gov/ was used to retrieve the proteins or nucleic acid sequences.
10. **EMBL:** EMBL at http://embl.org/was used to retrieve the primary sequence of proteins or nucleic acid.
11. **UniProt:** UniProt at https://www.uniprot.org/ was used to retrieve the primary sequence of proteins.
12. **Primer3:** Primer3 was used for analysis of the secondary structure of oligonucleotide primers. It is available at http://bioinfo.ut.ee/primer3-0.4.0/.
13. **Site for reverse-complement:** The sequence manipulation suite (SMS) software package was used to convert a DNA sequence into reverse-complement sequence. It is available at http://www.bioinformatics.org/sms/index.html.
14. **DNA binding site predictor for Cys_2His_2 Zinc Finger Proteins**: DNA binding site predictor for Cys_2His_2 Zinc Finger Proteins" (Persikov *et al.*, 2008; Persikov and Singh, 2013) was used for prediction of the CRZ-1 binding sites. It is available at http://zf.princeton.edu.
15. **RStudio® (v. 1.1.383)**: The ggplot2 package in RStudio® (v. 1.1.383; Rstudio Team, 2015; Wickham, 2016) was used to plot the box and whisker. It is available at https://www.rstudio.com/.

Chapter 3

Role of neuronal calcium sensor-1 (NCS-1) and associated proteins in tolerance to Ca^{2+} stress in *Neurospora crassa*

3.1 Introduction

Calcium (Ca^{2+}) acts as a universal signaling molecule and plays a pivotal role in in eukaryotic cell signaling (Berridge *et al.*, 1998; Clapham, 2007). The resting cytosolic free Ca^{2+} concentration ($[Ca^{2+}]_c$) is ~100 nM, which can rise transiently up to 1 µM, either by extracellular Ca^{2+} influx or Ca^{2+} release from the intracellular storage, triggering a Ca^{2+} signaling process (Chin and Means, 2000; Bootman *et al.*, 2001). Excessive $[Ca^{2+}]_c$ is toxic to the cell, since it causes inherent stress leading to cell death (Cerella *et al.*, 2010). In *N. crassa*, the $[Ca^{2+}]_c$ level is maintained by a coordinated mechanism involving active Ca^{2+} transport across the plasma membrane, Ca^{2+} buffering in cell organelles, and Ca^{2+} sequestration to vacuoles (Bowman *et al.*, 2011). A number of abiotic stresses including osmotic stress, high salt concentration, and temperature variation may lead to an increase in $[Ca^{2+}]_c$ in eukaryotes (Polisensky and Braam, 1996; Fang *et al.*, 1997; Knight, 1999; Kader and Lindberg, 2010). Transient increase in the $[Ca^{2+}]_c$ is sensed by various Ca^{2+} binding proteins containing EF-hand, including the neuronal calcium sensor-1 (NCS-1), which is a member of the NCS family of proteins (Pongs *et al.*, 1993; Bourne *et al.*, 2001; Tsujimoto *et al.*, 2002). Recoverin, which is a well-studied NCS protein acts as a Ca^{2+} sensor in rod and cone cells of retina and binds to rhodopsin kinase, regulating the rhodopsin desensitization (Dizhoor *et al.*, 1991; Kawamura, 1993; Chen *et al.*, 1995; Erickson *et al.*, 1998). Other NCS family proteins like hippocalcin (Tzingounis *et al.*, 2007) and neurocalcin (Hidaka and Okazaki, 1993) are reported to serve as Ca^{2+} sensors by regulating different ion channels.

In *S. cerevisiae*, *FRQ1*, the homolog of *N. crassa ncs-1*, is an essential gene and its knockout mutant is lethal (Hendricks *et al.*, 1999). The lethal phenotype of the *FRQ1* knockout is rescued by the overexpression of the *PIK1* gene that encodes phosphatidylinositol 4-kinase 1 (Pik1) protein, suggesting that Frq1 interacts with Pik1 (Hendricks *et al.*, 1999; Strahl *et al.*, 2005; Strahl *et al.*, 2007). In *S. pombe*, the NCS-1 homolog Ncs1p plays an important role in

protection against the Ca^{2+} stress by targeting the Yam8p Ca^{2+} permeable channel (Hamasaki-Katagiri and Ames, 2010). In *N. crassa, ncs-1* is involved in growth, Ca^{2+} and UV stress tolerance (Deka *et al.*, 2011) and Ca^{2+} dependent germling fusion (Palma-Guerrero *et al.*, 2013).

The calcineurin is another Ca^{2+} signaling protein having a critical role in normal growth, development, and maintaining apical Ca^{2+} gradient in *N. crassa* (Prokisch *et al.*, 1997; Kothe and Free, 1998; Tamuli *et al.*, 2016). The calcineurin is the only serine/threonine protein phosphatase activated by Ca^{2+} and CaM and contains a CaM binding catalytic subunit and a Ca^{2+} binding regulatory subunit (Klee *et al.*, 1979; Winkler *et al.*, 1984; Klee *et al.*, 1998; Rusnak and Mertz, 2000). The well-studied target of the calcineurin is the calcineurin responsive zinc finger 1 (Crz1) in fungi, while in mammals it is the nuclear factor of activated T cells (NFAT) (Chen *et al.*, 2010). The Crz1 and NFAT are transcription factors that translocate into the nucleus upon dephosphorylation by the activated calcineurin, and regulate the expression of the target genes (Chen *et al.*, 2010). In *S. cerevisiae*, the *CRZ-1* knockout mutant shows similar phenotypes, but less severe phenotypes like the calcineurin mutants, while *CRZ1* overexpression rescues the calcineurin mutants (Stathopoulos and Cyert, 1997). In *S. pombe*, Crz1 homologue Prz1p dephosphorylation by calcineurin causes nuclear localization and binding of the Prz1p to the promoter of *ncs1* upregulating its transcription during Ca^{2+} stress, which in turn closes the plasma membrane-localized Ca^{2+} permeable channel Yam8p to stop Ca^{2+} influx (Stathopoulos-Gerontides *et al.*, 1999; Hirayama *et al.*, 2003; Hamasaki-Katagiri and Ames, 2010). In *N. crassa*, Crz1 homolog is encoded by the gene *crz-1* (NCU07952) and it contains two DNA binding Cys_2His_2 (C_2H_2) Zinc-finger domains (Virgilio *et al.*, 2017).

In *N. crassa*, *the mid-1* gene (NCU06703) encodes the Yam8p homolog MID-1 (Lew *et al.*, 2008). In *S. cerevisiae*, Mid-1 is vital for matting and Ca^{2+} influx (Iida *et al.*, 1994).

Similarly, in *S. pombe*, Yam8p regulates Ca^{2+} influx essential for Ca^{2+} homeostasis (Hamasaki-Katagiri and Ames, 2010). In *N. crassa*, the *mid-1* has a role in growth, Ca^{2+} ion transport, and homeostasis (Lew *et al.*, 2008). In addition, the Δ*mid-1* mutant rescues the Ca^{2+} sensitive phenotype of the Δ*ncs-1* mutant, indicating that reduced Ca^{2+} influx due to the absence of MID-1 in the Δ*mid-1* mutant might protect from high extracellular Ca^{2+} (Deka and Tamuli, 2013). However, it remained unclear if NCS-1 physically interacts with MID-1 to regulate Ca^{2+} influx in response to the Ca^{2+} stress in *N. crassa*.

3.2 Results

3.2.1 The transcription of *ncs-1* increases in response to high Ca^{2+}

The *N. crassa* wild type strain shows tolerance to high Ca^{2+} stress, and therefore, grows in the presence very high $CaCl_2$ (0.4 M) in the medium (Deka *et al.*, 2011). However, the *N. crassa* Δ*ncs-1* mutant showed severe growth defect with increasing concentrations of $CaCl_2$ as compared to the wild type strain (Deka *et al.*, 2011). Therefore, I performed qRT-PCR analysis to test if *ncs-1* expression changes with changing Ca^{2+} concentration in the growth media. For qRT-PCR analysis, I isolated RNA isolated from the mycelia of the wild type strain cultured in the presence of $CaCl_2$ in four different concentrations (0.68 mM, 200 mM, 300 mM, and 400 mM). The protocols for RNA isolation, cDNA construction, and qRT-PCR performed using the primers (Table 2.2) were as described in the Chapter 2 describing Materials and Methods. The relative expression of *ncs-1* in the standard VM containing 0.68 mM $CaCl_2$ was taken as a control, and the expressions for the three different test concentrations of $CaCl_2$ (200 mM, 300 mM, and 400 mM) were expressed in terms of fold change by comparing with the control. The expression study showed a gradual increase in the *ncs-1* expression from ~4-fold to ~11-fold (Table 3.1; Fig. 3.1) with increasing concentrations of $CaCl_2$. The induction of *ncs-1*

expression by increased amounts of Ca^{2+} suggested an important role of the *ncs-1* in Ca^{2+} stress tolerance in *N. crassa*.

Table 3.1: Relative expression of *ncs-1* under different concentrations of $CaCl_2$ in the wild type strain

$CaCl_2$ Concentrations (mM)	**Relative expression[+]**	
	Median	**Mean ± Standard deviation (SD)**
0.68	1.0	1.0
200	3.9	3.9 ± 0.3 (***)
300	7.6	7.8 ± 0.5 (***)
400	10.8	11.1 ± 1.0 (***)

[+]Data are shown as both median and mean ± standard deviation calculated from three independent experiments done in triplicates (n = 9). The *p*-value <0.001 (***) compared with the wild type strain was measured by one-way ANOVA test.

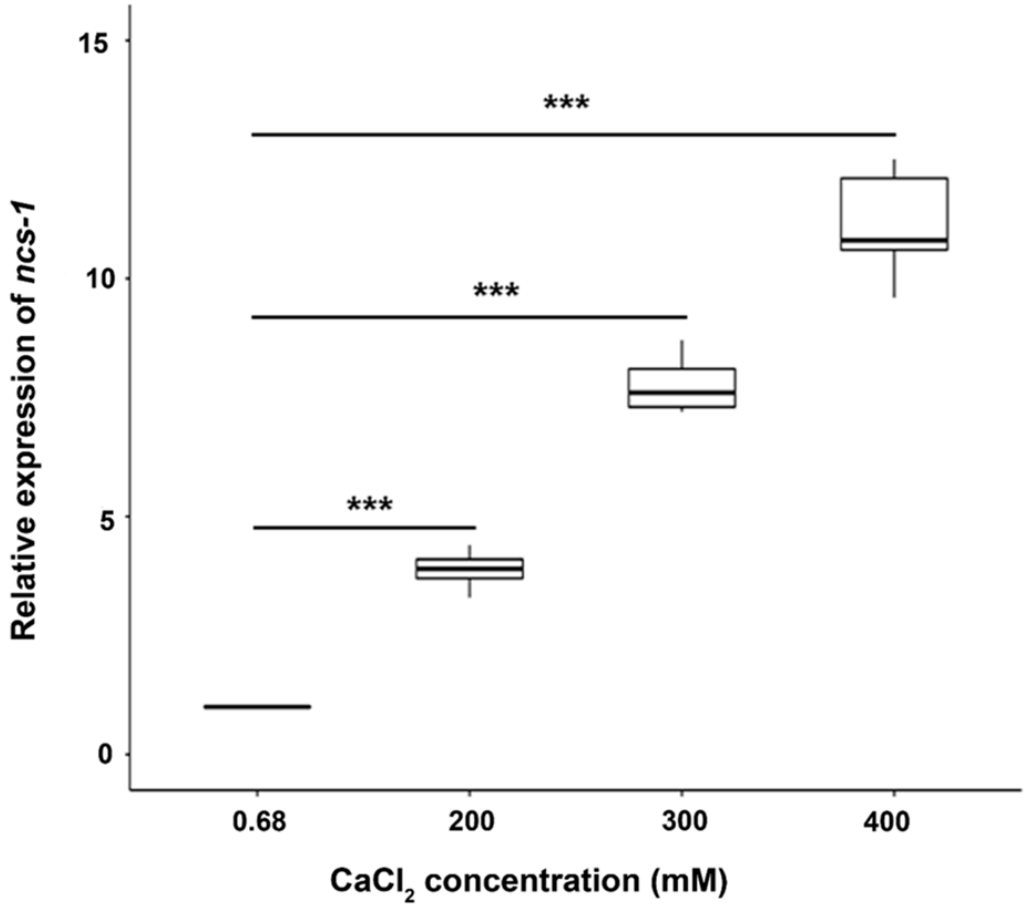

Fig. 3.1: Analysis of *ncs-1* expression under Ca^{2+} stress using qRT-PCR. RNA was isolated from the 16 h old mycelia of the *N. crassa* wild type strain cultured either in standard liquid VM (0.68 mM $CaCl_2$) or supplemented with various concentrations of $CaCl_2$ (200 mM, 300 mM and 400 mM) at 30 °C with 180 rpm shaking. The expression of *ncs-1* was normalized with the expression of *β*-tubulin. The relative expression of *ncs-1* in standard VM (0.68 mM $CaCl_2$) was taken as control and the expression for the other three conditions were expressed in the fold by comparing with it. RStudio® (R package) was used to plot the box and whisker plots. Each box represents 2nd and 3rd quartile, while the whiskers represent the maximum and minimum range of the data and the bold black line inside the box represents the median for each data group. The black dot indicates the outlier. One-way ANOVA was done to test the

significance of the fold change considering the p- values <0.05 (*), <0.01 (**), <0.001 (***) significant.

3.2.2 Generation of strain for NCS-1 overexpression

The increased level of the *ncs-1* transcript level in response to increased Ca^{2+} concentration indicated a Ca^{2+} induced overexpression of NCS-1 might have a role in survival under the Ca^{2+} stress condition. In a previous study, the cellular Ncs1p level was found to be upregulated to nearly 100-fold on increasing the extracellular Ca^{2+} concentration in *S. pombe* (Hamasaki-Katagiri and Ames, 2010). To test if the Ca^{2+}-induced overexpression of NCS-1 could complement the Ca^{2+} sensitive phenotype of the Δ*ncs-1* mutant, I generated *N. crassa* strains expressing *ncs-1* under the *nit-6* (NCU04720) promoter using the heterokaryotic strain NCS-1-P2- HT 3 (Table 2.1) that contains P_{nit-6}::*ncs-1*::*5xGly*::*V5*::*gfp* in the *pan-2* locus. The P_{nit-6}::*ncs-1*::*5xGly*::*V5* construct allows inducible expression of the NCS-1 under the *nit-6* promoter, which is controlled by the nitrogen source in the medium (Ouyang *et al.*, 2015). The NCS-1-P2- HT 3 strain was essentially generated by my senior colleague Dr. Rekha Deka in the Prof. Katherine A. Borkovich laboratory, University of California Riverside (UCR), USA. Briefly, for the generation of the NCS-1-P2- HT 3 strain, the *ncs-1* (NCU04379) open reading frame (ORF) of length 1162 bp was cloned in pRS426PVG/pnit-6_1.5 kb vector (Ouyang *et al.*, 2015) digested with SmaI and PacI. The pRS426PVG/pnit-6_1.5 kb vector contains a *pan-2* (NCU10048) UTRs, a regulatable *nit-6* (NCU04720) promoter (P_{nit-6}), 5XGly, *gfp* and *v5* tag. The P_{nit-6} regulatable promoter can be induced by the addition of $NaNO_3$ and repressed by glutamine in the medium as a nitrogen source (Exley *et al.*, 1993; Ouyang *et al.*, 2015). The *ncs-1* ORF was PCR amplified using the primer pairs NCS-1-NIT-6-GFP-FOR and NCS-1-NIT-6-GFP-REV (Table 2.2). Yeast recombinational cloning (Colot *et al.*, 2006) was used to perform the cloning, and plasmid constructs were isolated by yeast smash and grab method (Hoffman, 2001). The plasmid construct pRTNCS-1 (2) containing P_{nit-6}::*ncs-*

1::*5xGly*::*V5*::*gfp* (Fig. 3.2) was transformed into the *N. crassa* recipient strain 51-IV-8 (Table 2.1) by electroporation as described in the Chapter 2. One of the heterokaryotic strains, NCS-1-P2- HT 3 (Table 2.1) was crossed with the Δ*ncs-1* (FGSC11404) strain to obtain homokaryotic strains. The ascospores were germinated on FGS agar plate containing pantothenic acid, and homokaryotic progenies were initially screened for hygromycin resistance (*hyg*^{R}) and pantothenate auxotrophy (*pan-2*$^{-}$). Three homokaryotic strains were finally selected by verifying the presence of the *ncs-1* allele in the *pan-2* locus (Linkage group VI), and Δ*ncs-1*::*hph* allele in the endogenous locus (Linkage group IV) by PCR amplification (Fig. 3.3) using the primer pairs Pnit-6-Fw and GFP-Rv (Table 2.2), and HI-NCS-1F and 5HPHR (Table 2.2), respectively. Among the three homokaryotic strains, the P$_{nit-6}$::*ncs-1* (21) strain was used for further studies.

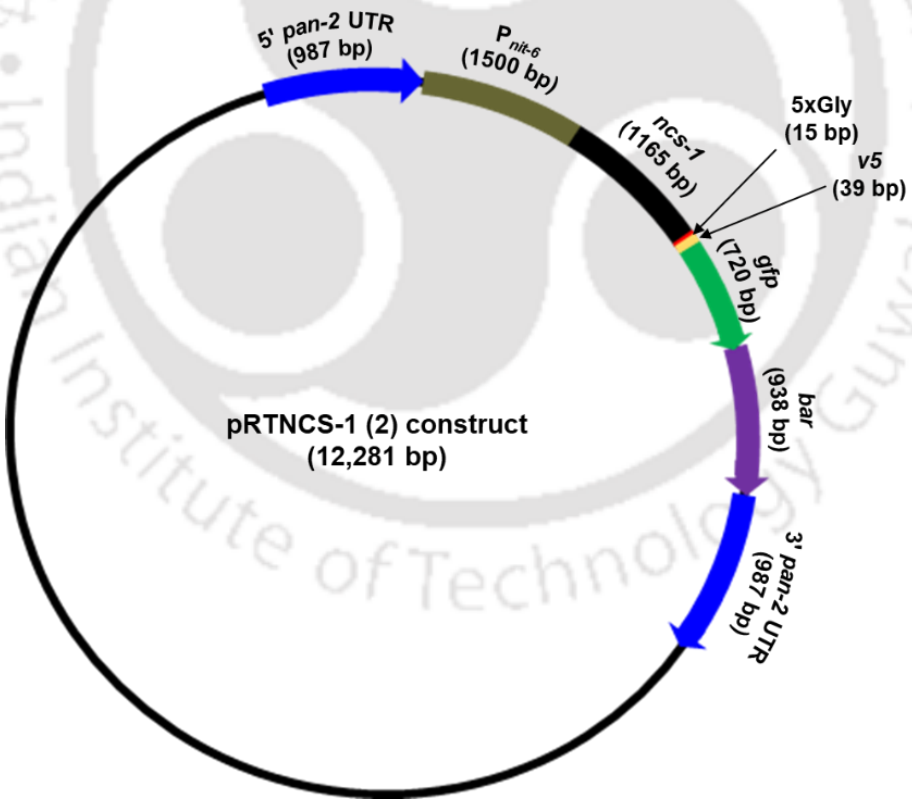

Fig. 3.2: Schematic diagram showing the pRTNCS-1 (2) plasmid construct containing the *ncs-1* ORF under the regulatable *nit-6* promoter (P$_{nit-6}$). The pRTNCS-1 (2) plasmid (12,382 bp), a modified pRS426 vector with *pan-2* UTRs, 5xGly, *gfp* and *v5* tag (Ouyang *et*

al., 2015), contains the *ncs-1* ORF cloned into the multiple cloning site (MCS) region. The numbers (in bp) in the parentheses indicate the size of the respective fragment.

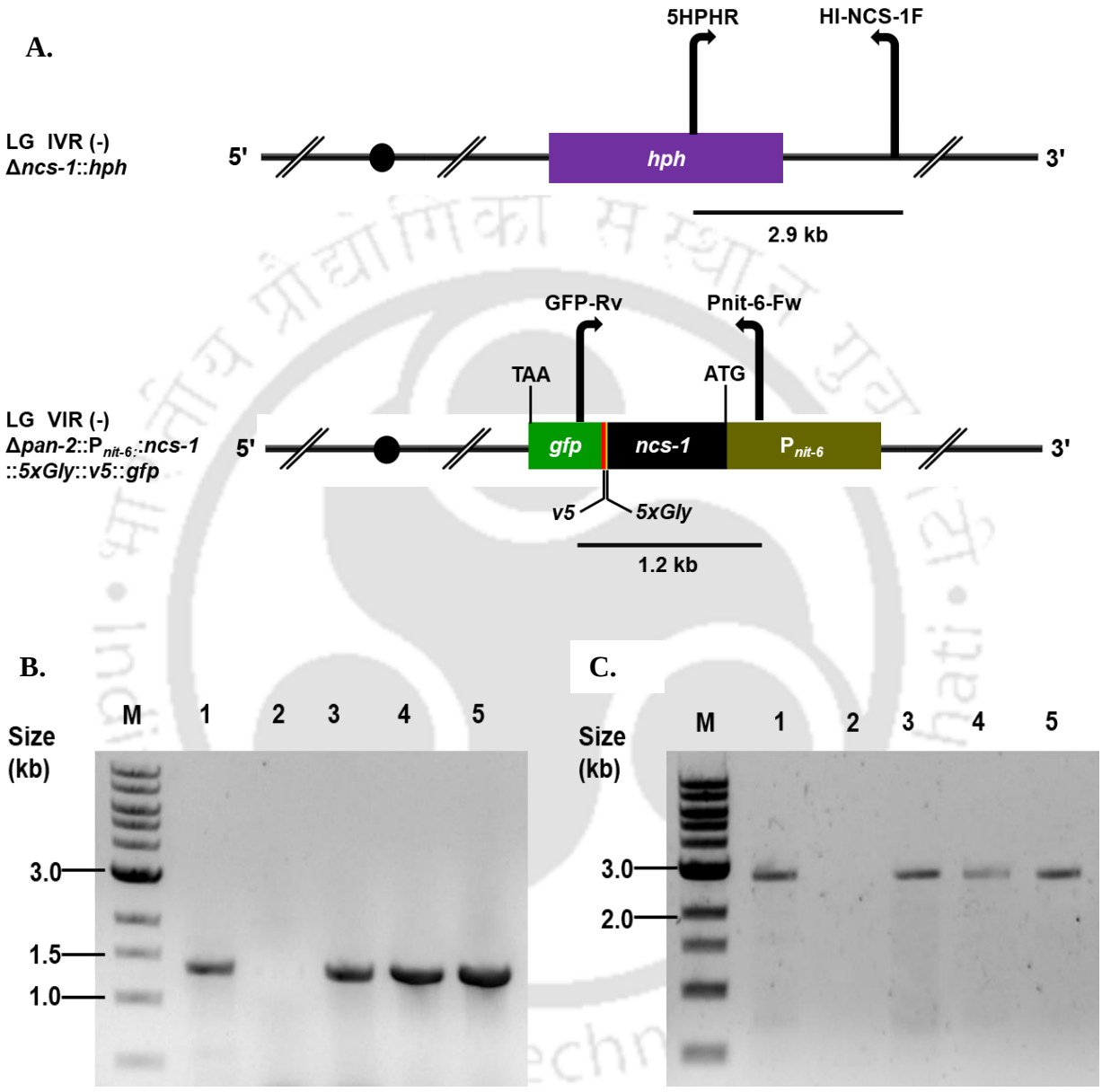

Fig. 3.3: Verification of the homokaryotic strains with *ncs-1* expressed under P_{nit-6}.

A. Schematic diagram showing the primer positions and 5'→3' orientation (shown using the direction of the arrow) used for the verification of the homokaryotic strains with the *ncs-1* expressed under P_{nit-6}. The primer pairs HI-NCS-1F and 5HPHR; Pnit-6-Fw and GFP-Rv (Table 2.2) amplify PCR products of sizes ~2.9 kb and ~1.2 kb respectively.

B. PCR amplification of the P_{nit-6}::*ncs-1*::*5xGly*::*V5*::*gfp* fragment using the primer pairs Pnit-6-Fw and GFP-Rv (Table 2.2). The three homokaryotic strains P_{nit-6}::*ncs-1* (8), P_{nit-6}::*ncs-1* (10), and P_{nit-6}::*ncs-1* (21) in lanes 3, 4 and 5 respectively showing the P_{nit-6}::*ncs-1*::*5xGly*::*V5*::*gfp* fragment of size ~1.2 kb. The pRTNCS-1 (2) plasmid in lane 1 and the wild type strain (FGSC 987) in lane 2 were used as positive and negative controls, respectively. PCR products were resolved in 1% agarose gel, using the 1 kb NEB DNA ladder (New England Biolabs, USA) as marker (M).

C. PCR amplification of the *hph* cassette using HI-NCS-1F and 5HPHR (Table 2.2). The homokaryotic strains P_{nit-6}::*ncs-1* (8), P_{nit-6}::*ncs-1* (10), and P_{nit-6}::*ncs-1* (21) in lanes 3, 4 and 5 respectively showing the *hph* fragment of size ~2.9 kb. The Δ*ncs-1* (FGSC 11404) strain in lane 1 and the wild type (FGSC 987) strain in lane 2 were used as positive and negative control, respectively. PCR products were resolved in a 1% agarose gel, using the 1 kb NEB DNA ladder (New England Biolabs, USA) as marker (M).

3.2.3 Expression of NCS-1 under P_{nit-6}

The pRTNCS-1 (2) construct expresses a fusion protein NCS-1::5xGly::V5::GFP (~51 kDa) under P_{nit-6}. I performed a western blot analysis to confirm the expression of the fusion protein in the P_{nit-6}::*ncs-1* (21) strain in both VM containing either $NaNO_3$ or glutamine as a nitrogen source for the induction and repression conditions, respectively. For the inducing media, VM liquid (without NH_4NO_3) was supplemented with 20 mM $NaNO_3$, and for repressing media 20 mM glutamine (Glu) was used as nitrogen source. The inducing and repressing conditions used for the P_{nit-6}::*ncs-1* (21) strain were of two different methods. In one method, the conidia were cultured for entire 16 h in either inducing or repressing condition. In the other method, first 12 h was given induction or repression, followed 4 h either in repression or induction condition. Total protein was isolated from the 16 h cultures and western blot was performed

using anti-GFP antibody (Cat. No. A6455, life Technologies, USA) as described in the Chapter 2. The western blot (Fig. 3.4) analysis showed that the induction and repression of the NCS-1::5xGly::V5::GFP in the respective media condition. There was ~8-fold increase in the expression in the inducing conditions compared with the expression when cultured either in the repression or in the standard VM liquid that contains 60 mM NH_4NO_3 as a nitrogen source. Therefore, NCS-1::5xGly::V5::GFP is nitrogen-regulatable construct under the $P_{nit\text{-}6}$ and NCS-1 was overexpressed in the inducing condition.

Strain	$P_{nit\text{-}6}$::*ncs-1* (21)					Wild type	
Standard VM (25 mM NH_4NO_3)	+	–	–	–	–	–	–
Repression (20 mM glutamine)	–	–	+	–	–	–	+
Induction (20 mM $NaNO_3$)	–	+	–	–	–	+	–
Repression → Induction	–	–	–	–	+	–	–
Induction → Repression	–	–	–	+	–	–	–
Lane	1	2	3	4	5	6	7

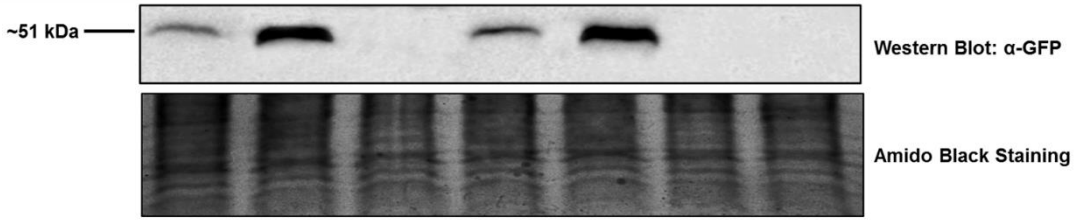

Fig. 3.4: Expression of NCS-1::5xGly::V5::GFP under $P_{nit\text{-}6}$ in inducing and repressing conditions. Western blot showing the expression of NCS-1::5xGly::V5::GFP (~51 kDa) under $P_{nit\text{-}6}$ in the $P_{nit\text{-}6}$::*ncs-1* (21) strain. Lane 1 shows expression of NCS-1::5xGly::V5::GFP in standard VM (25 mM NH_4NO_3), lanes 2 and 3 show expressions in inducing VM (20 mM $NaNO_3$) and repressing VM (20 mM glutamine), respectively, cultured for 16 h at 30°C with shaking at 180 rpm. The $P_{nit\text{-}6}$::*ncs-1* (21) strain was also grown first in inducing medium for 12 h and then in repressing medium for 4 hours (lane 4), or vice versa (lane 5). The wild type strain was grown in inducing and repressing conditions (lanes 6 and 7), respectively, for 16 h as a negative control and showed no expression. The amido black staining of the membrane is shown in the lower panel demonstrates the equal protein loading.

3.2.4 NCS-1 overexpression complemented the slow growth and Ca^{2+} sensitive phenotypes of the Δ*ncs-1* mutant

$P_{nit\text{-}6}$::*ncs-1* (21) strain contains a deletion for the *ncs-1* in its endogenous locus (Linkage group IV), and NCS-1 was expressed as an NCS-1::5xGly::V5::GFP fusion protein from the ectopic allele inserted at the *pan-2* locus. The apical growth of the $P_{nit\text{-}6}$::*ncs-1* (21) strain was studied using standard race tube assay (Ryan *et al.*, 1943; Ryan, 1950) in three media conditions- standard VM, inducing (standard VM + 20 mM $NaNO_3$) and repressing (standard VM + 20 mM glutamine). Agar plugs of the wild type (FGSC 987), Δ*ncs-1* (FGSC 11404), and $P_{nit\text{-}6}$::*ncs-1* (21) strains were inoculated at one end of the race tube containing 13 ml of VM agar and incubated at 30 °C for 72 h. The distance of the hyphal growth front from the point of inoculation was plotted against time. It was observed that the $P_{nit\text{-}6}$::*ncs-1* (21) strain was showing growth similar to the wild type in both the standard VM and inducing media (Tables 3.3, 3.4; Fig. 3.5). On the other hand in repressing media, the $P_{nit\text{-}6}$::*ncs-1* (21) strain had shown slow growth like the Δ*ncs-1* mutant strain (Table 3.5; Fig. 3.5 C). Thus, the $P_{nit\text{-}6}$::*ncs-1* (21) strain complemented the slow growth phenotype of the Δ*ncs-1* mutant strain.

To study tolerance to Ca^{2+} stress**,** a set of assays were performed in both inducing and repressing media to determine whether the overexpression of NCS-1 was able to complement the Ca^{2+} sensitive phenotype of the Δ*ncs-1* mutant or even confer better Ca^{2+} stress tolerance than the wild type. For the Ca^{2+} tolerance assay, the VM liquid medium (VGN without $CaCl_2$ and NH_4NO_3) was supplemented with four different concentrations (0, 0.2, 0.3, and 0.4 M) of $CaCl_2$. For the induction and repression, 20 mM $NaNO_3$ and 20 mM glutamine, respectively, were used as nitrogen source. The wild type and the Δ*ncs-1* mutant strains were used as controls. The Ca^{2+} sensitivity assay was performed as described in the Chapter 2. The average colony growth rate was calculated as cm h^{-1} based on the data obtained from three independent experiments (n = 3) for each strain. Average colony growth rate percentage (%) was calculated

relative to the colony diameter of the strains in VM without $CaCl_2$ (0 M) considering as 100%. In the inducing media, the overexpressed NCS-1::5xGly::V5::GFP in the $P_{nit\text{-}6}$::*ncs-1* (21) strain not only complemented the Ca^{2+} sensitive phenotype of the Δ*ncs-1* mutant but also conferred slightly better Ca^{2+} stress tolerance than the wild type (Table 3.5; Fig. 3.6 A). In the repressing media, the $P_{nit\text{-}6}$::*ncs-1* (21) strain displayed a lower average growth rate like the Δ*ncs-1* mutant strain (Table 3.6; Fig. 3.6 B). These results suggested that NCS-1 is involved in Ca^{2+} stress tolerance in *N. crassa*.

Table 3.2: Apical growth of the wild type, Δ*ncs-1*, and $P_{nit\text{-}6}$::*ncs-1* (21) strains in race tube in standard VM

Strains	**Distance (cm) in race tube at the indicated time interval**						
	0 h	**12 h**	**24 h**	**36 h**	**48 h**	**60 h**	**72 h**
Wild type	0.0 ± 0.0	2.4 ± 0.1	7.6 ± 0.2	13.6 ± 0.2	19.1 ± 0.2	24.8 ± 0.2	30.5 ± 0.2
Δ*ncs-1*	0.0 ± 0.0	1.1 ± 0.2	4.2 ± 0.3	8.5 ± 0.1	12.4 ± 0.2	16.8 ± 0.1	21.3 ± 0.1
$P_{nit\text{-}6}$::*ncs-1* (21)	0.0 ± 0.0	2.2 ± 0.1	7.0 ± 0.2	12.5 ± 0.2	17.6 ± 0.1	23.7 ± 0.3	28.9 ± 0.3

Table 3.3: Apical growth of the wild type, Δ*ncs-1*, and P_{nit-6}::*ncs-1* (21) strains in race tube in the inducing media (standard VM supplemented with 20 mM $NaNO_3$)

Strains	Distance (cm) in race tube at the indicated time interval						
	0 h	**12 h**	**24 h**	**36 h**	**48 h**	**60 h**	**72 h**
Wild type	0.0 ± 0.0	2.5 ± 0.2	7.6 ± 0.2	13.6 ± 0.2	19.1 ± 0.2	24.8 ± 0.2	30.3 ± 0.2
Δ*ncs-1*	0.0 ± 0.0	1.4 ± 0.2	4.5 ± 0.2	8.4 v	12.9 ± 0.2	17.2 ± 0.1	21.5 ± 0.2
P_{nit-6}::*ncs-1* (21)	0.0 ± 0.0	3.1 ± 0.1	8.3 ± 0.2	14.4 ± 0.2	20.0 ± 0.1	25.7 ± 0.3	31.9 ± 0.2

Table 3.4: Apical growth of the wild type, Δ*ncs-1*, and P_{nit-6}::*ncs-1* (21) strains in race tube in repressing media (standard VM supplemented with 20 mM glutamine)

Strains	Distance (cm) in race tube at the indicated time interval						
	0 h	**12 h**	**24 h**	**36 h**	**48 h**	**60 h**	**72 h**
Wild type	0.0 ± 0.0	2.7 ± 0.3	7.6 ± 0.2	13.7 ± 0.2	19.3 ± 0.2	24.8 ± 0.4	24.8 ± 0.5
Δ*ncs-1*	0.0 ± 0.0	1.1 ± 0.1	4.3 ± 0.1	8.4 ± 0.1	12.5 ± 0.2	16.8 ± 0.2	21.3 ± 0.1
P_{nit-6}::*ncs-1* (21)	0.0 ± 0.0	1.6 ± 0.1	4.8 ± 0.3	9.2 ± 0.4	13.3 ± 0.2	17.8 ± 0.1	22.7 ± 0.1

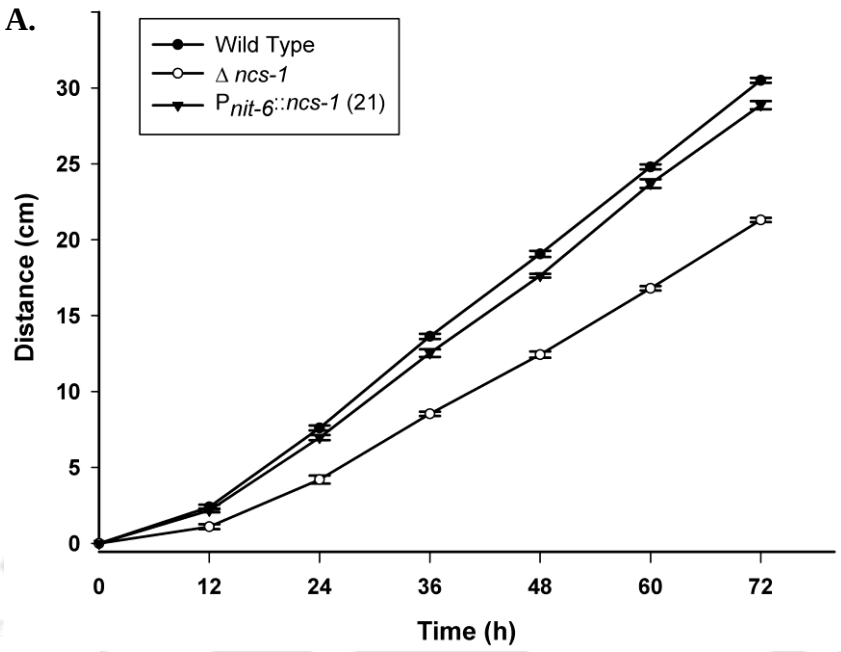

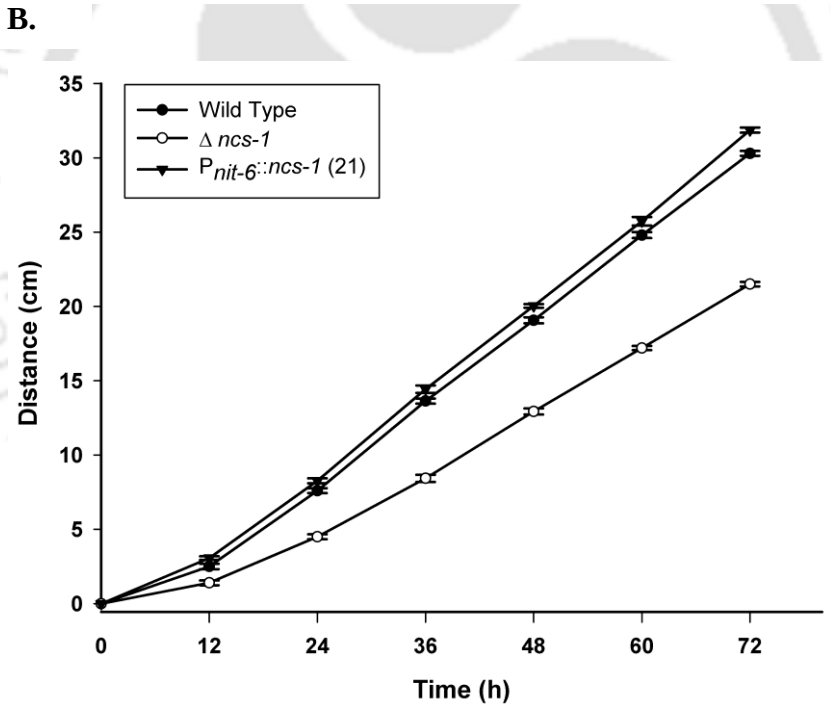

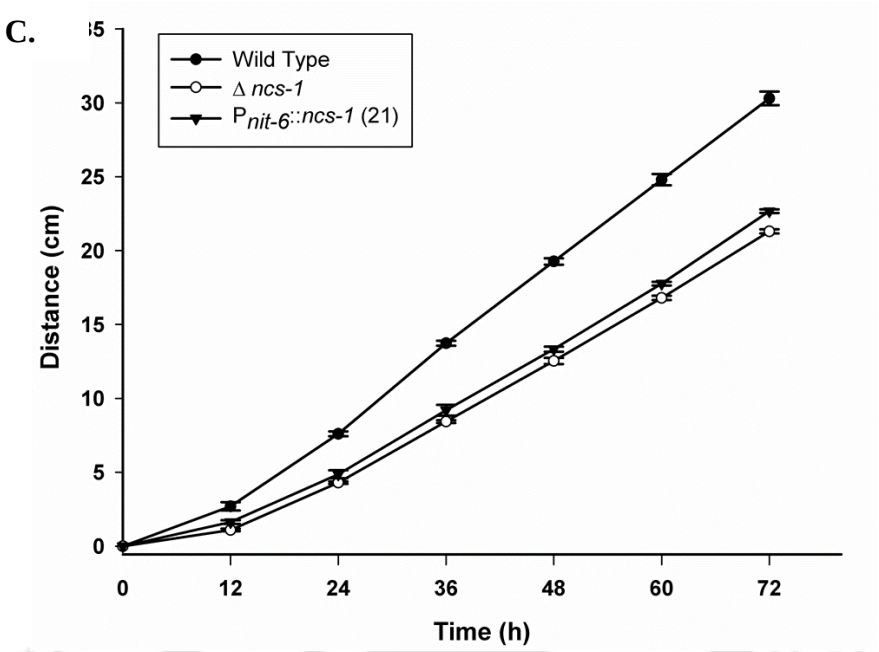

Fig. 3.5: Apical growth of the wild type, Δ*ncs-1*, and P$_{nit-6}$::*ncs-1* (21) strains in race tube. Error bars indicate the standard deviation calculated from the data for three independent experiments (n = 3).

A. Agar plugs of the wild type (FGSC 987), Δ*ncs-1*(FGSC 11404), and P$_{nit-6}$::*ncs-1* (21) strains were inoculated at one end of the race tube containing 13 ml of standard VM agar and incubated at 30 °C for 72 h. The P$_{nit-6}$::*ncs-1* (21) strain showed similar growth like the wild type strain.

B. Agar plugs of the wild type (FGSC 987), Δ*ncs-1*(FGSC 11404), and P$_{nit-6}$::*ncs-1* (21) strains were inoculated at one end of the race tube containing 13 ml of standard VM agar supplemented with 20 mM $NaNO_3$ as inducer and incubated at 30 °C for 72 h. The P$_{nit-6}$::*ncs-1* (21) strain showed similar growth like the wild type strain.

C. Agar plugs of the wild type (FGSC 987), Δ*ncs-1*(FGSC 11404), and P$_{nit-6}$::*ncs-1* (21) strains were inoculated at one end of the race tube containing 13 ml of standard VM agar supplemented with 20 mM glutamine as repressor and incubated at 30 °C for 72 h. The P$_{nit-6}$::*ncs-1* (21) strain showed similar slow growth like Δ*ncs-1* strain.

Table 3.5: Average colony growth rate (%) of the wild type, Δ*ncs-1*, and P_{nit-6}::*ncs-1* (21) strains at various concentrations of $CaCl_2$ in inducing media

Strains	Average colony growth rate percentage (%) at various concentrations of $CaCl_2$ (M)			
	0	**0.2**	**0.3**	**0.4**
Wild type	100.0 ± 0.0	82.7 ± 1.5	74.5 ± 1.7	68.2 ± 1.9
Δ*ncs-1*	100.0 ± 0.0	69.7 ± 2.2	49.7 ± 2.3	30.6 ± 1.4
P_{nit-6}::*ncs-1* (21)	100.0 ± 0.0	88.5 ± 2.3	79.6 ± 2.4	73.6 ± 2.4

Table 3.6: Average colony growth rate (%) of the wild type, Δ*ncs-1*, and P_{nit-6}::*ncs-1* (21) strains at various concentrations of $CaCl_2$ in repressing media

Strains	Average colony growth rate percentage (%) at various concentrations of $CaCl_2$ (M)			
	0	**0.2**	**0.3**	**0.4**
Wild type	100.0 ± 0.0	90.2 ± 1.5	84.0 ± 1.8	76.0 ± 2.2
Δ*ncs-1*	100.0 ± 0.0	71.3 ± 1.9	42.2 ± 2.4	34.0 ± 2.1
P_{nit-6}::*ncs-1* (21)	100.0 ± 0.0	79.3 ± 1.8	50.5 ± 2.5	42.4 ± 1.7

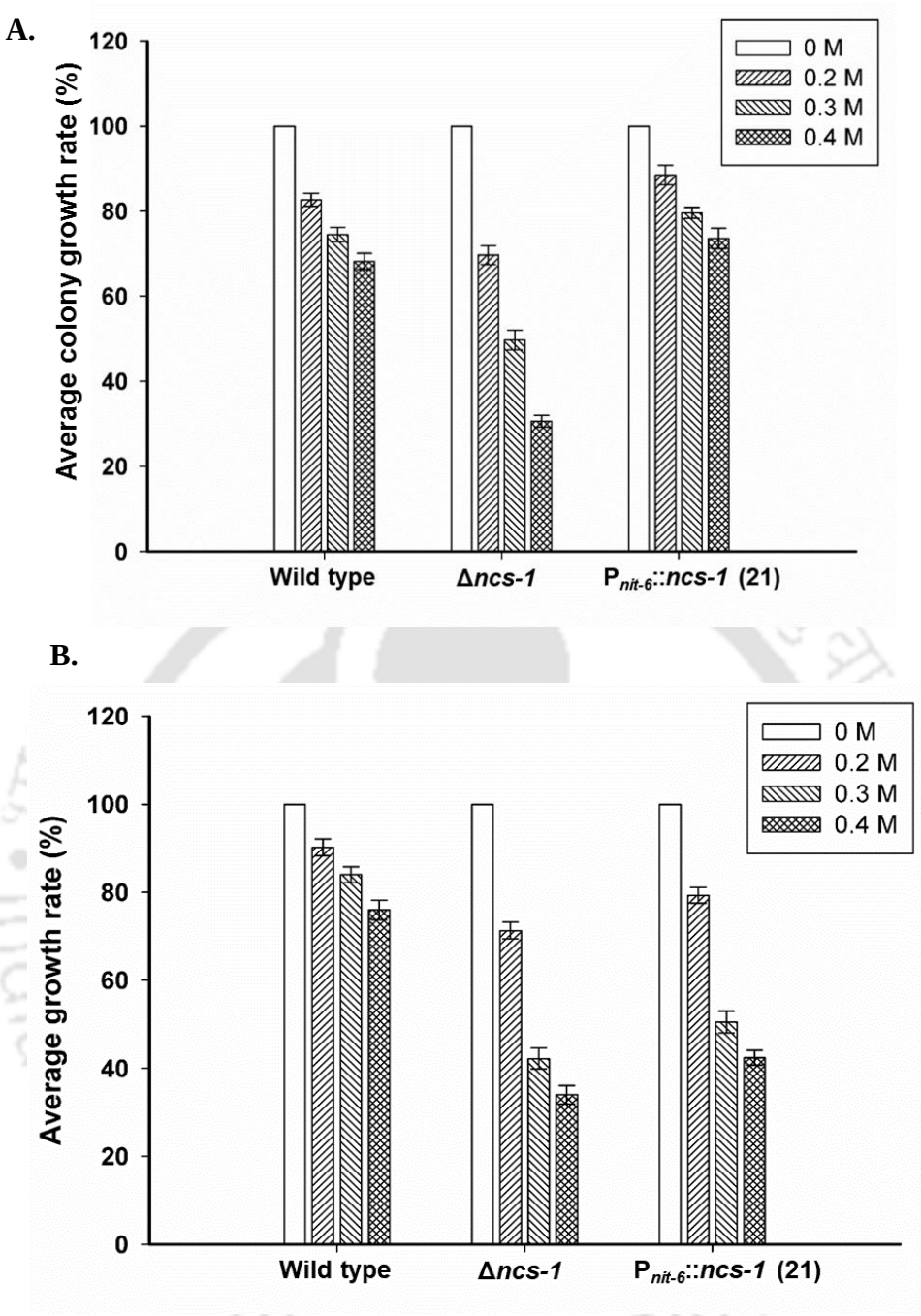

Fig. 3.6: Assay for tolerance to Ca^{2+} stress in $P_{nit\text{-}6}$::*ncs-1* (21) strain under inducing and repressing conditions. The *N. crassa* strains were grown in VM supplemented with various amounts of $CaCl_2$ and incubated at 30°C for 18 h. Error bars indicate the standard deviation calculated from the data of three individual experiments (n = 3).

A. For induction 20 mM $NaNO_3$ was added to the VM media. The $P_{nit\text{-}6}$::*ncs-1* (21) strain recovered the Ca^{2+} sensitive phenotype of the Δ*ncs-1* mutant in inducing medium.

B. For repression 20 mM glutamine was added to the VM media. The $P_{nit\text{-}6}$::*ncs-1* (21) strain was Ca^{2+} stress sensitive like the Δ*ncs-1* mutant in repressing medium.

3.2.5 The transcription of *ncs-1* is controlled by calcineurin and *crz-1*

The qRT-PCR and the NCS-1 overexpression studies, as described above, show that NCS-1 is a key player in the tolerance to Ca^{2+} stress in *N. crassa*. Therefore, I decided to elucidate the mechanism responsible for the *ncs-1* transcription from its endogenous locus in response to the increased Ca^{2+} level, which was not known previously. A possible mechanism for *ncs-1* transcription in the presence of high Ca^{2+} in *N. crassa* might involve the calcineurin pathway, similar to the established mechanism in other fungi. Calcineurin dephosphorylates the transcription factor Prz-1p in *S. pombe*, which upregulates the transcription of *ncs1* (Hamasaki-Katagiri and Ames, 2010). To investigate the role of the calcineurin pathway in Ca^{2+} stress tolerance in *N. crassa*, I evaluated the Ca^{2+} stress tolerance of the mutant lacking *crz-1*, the Prz-1 homologue. The Δ*crz-1* mutant showed Ca^{2+} sensitivity phenotype like the Δ*ncs-1* mutant (Table 3.7; Fig. 3.7), implicating the calcineurin-CRZ-1 pathway in Ca^{2+} stress tolerance in *N. crassa*.

Then I addressed the next question if the CRZ-1 is required for the *ncs-1* transcription under Ca^{2+} stress condition. A qRT-PCR assay was performed to test the expression of the *ncs-1* in the Δ*crz-1* mutant under the Ca^{2+} stress condition. For the qRT-PCR analysis, RNA was isolated from the respective *N. crassa* strains grown in the standard VM and the Ca^{2+} stress inducing medium containing 0.68 and 200 mM $CaCl_2$, respectively. The relative expression of *ncs-1* for the wild type strain in the standard VM media was considered as control, and the fold change for the remaining samples was calculated by comparing with the control. The *ncs-1* expression in the wild type under the Ca^{2+} stress was ~4.1-fold (Table 3.8; Fig. 3.8), which was similar as described above. But the *ncs-1* expression in the Δ*crz-1* mutant was reduced (~0.6-fold) for both normal and Ca^{2+} stress conditions (Table 3.8; Fig. 3.8). The reduced

expression of *ncs-1* in the Δ*crz-1* mutant suggested that expression of the transcription factor CRZ-1 is required for the induction of the *ncs-1* transcription under the Ca^{2+} stress condition.

Table 3.7: Average colony growth rate (%) of the wild type, Δ*ncs-1*, and Δ*crz-1* strains at various concentrations of $CaCl_2$

Strains	Average colony growth rate percentage (%) at various concentrations of $CaCl_2$ (M)			
	0	0.2	0.3	0.4
Wild type	100.0 ± 0.0	90.8 ± 1.2	85.1 ± 1.4	71.9 ± 1.3
Δ*ncs-1*	100.0 ± 0.0	71.2 ± 2.3	43.0 ± 2.4	32.9 ± 3.7
Δ*crz-1*	100.0 ± 0.0	79.1 ± 1.6	61.8 ± 1.3	51.8 ± 2.2

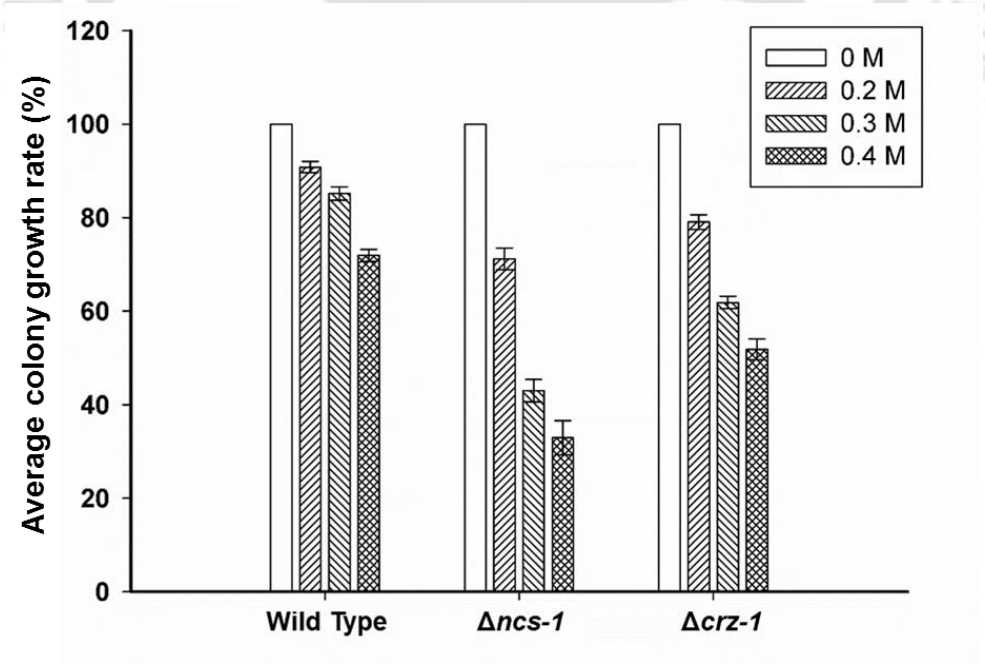

Fig. 3.7: Assay for tolerance to Ca^{2+} stress in the Δ*crz-1* mutant. Ca^{2+} stress tolerance assay showed the sensitivity of the Δ*crz-1* mutant to the Ca^{2+} stress. Error bars indicate the standard deviation calculated from the data of three individual experiments (n = 3).

Table 3.8: Relative expression of *ncs-1* in the wild type and Δ*crz-1* strain under Ca^{2+} stress

Concentration of $CaCl_2$ (mM)	Relative expression[+]			
	Wild type		Δ*crz-1*	
	Median	Mean ± SD	Median	Mean ± SD
0.68	1.0	1.0 ± 0.0	0.6	0.6 ± 0.2
200	4.1	4.0 ± 0.3 (***)	0.6	0.7 ± 0.2

[+]Data shown as both median and mean ± standard deviation calculated from three independent experiments done in triplicates (n = 9). The *p*-value <0.001 (***) compared with the wild type strain was measured by one-way ANOVA test.

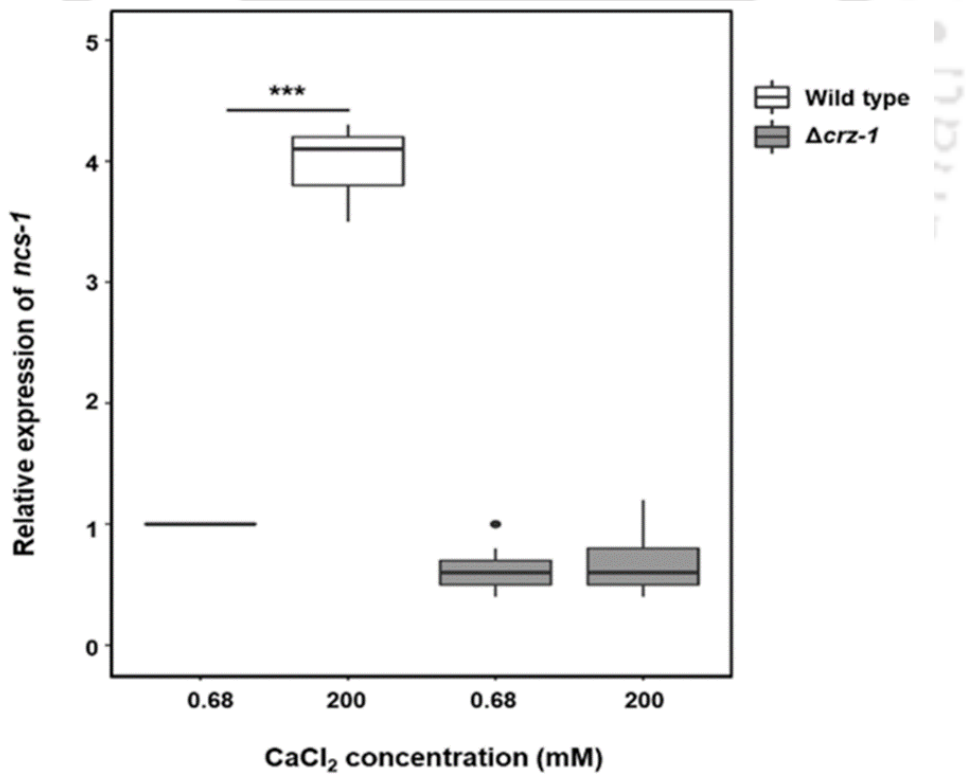

Fig. 3.8: Relative expression of *ncs-1* in the Δ*crz-1* strain grown under Ca^{2+} stress. Relative expression of *ncs-1* in the *N. crassa* strains in VM liquid containing indicated amounts of $CaCl_2$ (mM). The relative expression of *ncs-1* was normalized with the *β*-tubulin expression,

and compared with the expression in the wild type cultured in standard VM liquid containing 0.68 mM $CaCl_2$. RStudio® (R package) was used to plot the box and whisker plots. Each box represents 2nd and 3rd quartile, while the whiskers represent the maximum and minimum range of the data and the bold black line inside the box represents the median for each data group. The black dot indicates the outlier. One-way ANOVA was done to test the significance of the fold change considering the p- values <0.05 (*), <0.01 (**), <0.001 (***) significant.

3.2.6 The *ncs-1* transcription is controlled via the calcineurin -*crz-1* pathway

In *N. crassa*, *cna-1* is an essential gene (Prokisch *et al.*, 1997; Tamuli *et al.*, 2016), therefore, it is not possible to generate a direct knockout mutant of this gene. Therefore, to inhibit the calcineurin enzymatic activity, I used its known inhibitor FK506, also known as tacrolimus (Shapiro *et al.*, 1995; Testa and Klintmalm, 1997). Addition of 1 µg/ml of FK506 to the VM reduced the normal growth rate of the wild type, Δ*ncs-1*, and Δ*crz-1* mutants (Table 3.9; Fig. 3.9), which is consistent with the previous findings (Prokisch *et al.*, 1997; Tamuli *et al.*, 2016) that inhibition of calcineurin affects the normal growth in *N. crassa*. To test the effect of FK506 on *ncs-1*, *crz-1*, and *mid-1* expression during Ca^{2+} stress, the qRT-PCR assay was performed using the wild type strain. The RNA was isolated from the mycelia of the wild type strain (FGSC 987) cultured in three different conditions, namely, standard VM (0.68 mM $CaCl_2$), Ca^{2+} stress (200 mM $CaCl_2$), and Ca^{2+} stress together with the calcineurin inhibitor [$CaCl_2$ (200 mM) + FK506 (1 µg/ml)]. In the Ca^{2+} stress condition, the *ncs-1* and the *crz-1* transcriptions were increased by ~4-fold and ~3-fold, respectively, although, no significant difference in the *mid-1* transcription level was observed (Table 3.10; Fig 3.10). Interestingly, in the presence of FK506, the *ncs-1* expression was significantly reduced to ~0.6-fold, which is about 7-fold decrease, even under the Ca^{2+} stress condition (Table 3.10; Fig 3.10). However, the expressions of *crz-1* and *mid-1* did not show any significant difference in presence of the FK506 (Table 3.10; Fig 3.10). This analysis suggested that the calcineurin enzymatic activity

might be essential for the transcription of *ncs-1*, but not for *crz-1* and *mid-1*, under the Ca^{2+} stress condition. Therefore, the *ncs-1* transcription is regulated via the calcineurin -*crz-1* pathway.

Table 3.9: Average colony growth rates of the wild type, Δ*ncs-1* and Δ*crz-1* strains in presence of FK506

Strains	Average colony growth rate (cm/h)	
	Standard VM	**FK506**
Wild type	0.371 ± 0.012	0.290 ± 0.037
Δ*ncs-1*	0.232 ± 0.023	0.186 ± 0.025
Δ*crz-1*	0.280 ± 0.016	0.107 ± 0.018

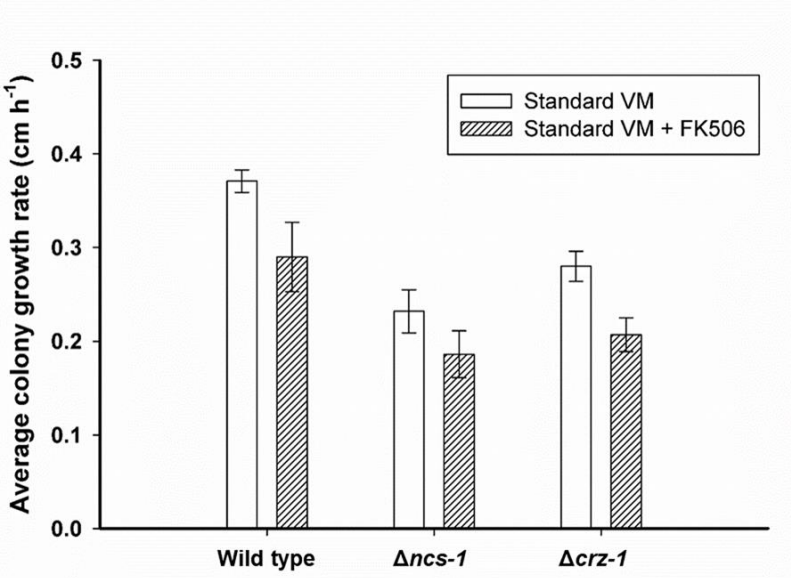

Fig. 3.9: Average colony growth rates of the wild type, Δ*ncs-1* and Δ*crz-1* mutant strains in presence of the calcineurin inhibitor FK506. Average colony growth rates of the wild type, Δ*ncs-1*, and Δ*crz-1* strains were reduced in the VM supplemented with the calcineurin

inhibitor FK506 (1 µg/ml). Error bars indicate the standard deviation calculated from the data of three individual experiments.

Table 3.10: Relative expression of *ncs-1*, *crz-1* and *mid-1* under Ca^{2+} stress and FK506

Concentration of $CaCl_2$	Relative expression[+]					
	0.68 mM		200 mM		200 mM + FK506	
Gene	**Median**	**Mean ± SD**	**Median**	**Mean ± SD**	**Median**	**Mean ± SD**
ncs-1	1.0	1.0 ± 0.0	3.9	3.9 ± 0.3	0.6	0.6 ± 0.3 (***)
crz-1	1.0	1.0 ± 0.0	2.7	2.6 ± 0.3	1.9	1.9 ± 0.2
mid-1	1.0	1.0 ± 0.0	1.5	1.4 ± 0.2	1.4	1.4 ± 0.2

[+]Data shown as both median and mean ± standard deviation calculated from three independent experiments done in triplicates (n = 9). The p-value <0.001 (***) compared with the wild type strain was measured by one-way ANOVA test.

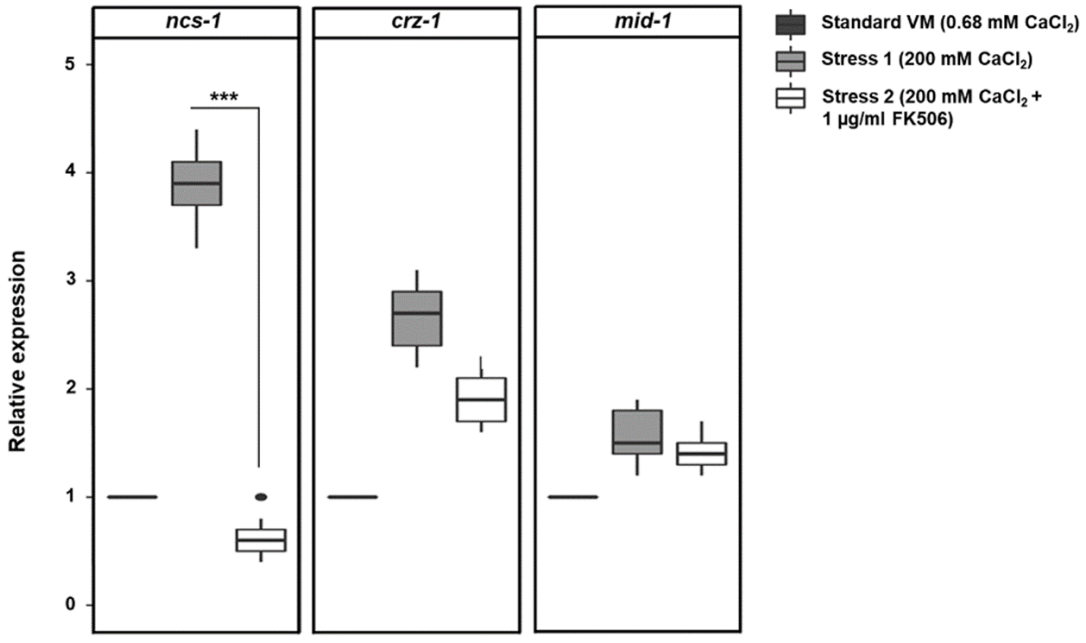

Fig. 3.10: Relative expressions of *ncs-1*, *crz-1*, and *mid-1* under the Ca^{2+} stress with and without the addition of the calcineurin inhibitor FK506. The expressions of *ncs-1*, *crz-1*,

and *mid-1* were normalized to the *β*-tubulin expression, and compared with the expression in standard VM (contains 0.68 mM $CaCl_2$) for each gene. RStudio® (R package) was used to plot the box and whisker plots. Each box represents 2nd and 3rd quartile, while the whiskers represent the maximum and minimum range of the data and the bold black line inside the box represents the median for each data group. The black dot indicates the outlier. One-way ANOVA was done to test the significance of the fold change considering the p- values <0.05 (*), <0.01 (**), <0.001 (***) significant.

3.2.7 Calcineurin regulates multiple targets in addition to CRZ-1 and NCS-1 for Ca^{2+} stress tolerance

The studies involving the Δ*crz-1* mutant and calcineurin inhibitor FK506 demonstrated that the calcineurin -*crz-1* pathway controls the *ncs-1* transcription under the high Ca^{2+} condition. Therefore, I hypothesize that the inhibition of calcineurin by FK506 would prevent the high Ca^{2+} induced expression of NCS-1, causing Ca^{2+} sensitivity phenotype in the wild type strain as displayed by the Δ*ncs-1* and Δ*crz-1* mutants. Therefore, I investigated the tolerance to high concentrations of Ca^{2+} in the wild type, Δ*ncs-1*, and Δ*crz-1* mutants in presence of the FK506 (1 µg/ml). Surprisingly, the wild type strain was able to grow equally well under the high concentrations of Ca^{2+} with or without the addition of FK506 (Table 3.11; Fig. 3.11), indicating that calcineurin inhibition has no effect on the tolerance to Ca^{2+} stress in the wild type. On the other hand, FK506 treatment rescued the Ca^{2+} sensitive phenotype of the Δ*ncs-1* and Δ*crz-1* mutants (Table 3.11; Fig. 3.11), indicating that calcineurin regulates additional target genes for tolerance to Ca^{2+} stress.

In *S. cerevisiae*, calcineurin directly inhibits Ca^{2+} exchanger Vcx1 by causing its dephosphorylation (Cunningham and Fink, 1996). In *N. crassa*, Vcx1 homolog CAX, expressed by the gene *cax* (NCU07075), is localized to vacuoles (Bowman *et al.*, 2009). The Δ*cax* mutant did not show sensitivity towards high concentration of Ca^{2+} and also Ca^{2+}

accumulation in the vacuoles was low (Bowman *et al.*, 2011). But in the presence of FK506, the Δ*cax* mutant displayed Ca^{2+} stress sensitivity like the Δ*ncs-1* and Δ*crz-1* mutants (Table 3.12; Fig. 3.12). This indicated that the calcineurin inhibits the CAX, and the addition of its inhibitor FK506 possibly activated the CAX resulting in increased sequestering of Ca^{2+} into the vacuoles to maintain the viable cytosolic Ca^{2+} level. This is a possible mechanism explaining the rescue of the Ca^{2+} sensitive phenotype of the Δ*ncs-1* and Δ*crz-1* mutants in the presence of FK506.

Table 3.11: Average colony growth rate (%) of the wild type, Δ*ncs-1* and Δ*crz-1* strains at various concentrations of $CaCl_2$ with or without the FK506 supplement

Strain (Supplement)	Average colony growth rate percentage (%) at various concentrations of $CaCl_2$ (M)			
	0	0.2	0.3	0.4
Wild type	100.0 ± 0.0	80.5 ± 1.2	75.2 ± 1.4	67.3 ± 1.9
Δ*ncs-1*	100.0 ± 0.0	65.7 ± 2.1	45.2 ± 2.3	29.3 ± 2.1
Δ*crz-1*	100.0 ± 0.0	69.3 ± 1.2	49.5 ± 1.5	30.9 ± 2.1
Wild type (FK506)	100.0 ± 0.0	79.1 ± 1.4	72.2 ± 1.7	64.3 ± 1.9
Δ*ncs-1* (FK506)	100.0 ± 0.0	74.2 ± 1.8	68.2 ± 1.9	60.2 ± 1.2
Δ*crz-1* (FK506)	100.0 ± 0.0	76.2 ± 1.5	70.1 ± 1.7	62.2 ± 1.9

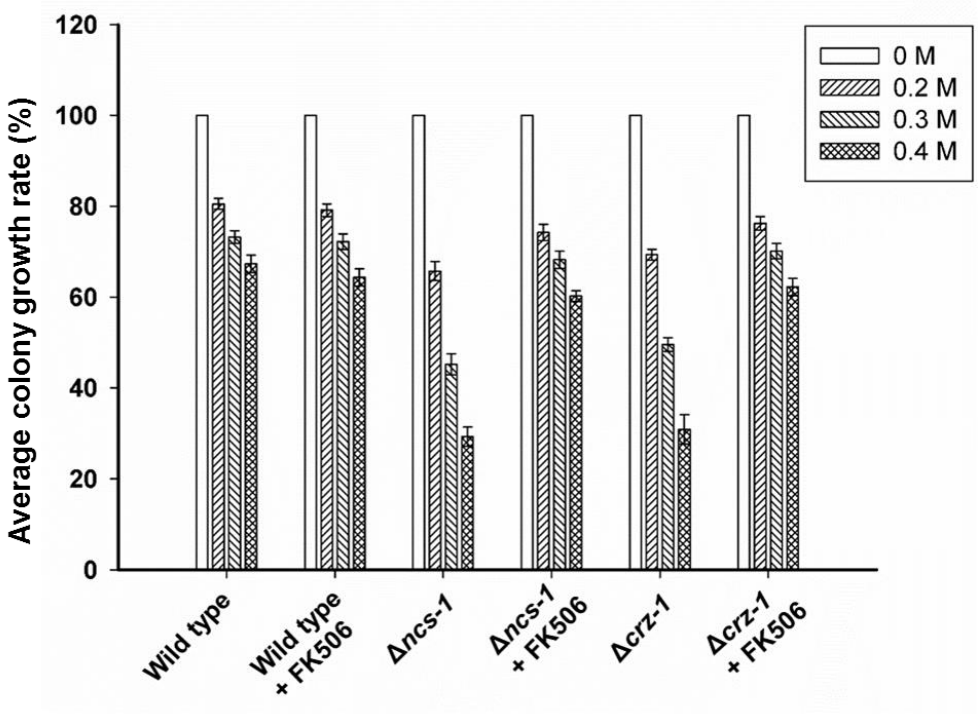

Fig. 3.11: Assay for the tolerance to Ca^{2+} stress in the wild type, Δ*ncs-1*, and Δ*crz-1* mutant strains in the presence of calcineurin inhibitor FK506. The Ca^{2+} sensitive phenotype of the Δ*ncs-1* and Δ*crz-1* mutant strains was rescued by addition of FK506 to VM. Error bars indicate the standard deviation calculated from the data of three individual experiments (n = 3).

Table 3.12: Average colony growth rate (%) of the wild type, Δ*cax* strains at various concentrations of $CaCl_2$ with or without FK506 supplement

Strain (Supplement)	**Average colony growth rate percentage (%) at various concentrations of $CaCl_2$ (M)**			
	0	**0.2**	**0.3**	**0.4**
Wild type	100.0 ± 0.0	80.5 ± 2.1	74.3 ± 2.2	68.2 ± 2.2
Δ*cax*	100.0 ± 0.0	78.3 ± 2.0	73.4 ± 1.8	64.3 ± 2.1
Δ*cax* (FK506)	100.0 ± 0.0	68.3 ± 1.8	44.3 ± 1.9	29.2 ± 2.4

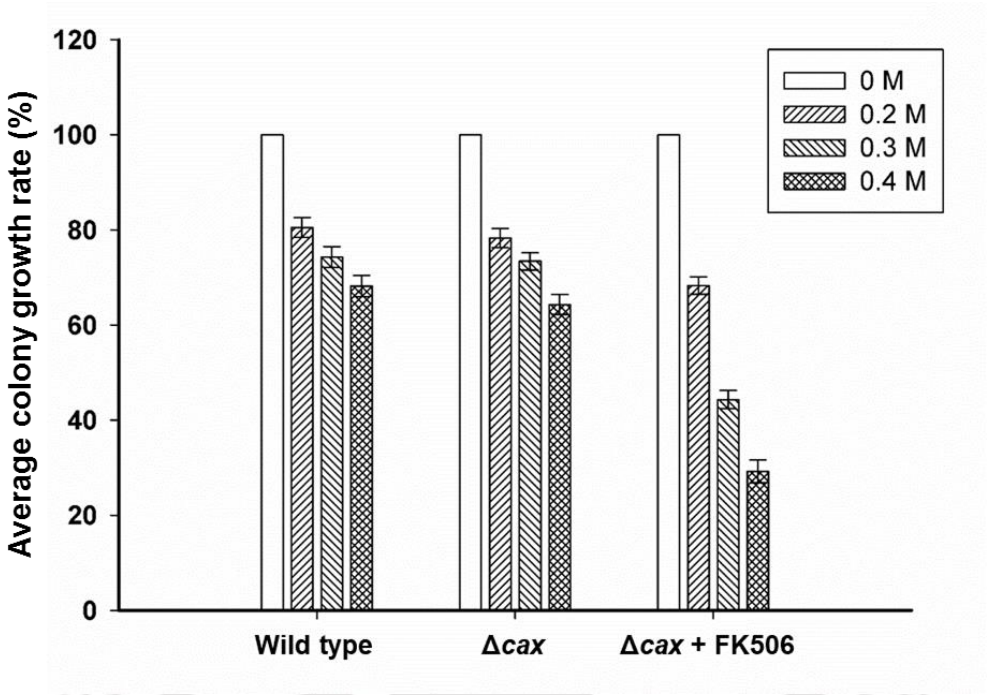

Fig. 3.12: Assay for the tolerance to Ca^{2+} stress in the Δ*cax* strain with or without the addition of FK506 in the VM. The Δ*cax* strain showed Ca^{2+} sensitivity in presence of the calcineurin inhibitor FK506, but it showed Ca^{2+} stress tolerance similar to the wild type in absence of the FK506 in the VM. Error bar indicates the standard deviation calculated from the data of three individual experiments (n = 3).

3.3 Discussion

In this chapter, I described the role of the NCS-1, calcineurin and its target transcription factor CRZ-1 for survival under the Ca^{2+} stress in *N. crassa*. The transcription of the *S. pombe ncs-1* homolog, *ncs1*, was induced by the Ca^{2+} ions (Hamasaki-Katagiri and Ames, 2010). In this study, a gradual increase in the *ncs-1* transcription in response to increasing $CaCl_2$ concentration was observed (Fig. 3.1), suggesting that *ncs-1* transcription is also induced by Ca^{2+} in *N. crassa*. In addition, I showed that NCS-1 overexpression, under the nitrogen-regulatable $P_{nit\text{-}6}$, was able to recover the Δ*ncs-1* Ca^{2+} sensitive phenotype, revealing that NCS-1 is a key player for the tolerance to Ca^{2+} stress in *N. crassa* (Fig. 3.6 A.).

To understand the regulation of the Ca^{2+} induced *ncs-1* transcription in *N. crassa*, I tested the hypothesis that the transcriptional regulation of the calcineurin-CRZ-1 pathway occurs in a manner similar to the *S. pombe*. Therefore, I performed a Ca^{2+} stress tolerance assay in the Δ*crz-1* mutant, which revealed the Ca^{2+} stress sensitive phenotype of the Δ*crz-1* mutant (Fig. 3.7). Therefore, the CRZ-1 transcription factor is also involved in survival under the high Ca^{2+} condition in *N. crassa*. The transcription level of the *ncs-1* was reduced drastically in the Δ*crz-1* mutant, and it remained reduced even under the high Ca^{2+} condition (Fig. 3.8). This result suggested the involvement of the CRZ-1 in the transcription of the *ncs-1* in *N. crassa*. In *S. cerevisiae*, the CRZ-1 homolog *TCN1/CRZ*-1 is dephosphorylated by calcineurin, localized to nucleus regulating the transcription of various target genes (Stathopoulos and Cyert, 1997). Similarly, in *S. pombe*, the CRZ-1 homologue Prz1p, upon dephosphorylation by the calcineurin, translocates into the nucleus (Hirayama *et al.*, 2003) and binds to a region of 130 bp in the *ncs1* promoter, which is upstream of the start codon (ATG), and upregulates the *ncs-1* transcription (Hamasaki-Katagiri and Ames, 2010). Calcineurin is the only reported serine/threonine protein phosphatase that is activated by Ca^{2+}/CaM (Klee *et al.*, 1979; Klee *et al.*, 1998). The other Ca^{2+} sensors CaM and the calcineurin subunit B (CNB) bind to the catalytic calcineurin subunit A (CNA) in response to the increased [$(Ca^{2+})_c$] (Klee *et al.*, 1979; Winkler *et al.*, 1984; Klee *et al.*, 1998; Rusnak and Mertz, 2000; Hogan *et al.*, 2003; Rumi-Masante *et al.*, 2012). In *N. crassa*, inhibition of the calcineurin by FK506 resulted in reduced growth rates in the wild type, the Δ*ncs-1*, and Δ*crz-1* mutants (Fig. 3.9), suggesting an important role of the calcineurin in growth. The qRT-PCR analysis revealed that the calcineurin inhibition by FK506 drastically reduced the transcript level of the *ncs-1* even under the Ca^{2+} stress condition (Fig. 3.10). However, the transcript level of *crz-1* and *mid-1* was not significantly varied due to the calcineurin inhibition in high Ca^{2+} (Fig. 3.10), which showed no significant role of the calcineurin in their transcription under the high Ca^{2+} condition.

Interestingly, inhibition of calcineurin using FK506 did not affect the Ca^{2+} stress tolerance significantly in the wild type, although, there was a moderate decrease in the normal growth rate (Fig. 3.11). Remarkably, the FK506 addition in the media rescued the Ca^{2+} sensitive phenotype of the Δ*ncs-1* and Δ*crz*-1 mutants (Fig. 3.11). This suggested that calcineurin regulates other targets independent of CRZ-1 and NCS-1 for tolerance to Ca^{2+} stress in *N. crassa*. In *S. cerevisiae*, the calcineurin directly inhibits Ca^{2+}/H^{+} exchanger Vcx1, which decreases the vacuolar Ca^{2+} transport (Cunningham and Fink, 1996). In *N. crassa*, CAX, the homolog of Vcx-1, is localized to the vacuoles (Bowman *et al.*, 2009). In addition, the Δ*cax* mutant did not display Ca^{2+} sensitive phenotype like the Δ*ncs-1* and Δ*crz*-1, and accumulated less Ca^{2+} in the vacuoles (Bowman *et al.*, 2011). I found that on the addition of FK506, the Δ*cax* mutant showed sensitivity to high Ca^{2+} (Fig. 3.12). This result indicated that calcineurin might inhibit the CAX by dephosphorylation, as reported in the *S. cerevisiae* (Cunningham and Fink, 1996), and inhibition of the calcineurin by FK506 possibly activates the CAX resulting in increased Ca^{2+} transport to the vacuoles for maintaining the viable $[Ca^{2+}]_c$ level. It might also be possible that the CAX sequesters excess Ca^{2+} into the vacuoles, while the calcineurin activated NCS-1 possibly closes MID-1 channel, and they antagonistically function for survival under Ca^{2+} stress in *N. crassa*. Thus, a possible model is that calcineurin promotes tolerance to Ca^{2+} stress by causing NCS-1 upregulation via the dephosphorylation of CRZ-1 and inhibition of CAX in *N. crassa*. This might explain the rescue of the Ca^{2+} sensitive phenotype in the Δ*ncs-1* and Δ*crz-1* mutants, and the emergence of Ca^{2+} sensitivity in the Δ*cax* mutant in the presence of calcineurin inhibitor FK506.

In summary, under the high Ca^{2+} concentration, the CRZ-1 transcription factor upregulates the expression of NCS-1, which could interact with the MID-1 Ca^{2+} permeable channel in *N. crassa*. Therefore, this study showed that the NCS-1 functions through the calcineurin-*crz-1* signaling pathway, possibly for interaction with the MID-1 channel to

prevent Ca^{2+} influx for survival under the high Ca^{2+} condition in *N. crassa*. In the next Chapter, the molecular mechanism of the NCS-1 mediated pathway for tolerance to Ca^{2+} stress e in *N. crassa* will be described in detail.

Chapter 4

Molecular mechanism of the NCS-1 mediated Ca^{2+} stress tolerance

4.1 Introduction

In the previous Chapter, the role of NCS-1 in the tolerance to Ca^{2+} stress was described. It was also established that the calcineurin and CRZ-1 was essential for the NCS-1 mediated pathway for the tolerance to Ca^{2+} stress. In *S. pombe*, the CRZ-1 homologue Prz1p binds to the *ncs-1* promoter at 130 bp upstream of the ATG start codon in response to Ca^{2+} stress (Hamasaki-Katagiri and Ames, 2010). Moreover, dephosphorylation of Prz1p by calcineurin is required for its nuclear localization and subsequent up-regulation of the *ncs1* promoter activity in the presence of high extracellular Ca^{2+}, indicating that the calcineurin facilitates the activation of Ca^{2+}-induced transcription of *ncs1* (Hamasaki-Katagiri and Ames, 2010). Therefore, in this Chapter, I examined the Ca^{2+} induced binding of the CRZ-1 to the *ncs-1* promoter and also determined the nucleotide sequence of the CRZ-1 binding site.

In *S. pombe*, Ncs-1p interacts with the MID-1 homologue Yam8p to regulate Ca^{2+} influx for maintaining Ca^{2+} homeostasis (Hamasaki-Katagiri and Ames, 2010). In *N. crassa*, the Δ*mid-1* mutant rescued the Ca^{2+} sensitive phenotype of the Δ*ncs-1* mutant, which indicated a possible reduction of Ca^{2+} influx due to the absence of the Ca^{2+}-permeable channel MID-1 providing protection against high extracellular Ca^{2+} (Deka and Tamuli, 2013). Interestingly, the Δ*ncs-1*; Δ*mid-1* double mutant was also able to rescue the Ca^{2+} sensitive phenotype of the Δ*ncs-1* mutant (Deka and Tamuli, 2013), suggesting an interaction between NCS-1 and MID-1 in *N. crassa* as observed in *S. pombe*. Therefore, to understand the molecular mechanism of the NCS-1 function, I examined if, NCS-1 and MID-1 directly interacts to confer tolerance to Ca^{2+} stress in *N. crassa*.

4.2 Results

4.2.1 Cloning of the *crz-1* gene under the coper regulatable *tcu-1* promoter (P_{tcu-1}) and expression of the CRZ-1::5xGly::V5::GFP tagged protein

The homokaryotic strain 559 (Table 2.1) was generated in the laboratory of Prof. Katherine A. Borkovich, and used for the expression of the CRZ-1::5xGly::V5::GFP fusion protein containing the V5 and GFP tags. To generate the 559 strain, the *crz-1* (NCU07952) ORF of length 2190 bp was amplified by PCR using the primers NCU07952-FOR and NCU07952-REV-gFP (Table 2.2) and cloned in the pRS426PVG/tcu-1 vector (Ouyang *et al.*, 2015) digested with SmaI and PacI. The pRS426PVG/tcu-1 vector has *pan-2* (NCU10048) UTRs, a coper regulatable *tcu-1* (NCU00830) promoter (P_{tcu-1}), 5xGly, *v5* and *gfp* tags (Ouyang *et al.*, 2015). P_{tcu-1} is induced by the addition of bathocuproine disulphonate (BCS) and repressed by $CuSO_4$ in the medium (Exley *et al.*, 1993). The plasmid construct pRTCRZ-1 (23) containing P_{tcu-1}::*crz-1*::5*xGly*::*V5*::*gfp* (Fig. 4.1) was transformed into the *N. crassa* recipient strain 52-4-9 (Table 2.1) by electroporation as described in the Chapter 2. The 45-23-crz (Table 2.1) heterokaryotic strain was crossed with 114994 (Δ*crz-1 a*) to generate the homokaryotic strain 559. The 559 strain was PCR-verified (Fig 4.2) for the presence of the *crz-1*::5*xGly*::*V5*::*gfp* allele in the *pan-2* locus (Linkage group VI), and Δ*crz-1*::*hph* allele in the endogenous locus (Linkage group IV) using the primer pairs Ptcu-1F and GFP-Rv (Table 2.2), and HI *crz-1*F and 5HPHR (Table 2.2), respectively.

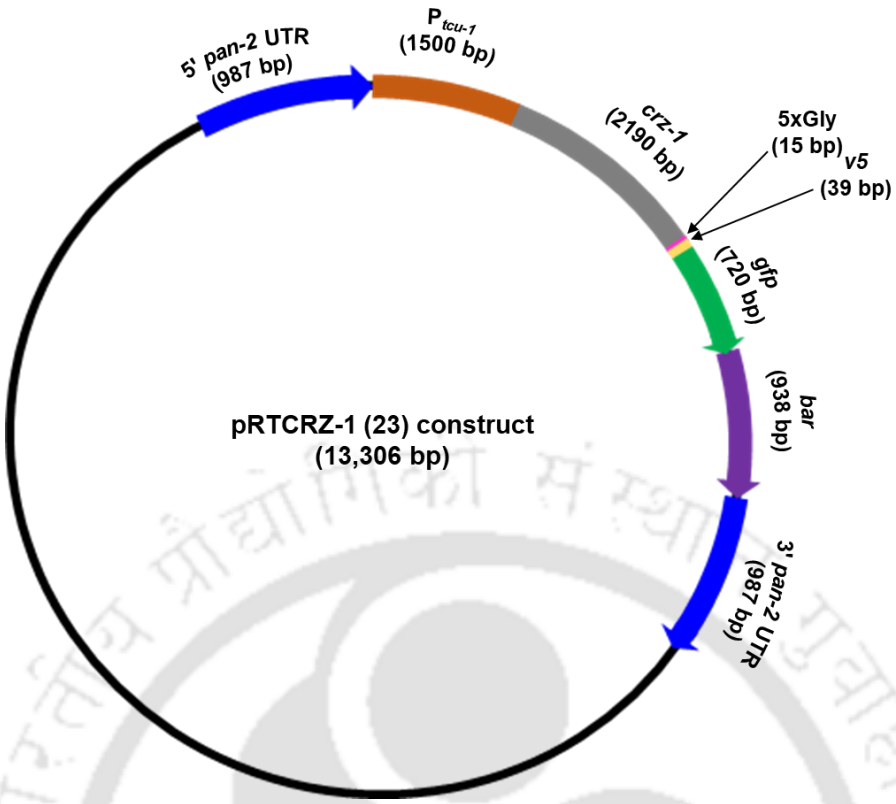

Fig. 4.1: Schematic diagram showing the pRTCRZ-1 (23) plasmid construct with the *crz-1* ORF under the regulatable *tcu-1* promoter (P_{tcu-1}). The pRTCRZ-1 (23) plasmid (13,306 bp) contains a modified pRS426 vector with *pan-2* UTRs, 5xGly, *V5* tag and *gfp* tags (Ouyang *et al.*, 2015), and the *crz-1* ORF cloned into the multiple cloning site (MCS) region. The numbers (in bp) in the parentheses indicate the size of the respective fragment.

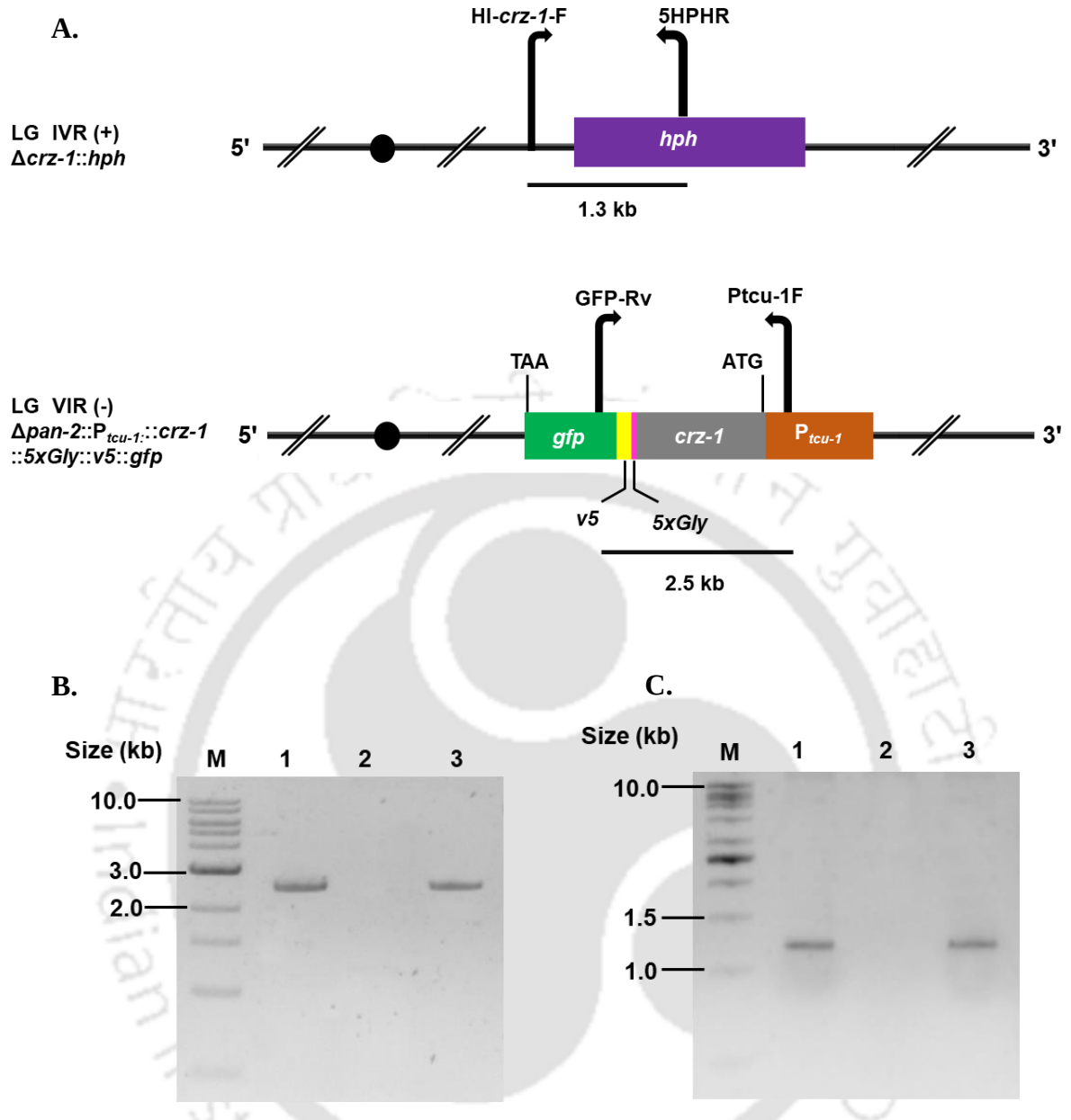

Fig. 4.2: PCR-verification of the homokaryotic strains with *crz-1* expressed under P_{tcu-1}.

A. Schematic diagram showing the primer positions and 5'→3' orientation (shown using the direction of the arrow) used for the verification of the homokaryotic strains containing the *crz-1* expressed under P_{tcu-1}. The primer pairs HI-*crz*-1F and 5HPHR, Ptcu-1F and GFP-Rv (Table 2.2) were used to PCR amplify the Δ*crz-1*::*hph* and *crz-1*::5*xGly*::*V5*::*gfp* alleles of ~1.3 kb and ~2.5 kb, respectively, in the 559 strain.

B. PCR amplification of the P_{tcu-1}::*crz-1*:: *5xGly*::*V5*::*gfp* fragment using the primer pairs Ptcu-1F and GFP-Rv (Table 2.2). The P_{tcu-1}::*crz-1*:: *5xGly*::*V5*::*gfp* fragment of size ~2.5 kb was PCR amplified in the homokaryotic strain 559 (lane 3). The pRTCRZ-1 (23) plasmid (lane 1) and the wild type (FGSC 987) strain (lane 2) were used as positive and negative controls, respectively. PCR products were resolved in 1% agarose gel, using the 1 kb NEB DNA ladder (New England Biolabs, USA) as marker (M).

C. PCR amplification of the Δ*crz-1*::*hph* allele using the primers HI-*crz*-1F and 5HPHR (Table 2.2). The *hph* fragment of size ~1.3 kb (lane 3), indicating the Δ*crz-1*::*hph* allele, is PCR amplified in the homokaryotic strain 559. The Δ*crz-1* 145 strain (lane 1) and the wild type (FGSC 987) strain (lane 2) were used as a positive and negative controls, respectively. PCR products were resolved in a 1% agarose gel, using the 1 kb NEB DNA ladder (New England Biolabs, USA) as marker (M).

4.2.2 Expression of the CRZ-1::5xGly::V5::GFP protein in inducing and repressing conditions

The pRTCRZ-1 (23) construct was transformed into the *N. crassa* strain 52-4-9 (Table 2.1) to express a fusion protein CRZ-1::5xGly::V5::GFP (~105 kDa) under P_{tcu-1}. In the *N. crassa* strain 559, the expression of the CRZ-1::5xGly::V5::GFP in both the induction and repression conditions was analyzed by western blot. For western blot, 559 strain was cultured in the standard VM liquid containing BCS (250 µM) for induction and $CuSO_4$ (250 µM) for repression and incubated at 30 °C with shaking at 180 rpm for 16 h. The wild type (FGSC 987) strain grown in both the inducing and repressing media was taken as negative controls. The western blot was performed by using anti-GFP rabbit antibody as described in the Chapter 2. The western blot analysis revealed that the CRZ-1::5xGly::V5::GFP expression was induced by BCS, and reduced by the addition of $CuSO_4$ (Fig. 4. 3). In addition, to test if, expression of

the CRZ-1::5xGly::V5::GFP fusion protein could complement the Ca^{2+} sensitive phenotype of the Δ*crz-1* mutant, I performed an assay for tolerance to Ca^{2+} stress assay in both the inducing and repressing media. The 559 strain displayed Ca^{2+} stress tolerance similar to the wild type strain in the inducing medium, suggesting that expression of the CRZ-1::5xGly::V5::GFP protein complements the Ca^{2+} sensitive phenotype in the Δ*crz-1* mutant (Table 4.1; Fig. 4.4A). On the other hand, the 559 strain was sensitive to the Ca^{2+} stress like the Δ*crz-1* mutant in the repressing medium (Table 4.2, Fig. 4.4B). The complementation assay showed that the CRZ-1::5xGly::V5::GFP fusion protein expressed in the 559 strain was functionally active, and therefore, further used for chromatin immunoprecipitation (CHIP) assay.

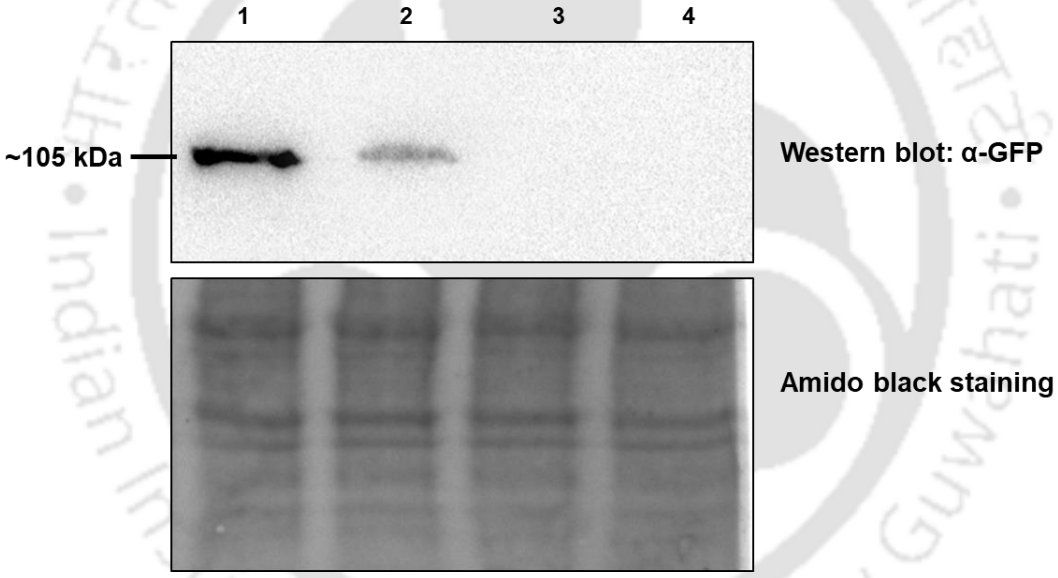

Fig. 4.3: Expression of CRZ-1::5xGly::V5::GFP under P_{tcu-1} in the inducing and repressing conditions. Western blot showing the expression of CRZ-1::5xGly::V5::GFP (~105 kDa) under P_{tcu-1} in the 559 strain. The CRZ-1::5xGly::V5::GFP is expressed in the inducing VM containing 250 µM BCS (lane 1), and reduced in the VM containing 250 µM $CuSO_4$ (lane 2), in the 559 strain cultured for 16 h at 30 °C with shaking at 180 rpm. The wild type strain was grown in inducing and repressing conditions (lanes 3 and 4), respectively, for

16 h as a negative control and showed no expression. The amido black staining of the membrane is shown in the lower panel demonstrates the equal protein loading.

Table 4.1: Average colony growth rate (%) of the wild type, Δ*crz-1*, and 559 strains at various concentrations of $CaCl_2$ in the inducing media

Strains	**Average colony growth rate (%) at various concentrations of $CaCl_2$ (M)**			
	0	**0.2**	**0.3**	**0.4**
Wild type	100.0 ± 0.0	90.2 ± 1.9	83.0 ± 1.8	72.0 ± 1.7
Δ*crz-1*	100.0 ± 0.0	79.3 ± 1.8	60.5 ± 2.7	52.4 ± 1.7
559	100.0 ± 0.0	93.3 ± 1.7	80.1 ± 1.6	74.2 ± 1.9

Table 4.2 Average colony growth rate (%) of the wild type, Δ*crz-1*, and 559 strains at various concentrations of $CaCl_2$ in the repressing media

Strain	**Average colony growth rate (%) at various concentrations of $CaCl_2$ (M)**			
	0	**0.2**	**0.3**	**0.4**
Wild type	100.0 ± 0.0	86.5 ± 1.4	77.5 ± 1.3	62.0 ± 1.4
Δ*crz-1*	100.0 ± 0.0	62.5 ± 1.5	40.5 ± 1.7	26.2 ± 1.9
559	100.0 ± 0.0	60.1 ± 1.7	38.5 ± 2.2	23.8 ± 1.9

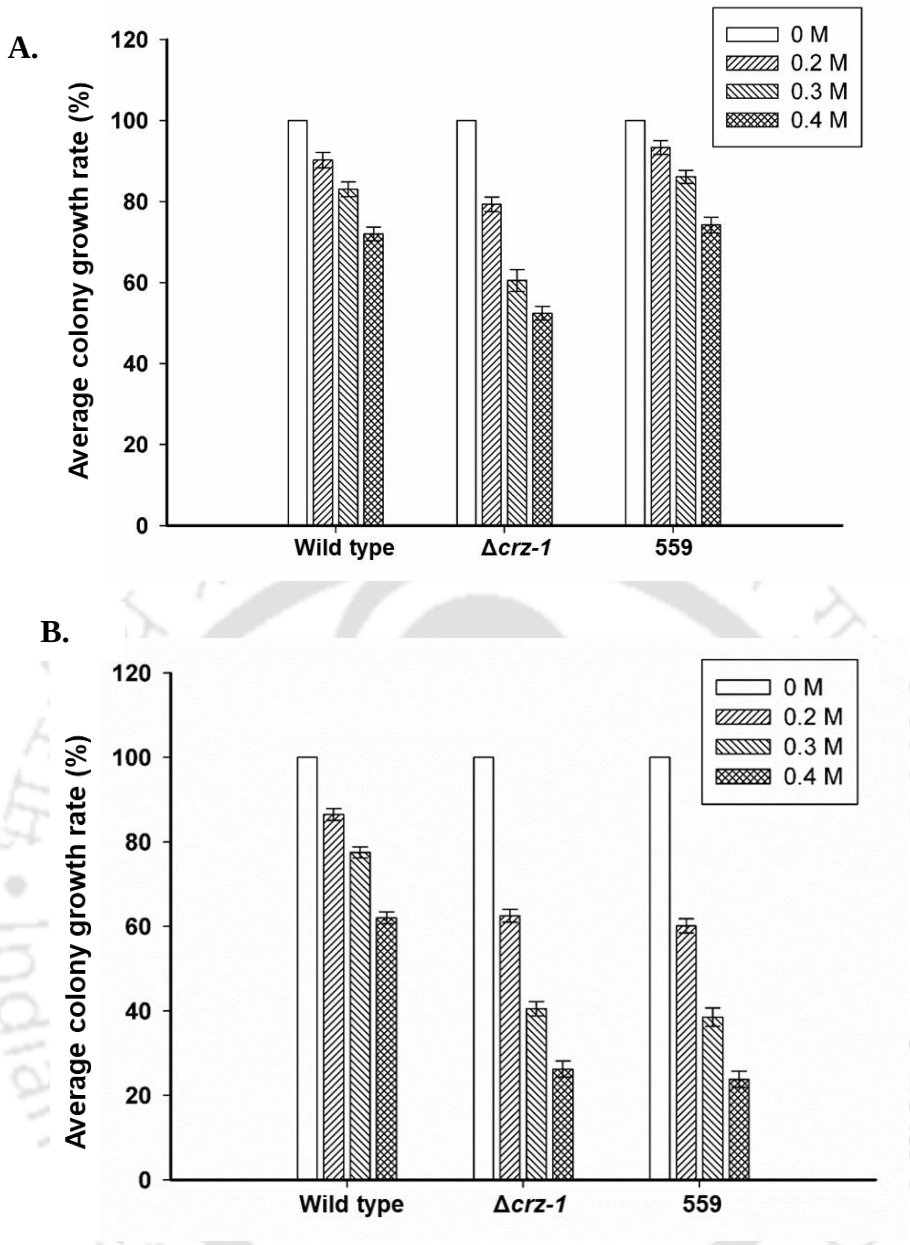

Fig. 4.4: Assay for the tolerance to Ca^{2+} stress for the 559 strain under the inducing and repressing conditions. Error bars indicate the standard deviation calculated from the data of three individual experiments (n = 3).

A. For the induction of $P_{tcu\text{-}1}$::*crz-1*::*5xGly*::*V5*::*gfp*, 250 µM BCS was added to the VM liquid medium. The Ca^{2+} sensitive phenotype of the Δ*crz-1* mutant is recovered in the 559 strain under the inducing condition.

B. For the repression of $P_{tcu\text{-}1}$::*crz-1*::*5xGly*::*V5*::*gfp*, 250 µM $CuSO_4$ was added to the VM. The 559 strain showed sensitivity to Ca^{2+} stress like the Δ*crz-1* mutant in the repressing condition.

4.2.3 Chromatin immunoprecipitation assay

Chromatin immunoprecipitation (CHIP) assay was performed using 5 h old germlings of the 559 strain (Table 2.1). Approximately 5 x 10^6 conidia/ml were inoculated in 50 ml standard VM liquid (0.68 mM), and VM supplemented with 0.2 M $CaCl_2$, and grown for 5 h at 30 ºC and shaking at 180 rpm. Both the growth media were supplemented with 50 µM BCS and 10 µg/ml pantothenic acid. The germlings were harvested and washed twice with 1X phosphate-buffered saline (PBS, pH 7.4), then 1% formaldehyde was added to the cultures and incubated at room temperature on a rotating platform for 30 min for chemical crosslinking. To quench the reaction, 125 mM glycine was added and incubated for 10 min at room temperature. Germlings were harvested and washed twice with 1X PBS and suspended in CHIP lysis buffer. Chromatin was sheared by sonication in a sonicator (Vibra cell sonics, USA) on ice. The parameters for the sonication were 33% amplitude, 8 s ON pulse, 10 s OFF pulse, 120 cycles, and 16 min time. CHIP was performed as described in the Chapter 2. Three pairs of overlapping PCR primers, CHIP-1F and CHIP-1R, CHIP-2F and CHIP-2R, and CHIP-3F and CHIP-3R covering the entire 1548 bp of the *ncs-1* promoter region, to PCR amplify six overlapping fragments of different sizes (Table 2.2; Fig. 4.5) were designed for determining the binding position of the CRZ-1 to the *ncs-1* promoter. All the PCRs were performed by using Phusion® High-Fidelity DNA polymerase (Cat. no. M0530S, New England Biolabs, USA) using the reaction conditions- 98 ºC for 30 s, 25 cycles of 98 ºC for 10 s, 63 ºC for 30 s and 72 ºC for 30 s, and then 72 ºC for 5 min. The PCR products were run on 1% agarose gel containing EtBr (0.5 µg/ml) and visualized in a gel doc (Bio-Print ST4, Vilber Lourmat, France).

In the ChIP analysis, positive PCR bands were observed only for the 1135 bp (III) and 535 bp (VI) fragments, amplified using the primers Chip 2F and Chip 1R, and ChIP 1F and ChIP 1R, respectively (Fig. 4.6). The band intensity of the positive ChIP was higher for the 535 bp (VI) fragment. The PCR product for the 535 bp (VI) fragment was further verified by sequencing (Figs. 4.7, 4.8), which confirmed that the CRZ-1 transcription factor binds to the *ncs-1* promoter. Moreover, there was ~6-fold increase in the band intensity of the positive ChIP for the strain grown in the medium supplemented with 0.2 M $CaCl_2$ compared to the strain grown in the normal VM, indicating that binding of CRZ-1 to the *ncs-1* promoter was increased during high Ca^{2+} condition.

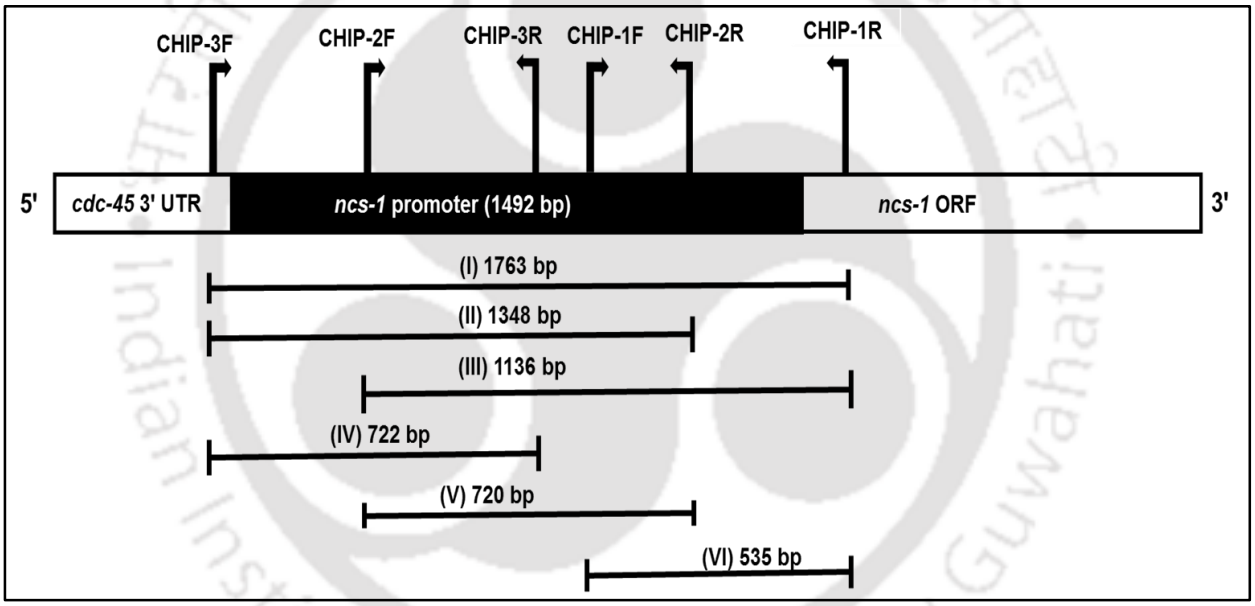

Fig. 4.5: Schematic showing the primer pairs and their position for the CHIP analysis. The primers designed to perform PCR for the *ncs-1* promoter region using the DNA template obtained in the ChIP are located between the 3′ UTR of *cdc-45* (5′ proximal gene of *ncs-1*) and the *ncs-1* ORF. The primers CHIP-3F and CHIP-1R, CHIP-3F and CHIP-2R, CHIP-3F and CHIP-1R, CHIP-2F and CHIP-1R, CHIP-3F and CHIP-3R, CHIP-2F and CHIP-2R, and CHIP-1F and CHIP-1R, were used to PCR amplify six fragments I, II, III, IV, V, and VI, respectively, of different sizes as indicated in the diagram.

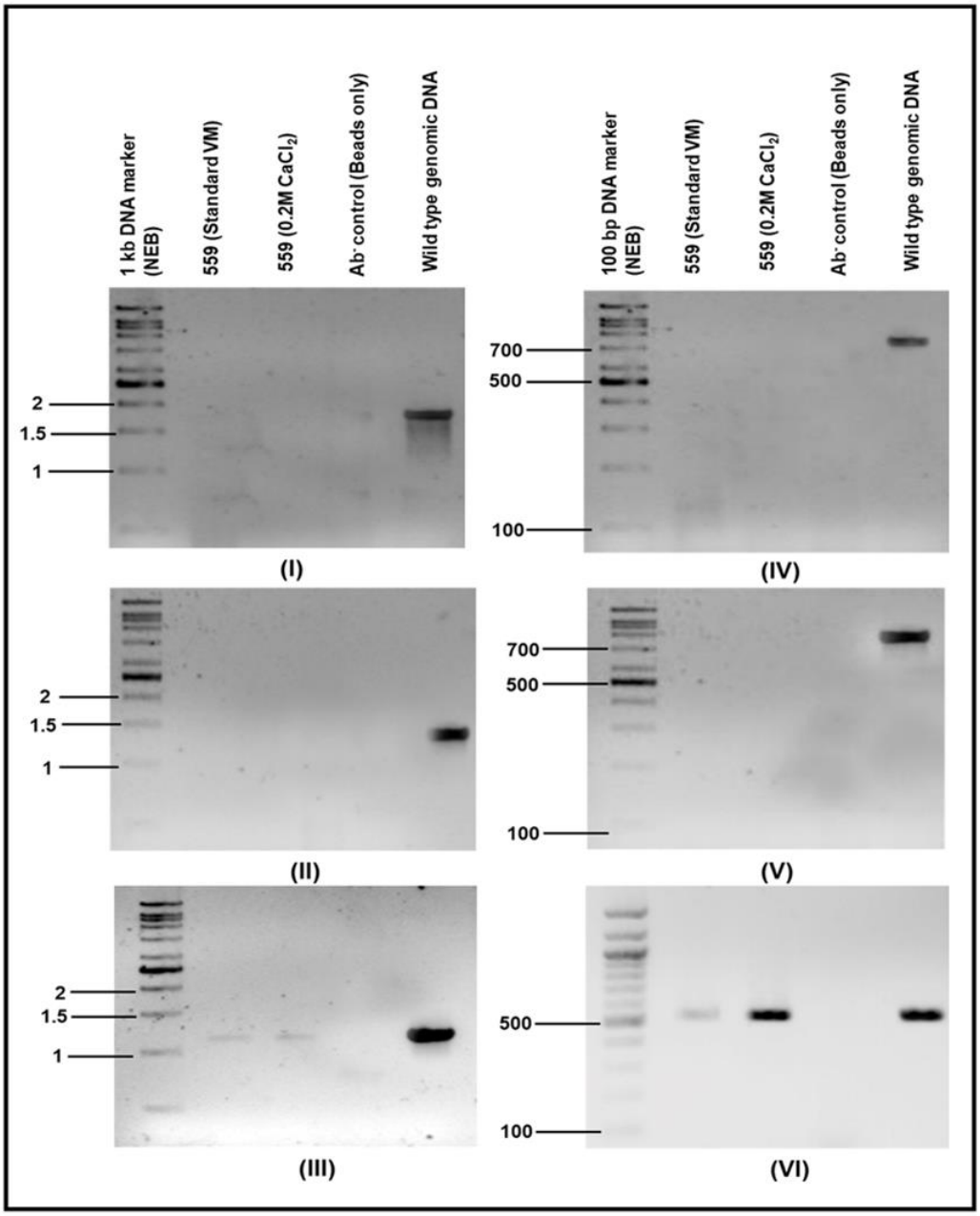

Fig. 4.6: CHIP assay to determine the binding of CRZ-1 to the *ncs-1* promoter sequence. PCR products were analyzed using a 1% agarose gel to identify the CRZ-1 binding region in the *ncs-1* promoter sequence. The PCR amplification for each of the six fragments (I to VI) is indicated below the gel. The analysis of the PCR revealed a positive product for the fragment VI of 535 bp in size, and the band intensity was further enhanced, when the 559 strain was grown in the presence of $CaCl_2$ stress condition. The PCR amplified fragment VI was further confirmed by sequencing. PCR amplification for the fragment III was also observed, however,

the intensities of products were similar in both normal and in the $CaCl_2$ stress condition. The antibody control (Ab^-) indicates the control PCR for the sample, where, only beads were used for immunoprecipitation. The wild type genomic DNA has used a positive PCR control for amplification of all the six fragments.

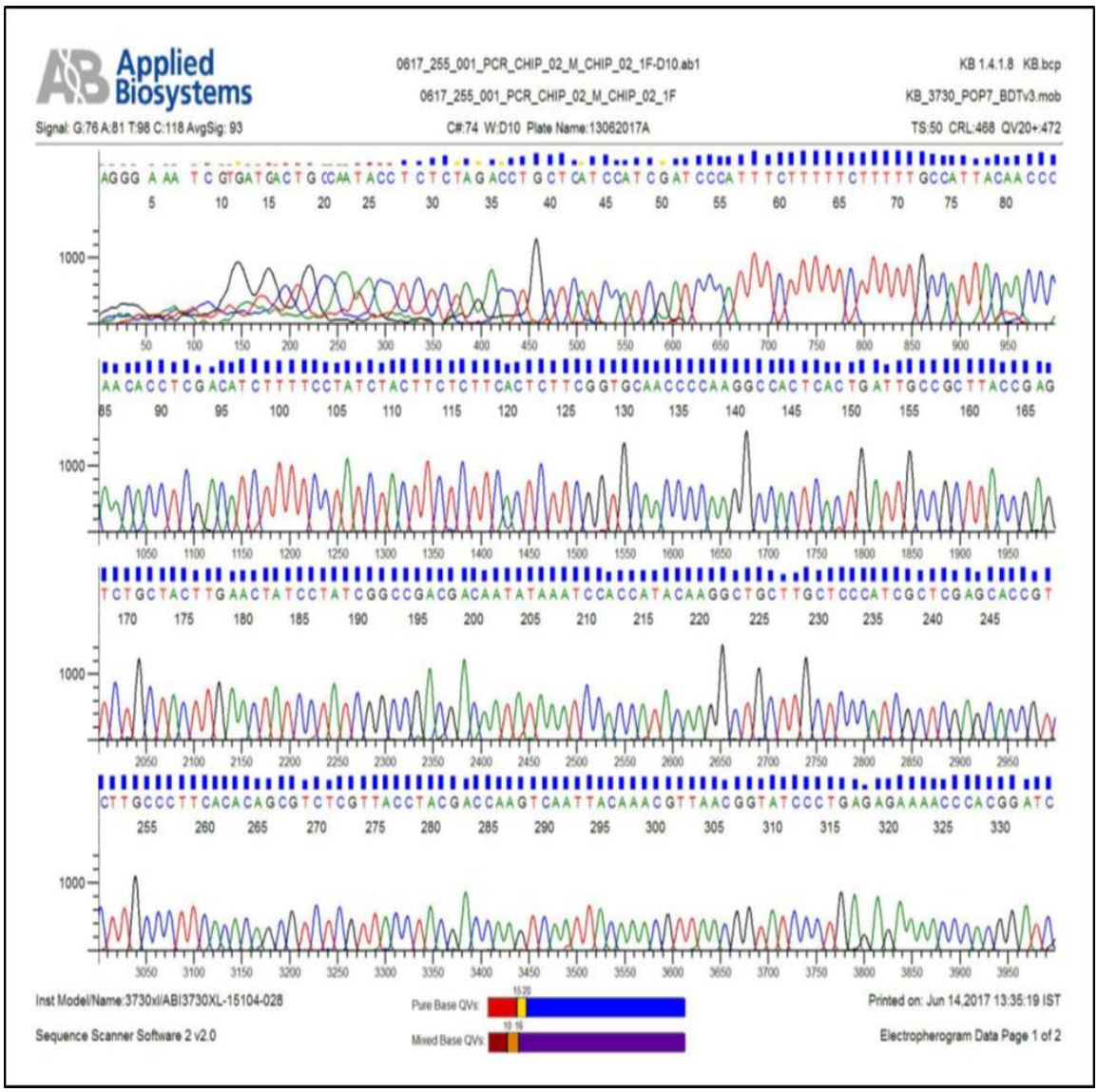

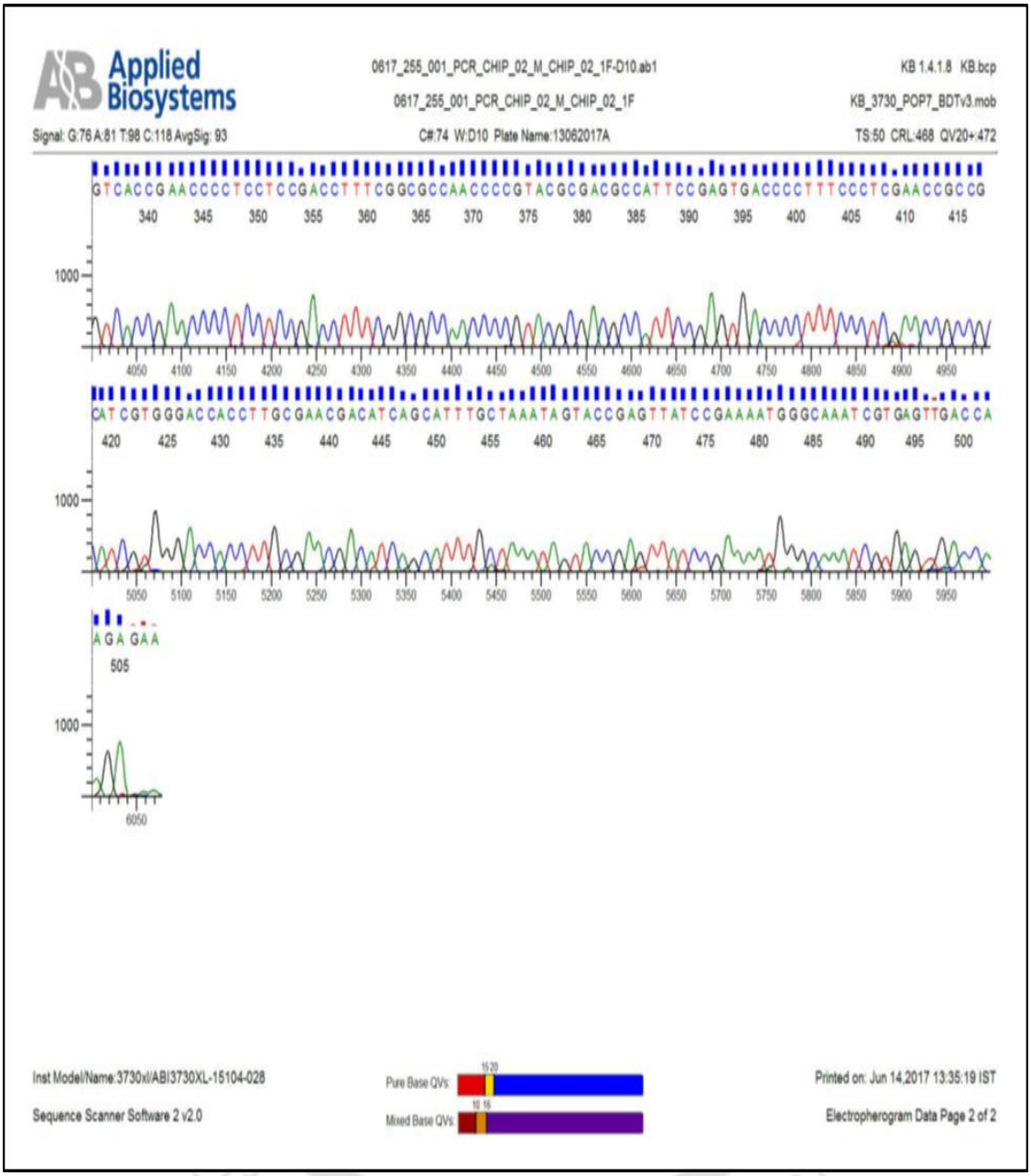

Fig. 4.7: Chromatogram profile of the *ncs-1* promoter fragment generated by sequencing of the fragment VI. The PCR product fragment VI of size 535 bp was obtained from the immunoprecipitated chromatin fraction by using the primers CHIP-1F and CHIP-1R. Sequencing was performed by using the forward primer CHIP-1F.

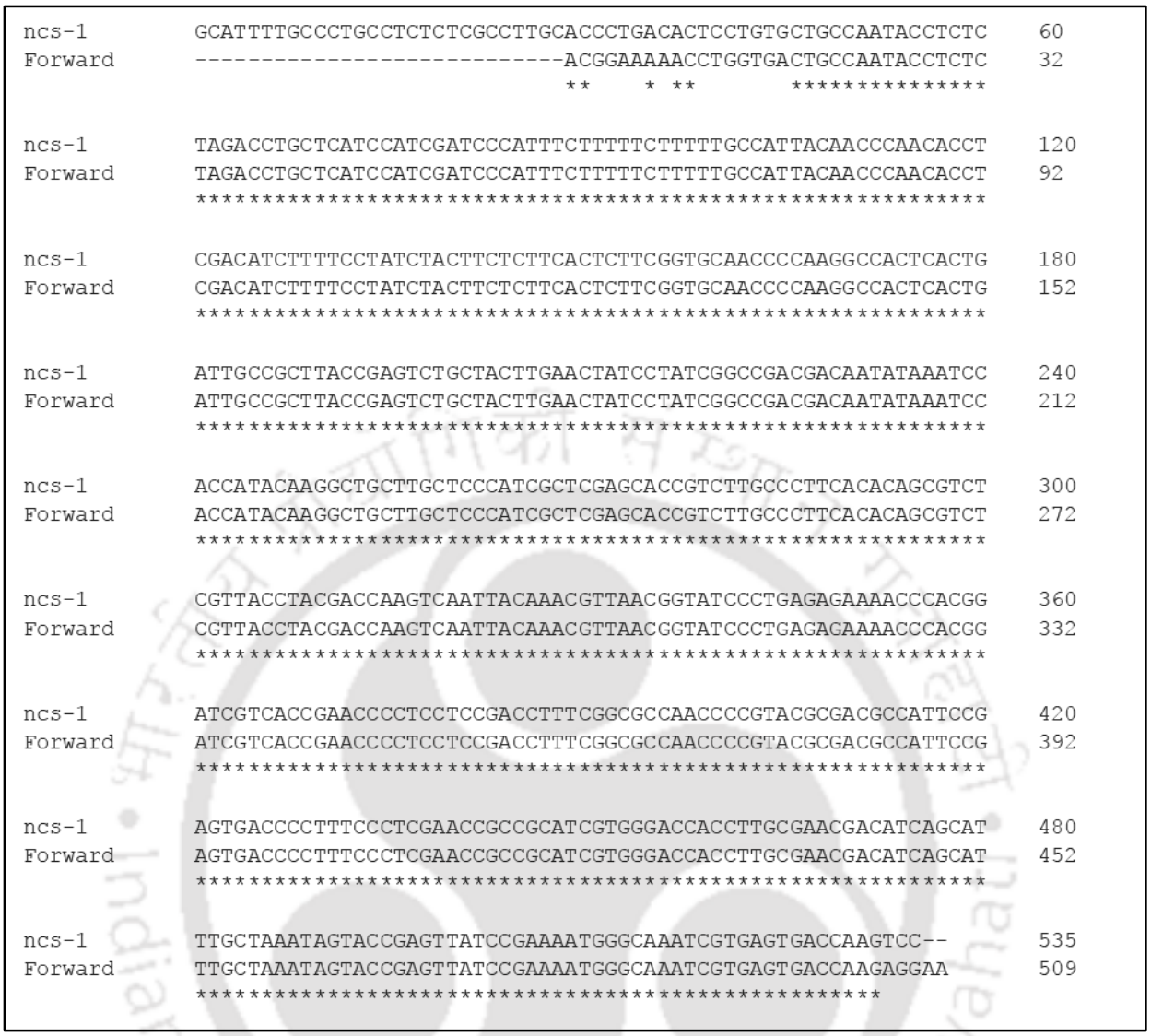

Fig. 4.8: Confirmation of the PCR product fragment VI as the *ncs-1* promoter fragment.

The sequence of the PCR product fragment VI of size 535 bp, obtained by DNA sequencing, was aligned with the corresponding promoter sequence using the ClustralX. Asterisks below the alignment indicate the identical nucleotide and absence of asterisk below indicates unmatched nucleotides in the alignment. The sequencing confirmed that CRZ-1 binds to a 535 bp fragment of the *ncs-1* promoter.

4.2.4 The electrophoretic mobility shift assay revealed that the CRZ-1 binding site in the *ncs-1* promoter is located upstream of the TATA box

The ChIP assay revealed that the CRZ-1 transcription factor binds to the *ncs-1* promoter and the binding increases with the increasing Ca^{2+} concentration. But, the CRZ-1 binding sequence in the *ncs-1* promoter remained unknown. Therefore, to determine the CRZ-1 binding sequence, I designed and performed an electrophoretic mobility shift assay (EMSA). EMSA was performed using a Molecular probes™ EMSA Kit (Cat no. E33075, Life Technologies, USA) as per the manufacturer's protocol. The TATA box is present 270 bp upstream of the start codon (ATG), which is within the 535 bp fragment identified by the CHIP analysis (Fig. 4.6). I designed four DNA probes of sizes 297 bp, 231 bp, 150 bp and 147 bp for EMSA. (Fig. 4.9). The 231 bp and 297 bp probes lie upstream and downstream of the TATA box, respectively, and the 150 bp and 147 bp probes lie within the 297 bp fragment downstream of the TATA box (Fig. 4.9). The DNA probes were prepared by PCR from the wild type *N. crassa* genomic DNA using the PCR primers CHIP-1F, CHIP-1R, EMSA-1F, EMSA-1R, EMSA-2F, and EMSA-2R in appropriate pairs (Table 2.2; Fig. 4.9), and Phusion® High-Fidelity DNA polymerase (Cat. no. M0530S, New England Biolabs, USA). The PCR products were analyzed in a 1% agarose gel and later purified by using PCR purification kit (Cat. No. 28104, Qiagen, Germany). The CRZ-1::5xGly::V5::GFP (~105 kDa) and V5::GFP (~28 kDa) proteins were isolated and purified from the 559 and P*ccg-1*::GFP strains (Table 2.1) as described in the Chapter 2 and were run on a 10% SDS- polyacrylamide (30:1) gel to check the purity (Fig. 4.10). To test protein-DNA binding, the purified CRZ-1::5xGly::V5::GFP protein (50 µM) was incubated with the respective DNA probes (5 µM**).** Protein-DNA complexes were resolved in a 10% non-denaturing polyacrylamide (30:1)/1X TBE gel at 200 volts for 1 h in 1 X TBE running buffer and stained with SYBR® Green provided with the EMSA kit. The gel was visualized in a gel doc (Bio-Print ST4, Vilber Lourmat, France). Band shifts were

observed only for the probes VI-I (297 bp) and VI-IV (47 bp) in the EMSA (Fig. 4.10). Therefore, CRZ-1 binding site is located within the147 bp fragment located upstream of the TATA box in the *ncs-1* promoter.

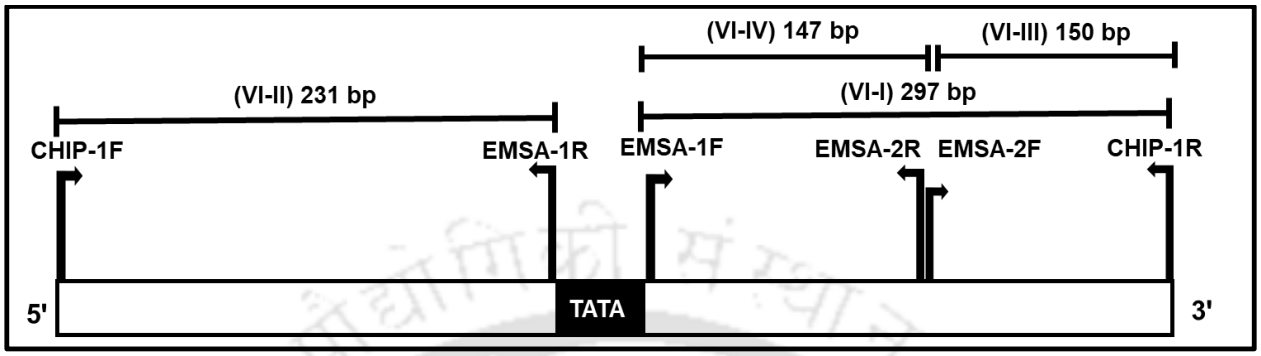

Fig. 4.9: Schematic showing the position of the PCR primers to map the CRZ-1 binding sequence in the fragment VI of the *ncs-1* promoter shown using a bar. The primers, indicated using arrows, were used for PCR amplification of four different DNA probes, VI-I to VI-IV, of indicated size (bp) for the EMSA. The relative position of the TATA box with respect to the primer position is shown.

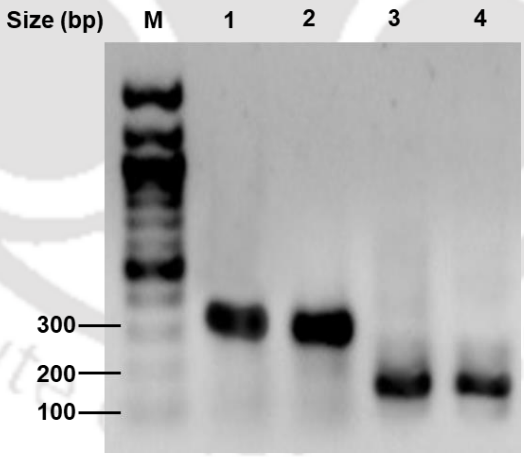

Fig. 4.10: Verification of the DNA probes obtained by PCR. The four DNA probes VI-I to VI-IV were obtained by PCR amplification using the *N. crassa* wild type (FGSC 987) genomic DNA as a template and the primers CHIP-1F, CHIP-1R, EMSA-1F, EMSA-1R, EMSA-2F, and EMSA-2R in appropriate combination as shown in the Fig. 4.9. The probes were verified by running on a 1% agarose gel using 100 bp NEB DNA ladder (New England Biolabs, USA)

indicated as M. Lanes 1, 2, 3 and 4 indicate the DNA probes VI-I, VI-II, VI-III, and VI-IV, respectively.

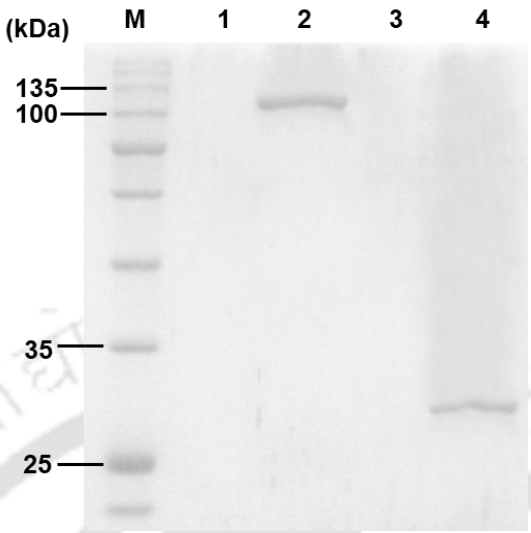

Fig. 4.11: Purification of the CRZ-1::5xGly::GFP::V5 and GFP::V5 proteins. The purified CRZ-1::5xGly::V5::GFP and V5::GFP protein samples were run on a 10% SDS-PAGE gel and visualized by Coomassie Brilliant Blue (CBB) staining. Single bands were observed in the lanes 2 and 4 loaded with CRZ-1::5xGly::V5::GFP (~105 kDa) and V5::GFP (~28 kDa) proteins, respectively, which indicate purified proteins. Prestained protein marker (Himedia, India) was loaded in the lane indicated as M. Lanes 1 and 3 were kept as blanks.

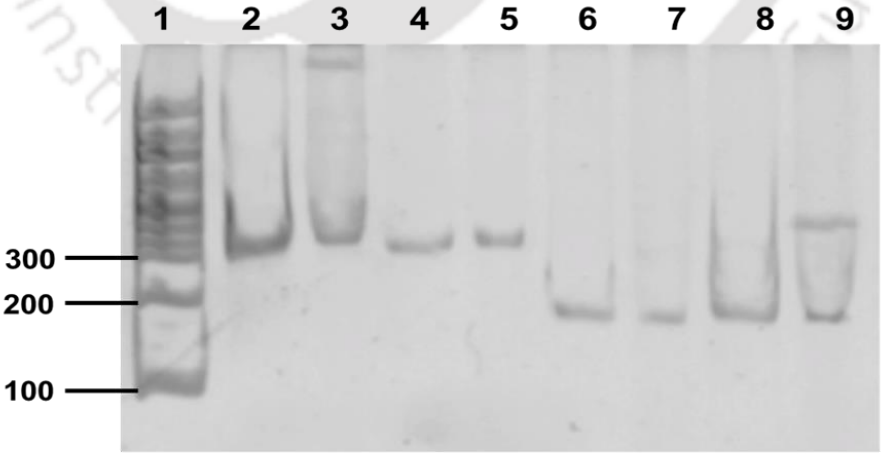

Fig. 4.12: CRZ-1 binding to the specific DNA probe. The 100 bp DNA ladder (New England Biolabs, USA) (lane 1), DNA probes only controls (lanes 2, 4, 6, and 8), and the reaction

mixture containing both the DNA probe and the CRZ-1::5xGly::V5::GFP protein (lanes 3, 5, 7, and 9) were resolved in a 10% non-denaturing polyacrylamide gel and stained with SYBR® Green. The DNA probe VI-I (lanes 2 and 3), VI-II (lanes 4 and 5), VI-III (lanes 6 and 7), and VI-IV (lanes 8 and 9) were used either alone or with the protein as described above. The gel shifts were observed for the probes I of 297 bp (lane 3) and IV of 147 bp (lane 9), which further maps the CRZ-1::5xGly::V5::GFP protein binding region in the *ncs-1* promoter.

4.2.5 Prediction of the putative nucleotide sequence of the CRZ-1 binding site and preparation of duplex probes

The EMSA revealed that the CRZ-1 binding site of the *ncs-1* promoter is located upstream of the TATA box within the 147 bp fragment. To identify the specific nucleotide sequence essential for CRZ-1 binding within this 147 bp region in the *ncs-1* promoter, 10 putative binding sites of 8 bp in size were predicted (Table 4.3) using the online tool "DNA binding site predictor for Cys_2His_2 Zinc Finger Proteins" (http://zf.princeton.edu; Persikov *et al.*, 2008; Persikov and Singh, 2013). Based on the predicted results (Table 4.3), I designed three 30 bp duplex DNA probes (Fig. 4.13) containing the first two putative nucleotide sequences with highest support vector machine (SVM) score and the lowest *p*-value for performing the second round of EMSA. Among the three probes, two were normal probes (A and C) the remaining one was mutated probe (C) which was to be used as negative control. The 30 bp duplex DNA probes were prepared from the complementary primer pairs, Dup-1F and Dup-1R, Dup-2F and Dup-2R, and Dup-2MF and Dup-2MR (Table 2.2) as described in the Chapter 2. The three duplex probes were run on a 15% non-denaturing polyacrylamide (30:1)/1 X TBE gel at 200 volts for 1 h in 1 X TBE running buffer and stained with EtBr to test whether the probes were generated properly (Fig. 4.14).

Table 4.3: Predicted CRZ-1 binding sequence

Predicted DNA sequence (5'→3')	SVM score	+*p*-value
CCTTCACA	5.9687	0.006
CCATCGCT	5.9630	0.006
CCTCCTCC	5.9122	0.006
AGCGTCTC	5.7584	0.006
CCTCCGAC	5.0652	0.012
GCTGCTTG	5.0586	0.012
CCTACGAC	5.0257	0.012
CACACAGC	4.7290	0.018
GCGTCTCG	4.6137	0.021
CGAGCACC	4.5953	0.021

+*p*-values were calculated using following background nucleotide Probabilities-*P*(a)=0.2500: P(c)=0.2500: P(g)=0.2500: P(t)=0.2500

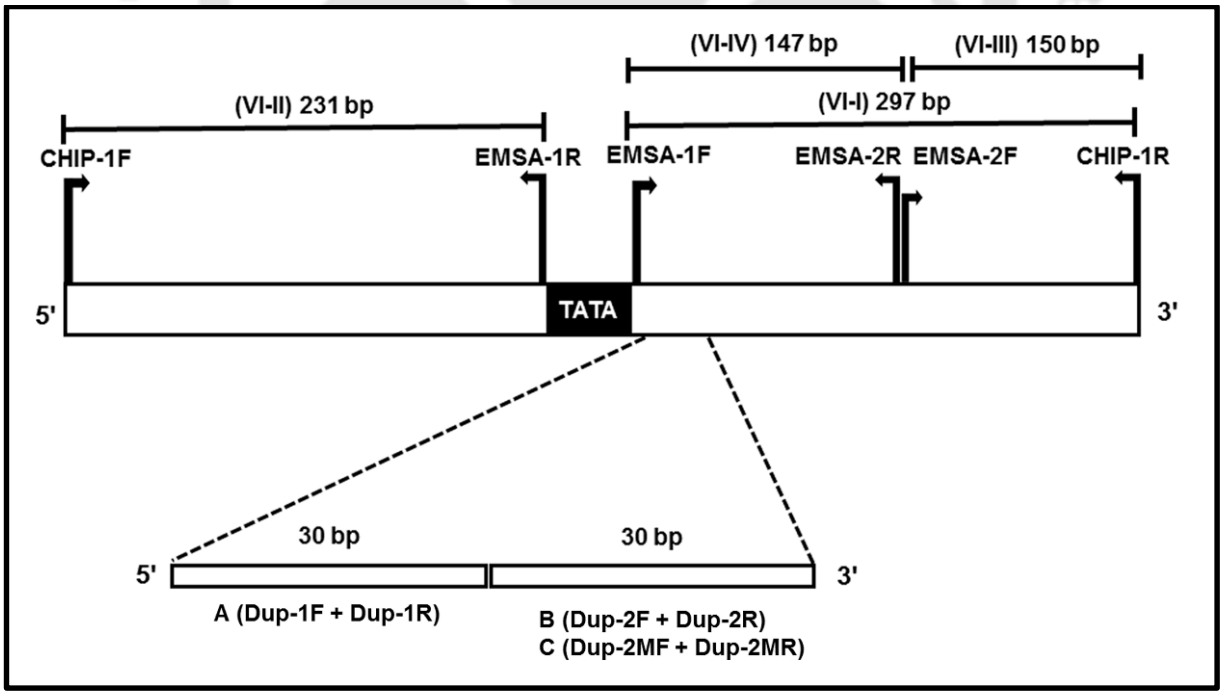

Fig. 4.13: Schematic showing the position of the duplex DNA probes in the CRZ-1 binding 147 bp fragment of the *ncs-1* promoter. The positions of the two duplex DNA probe A and

B of 30 bp each is indicated below the *ncs-1* promoter. The position of mutated probe C is same as the B. The primers to obtain each of the probes are indicated in the parentheses for the respective probe.

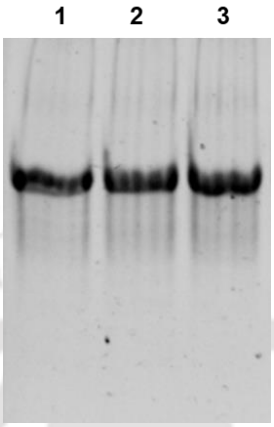

Fig. 4.14: Verification of the synthesis of the duplex DNA probes. The three 30 bp DNA probes were run on a 15% non-denaturing polyacrylamide (30:1)/1 X TBE gel at 200 volts for 1 h in 1 X TBE running buffer and visualized using ethidium bromide (EtBr) staining. Lanes 1, 2, and 3 were loaded with probes A, B, and C, respectively, and single band in each lane shows the successful synthesis of all the three probes.

4.2.6 Identification of an 8 bp fragment essential for the CRZ-1 binding to the *ncs-1* promoter

An EMSA was performed using the purified CRZ-1::5xGly::V5::GFP protein and the respective duplex DNA probes as described in the Chapter 2. Additionally, the purified V5::GFP protein was also incubated with the probes as a control. Protein-DNA complexes were resolved in a 15% non-denaturing polyacrylamide (30:1)/1 X TBE gel at 200 volts for 1 h in 1 X TBE running buffer and stained with SYBR® Green provided in the EMSA kit. The gel was visualized in a Gel Doc (Bio-Print ST4, Vilber Lourmat, France). Band shift was observed for the probe C containing the sequence 5′-CCTTCACA-3′ (Fig. 4.15), suggesting the CRZ-1 binding to the probe C. Furthermore, no shift was observed for either the probe A

containing the 8 bp sequence 5′-CCATCGCT-3′ or the probe C where the 8 bp 5′-CCTTCACA-3′ nucleotide sequence was mutated to 5′-AAGGACAA-3′ (Fig. 4.15). Therefore, *N crassa* CRZ-1 specifically binds to an 8 bp nucleotide sequence 5′-CCTTCACA-3′, located 216 bp upstream of the ATG start codon. Based on the data from the results described in the previous section, I extrapolated that binding of CRZ-1 upregulates the expression of the *ncs-1* during Ca^{2+} stress.

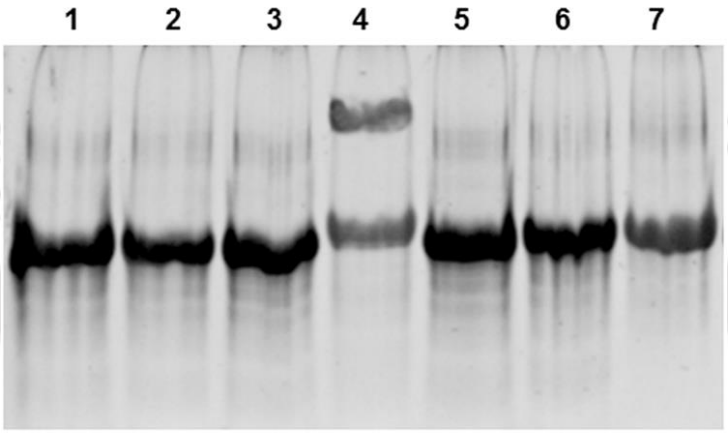

Fig. 4.15: Identification of the CRZ-1 binding sequence in the *ncs-1* promoter region. The DNA probes A, B, and C were used alone as controls (lanes 1, 3, and 5, respectively) or together with the CRZ-1::5xGly::V5::GFP protein (lanes 2, 4, and 6, respectively). A shift was observed when probe B was used together with the protein (lane 4), showing that CRZ-1::5xGly::V5::GFP binds to probe B that contains the predicted CRZ-1 binding sequence site 5´-CCTTCACA-3´. The shift was not observed for the probe C containing mutations in the predicted CRZ-1 binding site (lane 6). In lane 7, 5xGly::V5::GFP protein with probe B was used as a negative control and no shift was observed.

4.2.7 Confocal microscopy showed that NCS-1 localized to the plasma membrane during Ca^{2+} stress indicating a putative interaction with the Ca^{2+}-permeable channel MID-1

In *S. pombe*, Ncs1p interacts directly with Yam8p channel present in the plasma membrane to prevent the Ca^{2+} efflux providing tolerance during Ca^{2+} stress (Hamasaki-Katagiri and Ames, 2010). In *N. crassa*, Ca^{2+} permeable channel MID-1 is the homolog of the *S. pombe* Yam8p and it is also localized to the plasma membrane (Lew *et al*., 2008; Deka and Tamuli, 2013). Therefore, I examined, if the *N. crassa* NCS-1 also interacts with MID-1 during Ca^{2+} stress. I performed confocal microscopy using the strain $P_{nit\text{-}6}$::*ncs-1* (21) to test if, NCS-1 localizes to the plasma membrane in presence high Ca^{2+}. For confocal microscopy, conidia of $P_{nit\text{-}6}$::*ncs-1* (21) strain were harvested in sterile water from the three days old cultures grown on standard VM agar plates supplemented with pantothenic acid. An equal amount of conidial suspension was inoculated in 20 ml VM liquid in two 100 ml flasks one containing 0.2 M $CaCl_2$ and the other without $CaCl_2$. The tubes were incubated for 4 h at 30 ºC and shaking at 180 rpm. For visualization of the plasma membrane, FM™4-64 dye (Cat. No. T3166, Life Technologies, USA) was used as per standard protocol from the manufacturer. Microscopy was performed using a Leica TCS SP8 (DMi8) confocal microscope with a 63x oil objective, 4x zoom, 1024x1024 pixels resolution, and 400 Hz scan speed visualized with the Hybrid Detection system (HyD) laser (Leica Microsystems CMS, GmbH, Germany). Images were captured sequentially; plasma membrane images stained with FM™4-64 were obtained with excitation at 515 nm and emission from 600–700 nm, and GFP images were obtained by excitation at 488 nm, with emission collected from 500–535 nm and were merged to observe the co-localization. Image acquisition and analysis were performed using Leica Application Suite X (LAS X; Leica Microsystems CMS, GmbH, Germany). From the confocal image analysis, NCS-1 appeared to be localized to the plasma membrane during the high Ca^{2+} condition (0.2 M $CaCl_2$), but cytosolic in the medium lacking high Ca^{2+} (Fig. 4.16).

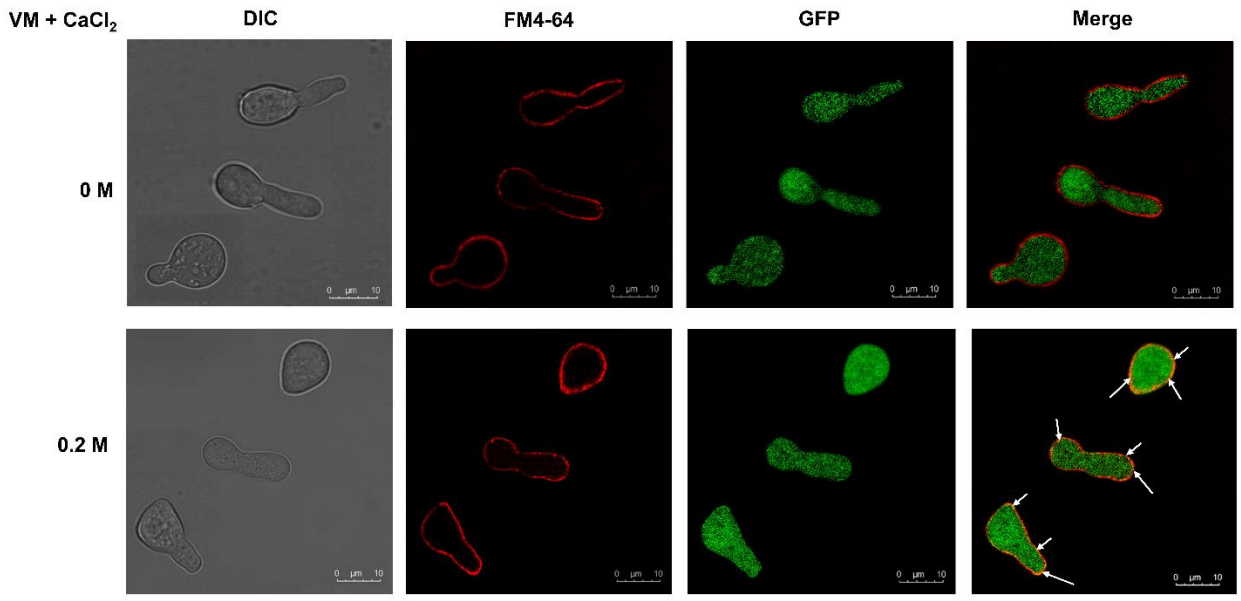

Fig. 4.16: Microscopic analysis for localization of NCS-1 during Ca^{2+} stress. The DIC, FM™4-64 dye, GFP, and merge images are shown for both in the VM medium without $CaCl_2$ (upper panel) and with 0.2 M $CaCl_2$ (lower panel). Confocal microscopy was performed using a Leica TCS SP8 (DMi8) confocal microscope with a 63x oil objective, 4x zoom, 1024 x 1024 pixels resolution, and 400 Hz scan speed visualized with the Hybrid Detection system (HyD) laser (Leica Microsystems CMS, GmbH, Germany as described in the Chapter 2. The localization of NCS-1::5xGly::V5::GFP to the plasma membrane was observed in the presence (0.2 M) or absence (0 M) of high concentration of $CaCl_2$. The NCS-1::5xGly::V5::GFP localization to the plasma membrane (yellow colour) is shown using white arrows (in the bottom panel). Three separate images were combined to show three different cells together. Scale bar = 10 µM.

4.2.8 Membrane binding assay showed NCS-1 interaction with MID-1

The pulldown assay using *N. crassa* membrane fractions were performed to determine the interaction of NCS-1 to MID-1. The membrane binding assay was performed both *in vivo* and *in vitro*. For the *in vivo* assay, Δ*ncs-1*; Δ*mid-1*; $P_{nit\text{-}6}$::*ncs-1* (4) strain (Table 2.1) was generated from a cross between the $P_{nit\text{-}6}$::*ncs-1* (21) and Δ*ncs-1*; Δ*mid-1* (2) strain (Table 2.1; Fig. 4.17).

The ascospores obtained from the cross were germinated in FGS agar plate supplemented with pantothenic acid. The pantothenic acid auxotroph progenies were selected and the presence of Δ*ncs-1*::*hph*, Δ*mid-1*::*hph*, P_{nit-6}::*ncs-1*::*5xGly*::*V5*::*gfp* alleles in the Δ*ncs-1*; Δ*mid-1*; P_{nit-6} ::*ncs-1* (4) strain were verified by PCR using the primer pairs HI-NCS-1-F and 5HPHR, HI-NCU06703-F and 5HPHR, Pnit-6-Fw and GFP-Rv (Table 2.2), respectively (Fig. 4.18). For the isolation of the membrane fractions, conidia of the P_{nit-6}::*ncs-1* (21) and Δ*ncs-1*; Δ*mid-1*; P_{nit-6}::*ncs-1* (4) strains (~ 1 x 10^6 conidia/ml) were inoculated in 50 ml VM liquid without $CaCl_2$ and with 0.2 M $CaCl_2$ in 250 ml flasks and incubated at 30 ºC for 6 h with shaking at 180 rpm. Germlings of these cultures were harvested by centrifugation at 4000 x *g* for 15 min at 4 ºC. The membrane fractions from the harvested germlings were isolated as described in the Chapter 2). Then, 18 µl of the membrane fractions and total crude protein sample from the P_{nit-6}::*ncs-1* (21) as a positive control mixed with 2 µl of 5X SDS-PAGE sample buffer were run in an SDS-PAGE (10% acrylamide) gel. Western blot was performed using rabbit anti-GFP antibody (Cat. No. A6455, Life Technologies, USA) as described in the Chapter 2. An intense band corresponding to the NCS-1::5xGly::V5::GFP protein (~51 kDa) was observed under the high concentration of Ca^{2+} (0.2 M $CaCl_2$) and a faint band was observed in the absence of high Ca^{2+} (0 M $CaCl_2$) for the P_{nit-6} ::*ncs-1* (21) membrane fraction (Fig. 4.19). But, no band was observed for the Δ*ncs-1*; Δ*mid-1*; P_{nit-6}::*ncs-1* (4) membrane fraction in both the presence of high concentration of Ca^{2+} (0.2 M $CaCl_2$) and in the absence of high Ca^{2+} (0 M $CaCl_2$) in the media (Fig. 4.19). Therefore, the *in vivo* membrane binding assay showed that NCS-1 binds to the MID-1 in the membrane during high concentration of Ca^{2+}.

For the *in vitro* assay, the membrane fractions were isolated from the Δ*ncs*-1 (FGSC 11404) and Δ*ncs-1*; Δ*mid-1* (2) strains (Table 2.1) as described in the Chapter 2. The NCS-1::5xGly::V5::GFP protein was isolated and purified from the P_{nit-6}::*ncs-1* (21) strain (Table 2.1) as described in the Chapter 2 and were run on a 10% SDS- polyacrylamide (30:1) gel to

check the purity (Fig. 4.20). A 10 µl aliquot of the plasma membrane fraction (~50 µg) was treated with 10 µl of purified NCS-1::5xGly::V5::GFP (~50 µg) in two different conditions of either Ca^{2+} free (1 mM EGTA) or Ca^{2+} bound (1 mM $CaCl_2$), and incubated for 1 h at 4 ºC. Each sample was treated with 1% formaldehyde at room temperature on a rocking platform for 30 min for chemical crosslinking and the reaction was quenched by adding 125 mM glycine for 10 min at room temperature. Washing step was not performed in order to visualize the unbounded NCS-1::5xGly::V5::GFP could be visualized in the western blot. The NCS-1::5xGly::V5::GFP treated membranes were subjected to SDS-PAGE (10% acrylamide). Western blot was performed using rabbit anti-GFP antibody (Cat. No. A6455, Life Technologies, USA) as described in the Chapter 2. The western blot analysis revealed the binding of NCS-1 with the membrane fraction isolated from the Δ*ncs-1* strain (Fig. 4.21). In the presence of Ca^{2+} chelating agent (1 mM EGTA), a very faint band (~125 kDa) was observed, indicating a very weak binding of the NCS-1::5xGly::V5::GFP recombinant protein with MID-1. Additionally, in the pull-down assay, the intensity of the band was increased by ~5-fold in the presence of Ca^{2+} (1 mM $CaCl_2$). However, the membrane fractions from the Δ*ncs-1*; Δ*mid-1* (2) strain showed no band at ~125 kDa, instead, a band was observed corresponding to the NCS-1::5xGly::V5::GFP (~51 kDa) recombinant protein representing the unbound protein (Fig. 4.21). Therefore, like the *in vivo* assay, and the *in vitro* membrane binding assay further supported that NCS-1 specifically binds to the MID-1 in the membrane during high Ca^{2+} condition.

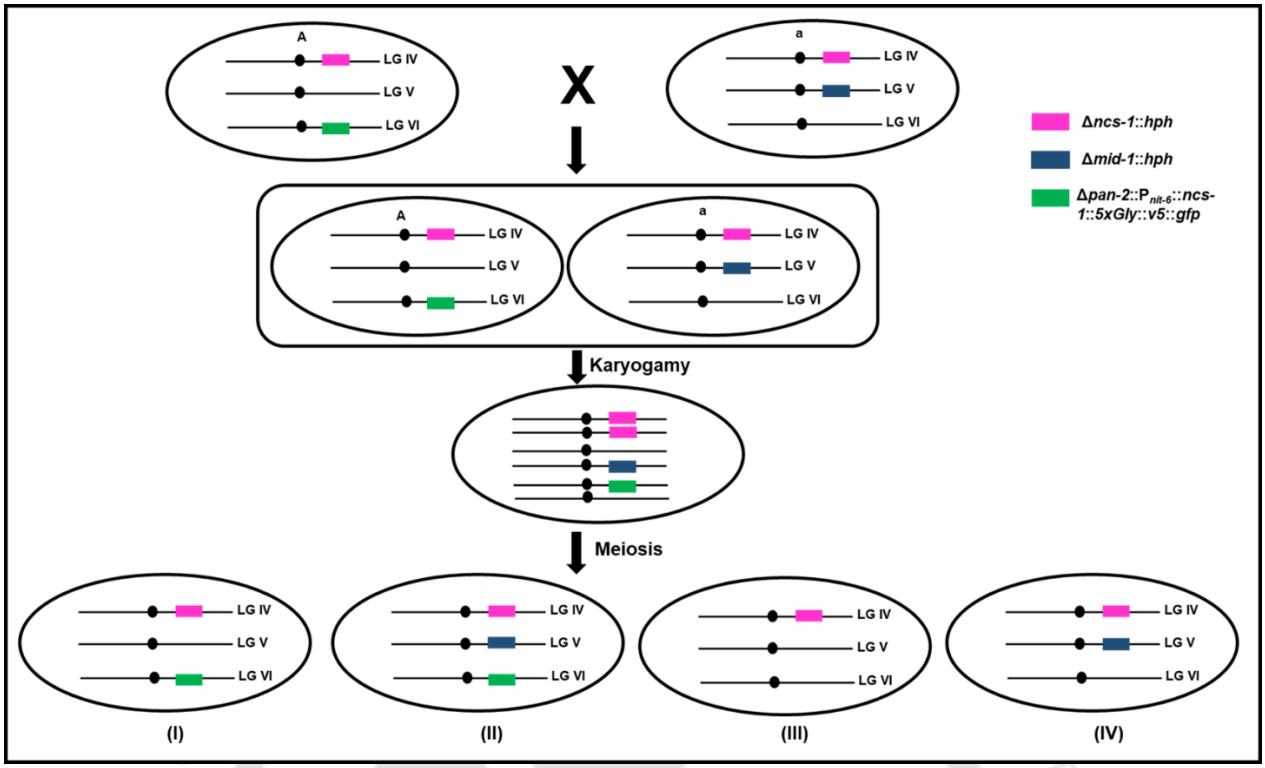

Fig. 4.17: Schematic representation of the cross to generate strain with Δ*ncs-1*, Δ*mid-1* and Δ*pan-2*::P$_{nit-6}$::*ncs-1*::*5xGly*::*V5*::*gfp* alleles. Cross was set up between the P$_{nit-6}$::*ncs-1* (21) *A* and Δ*ncs-1*; Δ*mid-1* (2) *a* strains in SCM media supplemented with pantothenic acid and the ascospores were harvested after 21 days. The progenies were germinated and screened to identify the type (II) progeny containing the Δ*ncs-1*::*hph*, Δ*mid-1*::*hph*, P$_{nit-6}$::*ncs-1*::*5xGly*::*V5*::*gfp* alleles.

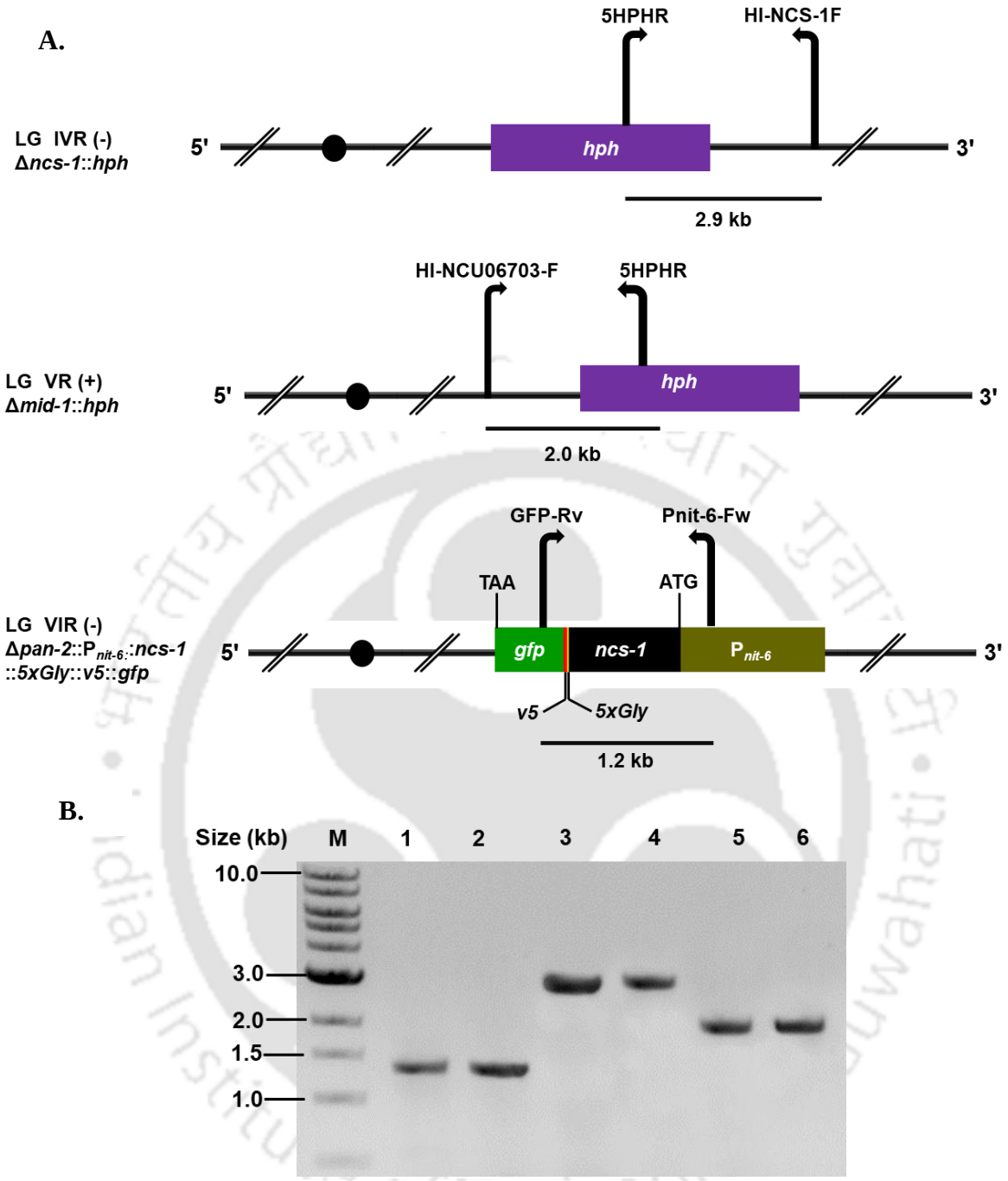

Fig. 4.18: PCR verification of the Δ*ncs-1*, Δ*mid-1* and Δ*pan-2*::P$_{nit-6}$::*ncs-1*::*5xGly*::*V5*::*gfp* alleles in the Δ*ncs-1*; Δ*mid-1*; P$_{nit-6}$::*ncs-1* (4) strain.

A. Schematic diagram showing the primer positions and 5'→3' orientation (shown using the direction of the arrow) used for the verification of the Δ*ncs-1*, Δ*mid-1*, and Δ*pan-2*::P$_{nit-6}$::*ncs-1*::*5xGly*::*V5*::*gfp* alleles in the Δ*ncs-1*; Δ*mid-1*; P$_{nit-6}$::*ncs-1* (4) strain. The primer pairs HI-

NCS-1F and 5HPHR, HI-NCU06703-F and 5HPHR, and Pnit-6-Fw and GFP-Rv (Table 2.2) were used to amplify PCR products of sizes ~2.9 kb, ~2.0 kb, and ~1.2 kb, respectively.

B. PCR amplification of the fragments of the $P_{nit\text{-}6}$::*ncs-1*::*5xGly*::*V5*::*gfp*, Δ*ncs-1*::*hph*, and Δ*mid-1*::*hph* alleles using the primer pairs Pnit-6-Fw and GFP-Rv, HI-NCS-1F and 5HPHR, and HI-NCU06703-F and 5HPHR, respectively. The PCR using the DNA from the Δ*ncs-1*; Δ*mid-1*; $P_{nit\text{-}6}$::*ncs-1* (4) strain as template DNA showed the $P_{nit\text{-}6}$::*ncs-1*::*5xGly*::*V5*::*gfp*, Δ*ncs-1*::*hph* and Δ*mid-1*::*hph* fragments of size ~1.2 kb (lane 2), ~2.9 kb (lane 4), and ~2.0 kb (lane 6), respectively. The products obtained using the template DNA of the $P_{nit\text{-}6}$::*ncs-1* (21), Δ*ncs-1 A* (FGSC 11404), and Δ*mid-1 a* (FGSC 11707) strains in lanes 1, 3, and 5, respectively, were controls in the PCR reactions. PCR products were resolved in a 1% agarose gel, using the 1 kb NEB DNA ladder (New England Biolabs, USA) as marker (M).

Sample	$P_{nit\text{-}6}$ ::*ncs-1* (21)	Blank	$P_{nit\text{-}6}$ ::*ncs-1* (21)		Δ*ncs-1*; Δ*mid-1*; $P_{nit\text{-}6}$ ::*ncs-1*	
$CaCl_2$ (mM)	0.68	-	200	0	200	0
Sample type	Crude Protein	-	Membrane fraction	Membrane fraction	Membrane fraction	Membrane fraction
Lane	1	2	3	4	5	6

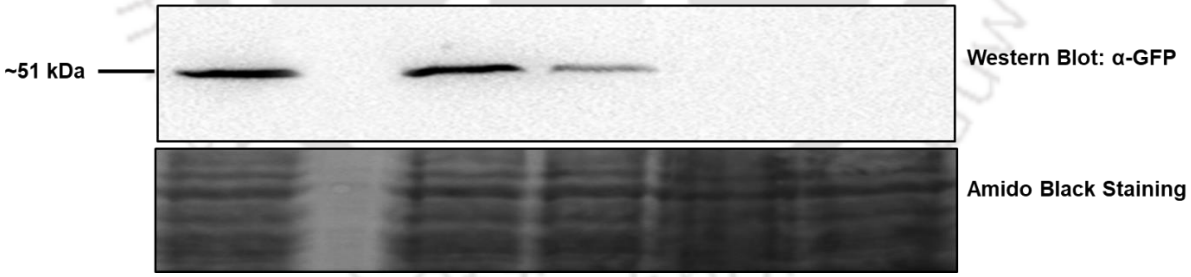

Fig. 4.19: *In vivo* membrane binding pulldown assay for NCS-1 and MID-1 interaction. Plasma membrane fractions of the $P_{nit\text{-}6}$::*ncs-1* (21) and Δ*ncs-1*; Δ*mid-1*; $P_{nit\text{-}6}$ ::*ncs-1* (4) strains grown in the VM medium containing the indicated amounts of $CaCl_2$ were resolved in a 10% SDS-PAGE and analyzed in a western blot. The crude NCS-1::5xGly::V5::GFP protein obtained from the $P_{nit\text{-}6}$ ::*ncs-1* (21) cultured in normal VM liquid (0.068 M $CaCl_2$) was used as control (lane 1). The lane 2 was kept as blank without any sample. The NCS-

1::5xGly::V5::GFP protein bands (~51 kDa) were observed in the membrane fractions of the $P_{nit\text{-}6}$ ::*ncs-1* (21) strain (lanes 3 and 4). The band intensity was very faint in the absence of $CaCl_2$ (lane 4), indicating that the interaction of NCS-1 with MID-1 was promoted by the high Ca^{2+} condition. No band was observed in the membrane fractions of the Δ*ncs-1*; Δ*mid-1*; $P_{nit\text{-}6}$::*ncs-1* (4) strain, both in the presence and absence of $CaCl_2$ in the media (lanes 5 and 6), which established that NCS-1 specifically binds to MID-1 in the plasma membrane.

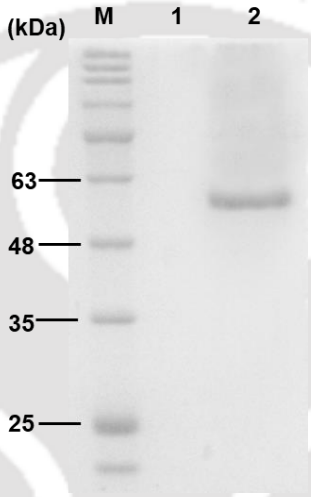

Fig. 4.20: Purification of the NCS-1::5xGly::GFP::V5 protein. The purified NCS-1::5xGly::V5::GFP protein sample was run on a 10% SDS-PAGE gel and visualized by Coomassie Brilliant Blue (CBB) staining. A single band was observed for the lane 2 loaded with NCS-1::5xGly::V5::GFP (~51 kDa) protein which indicates purified protein. Prestained protein marker (Himedia, India) was loaded in the lane indicated as M. Lanes 1 was kept as blank.

Sample	Control		Δ*ncs-1*		Δ*ncs-1*; Δ*mid-1*	
NCS-1::5xGly::V5::GFP protein	+	–	+	+	+	+
Membrane fraction	–	+	+	+	+	+
1 mM EGTA [- (Ca^{2+})]	–	–	+	–	+	–
1 mM $CaCl_2$ [+ (Ca^{2+})]	–	–	–	+	–	+
Lane	1	2	3	4	5	6

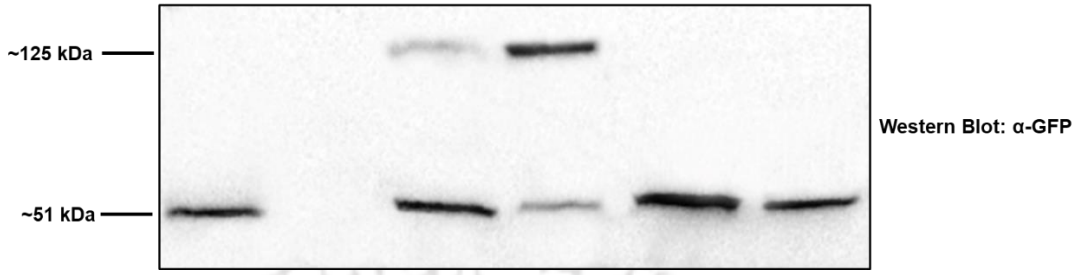

Fig. 4.21: *In vitro* membrane binding pulldown assay for NCS-1 and MID-1 interaction. Plasma membrane fractions of the Δ*ncs-1*, and Δ*ncs-1*; Δ*mid-1* strains (Table 1) were treated with either the NCS-1::5xGly::V5::GFP protein in presence of 1 mM $CaCl_2$ (lanes 4 and 6), or 1 mM EGTA (lanes 3 and 5). The purified NCS-1::5xGly::V5::GFP protein (lane 1) and membrane fraction of the Δ*ncs-1* mutant (lane 2) were used as controls. The NCS-1::5xGly::V5::GFP protein band (~125 kDa) was observed in the membrane fractions of the Δ*ncs-1* (lanes 4 and 5), but not in the membrane fractions of the Δ*ncs-1*; Δ*mid-1* (2) strain (lanes 5 and 6). The band intensity was very faint in absence of $CaCl_2$ (lane 3). The unbound NCS-1::5xGly::V5::GFP protein (~51 kDa) bands are shown using an asterisk.

4.2.9 Generation of strain for the expression of MID-1 tagged with S-tag and RFP

For the generation of the strain expressing MID-1 tagged with S-tag and RFP, 2,097 bp *mid-1* (NCU06703) open reading frame (ORF) was amplified by PCR using the primes DGMID-1-F and DGMID-1-R (Table 2.2) and ligated into the SmaI (Cat. No. R0141S, New England Biolabs, USA) digested pRS426PVG/tcu-1 vector (Ouyang *et al.*, 2015) using Quick Ligation™ Kit (Cat. no. M2200S, New England Biolabs, USA). The ligated product was transformed into ultra-competent *E. coli* DH5α (Inoue *et al.*, 1990) and plasmid constructs were isolated. The plasmid containing the containing $P_{tcu\text{-}1}$::*mid-1*::*5xGly*::*S-tag*::*rfp* was verified by PCR amplification (Fig. 4.22) using the primer pairs Ptcu-1F and DGMID-1-R (Table 2.2)

and named as pDGMID-1 (17) construct (Fig. 4.23). The plasmid construct pDGMID-1 (17) was transformed into the *N. crassa* recipient strain 52-4-9 (Table 2.1), essentially as described in the Chapter 2. The initial heterokaryotic transformants were selected on FGS agar plates supplemented with BASTA™ and inositol. The heterokaryotic transformant MID-1-17-HT 21 (Table 2.1) was further verified for the P_{tcu-1}::*mid-1*::*5xGly*::*S-tag*::*rfp* allele by PCR amplification (Fig. 4.24) using the primer pairs Ptcu-1F and DGMID-1-R (Table 2.2). The heterokaryotic transformant MID-1-17-HT 21 (Table 2.1) crossed with Δ*mid-1 a* (FGSC 11707) to generate the homokaryotic strain expressing MID-1::5xGly::S-tag::RFP. The ascospores from this cross were germinated on FGS agar medium containing inositol, and homokaryotic strains were initially identified based on hygromycin resistance and inositol auxotrophy. In the homokaryotic strains, the presence of *mid-1* allele in the *inl* locus, and Δ*mid-1*::*hph* allele in the endogenous locus were verified by PCR amplification (Fig. 4.25) using the primer pairs Ptcu-1F and DGMID-1-R (Table 2.2), and HI-NCU06703-F and 5HPHR (Table 2.2), respectively. Thus, I isolated the P_{tcu-1}::*mid-1* (11) homokaryotic strain (Table 2.1) and used in this study.

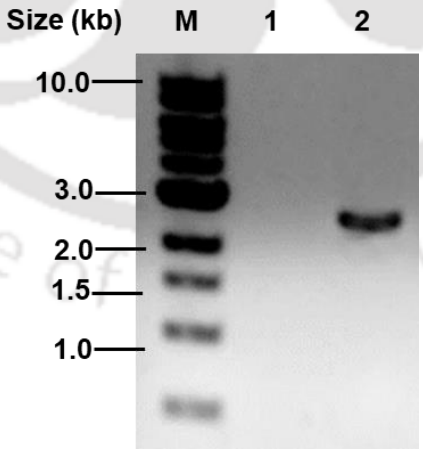

Fig. 4.22: Cloning of *mid-1* in the pRS426PVG/tcu-1 vector for the expression of MID-1 tagged with S-tag and RFP. The *mid-1* ORF of size 2,097 bp was ligated in the SmaI digested pRS426PVG/tcu-1 vector and transformed into *E. coli* DH5α ultracompetent cells. The plasmid pDGMID-1 (17) isolated from the transformed colonies was confirmed by PCR using

the primers Ptcu-1F and DGMID-1-R (Table 2.2). The PCR products were resolved in a 1% agarose gel, amplicon of size ~2.5 kb was observed for the pDGMID-1 (17) plasmid construct (lane 2). The pRS426PVG/tcu-1 vector was used as negative control in the PCR reaction, and the 1 kb NEB DNA ladder (New England Biolabs, USA) was used as marker (M).

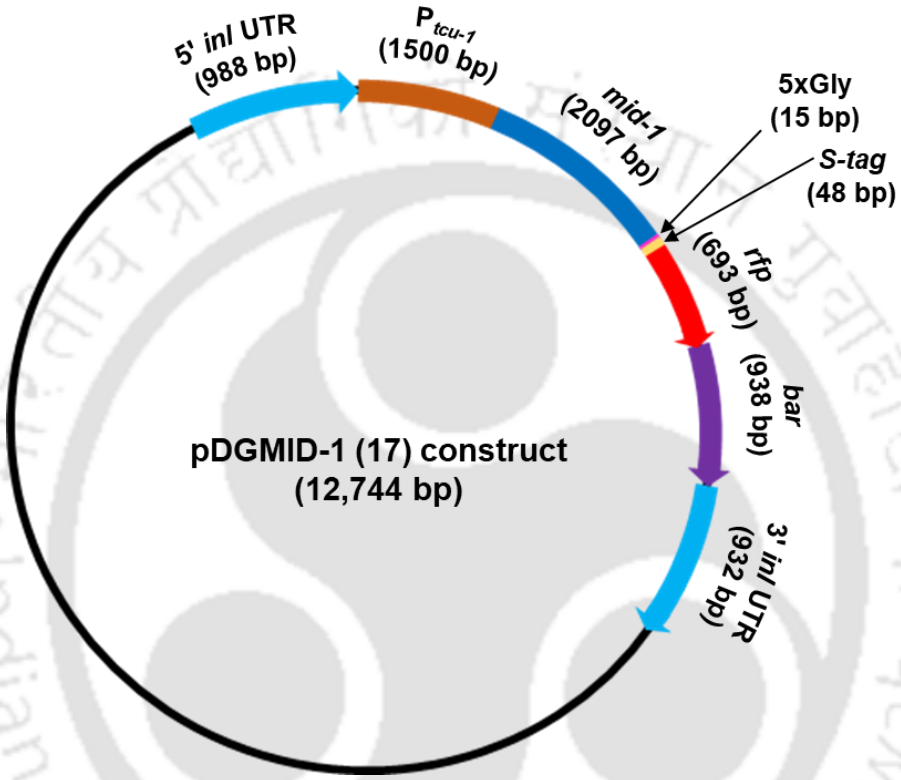

Fig. 4.23: Schematic diagram showing the pDGMID-1 (17) plasmid construct containing *mid-1* ORF under the regulatable *tcu-1* promoter (P_{tcu-1}). The pDGMID-1 (17) plasmid (12,744 bp) is a modified pRS426 vector, which contains *inl* UTRs, 5xGly, S-tag, and *rfp* (Ouyang *et al.*, 2015). The *mid-1* ORF cloned into the multiple cloning site (MCS) region in the pDGMID-1 (17) digested with SmaI. The numbers (in bp) in the parentheses indicate the size of the respective fragment.

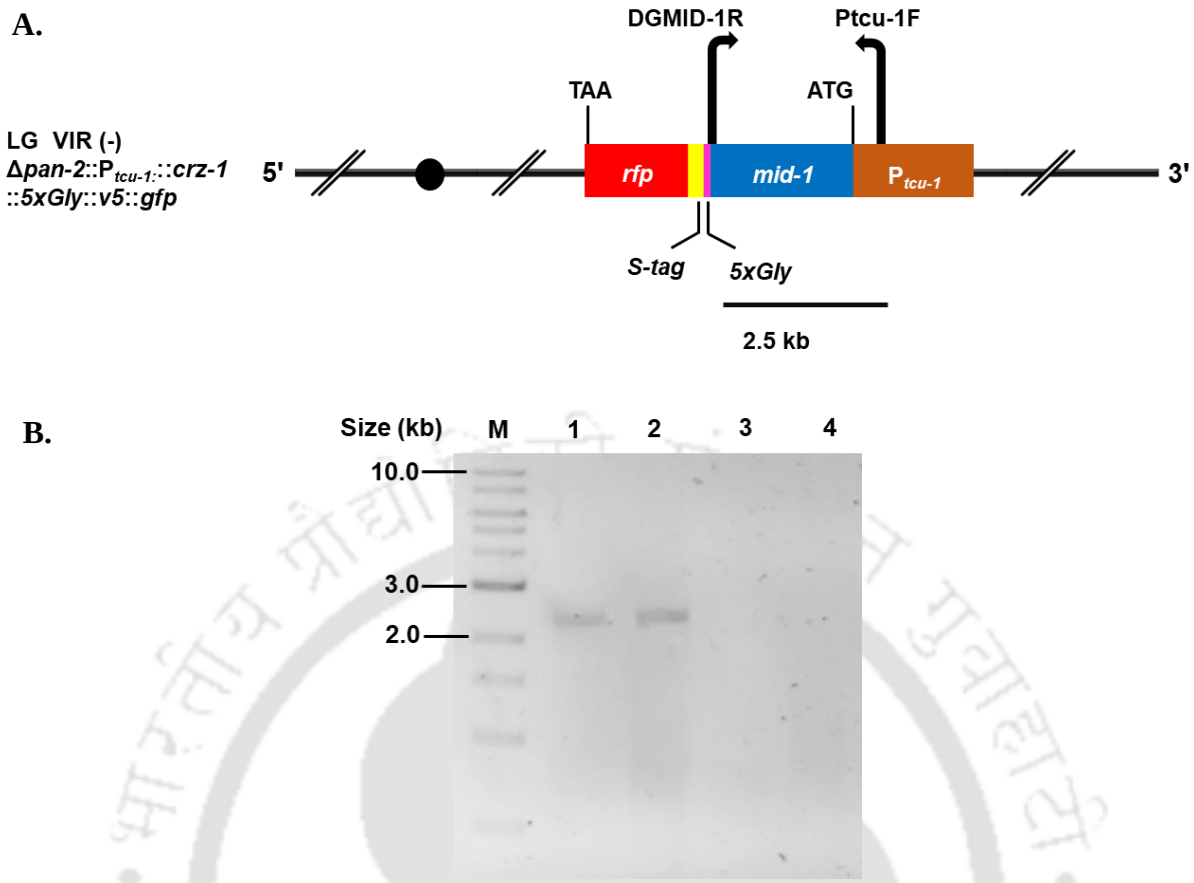

Fig. 4.24: PCR verification of the heterokaryotic MID-1-17-HT 21 strain for the presence of the Δ*inl*::P$_{nit-6}$::*mid-1*::*5xGly*::*S-tag*::*rfp* allele.

A. Schematic diagram showing the primer positions and 5'→3' orientation (shown using the direction of the arrow) used for the PCR verification of the Δ*inl*::P$_{nit-6}$::*mid-1*::*5xGly*::*S-tag*::*rfp* allele in the heterokaryotic MID-1-17-HT 21 strain. The size of the PCR product is shown below the primer positions.

B. PCR confirmation of the Δ*inl*::P$_{nit-6}$::*mid-1*::*5xGly*::*S-tag*::*rfp* allele in the heterokaryotic MID-1-17-HT 21 strain. The PCR, performed using the primers Ptcu-1F and DGMID-1-R (Table 2.2), followed by a 1% agarose gel analysis revealed the PCR amplicons of size ~2.5 kb for the pDGMID-1 (17) construct and heterokaryotic MID-1-17-HT (21) strain in the lanes 1 and 2, respectively. The 1 kb NEB DNA ladder (New England Biolabs, USA) was used as marker (M). PCR using the template of the pDGMID-1 (17) construct in lane 1 was positive

control, while the wild type (FGSC 987) and the recipient 52-4-9 (FGSC 2479) strains in lanes 3 and 4, respectively, were negative controls.

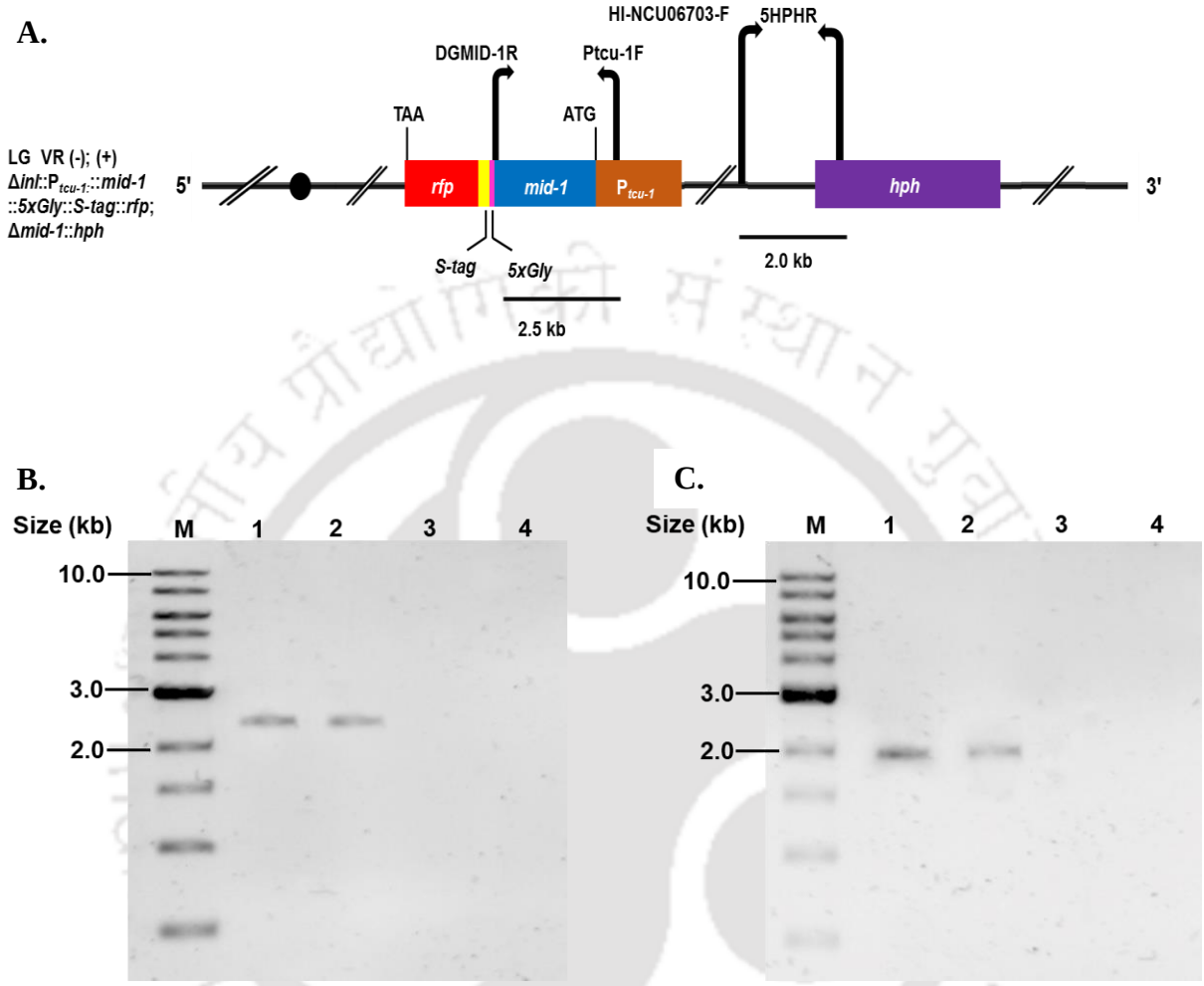

Fig. 4.25: PCR verification of the homokaryotic strain with the *mid-1* expressed under P_{tcu-1}.

A. Schematic diagram showing the primer positions and 5'→3' orientation (shown using the direction of the arrow) used for the PCR verification of the Δ*inl*::P_{nit-6}::*mid-1*:: *5xGly*::*S-tag*::*rfp* allele in the homokaryotic P_{tcu-1}::*mid-1* (11) strain. The size of the PCR product is shown below the primer positions.

B. PCR confirmation of the Δ*inl*::P_{nit-6}::*mid-1*:: *5xGly*::*S-tag*::*rfp* allele in the homokaryotic P_{tcu-1}::*mid-1* (11) strain using the primers Ptcu-1F and DGMID-1-R (Table 2.2). The PCR

amplicons of size ~2.5 kb were observed for the pDGMID-1 (17) construct and homokaryotic $P_{tcu\text{-}1}$::*mid-1* (11) strain in the lanes 1 and 2, respectively, when resolved in a 1% agarose gel. The 1 kb NEB DNA ladder (New England Biolabs, USA) was used as marker (M). The pDGMID-1 (17) construct in lane 1 was used as a positive control, while the wild type (FGSC 987) and the recipient 52-4-9 (FGSC 2479) strain in lanes 3 and 4, respectively, were used as negative controls.

C. PCR confirmation of the Δ*mid-1*::*hph* allele in the homokaryotic $P_{tcu\text{-}1}$::*mid-1* (11) strain using the primers HI-NCU06703-F and 5HPHR (Table 2.2). The *hph* cassette fragment of length ~2.0 kb was observed for the Δ*mid-1 a* (FGSC 11707) and homokaryotic $P_{tcu\text{-}1}$::*mid-1* (11) strains in the lanes 1 and 2, respectively, when resolved in a 1% agarose gel with 1 kb NEB DNA ladder (New England Biolabs, USA) as marker (M). The Δ*mid-1 a* (FGSC 11707) strain in lane 1 was positive control, while the wild type (FGSC 987) and the recipient 52-4-9 (FGSC 2479) strain in lanes 3 and 4, respectively, were negative controls in the PCR reactions.

4.2.10 Co-IP of NCS-1::5xGly::V5::GFP and MID-1::5xGly::S-tag::RFP proteins

For Co-IP assay, two forced heterokaryons NCS-1GFP + MID-1RFP and GFP + RFP (Table 2.1) were generated by co-inoculating the individual strains, $P_{nit\text{-}6}$ ::*ncs-1* (21) + $P_{tcu\text{-}1}$::*mid-1* (11) and pccg-1_GFP + pccg-1_RFP, respectively, in 250 ml flasks containing 50 ml normal VM agar and incubating at 30 °C in the dark for 3 days and at room-temperature for 4 days under constant light (Fig. 4.26). The heterokaryon NCS-1GFP + MID-1RFP was used as the test strain, while the heterokaryon GFP + RFP and wild type (FGSC 987) were used as control strains. Conidia of the wild type (FGSC 987) and the heterokaryons NCS-1GFP + MID-1RFP and GFP + RFP (~ 1 x 10^6 conidia/ml) were inoculated in 50 ml VM liquid supplemented with 0.2 M $CaCl_2$ in 250 ml flasks and incubated at 30 ºC for 6 h with shaking at 180 rpm. The membrane fractions and cytosolic protein fractions were isolated as described in the Chapter 2. Co-IPs were performed in two sets, one using the membrane fraction and other using the

cytosolic fraction. Initial precipitations were performed using Dynabeads™ Protein A magnetic beads (Cat. No. 10001D, Life Technologies, USA) conjugated and cross-linked with rabbit anti-GFP antibody (Cat. No. A6455, Life Technologies, USA) and eluted as described in the Chapter 2. The eluted samples were run in SDS-PAGE (10% acrylamide) gels. Western blots were performed in two sets, one using rabbit anti-GFP antibody (Cat. No. A6455, Life Technologies, USA) and another using rabbit anti-RFP antibody (Cat. No. 710530, Life Technologies, USA). It was observed that the NCS-1::5xGly::V5::GFP protein (~51 kDa) was immunoprecipitated in all strains for both the plasma membrane and cytosolic fractions (Fig. 4.27). Interestingly, the MID-1::5xGly::S-tag::RFP protein (~102 kDa) was visible in the input from the heterokaryotic NCS-1GFP + MID-1RFP strain (Table 2.2) and also co-immunoprecipitated with the NCS-1::5xGly::V5::GFP protein only for the membrane fraction (Fig. 4.27). In case of the cytosolic fraction, the MID-1::5xGly::S-tag::RFP protein was observed neither for the input nor for the IP, which showed that the interaction between NCS-1 and MID-1 takes place only in the plasma membrane. In the control reactions using the heterokaryotic GFP + RFP strain, no S-tag::RFP protein was co-immunoprecipitated with the V5::GFP protein indicating no interaction between the tagged proteins. No protein bands were observed for the wild type strain in any case due to the absence of any fluorescent tag. Therefore, these results demonstrated that in response to Ca^{2+} stress, NCS-1 directly interacts with MID-1, which might close the Ca^{2+}-permeable channel MID-1 to prevent Ca^{2+} influx.

A.

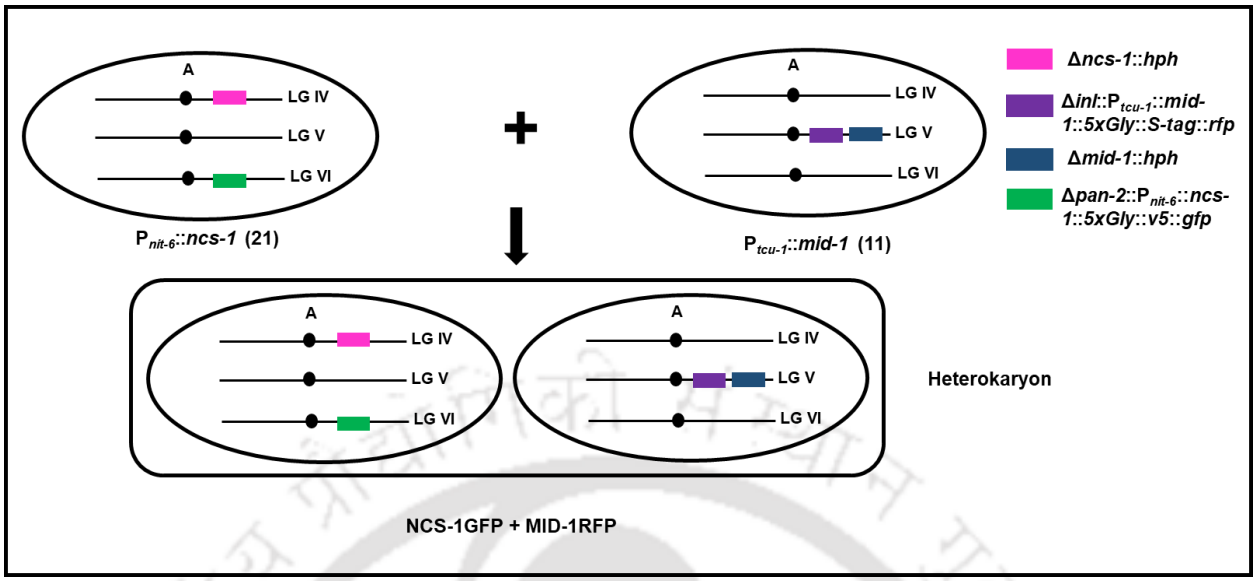

B.

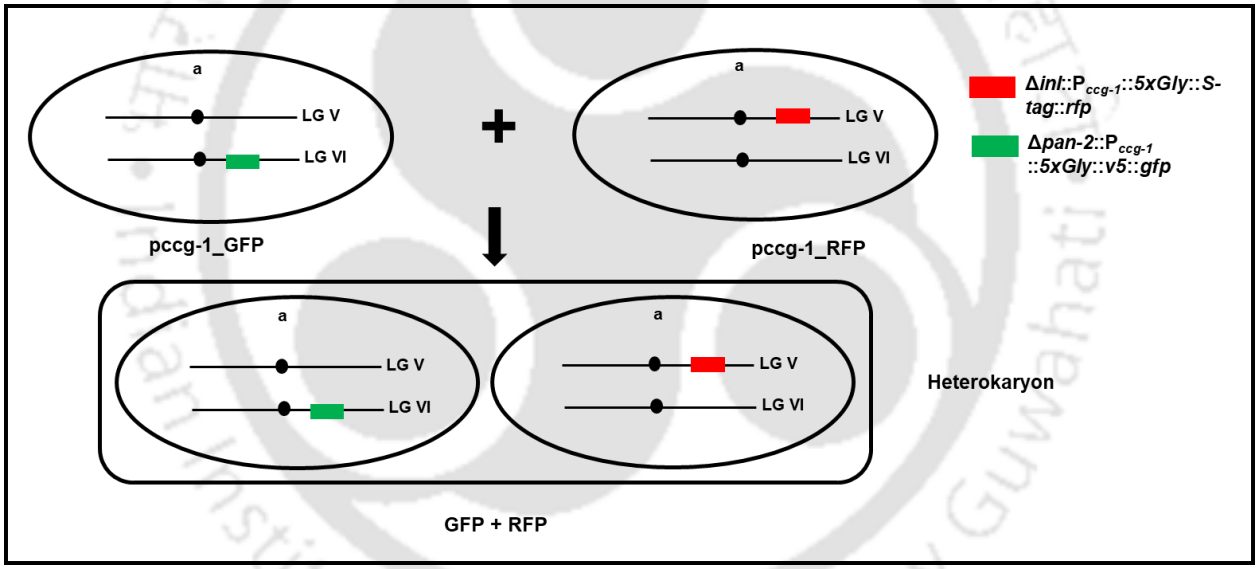

Fig. 4.26: Schematics for the generation of the forced heterokaryons. Two forced heterokaryons were generated for the Co-IP experiment to demonstrate the interaction between NCS-1 and MID-1.

A. The heterokaryon NCS-1GFP + MID-1RFP was generated by co-inoculating the individual strains- $P_{nit\text{-}6}$::*ncs-1* (21) + $P_{tcu\text{-}1}$::*mid-1* (11) in 50 ml normal VM agar in 250 ml flasks. The cultures were that incubated at 30 °C in the constant dark for 3 days and at room temperature for 4 days under constant light.

B. The heterokaryon GFP + RFP was generated by co-inoculating the individual strains pccg-1_GFP + pccg-1_RFP 50 ml normal VM agar in 250 ml flasks. The cultures were incubated at 30 °C in the constant dark for 3 days and at room temperature for 4 days under constant light.

Sample	NCS-1GFP + MID-1RFP		Wild type		GFP + RFP	
Input or IP	Input	IP	Input	IP	Input	IP
NCS-1::5xGly::V5::GFP	+	+	–	–	–	–
MID-1::5xGly::S-tag::RFP	+	+	–	–	–	–
V5::GFP	–	–	–	–	+	+
S-tag::RFP	–	–	–	–	+	+
Lane	1	2	3	4	5	6

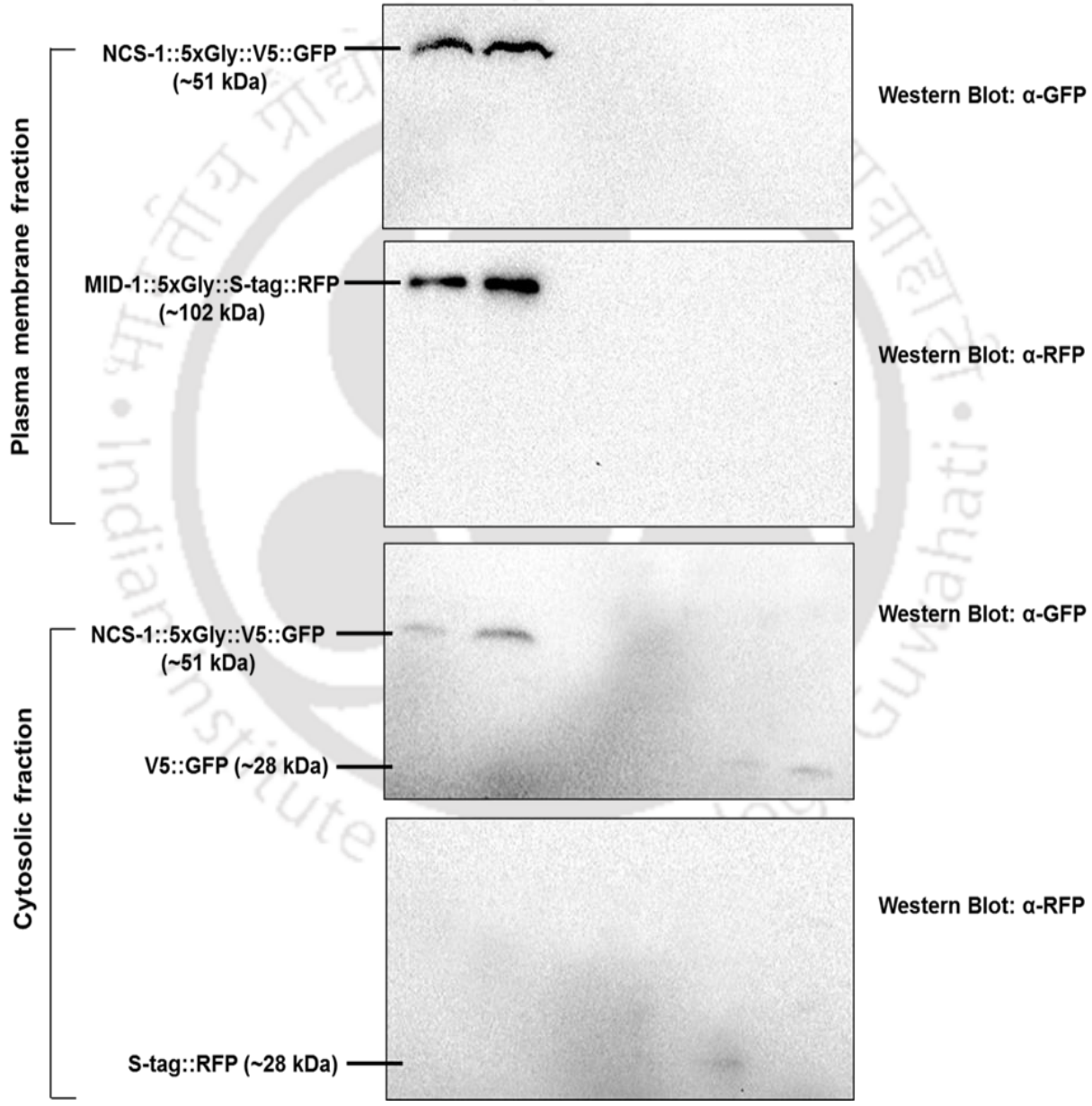

Fig. 4.27: Co-immunoprecipitation of NCS-1 and MID-1. The indicated heterokaryons, NCS-1GFP + MID-1RFP and GFP + RFP, and the wild type strain (FGSC 987) were grown

for 6 h in submerged culture as described in the previous section. The soluble plasma membrane and cytosolic fractions were isolated and immunoprecipitated using anti-GFP antibody coupled Dynabeads™ Protein A magnetic beads. Samples of either whole plasma membrane and cytosolic fraction (Input) and immunoprecipitated proteins (IP) were subjected to western blot analysis using anti-GFP (top), and anti-RFP (bottom) antibodies as described in the previous section. The line indicates position for bands of the NCS-1::5xGly::V5::GFP (~51 kDa) and MID-1:: 5xGly::S-tag::RFP (~102 kDa) proteins.

4.3 Discussion

In this Chapter, I described the molecular mechanism of the NCS-1 mediated pathway for tolerance to Ca^{2+} stress in *N. crassa*. The ChIP analysis revealed that the CRZ-1 transcription factor binds to the promoter of *ncs-1*, possibly to upregulate its expression under the high Ca^{2+} condition. Moreover, Ca^{2+} promotes the binding of CRZ-1 to the *ncs-1* promoter since the binding intensity increased with increasing Ca^{2+} level. In *S. cerevisiae*, calcineurin dephosphorylates the CRZ-1 homologue *TCN1/CRZ-1*, for its nuclear localization, which subsequently regulates the transcription of the target genes (Stathopoulos and Cyert, 1997). Similarly, the *S. pombe* CRZ-1 homologue Prz1p, binds to the *ncs1* promoter at 130 bp upstream of the ATG start codon and the binding was induced by an increased level of intracellular Ca^{2+} (Hamasaki-Katagiri and Ames, 2010). Furthermore, the enzymatic activity of the calcineurin and its target Prz1p is essential in the up-regulation of the *ncs1* promoter activity in the presence of high extracellular Ca^{2+} and indicates the calcineurin-mediated activation of *ncs1* transcription induced by Ca^{2+} (Hamasaki-Katagiri and Ames, 2010). In addition, the EMSA revealed that CRZ-1 specifically binds to an 8 bp nucleotide sequence 5′-CCTTCACA-3′ in the *ncs-1* promoter, which is located 216 bp upstream of the start codon. Remarkably, unlike the *S. cerevisiae*, the CRZ-1 binding site of the *ncs-1* promoter is not a CDRE sequence. Similarly, in *S. pombe*, the Prz1p binding site sequence 5′-CAACT-3′ in the

ncs1 promoter is also different from the *S. cerevisiae* CDRE sequence (Hamasaki-Katagiri and Ames, 2010). The *N. crassa* CDRE sequence 5′-AGCCTC-3′ (Kumar *et al.*, 2006) was also absent in the *ncs-1* promoter.

In *S. cerevisiae*, a genome-wide microarray screening revealed that the *ncs-1* homologue *FRQ1* was not regulated by TCN1/CRZ1 (Yoshimoto *et al.*, 2002). In mammals, during the activation of T-lymphocyte, the transcription factor NFAT is regulated by calcineurin (Crabtree and Olson, 2002) and recognizes the sequence 5′-GGAAA-3′ present in the promoters of both recoverin and mammalian NCS-1 (Hamasaki-Katagiri and Ames, 2010). However, the exact mechanism of the regulation of NCS protein by calcineurin is not clear.

Therefore, to understand the mechanism of NCS-1 mediated pathway for tolerance to Ca^{2+} stress in *N. crassa*, I examined, if NCS-1 interacts with the Ca^{2+}-permeable channel MID-1 protein that might prevent Ca^{2+} entry to the cell. *N. crassa* possesses three Ca^{2+} permeable channels (Galagan *et al.*, 2003; Borkovich *et al.*, 2004; Zelter *et al.*, 2004; Tamuli *et al.*, 2013), including the *S. pombe* Yam8p homologue MID-1, which is necessary for Ca^{2+}-homeostasis (Lew *et al.*, 2008). Besides, both Δ*mid-1* single and Δ*ncs-1*; Δ*mid-1* double mutants were able to recover the Ca^{2+} sensitive phenotype of the Δ*ncs-1*, indicating a genetic interaction of *mid-1* and *ncs-1* during Ca^{2+} stress condition (Deka and Tamuli, 2013). In addition, Ca^{2+} induced closure of the MID-1 homologue Yam8p ion channel by Ncs1p was demonstrated in *S. pombe* (Hamasaki-Katagiri and Ames, 2010). In this study, I demonstrated that during high Ca^{2+} condition, NCS-1 promotes the closure of the Ca^{2+}-permeable channel MID-1. The confocal microscopy study suggested that high concentration of Ca^{2+} promotes NCS-1 localization to the plasma membrane, which, otherwise mostly remained in the cytosol. In an earlier study, G2A mutation in the N-terminal myristoylation domain of *N. crassa* NCS-1 was found not to affect the normal vegetative growth and Ca^{2+} stress tolerance (Gohain *et al.*, 2016). In recoverin, which is an NCS family protein, the N-terminal myristoyl group is sequestered in a

deep hydrophobic cavity and exposed to interact with a lipid bilayer membrane only on the binding of Ca^{2+} to the EF-hands (Ames *et al.*, 1997). Therefore, it may be speculated that during Ca^{2+}-stress, the increased level of $[Ca^{2+}]_c$ causes Ca^{2+} binding to the NCS-1 exposes the myristoyl group and resulting in its plasma membrane localization, which otherwise remains cytosolic. Furthermore, both in *vivo* and *in vitro* membrane pulldown assays revealed that NCS-1 was unable to bind to the membrane fraction lacking MID-1, suggesting that NCS-1 specifically binds to MID-1. The Co-IP assay established a direct physical interaction between NCS-1 and MID-1

A model was proposed based on this and earlier studies to describe the Ca^{2+}-stress tolerance in *N. Crassa* (Fig. 4.28). Ca^{2+} influx through the plasma membrane localized Ca^{2+}-permeable channel MID-1 increases the $[Ca^{2+}]_c$, resulting in the activation of calmodulin (CaM). CaM activates calcineurin which dephosphorylates the target transcription factor CRZ-1 and causes its nuclear localization. In the nucleus, CRZ-1 binds upstream to the start codon in the *ncs-1* promoter (~1.4 kb) to upregulate its mRNA expression. The NCS-1 protein is activated by the $[Ca^{2+}]_c$ and interacts with MID-1, possibly causing its closure to prevent further Ca^{2+} influx for stress tolerance. As described in the previous chapter, the Ca^{2+}/H^+ exchanger protein CAX, located in the vacuole serving as the intracellular Ca^{2+} store, possibly pumps Ca^{2+} to maintain the resting level of the $[Ca^{2+}]_c$. Calcineurin might act as the inhibitor of CAX, and the inhibition is relieved when the calcineurin inhibitor FK506 is present. In addition, the Ca^{2+} -ATPase NCA-2, another possible target of CRZ-1, also contributes to the tolerance to Ca^{2+} stress by pumping Ca^{2+} out of the cell and presumably into vacuole to reduce $[Ca^{2+}]_c$ as reported previously (Bowman *et al.*, 2009, 2011; Zelter *et al.*, 2004). Further work will reveal additional molecular details of the pathway involving calcineurin, CRZ-1, and the Ca^{2+} transporters in conferring tolerance to Ca^{2+} stress in *N. crassa*.

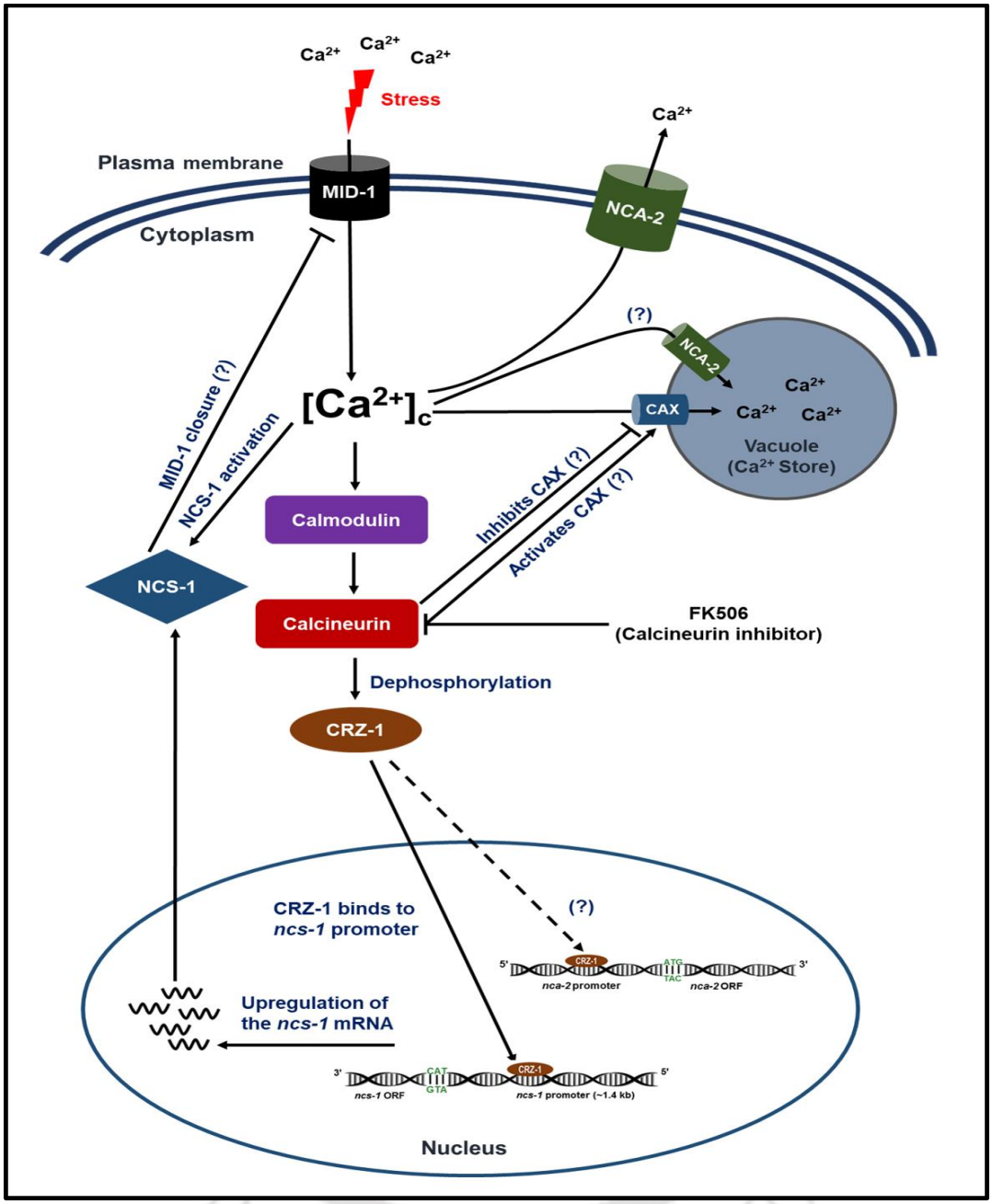

Fig. 4.28: Model for Ca^{2+} stress tolerance in *N. crassa*. Ca^{2+} influx through MID-1 during stress increases the level of $[Ca^{2+}]_c$. Calmodulin, activated by $[Ca^{2+}]_c$, activates calcineurin which dephosphorylates CRZ-1. Dephosphorylated CRZ-1 enters the nucleus and increases the transcription of *ncs-1*. NCS-1 is activated by $[Ca^{2+}]_c$ interacts with MID-1 to prevent the Ca^{2+} influx. Calcineurin might act as the inhibitor of CAX, and the inhibition is relieved when the calcineurin inhibitor FK506 is present. CAX sequesters excess Ca^{2+} into the vacuoles for maintaining the resting level of $[Ca^{2+}]_c$. NCA-2, another possible target of CRZ-1, also

contributes to the tolerance to Ca^{2+} stress by pumping Ca^{2+} out of the cell and presumably into vacuole to reduce $[Ca^{2+}]_c$. Possible interaction between CRZ-1 and the *nca-2* promoter is shown with dashed line and arrow. Possible mechanism of action, which has not yet established, is indicated using question marks in the parentheses.

Chapter 5

Neurospora and rat orthologs of neuronal calcium sensor-1 (NCS-1) show functional conservation

5.1 Introduction

Neuronal calcium sensor-1 (NCS-1) belongs to the neuronal calcium sensor (NCS) family of proteins, first discovered member was frequenin (FRQ) that binds to Ca^{2+} in *Drosophila melanogaster* (Pongs *et al.*, 1993). The NCS-1 protein contains a highly conserved N-myristoylation domain and four EF-hand domains, and its orthologs are identified in yeast, filamentous fungi, insects, nematodes, birds, mammals including human (Nef, 1996; Tamuli *et al.*, 2011). NCS proteins are Ca^{2+}-myristoyl switch proteins with N-myristoylation and four Ca^{2+} binding EF-hand domains (Burgoyne *et al.*, 2004; Burgoyne, 2007). NCS-1 protein is encoded by the *ncs-1* gene (NCU04379) in *N. crassa*. NCS-1 from *N. crassa* shows significant sequence similarities with its orthologs from fission yeast, other filamentous fungi like *M. grisea*, and *A. fumigatus*, and mammals including rat and human (Deka *et al.*, 2011). Therefore, to test if the fungal and mammalian NCS-1 orthologs are functionally conserved, I expressed the *Rattus norvegicus* ortholog of the NCS-1 in *N. crassa* to study inter-specific complementation.

5.2 Results

5.2.1 Sequence analysis of the *N. crassa*, rat, and human NCS-1 orthologs

The protein sequences of NCS-1 orthologs in *N. crassa*, *Rattus norvegicus* (rat) and *Homo sapiens* (human) with GenBank accession numbers EAA28220.1, AAA88510.1 and AAF01804.1, respectively, were obtained from the NCBI protein database (https://www.ncbi.nlm.nih.gov/protein) as described previously (Deka *et al.*, 2011). The protein sequences were aligned with ClustralX 2.0 (Larkin *et al.*, 2007) and visualized using GeneDoc (Nicholas, 1997). Interestingly, the rat and human NCS-1 orthologs are 100% identical. A BLASTp (https://blast.ncbi.nlm.nih.gov/Blast.cgi; Altschul *et al.*, 1990) analysis of NCBI using the *N. crassa* NCS-1 as the query sequence revealed 82% similarity and 66%

identity with *e*-value 8e-96 with its rat and human orthologs. The multiple sequence alignment showed that all the three NCS-1 orthologs possess a conserved N- myristoylation domain and four EF-hand domains (Fig. 5.1).

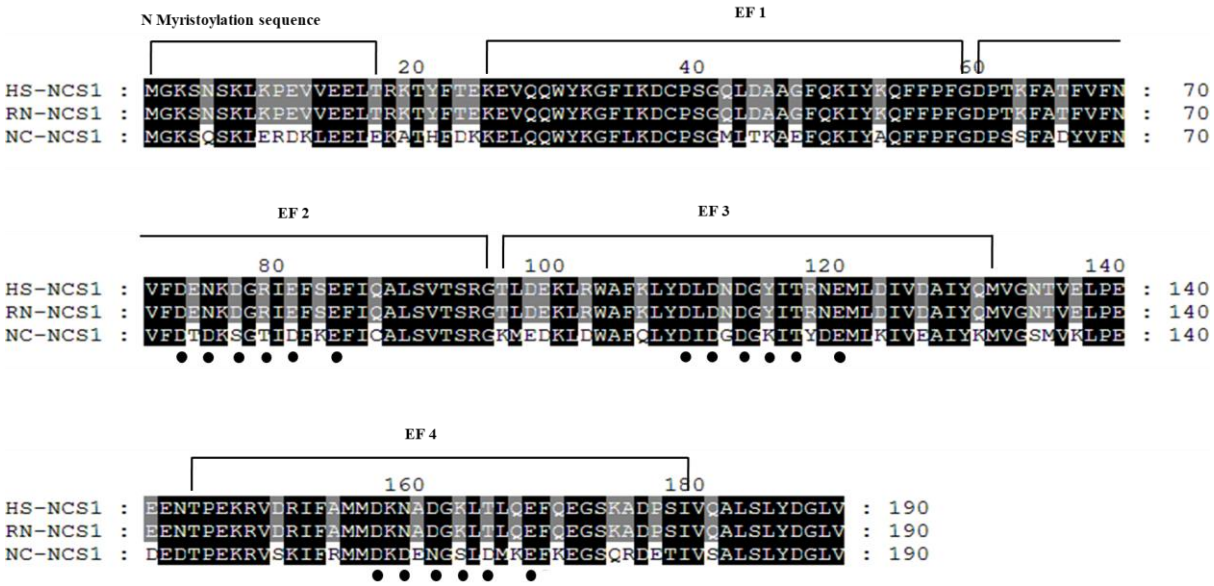

Fig. 5.1: Sequence alignment of NCS-1 orthologs from *N. crassa*, rat, and human. Conserved amino acids are indicated in black (100%) and light grey (>60%). The positions of the N-terminal myristoylation sequence and the four EF-hands (EF1, EF2, EF3 and EF4) are indicated above the sequence. The amino acid residues responsible for providing the oxygen ligands for Ca^{2+} coordination are indicated below the sequence using black dots.

5.2.2 Generation of the *N. crassa* strain for the expression of rat NCS-1

To generate the *N. crassa* strain expressing rat NCS-1 (NCS-1^{Rat}), the *ncs-*1^{Rat} cDNA (GenBank™ accession no. L27421; McFerran *et al.*, 1999) was PCR amplified using the pET5α-*ncs-*1^{Rat} plasmid construct as template, and the primers Rat *ncs-1* pMF272 F and Rat *ncs-1* pMF272 R (Table 2.2) containing the *Xba*I and *Pac*I restriction sites, respectively, for directional cloning. The pET5α-*ncs-*1^{Rat} plasmid construct contains the rat *ncs-1* cDNA (*ncs-*1^{Rat}) and was a kind gift from Prof. Robert D. Burgoyne (Physiological laboratory, University of Liverpool, UK). The *N. crassa his-3* (NCU03139), located in linkage group I (LG I),

targeting vector pMF272 vector (Freitag *et al.*, 2004) that contains an N-terminal GFP tag, was used for cloning the PCR amplified *ncs-1*^{Rat}. The PCR product and the pMF272 vector were double digested using the restriction enzymes PacI (Cat. No. R0547S, New England Biolabs, USA) and XbaI (Cat. No. R0145S, New England Biolabs, USA), then ligated using the Quick Ligation Kit (M2200S, New England Biolabs, USA), and transformed into the *E. coli* DH5α ultra-competent cells (Inoue *et al.*, 1990). The plasmids were then isolated from the transformed *E. coli* DH5α cells and screened by PCR using the primers Rat *ncs-1* F and Rat *ncs-1* R (Table 2.2) and digestion with PacI (Cat. No. R0547S, New England Biolabs, USA) and XbaI (Cat. No. R0145S, New England Biolabs, USA) restriction enzymes (Fig. 5.2) to identify the plasmid containing the *ncs-1*^{Rat} insert. The plasmid construct, pDG-5 (Fig. 5.3) containing the *ncs-1*^{Rat} insert was identified and isolated using the plasmid mini-preparation method as described in the Chapter 2. The pDG-5 construct was transformed into the *N. crassa his-3*; Δ*ncs-1* (11) strain (Table 2.1) by electroporation as described in the Chapter 2. The heterokaryotic transformants were selected on FGS agar plates incubated at 30 °C for 2 days . The initial heterokaryotic transformants were verified by PCR using the primers Rat *ncs-1* F and Rat *ncs-1* R (Table 2.2) for integration of the *ncs-1*^{Rat} insert, and a heterokaryotic transformant *ncs-1*^{Rat} HT (RB10) was isolated (Fig. 5.4). The heterokaryotic transformant *ncs-1*^{Rat} HT (RB10) was crossed with the Δ*ncs-1 a* (FGSC 11403) strain to generate homokaryotic progenies. The ascospores obtained were germinated in minimal FGS agar plate, and the homokaryotic progenies were initially screened for hygromycin resistance on FGS agar plate supplemented with hygromycin (220 µg/ml). The homokaryotic progenies showing hygromycin resistance were further verified by PCR using two different primers sets, Rat *ncs-1* F and Rat *ncs-1* R for *ncs-1*^{Rat} allele, and HI-NCS-1F and 5*hph*-RV for Δ*ncs-1*::*hph* allele (Table 2.2; Fig. 5.5). Thus, I isolated two homokaryotic strains *ncs-1*^{Rat} hop (RB10-7) and *ncs-1*^{Rat} hop (RB10-14) (Table 2.2) and used for further studies.

First, I performed the mRNA and protein expression analysis of the NCS-1^{Rat}. To isolate RNA and protein, the *N. crassa* wild type (FGSC 987), Δ*ncs-1 A* (FGSC 11404), *ncs-1*^{Rat} hop (RB10-7) and *ncs-1*^{Rat} hop (RB10-14) strains (Table 2) were cultured in 100 ml conical flasks containing 10 ml VM liquid and incubated at 30 °C with shaking at 180 rpm for 16 h. Total RNA and protein from these cultures were isolated as described in the Chapter 2. To determine the mRNA expression, a reverse transcriptase PCR (RT-PCR) was performed using about 1 µg of the total RNA from each sample, primers Rat *ncs-1* F and Rat *ncs-1* R (Table 2.2), and Verso™ cDNA Synthesis Kit (Cat. no. AB-1453/A, Thermo Fisher Scientific, USA). PCR products were analysed using a 1 % agarose gel, the presence of a PCR product of size 570 bp confirmed the expression of the *ncs-1*^{Rat} mRNA (Fig 5.6 A). In addition, protein concentration was quantified by Bradford Assay using Bradford Reagent (Cat. No. ML106-100ML, Himedia, India). Samples containing 50 µg of total protein were run on a 10% SDS gel, and western blot was performed using rabbit anti-GFP antibody (Cat. No. A6455, Life Technologies, USA) and detected by chemiluminescence as described in the Chapter 2. The appearance of a band of size ~49.4 kDa (Fig. 5.6 B) in the protein sample isolated from the homokaryotic transformants confirmed the successful heterologous expression of the NCS-1^{Rat}::GFP fusion protein in *N. crassa.*

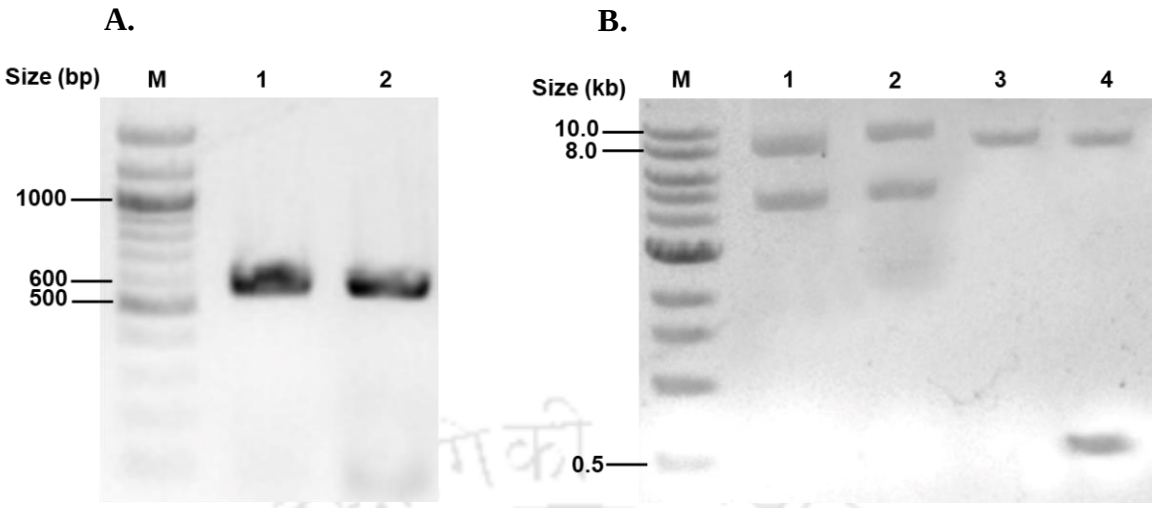

Fig. 5.2: Cloning of the *ncs-1*^{rat} cDNA in the pMF272 vector for interspecific complementation.

A. Confirmation of the *ncs-1*^{Rat} cDNA clones by PCR using the primers Rat *ncs-1* F and Rat *ncs-1* R (Table 2.2). The PCR products were resolved in 1% agarose gel, amplicons of size 570 bp were observed for the pET5α- *ncs-1*^{Rat} construct (lane 1) and pDG-5 construct (lane 2). The pET5α- *ncs-1*^{Rat} construct was used as a control, and the 100 bp NEB DNA ladder (New England Biolabs, USA) was used as marker (M).

B. Confirmation of the *ncs-1*^{Rat} cDNA clones by digesting with restriction endonucleases. The pDG-5 construct was digested with the restriction enzymes PacI and XbaI (New England Biolabs, USA) and resolved in 1% agarose gel, using the 1 kb NEB DNA ladder (New England Biolabs, USA) as marker (M). Two DNA bands of size ~8.4 kb and ~0.5 kb were observed (lane 4) for the clone containing the *ncs-1*^{Rat} cDNA insert. The undigested pMF272 vector (lane 1), undigested pDG-5 construct (lane 2), and PacI and XbaI digested pMF272 vector (lane3) were used as controls.

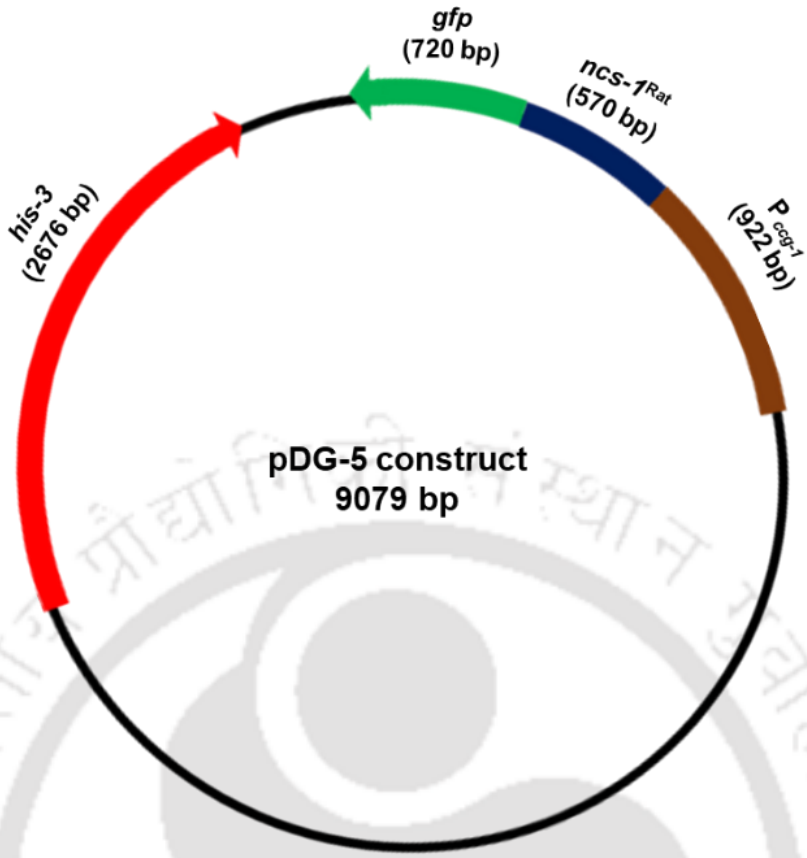

Fig. 5.3: Schematic diagram showing the pDG-5 plasmid construct containing the *ncs-1*^{Rat} cDNA under the *ccg-1* promoter (P_{ccg-1}). The pDG-5 plasmid (9,079 bp) contains the *ncs-1*^{Rat} cDNA cloned in the multiple cloning sites (MCS) region of the pMF272 vector. The numbers (in bp) in the parentheses indicate the size of the respective fragments.

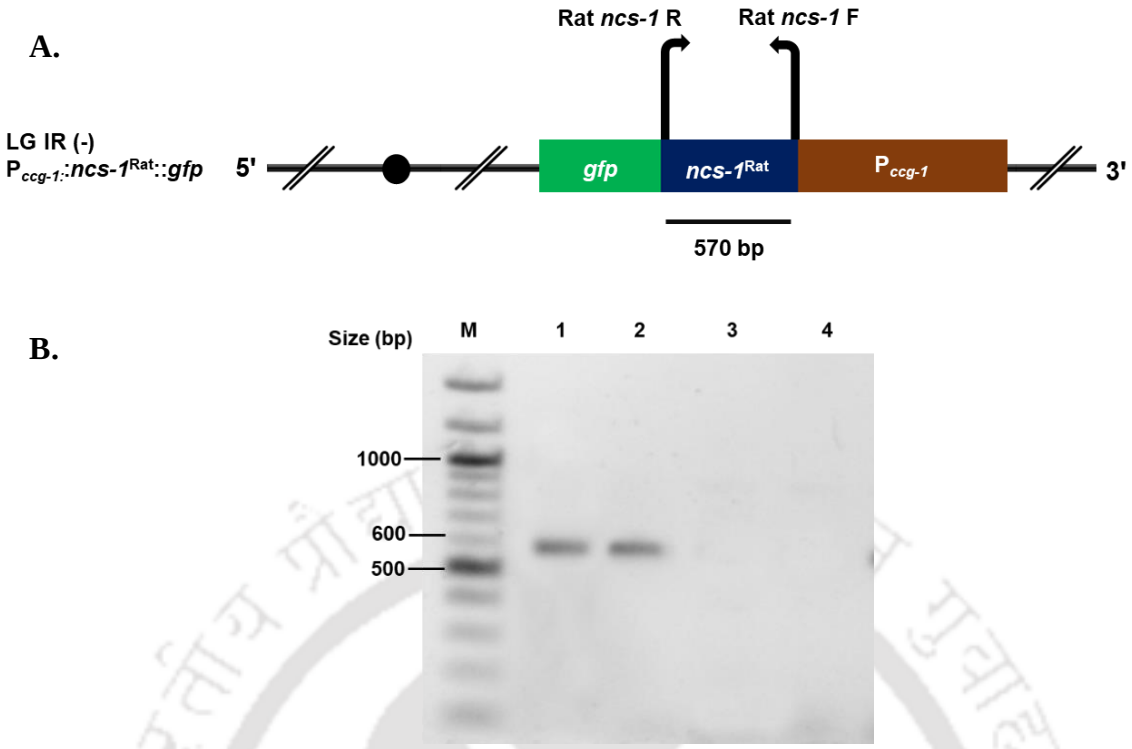

Fig. 5.4: Verification of the heterokaryotic *ncs-1*^{Rat} HT (RB10) strain for the presence of the P$_{ccg-1}$::*ncs-1*^{Rat}::*gfp* allele.

A. Schematic diagram showing the primer positions and 5'→3' orientation (shown using the direction of the arrow) used for the verification of the *ncs-1*^{Rat} allele in the heterokaryotic *ncs-1*^{Rat} HT (RB10) strain. The size of the PCR product is shown below the primer positions.

B. PCR confirmation of the P$_{ccg-1}$::*ncs-1*^{Rat}::*gfp* allele in the heterokaryotic *ncs-1*^{Rat} HT (RB10) strain. The PCR, performed using the primers Rat *ncs-1* F and Rat *ncs-1* R (Table 2.2), followed by a 1% agarose gel analysis revealed the PCR amplicons of size 570 bp for the pDG-5 construct and heterokaryotic *ncs-1*^{Rat}-HT (RB-10) strain in the lanes 1 and 2, respectively. The 100 bp NEB DNA ladder (New England Biolabs, USA) was used as marker (M). The pDG-5 construct in lane 1 was used as positive control, while the wild type (FGSC 987) and the recipient *his-3*$^{-}$Δ*ncs-1* (11) strain in lanes 3 and 4, respectively, were used as negative controls.

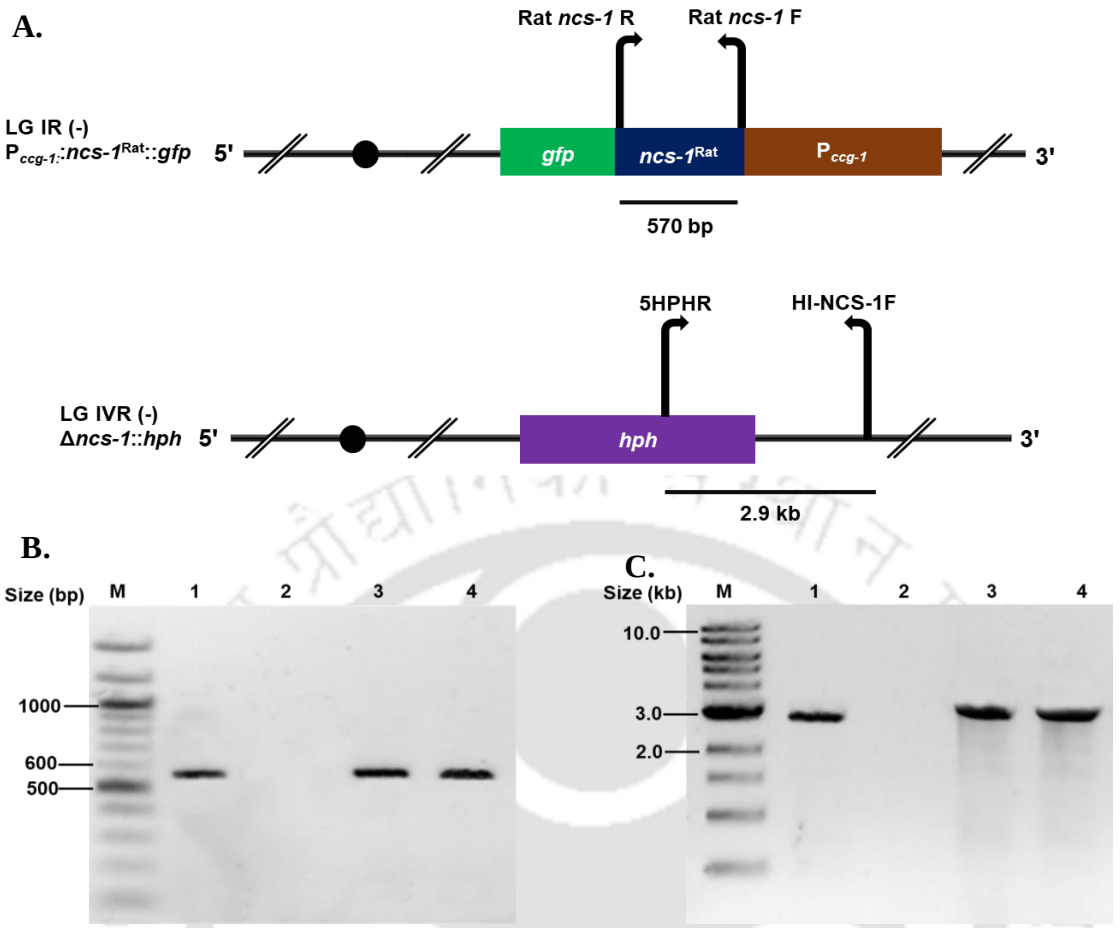

Fig. 5.5: PCR verification of the $P_{ccg\text{-}1}$::*ncs-1*^{Rat}::*gfp* and Δ*ncs-1*::*hph* alleles in the *N. crassa* homokaryotic strains.

A. Schematic diagram showing the primer positions and 5'→3' orientation (shown using the direction of the arrow) used for the PCR verification of the homokaryotic strains for the presence of the $P_{ccg\text{-}1}$::*ncs-1*^{Rat}::*gfp* and Δ*ncs-1*::*hph* alleles. The size of the PCR product is shown below the primer positions.

B. PCR confirmation of the $P_{ccg\text{-}1}$::*ncs-1*^{Rat}::*gfp* allele in the homokaryotic *ncs-1*^{Rat} hop (RB10-7) and *ncs-1*^{Rat} hop (RB10-14) strains using the primers Rat *ncs-1* F and Rat *ncs-1* R (Table 2.2). The PCR amplicons of size 570 bp for the pDG-5 construct, and the *ncs-1*^{Rat} hop (RB10-7) and *ncs-1*^{Rat} hop (RB10-14) homokaryotic strains were observed in the lanes 1, 3, and 4, respectively, when resolved in 1 % agarose gel. The 100 bp NEB DNA ladder (New England

Biolabs, USA) was used as marker (M). The pDG-5 construct in lane 1 was used as positive control, while the wild type (FGSC 987) strain in lane 2 was used as negative control.

C. PCR confirmation of the Δ*ncs-1*::*hph* allele in the homokaryotic *ncs-1*^{Rat} hop (RB10-7) and *ncs-1*^{Rat} hop (RB10-14) strains using the primers HI-NCS-1F and 5HPHR (Table 2.2). The *hph* cassette fragment of length ~2.9 kb was observed for the Δ*ncs-1 A* (FGSC 11404) and homokaryotic *ncs-1*^{Rat} hop (RB10-7) and *ncs-1*^{Rat} hop (RB10-14) strains in the lanes 1, 3 and 4, respectively, when resolved in 1% agarose gel with 1 kb NEB DNA ladder (New England Biolabs, USA) as marker (M). The Δ*ncs-1 A* (FGSC 11404) strain in lane 1 was used as positive control and wild type (FGSC 987) strain in lane 2 was used as negative control.

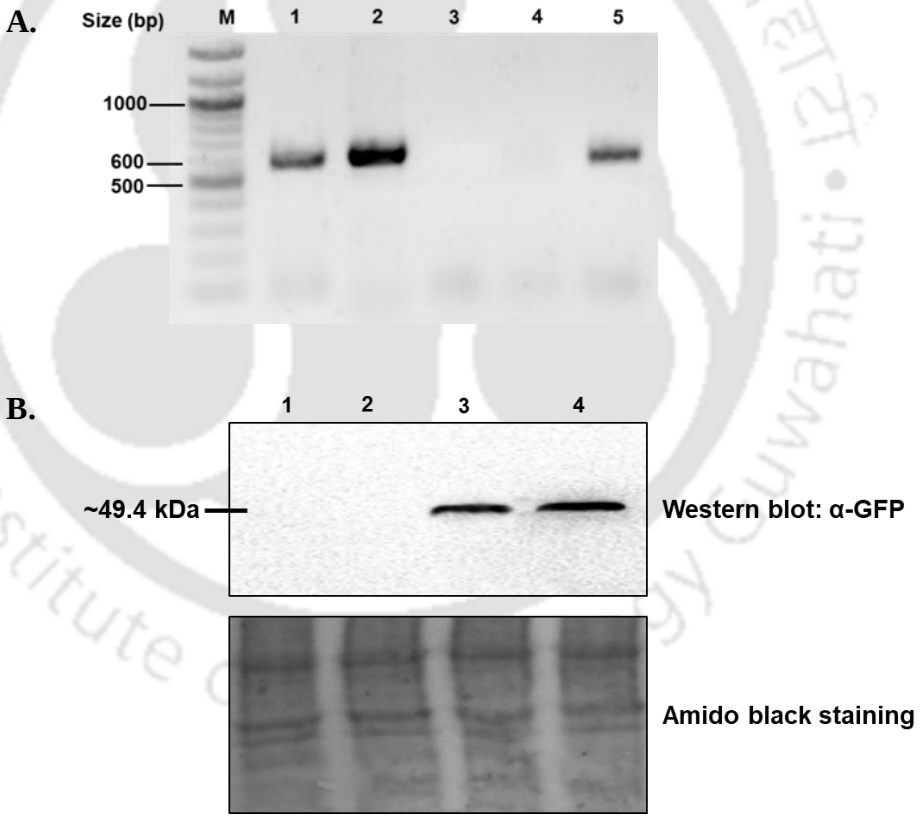

Fig. 5.6: Expression analysis of *ncs-1*^{Rat} under P$_{ccg-1}$.

A. Heterologous expression of *ncs-1*^{Rat} in *N. crassa*. About 1 µg of the total RNA isolated from the indicated *N. crassa* strains were used for the reverse transcriptase PCR (RT-PCR) and analysed using a 1 % agarose gel. Amplification of 570 bp of *ncs-1*^{Rat} cDNA for the

homokaryotic *ncs-1*^{Rat} hop (RB10-7) and *ncs-1*^{Rat} hop (RB10-14) strains, as observed in the lanes 1 and 2, respectively, confirmed the heterologous expression of *ncs-1*^{Rat} at mRNA level. The wild type (FGSC 987) and Δ*ncs-1 A* (FGSC 11404) strains, shown in the lane 3 and 4, respectively, were used as negative controls in the PCR, and pDG-5 construct shown in lane 5 was used as a positive PCR control. The 100 bp NEB DNA ladder (New England Biolabs, USA) was used as marker (M).

B. Western blot showing the expression of rat NCS-1::GFP (~49.4 kDa) under P_{ccg-1} in the homokaryotic *ncs-1*^{Rat} strains using anti-GFP antibody. Lanes 3 and 4 show the expression of rat NCS-1::GFP for the homokaryotic *ncs-1*^{Rat} hop (RB10-7) and *ncs-1*^{Rat} hop (RB10-14) strains respectively. The wild type (FGSC 987) and Δ*ncs-1 A* (FGSC 11404) strains in lane 3 and 4 were used as negative controls. The amido black staining of the membrane, shown in the lower panel, demonstrates the equal protein loading.

5.2.3 Interspecific complementation studies

The *N. crassa* Δ*ncs-1* mutant displayed slow growth, sensitivity to Ca^{2+} and UV stress conditions (Deka *et al.*, 2011). The *ncs-1*^{Rat} homokaryotic strains had shown successful expression of the NCS-1^{Rat} protein. To test whether NCS-1^{Rat} could complement the phenotypes of the Δ*ncs-1* mutant strain, I performed a series of complementation studies including the apical growth rate, Ca^{2+} and UV stress survival assays.

5.2.3.1 The *ncs-1*^{Rat} homokaryotic strains grew like wild type

The growth behaviour of the *ncs-1*^{Rat} homokaryotic strains was studied using standard race tube assay (Ryan *et al.*, 1943; Ryan, 1950). Agar plugs of the wild type (FGSC 987, 988), Δ*ncs-1* (FGSC 11403, 11404) and homokaryotic *ncs-1*^{Rat} strains, Rat *ncs-1* hop (RB10-7) and Rat *ncs-1* hop (RB10-14), were inoculated at one end of the race tube containing 13 ml of VM agar and incubated at 30 °C for 72 h. The hyphal growth front was marked periodically at

every 12 h interval. The distance of the hyphal growth front from the point of inoculation was plotted against time (Table 5.1; Fig. 5.7). The average growth rates of the wild type, Δ*ncs-1* and *ncs-1*^{Rat} strains were 0.362 ± 0.079, 0.236 ± 0.071 and 0.347 ± 0.083 cm h^{-1}, respectively, calculated from the growth data of three individual experiments (n = 3).

Table 5.1: Apical growth of the wild type, Δ*ncs-1*, and homokaryotic *ncs-1*^{Rat} strains in race tube

Strains	Distance (cm) in race tube at the indicated time interval						
	0 h	12 h	24 h	36 h	48 h	60 h	72 h
Wild type	0.0 ± 0.0	2.6 ± 0.2	7.8 ± 0.3	13.8 ± 0.4	19.5 ± 0.4	25.0 ± 0.4	30.5 ± 0.4
Δ*ncs-1*	0.0 ± 0.0	1.4 ± 0.1	4.6 ± 0.2	8.8 ± 0.2	13.3 ± 0.3	17.3 ± 0.3	21.6 ± 0.3
ncs-1^{Rat} hop	0.0 ± 0.0	2.4 ± 0.2	7.5 ± 0.3	12.9 ± 0.4	18.7 ± 0.4	24.3 ± 0.4	30.2 ± 0.4

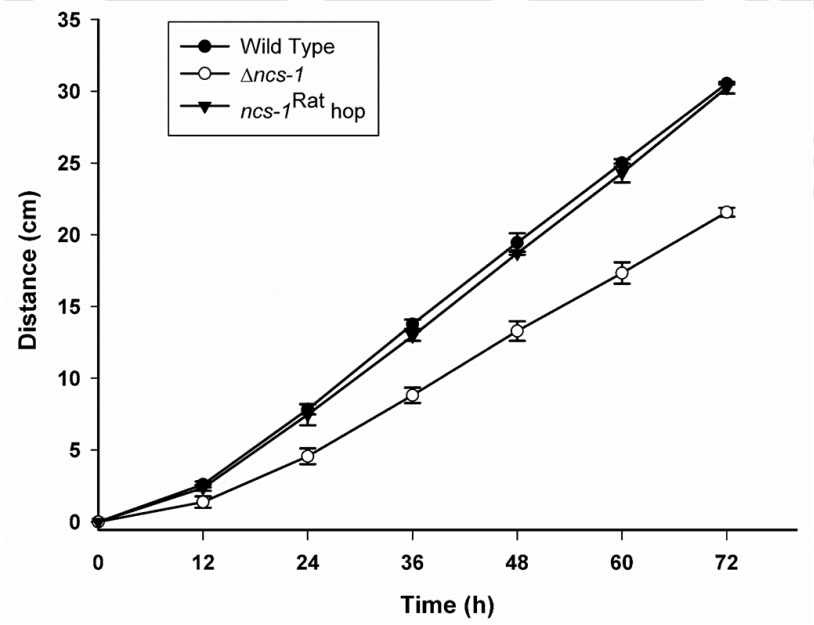

Fig. 5.7: The *ncs-1*^{Rat} allele complements the slow growth phenotype of the Δ*ncs-1* mutant. Agar plugs of the wild type, Δ*ncs-1*, and *ncs-1*^{Rat} homokaryotic (hop) strains were inoculated

at one end of the race tube containing 13 ml of VM agar and incubated at 30°C for 72 h. The *ncs-1*^{Rat} hop strain showed similar growth rate as the wild type strain, thus complements the slow growth phenotype of the Δ*ncs-1* mutant. Error bars indicate the standard deviation calculated from the data for three independent experiments (n = 3).

5.2.3.2 The *ncs-1*^{Rat} strains showed tolerance to the Ca^{2+} stress like the wild type

To test if the *ncs-1*^{Rat} homokaryotic strains were able to complement the Ca^{2+} sensitive phenotype of the Δ*ncs-1* mutant, I performed a Ca^{2+} stress tolerance assay. The wild type (FGSC 987, 988), Δ*ncs-1* (FGSC 11403, 11404), and the homokaryotic *ncs-1*^{Rat} strains, Rat *ncs-1* hop (RB10-7) and Rat *ncs-1* hop (RB10-14), were grown on VM medium was supplemented with four different concentrations of $CaCl_2$ (0, 0.2, 0.3, and 0.4 M). The average colony growth rates percentage on medium supplemented with different $CaCl_2$ concentrations were obtained by dividing the growth rate at the respective medium with the average colony growth rate at 0 M $CaCl_2$ and multiplying with 100. The homokaryotic *ncs-1*^{Rat} strains displayed similar colony growth rate like the wild type under different $CaCl_2$ concentrations (Table 5.2; Fig. 5.8).

Table 5.2: Average colony growth rate (%) of the wild type, Δ*ncs-1* and homokaryotic *ncs-1*^{Rat} strains at various concentrations of $CaCl_2$

Strains	Average colony growth rate (%) at various concentrations of $CaCl_2$ (M)			
	0	0.2	0.3	0.4
Wild type	100.0 ± 0.0	90.6 ± 3.2	81.4 ± 1.6	72.2 ± 2.6
Δ*ncs-1*	100.0 ± 0.0	72.1 ±2.9	56.8 ±2.6	30.7 ± 2.3
ncs-1^{Rat} hop	100.0 ± 0.0	88.2 ± 1.5	77.7 ± 1.6	64.5 ± 1.1

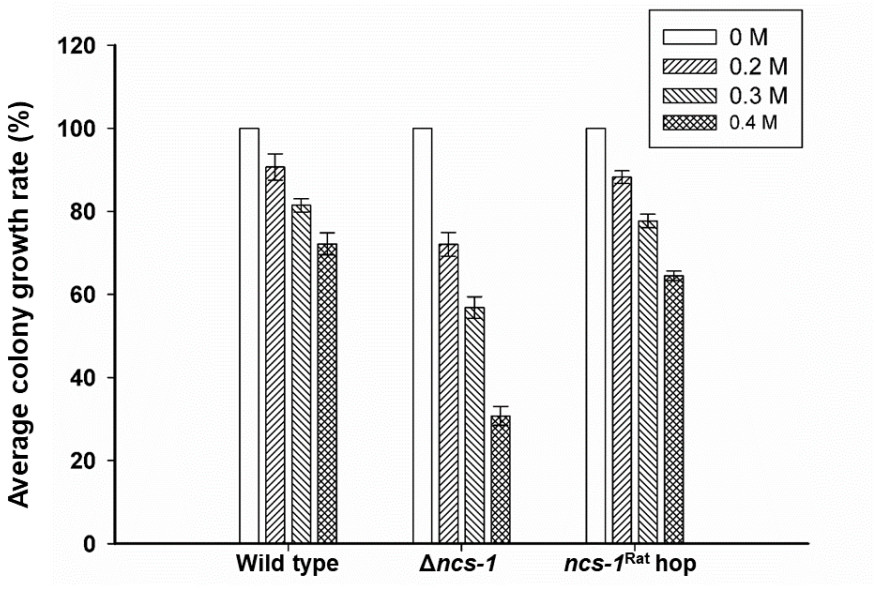

Fig. 5.8: The *ncs-1*^{Rat} allele complements the Ca^{2+} sensitive phenotype of the Δ*ncs-1*. The *N. crassa* strains were grown in VM supplemented with various amounts of $CaCl_2$ and incubated at 30 °C with shaking at 180 rpm for 18 h. Error bars indicate the standard deviation calculated from the data of three individual experiments (n = 3).

5.2.3.3 The *ncs-1*^{Rat} strains complemented the ultraviolet sensitivity of the Δ*ncs-1* mutant

I tested the ultraviolet (UV) sensitivity of the *ncs-1*^{Rat} strains towards UV using both qualitative and quantitative assays. The *upr-1* (34-97-3; Table 2.1) strain, which showed hypersensitivity to UV exposure, was used for comparing the relative UV sensitivity (Tamuli *et al.*, 2006). For qualitative analysis, conidia of the wild type, Δ*ncs-1*, *upr-1* (34-97-3), and *ncs-1*^{Rat} strains were grown in 250 ml conical flasks containing 50 ml VM agar medium for 4 days in dark followed by 1 day under light at 30 °C, conidia were then harvested, washed with sterile water, and finally re-suspended in 1 ml sterile water. For the qualitative assay, a serial dilution (10^0, 10^{-1}, 10^{-2}, 10^{-3}, 10^{-4}, 10^{-5}, and 10^{-6}) was performed, then 5 µl conidial suspensions of each dilution were spotted on FGS agar plate and irradiated with UV doses of 0, 100, 200 and 300 J m^{-2} in a UV cross-linker (UVC 500, Hoefer, UK). For the quantitative assay, ~1000 conidia were plated on the FGS agar plate and irradiated with the same UV doses as in the qualitative assay.

The qualitative and quantitative UV survival assays (Table 5.3; Fig. 5.9) revealed that viability of the *ncs-1*^{rat} strains were like the wild type strain, therefore, the *ncs-1*^{rat} allele complements the UV sensitivity of the Δ*ncs-1* mutant.

Table 5.3: Relative UV-sensitivity of the wild type, Δ*ncs-1*, *ncs-1*^{Rat}, and *upr-1* strains

Strains	**% Survival in various doses of UV irradiation (Jm^{-2})**			
	0	**100**	**200**	**300**
Wild type	100.0 ± 0.0	65.2 ± 0.7	15.1 ± 0.5	1.1 ± 0.3
Δ*ncs-1*	100.0 ± 0.0	27.2 ± 1.4	1.1 ± 0.3	0.0 ± 0.0
ncs-1^{rat} hop	100.0 ± 0.0	62.1 ± 0.8	13.9 ± 0.4	1.0 ± 0.2
upr-1	100.0 ± 0.0	4.0 ± 0.2	0.0 ± 0.0	0.0 ± 0.0

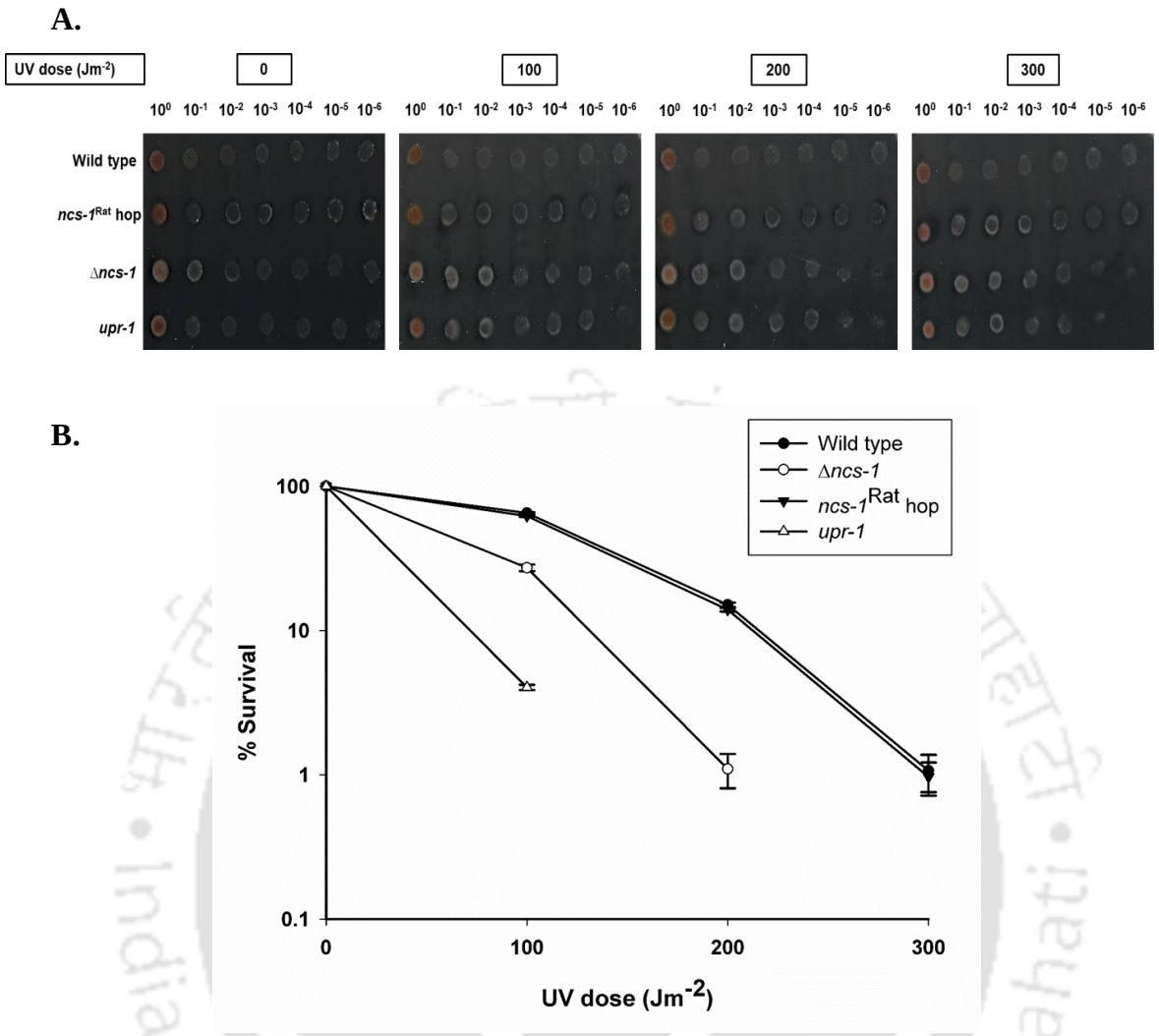

Fig. 5.9: Complementation of the UV stress-sensitive phenotype of the Δ*ncs-1* mutant by *ncs-1*^{Rat}.

A. Qualitative assay for UV sensitivity. An aliquot of 5 µl conidial suspensions of the indicated dilutions (10^0 - 10^{-6}) of the wild type, Δ*ncs-1*, *ncs-1*^{Rat} hop, and *upr-1* strains were spotted left to right on FGS agar plate and irradiated with UV doses of 0, 100, 200 and 300 J m^{-2} in a UV cross-linker (UVC 500, Hoefer, UK). The Δ*ncs-1* strain was more sensitive to UV exposure than the wild type, while the *ncs-1*^{Rat} hop strain displayed UV sensitivity similar to the wild type strain.

B. Quantitative assay for UV sensitivity. Approximately 1000 conidia of the wild type, Δ*ncs-1* mutant, *ncs-1*^{Rat} hop, and *upr-1* strains were platted on FGS agar plates and irradiated with UV doses of 0, 100, 200 and 300 J m^{-2}. A semi-logarithmic plot was obtained by plotting the survival percentage on logarithmic Y-axis against the UV doses on linear X-axis. The *ncs-1*^{Rat} hop strain had shown similar survival percentage like the wild type strain. Percent survival was obtained by dividing the number of colonies from plates irradiated with different doses of UV by the number of colonies on control plates with no UV irradiation (0 J m^{-2}). Error bars indicate the standard deviation calculated from the data of three individual experiments.

5.2.4 Site-directed mutagenesis of the NCS-1^{Rat} to mutate glutamic acid at position 120 to a glutamine residue

Previously, a site-directed mutation (SDM) study revealed that three key amino acid residues, glycine (G), glutamic acid (E), and arginine (R) at positions 2, 120, and 175, respectively, were important for NCS-1 functions in *N. crassa* (Gohain *et al.*, 2016). The glutamic acid (E) at position 120 was found to be most critical, since mutating this residue to glutamine (E→Q) resulted in a mutant displaying phenotypes identical to the Δ*ncs-1* strain, suggesting that E120Q causes complete loss of the function (Gohain *et al.*, 2016). The E120 residue is located in the Ca^{2+} binding site of the EF-hand 3 (EF3) of the *N. crassa* NCS-1 (Fig. 5.1). Interestingly, E120 residue in the EF3 of NCS-1 is highly conserved from lower to higher eukaryotes (Deka *et al.*, 2011; Gohain *et al.*, 2016). The E120Q mutation was also shown to impair Ca^{2+} dependent conformational activity of NCS-1^{Rat}, although, the mutant protein was binding to cellular proteins (Weiss *et al.*, 2000; Burgoyne and Weiss, 2001). Therefore, I generated E120Q mutation in the EF3 domain of the rat NCS-1 to test its function in *N. crassa*. For introducing the E120Q mutation, the glutamic acid codon GAG in the *ncs-1*^{Rat} cDNA was mutated to glutamine codon CAG using the mutagenic primer pairs Rat *ncs-1* E120Q-F and Rat *ncs-1* E120Q-R (Table 2.2) and the pDG-5 construct (Fig. 5.3). The mutagenic PCR was

performed by using Q5® high-fidelity DNA Polymerase (Cat No. M0491S, New England Biolabs, USA) with cycling parameters of initial denaturation at 98 ℃ for 2 min, followed by 25 cycles of denaturation at 98 ℃ for 10 s, annealing at 70 ℃ for 15 s and extension at 72 ℃ for 7 min, and final extension at 72 ℃ for 10 min. The PCR product was digested using DpnI restriction enzyme (Cat. No. M0491S, New England Biolabs, USA) to remove the methylated parental and hemimethylated template DNA, and transformed into ultra-competent *E. coli* DH5α cells (Inoue *et al.*, 1990) for plasmid nick repair and replication. The transformant colonies were selected on LB agar medium supplemented with ampicillin (100 µg/ml). Plasmid DNA from the transformed *E. coli* DH5α cells was isolated and the desired E120Q mutation in the plasmids was confirmed by DNA sequencing (Figs. 5.10, 5.11; GenBank accession number KU991935). Based on sequence analysis, a plasmid construct named as pDG-5^{E120Q} containing the E120Q mutation was isolated (Fig. 5.12).

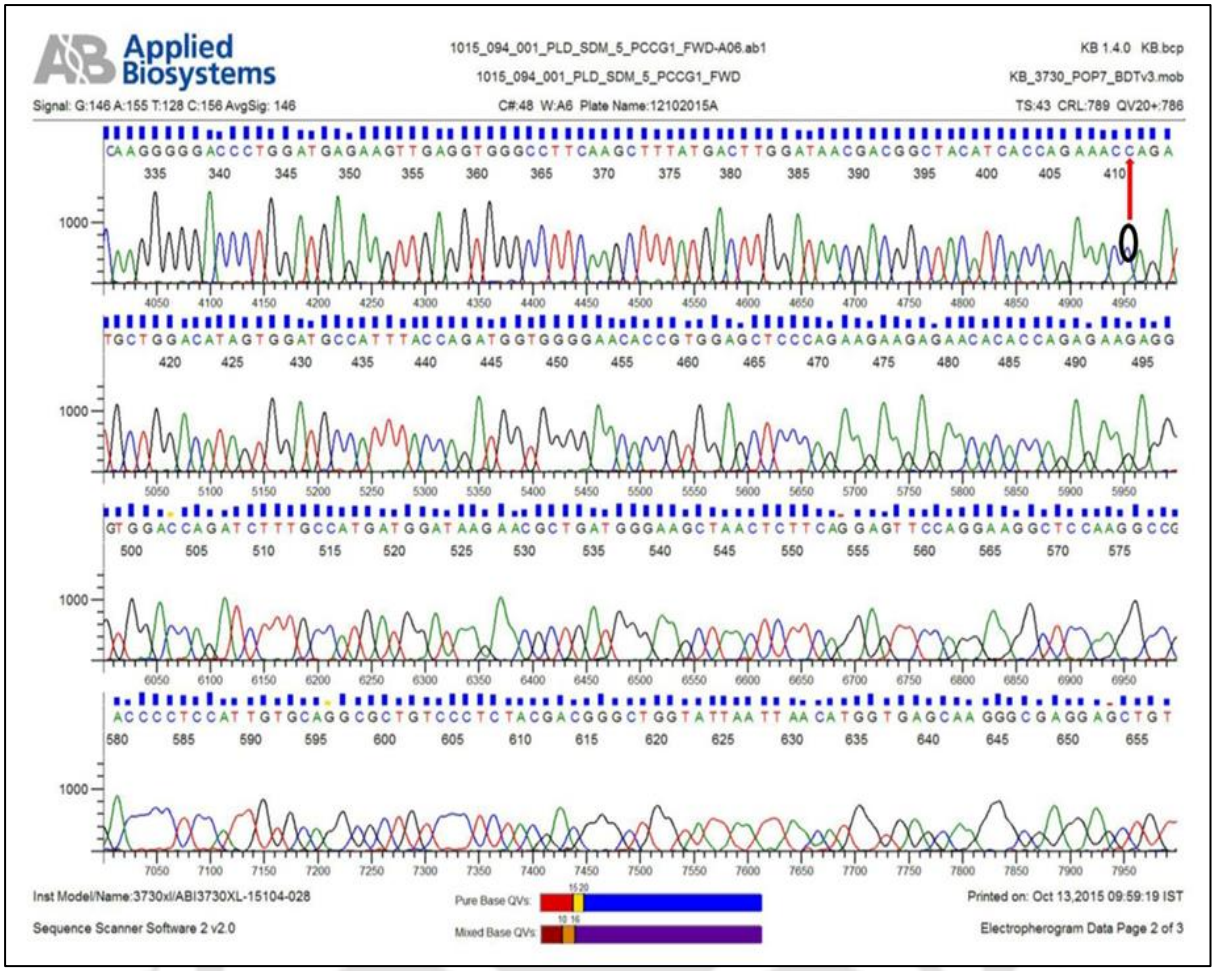

Fig. 5.10: Chromatogram profile of the *ncs-1*$^{Rat\ (E120Q)}$ mutant allele generated by sequencing of the pDG-5^{E120Q} construct. The point mutation in the triplet codon GAG to CAG (or CTC to GTC) changes glutamic acid at position 120 to glutamine in the NCS-1^{Rat} protein. The position of the point mutation is shown using a black circle in the chromatogram, and a red arrowhead in the corresponding sequence.

A.

```
ncs-1Rat            ----------------------ATGGGGAAATCCAACAGCAAGTTGAAGCCTGA 32
ncs-1Rat(E120Q) ACAACCCCTCACATCAACCAAATCTAGAATGGGGAAATCCAACAGCAAGTTGAAGCCTGA 60
                                          ********************************

ncs-1Rat        AGTTGTGGAGGAGCTGACCAGAAAAACCTACTTCACTGAAAAGGAAGTACAGCAGTGGTA 92
ncs-1Rat(E120Q) AGTTGTGGAGGAGCTGACCAGAAAAACCTACTTCACTGAAAAGGAAGTACAGCAGTGGTA 120
                ************************************************************

ncs-1Rat        AAGGGTTTCATTAAGGACTGCCCCAGTGGGCAGCTGGACGCCGCTGGCTTCCAGAAGAT  152
ncs-1Rat(E120Q) CAAGGGTTTCATTAAGGACTGCCCCAGTGGGCAGCTGGACGCCGCTGGCTTCCAGAAGAT 180
                ************************************************************

ncs-1Rat        CTACAAACAGTTCTTCCCATTTGGAGACCCCACCAAGTTCGCCACGTTTGTTTTCAACGT 212
ncs-1Rat(E120Q) CTACAAACAGTTCTTCCCATTTGGAGACCCCACCAAGTTCGCCACGTTTGTTTTCAACGT 240
                ************************************************************

ncs-1Rat        CTTCGACGAGAACAAGGATGGCAGGATCGAGTTCTCCGAATTCATCCAGGCTCTATCGGT 272
ncs-1Rat(E120Q) CTTCGACGAGAACAAGGATGGCAGGATCGAGTTCTCCGAATTCATCCAGGCTCTATCGGT 300
                ************************************************************

ncs-1Rat        GACCTCAAGGGGGACCCTGGATGAGAAGTTGAGGTGGGCCTTCAAGCTTTATGACTTGGA 332
ncs-1Rat(E120Q) GACCTCAAGGGGGACCCTGGATGAGAAGTTGAGGTGGGCCTTCAAGCTTTATGACTTGGA 360
                ************************************************************

ncs-1Rat        TAACGACGGCTACATCACCAGAAACGAGATGCTGGACATAGTGGATGCCATTTACCAGAT 392
ncs-1Rat(E120Q) TAACGACGGCTACATCACCAGAAACCAGATGCTGGACATAGTGGATGCCATTTACCAGAT 420
                ************************ ********************************

ncs-1Rat        GGTGGGGAACACCGTGGAGCTCCCAGAAGAAGAGAACACACCAGAGAAGAGGGTGGACCG 452
ncs-1Rat(E120Q) GGTGGGGAACACCGTGGAGCTCCCAGAAGAAGAGAACACACCAGAGAAGAGGGTGGACCG 480
                ************************************************************

ncs-1Rat        GATCTTCGCCATGATGGATAAGAACGCTGATGGGAAGCTAACTCTTCAGGAGTTCCAGGA 512
ncs-1Rat(E120Q) GATCTTCGCCATGATGGATAAGAACGCTGATGGGAAGCTAACTCTTCAGGAGTTCCAGGA 540
                ************************************************************

ncs-1Rat        AGGCTCCAAGGCCGACCCCTCCATTGTGCAGGCGCTGTCCCTCTACGACGGGCTGGTA-- 570
ncs-1Rat(E120Q) AGGCTCCAAGGCCGACCCCTCCATTGTGCAGGCGCTGTCCCTCTACGACGGGCTGGTATT 600
                ************************************************************

ncs-1Rat        -------------------------- 570
ncs-1Rat(E120Q) AATTAACATGGTGAGCAAGGGCGAGG 626
```

B.

```
NCS-1Rat        MGKSNSKLKPEVVEELTRKTYFTEKEVQQWYKGFIKDCPSGQLDAAGFQKIYKQFFPFGD 60
NCS-1Rat(E120Q) MGKSNSKLKPEVVEELTRKTYFTEKEVQQWYKGFIKDCPSGQLDAAGFQKIYKQFFPFGD 60
                ************************************************************

NCS-1Rat        PTKFATFVFNVFDENKDGRIEFSEFIQALSVTSRGTLDEKLRWAFKLYDLDNDGYITRNE 120
NCS-1Rat(E120Q) PTKFATFVFNVFDENKDGRIEFSEFIQALSVTSRGTLDEKLRWAFKLYDLDNDGYITRNQ 120
                ************************************************************

NCS-1Rat        MLDIVDAIYQMVGNTVELPEEENTPEKRVDRIFAMMDKNADGKLTLQEFQEGSKADPSIV 180
NCS-1Rat(E120Q) MLDIVDAIYQMVGNTVELPEEENTPEKRVDRIFAMMDKNADGKLTLQEFQEGSKADPSIV 180
                ************************************************************

NCS-1Rat        QALSLYDGLV 190
NCS-1Rat(E120Q) QALSLYDGLV 190
                **********
```

Fig. 5.11: Confirmation of the E120Q mutation in pDG-5^{E120Q} construct.

A. The sequence of the *ncs-1*$^{Rat\ (E120Q)}$ allele, obtained by DNA sequencing, was aligned with the *ncs-1*^{Rat} cDNA sequence using ClustalX. Asterisks below the alignment indicate the

identical nucleotide. The absence of asterisk below the unmatched nucleotide (indicated with grey shade) in the alignment confirmed the changed nucleotide of the triplet codon GAG to CAG.

B. The nucleotide sequence of the *ncs-1*$^{\text{Rat (E120Q)}}$ allele, obtained by DNA sequencing, and the *ncs-1*$^{\text{Rat}}$ cDNA sequence was translated to amino acid sequence by ExPASy translate tool (https://web.expasy.org/translate/) and aligned using ClustalX. Asterisks below the alignment indicate the identical amino acid residues. The absence of asterisk below the unmatched amino acid residue (indicated with grey shade) in the alignment confirmed the change of glutamic acid (E) at position 120 to glutamine (Q).

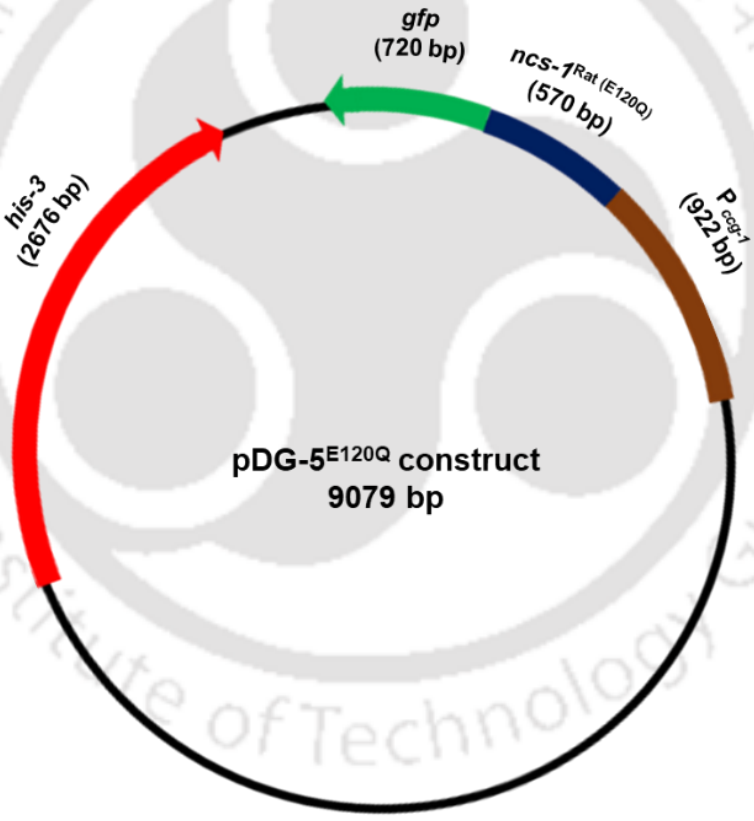

Fig. 5.12: Schematic diagram showing the pDG-5$^{\text{E120Q}}$ plasmid construct containing the *ncs-1*$^{\text{Rat (E120Q)}}$ allele under the *ccg-1* promoter (P$_{ccg-1}$). The pDG-5$^{\text{E120Q}}$ plasmid (9,079 bp) contains the mutated *ncs-1*$^{\text{Rat (E120Q)}}$ cDNA cloned into the multiple cloning sites (MCS) region

of the pMF272 vector. The numbers (in bp) in the parentheses indicate the size of the respective fragment.

5.2.5 Generation of the *ncs-1*$^{\text{Rat (E120Q)}}$ strain and expression of rat NCS-1$^{\text{E120Q}}$::GFP

The pDG-5$^{\text{E120Q}}$ construct was transformed into the *his-3* Δ*ncs-1* (11) strain (Table 2.1) by electroporation as described in the Chapter 2. The initial heterokaryotic transformants were selected on normal FGS agar medium and crossed with the Δ*ncs-1a* (FGSC 11403) strain to generate the homokaryotic strain. The homokaryotic progenies were initially screened for hygromycin resistance on FGS agar plate supplemented with hygromycin (220 µg/ml). The homokaryotic progenies with hygromycin resistance were selected and then verified using two sets of PCR primers, Rat *ncs-1* F and Rat *ncs-1* R (Table 2.2) for *ncs-1*$^{\text{Rat (E120Q)}}$ allele, and HI-NCS-1F and 5*hph*-RV for Δ*ncs-1*::*hph* allele (Fig. 5.13). Based on the PCR verification, two homokaryotic strains *ncs-1*$^{\text{Rat (E120Q)}}$ hop (E5-3) and *ncs-1*$^{\text{Rat (E120Q)}}$ hop (E5-28) were isolated and used for subsequent studies (Table 2.1).

I performed the mRNA and protein expression analysis of the *ncs-1*$^{\text{Rat (E120Q)}}$ allele in the *ncs-1*$^{\text{Rat (E120Q)}}$ (E5-3) and *ncs-1*$^{\text{Rat (E120Q)}}$ (E5-28) strains. For the isolation of RNA, wild type (FGSC 987), Δ*ncs-1 A* (FGSC 11404), *ncs-1*$^{\text{Rat}}$ hop (RB10-7), *ncs-1*$^{\text{Rat}}$ hop (RB10-14), *ncs-1*$^{\text{Rat (E120Q)}}$ hop (E5-3) and *ncs-1*$^{\text{Rat (E120Q)}}$ hop (E5-28) strains were cultured in 100 ml conical flasks containing 10 ml VM liquid and incubated at 30 °C with shaking at 180 rpm for 16 h. The total RNA was isolated as described in the Chapter 2. A reverse transcriptase PCR (RT-PCR) was performed using the primers Rat *ncs-1* F and Rat *ncs-1* R and Verso™ cDNA Synthesis Kit (Cat. no. AB-1453/A, Thermo Fisher Scientific, USA). PCR products were analysed using a 1% agarose gel. A positive PCR product of size 570 bp confirmed the mRNA expression of the *ncs-1*$^{\text{Rat (E120Q)}}$ allele (Fig 5.14 A).

For the isolation of protein, the wild type wild type (FGSC 987), Δ*ncs-1 A* (FGSC 11404), *ncs-1*$^{\text{Rat}}$ hop (RB10-7), *ncs-1*$^{\text{Rat}}$ hop (RB10-14), *ncs-1*$^{\text{Rat (E120Q)}}$ hop (E5-3) and *ncs-1*$^{\text{Rat}}$

$^{(E120Q)}$ hop (E5-28) strains were cultured in 100 ml conical flasks containing 10 ml VM liquid at 30°C with shaking at 180 rpm for 16 h. The crude total protein was extracted from the samples as described in the Chapter 2. Protein concentration was quantified by Bradford Assay using Bradford reagent, (Cat. No. ML106-100ML, Himedia, India). Samples containing 50 µg of total protein were resolved using a 12% SDS gel and western blot was performed using anti-GFP antibody (Cat. No. A6455, Life Technologies, USA) and detected by chemiluminescence as described in the Chapter 2. The band of size ~49.4 kDa observed for the homokaryotic transformants confirmed the successful expression of the rat NCS-1^{E120Q}::GFP fusion protein in *N. crassa* (Fig. 5.14 B).

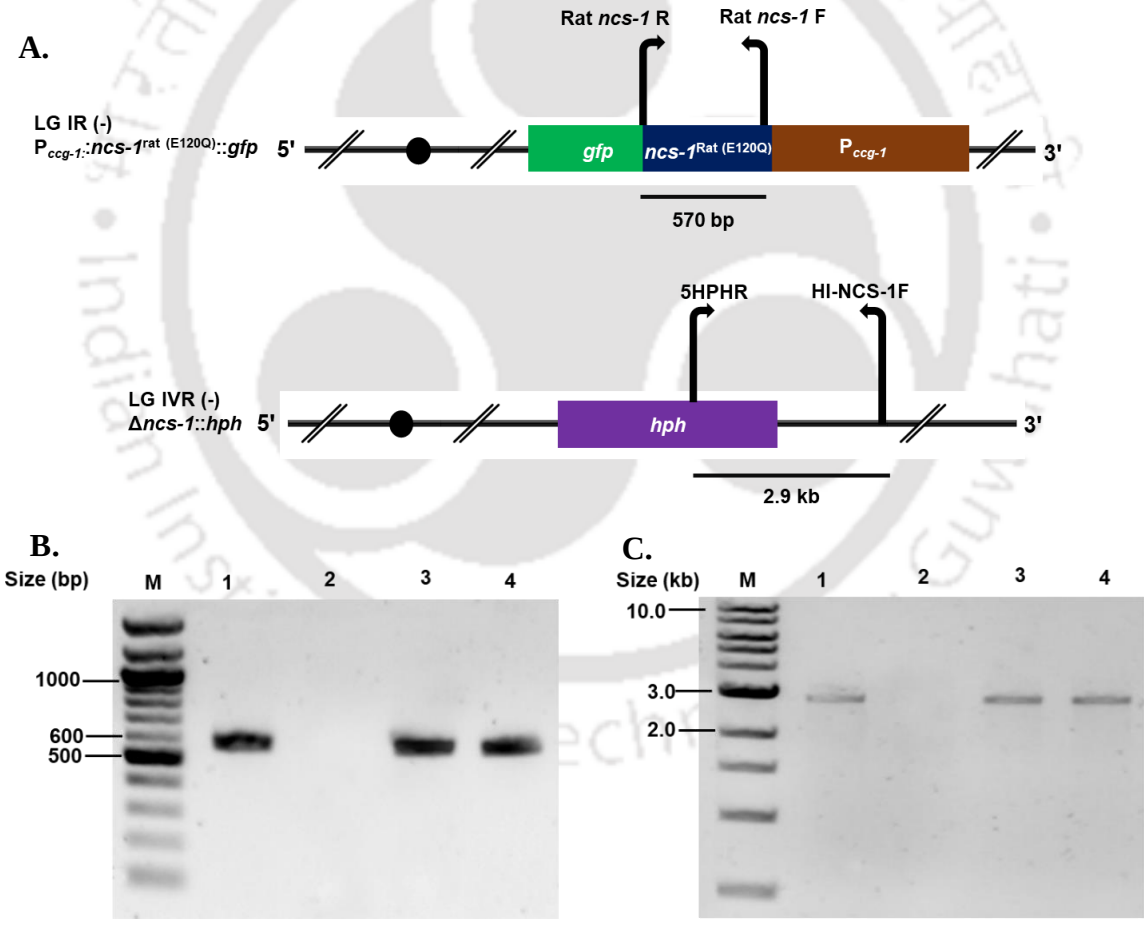

Fig. 5.13: Verification of the P$_{ccg-1}$::*ncs-1*$^{Rat\ (E120Q)}$::*gfp* and Δ*ncs-1*::*hph* alleles in the *N. crassa* homokaryotic strains.

A. Schematic diagram showing the primer positions with 5'→3' orientation (shown using the direction of the arrow) used for the verification of the homokaryotic strains for the presence of the $P_{ccg\text{-}1}$::*ncs-1*$^{Rat\ (E120Q)}$::*gfp* and Δ*ncs-1*::*hph* alleles.

B. Confirmation of the $P_{ccg\text{-}1}$::*ncs-1*$^{Rat\ (E120Q)}$::*gfp* allele in the homokaryotic *ncs-1*$^{Rat\ (E120Q)}$ hop (E5-28) and *ncs-1*$^{Rat\ (E120Q)}$ hop (E5-3) strains by PCR using the primers Rat *ncs-1* F and Rat *ncs-1* R (Table 2.2). The PCR amplicons, resolved in 1.2% agarose gel, of size 570 bp were observed for the pDG-5 construct and homokaryotic *ncs-1*$^{Rat\ (E120Q)}$ hop (E5-28) and *ncs-1*$^{Rat\ (E120Q)}$ hop (E5-3) strains, in the lanes 1, 3 and 4, respectively. The 100 bp NEB DNA ladder (New England Biolabs, USA) was used as marker (M), the pDG-5 construct in lane 1 was used as positive control, and DNA from the wild type (FGSC 987) strain in lane 2 was used as negative control.

C. Confirmation of the Δ*ncs-1*::*hph* allele in the homokaryotic *ncs-1*$^{Rat\ (E120Q)}$ hop (E5-28) and *ncs-1*$^{Rat\ (E120Q)}$ hop (E5-3) strains by PCR using the primers HI-NCS-1F and 5HPHR (Table 2.2). The *hph* cassette of length ~2.9 kb was observed for the Δ*ncs-1 A* (FGSC 11404) and homokaryotic *ncs-1*$^{Rat\ (E120Q)}$ hop (E5-28), and *ncs-1*$^{Rat\ (E120Q)}$ hop (E5-3) strains were observed in the lanes 1, 3, and 4, respectively, when resolved in 1% agarose gel with 1 kb NEB DNA ladder (New England Biolabs, USA) as marker (M). The Δ*ncs-1 A* (FGSC 11404) strain in lane 1 was used as positive control, and wild type (FGSC 987) strain in lane 2 was used as negative control.

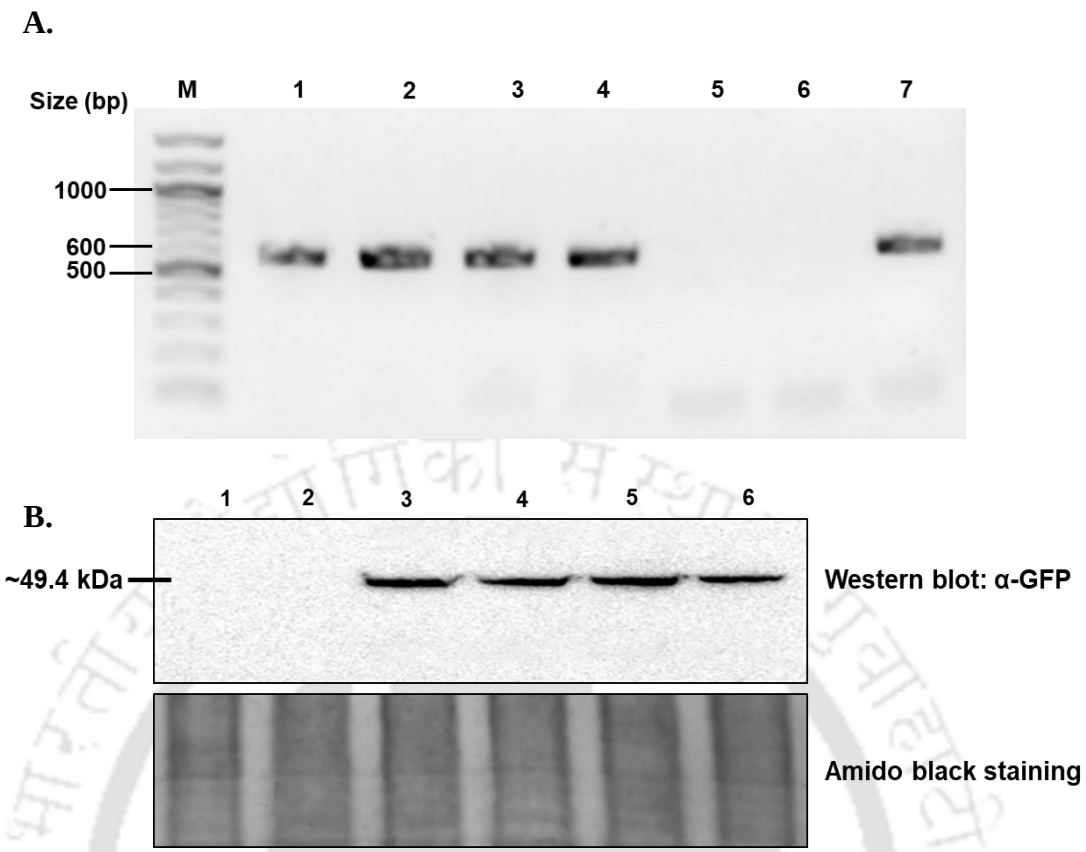

Fig. 5.14: Expression analysis of *ncs-1*$^{\text{Rat (E120Q)}}$ under P$_{ccg\text{-}1}$.

A. Heterologous expression of *ncs-1*$^{\text{Rat (E120Q)}}$ in *N. crassa*. About 1 µg of the total RNA isolated from the indicated *N. crassa* strains were used for the reverse transcriptase PCR (RT-PCR) and analysed using 1 % agarose gel. Amplification of 570 bp of mutated *ncs-1*$^{\text{Rat (E120Q)}}$ cDNA for the homokaryotic *ncs-1*$^{\text{Rat (E120Q)}}$ hop (E5-3) and *ncs-1*$^{\text{Rat (E120Q)}}$ hop (E5-28) strains, as observed in the lanes 3 and 4, respectively, confirmed the heterologous expression of the *ncs-1*$^{\text{Rat (E120Q)}}$ mRNA. The wild type (FGSC 987) and Δ*ncs-1* A (FGSC 11404) strains in lane 3 and, respectively, were used as negative controls, while *ncs-1*$^{\text{Rat}}$ hop (RB10-7) and *ncs-1*$^{\text{Rat}}$ hop (RB10-14) strains, pDG-5 construct in lanes 1, 2, and 7, respectively, were used as positive control in the PCR analysis. The 100 bp NEB DNA ladder (New England Biolabs, USA) was used as marker (M).

B. Western blot showing the expression of rat NCS-1$^{\text{E120Q}}$::GFP (~49.4 kDa) under P$_{ccg\text{-}1}$ in the homokaryotic *ncs-1*$^{\text{Rat (E120Q)}}$ strains using anti-GFP antibody. The expression of NCS-

1$^{Rat(E120Q)}$::GFP in the homokaryotic *ncs-1*$^{Rat\ (E120Q)}$ hop (E5-3) and *ncs-1*$^{Rat\ (E120Q)}$ hop (E5-28) strains was observed in the lanes 5 and 6, respectively. The wild type (FGSC 987) and Δ*ncs-1 A* (FGSC 11404) strains in lane 1 and 2 were used as negative controls, while *ncs-1*^{Rat} hop (RB10-7) and *ncs-1*^{Rat} hop (RB10-14) strains in lanes 3 and 4, respectively, were used as positive control. The band of size ~49.4 kDa observed for the homokaryotic strains (lanes 3-6) confirmed the successful expression of the NCS-1^{Rat}::GFP and NCS-1$^{Rat(E120Q)}$::GFP fusion proteins in *N. crassa*. The amido black staining of the membrane, as shown in the lower panel, demonstrates the equal protein loading.

5.2.6 The *ncs-1*$^{Rat\ (E120Q)}$ mutant displayed slow growth phenotype like the Δ*ncs-1* mutant

The apical growth of the homokaryotic *ncs-1*$^{Rat\ (E120Q)}$ mutants was studied using standard race tube assay (Ryan *et al.*, 1943; Ryan, 1950). Agar plugs of the wild type (FGSC 987, 988), Δ*ncs-1* (FGSC 11403, 11404), *ncs-1*^{Rat} hop (RB10-7), *ncs-1*^{Rat} hop (RB10-14), *ncs-1*$^{Rat\ (E120Q)}$ hop (E5-3), and *ncs-1*$^{Rat\ (E120Q)}$ hop (E5-28) strains were inoculated at one end of the race tube containing 13 ml of VM agar and incubated at 30 °C for 72 h. The distance of the hyphal growth front from the point of inoculation was plotted against time (Table 5.3; Fig. 5.15). The average growth rates of the wild type, Δ*ncs-1*, *ncs-1*^{Rat}, and *ncs-1*$^{Rat\ (E120Q)}$ strains were 0.356 ± 0.081, 0.222 ± 0.077, 0.336 ± 0.088, and 0.236 ± 0.080 cm h^{-1}, respectively which were calculated from the growth data of three individual experiments (n = 3). Thus, the *ncs-1*$^{Rat\ (E120Q)}$ mutant grows slowly like the Δ*ncs-1* mutant.

Table 5.4: Apical growth of the wild type, Δ*ncs-1*, homokaryotic *ncs-1*^{Rat} and *ncs-1*$^{Rat\ (E120Q)}$ strains in race tube

Strains	Distance (cm) in race tube at the indicated time interval						
	0 h	**12 h**	**24 h**	**36 h**	**48 h**	**60 h**	**72 h**
Wild Type	0.0 ± 0.0	2.5 ± 0.1	7.6 ± 0.2	13.6 ± 0.2	19.1 ± 0.2	24.8 ± 0.1	30.3 ± 0.2
Δ*ncs-1*	0.0 ± 0.0	1.1 ± 0.1	4.2 ± 0.1	8.4 ± 0.1	12.6 ± 0.2	16.8 ± 0.1	21.3 ± 0.1
ncs-1^{Rat} hop	0.0 ± 0.0	2.2± 0.1	7.0 ± 0.1	12.5 ± 0.3	18.6 ± 0.1	23.7 ± 0.3	29.9 ± 0.2
ncs-1$^{Rat(E120Q)}$ hop	0.0 ± 0.0	1.2 ± 0.1	4.4 ± 0.2	8.8 ± 0.1	13.3 ± 0.2	17.8 ± 0.1	22.5 ± 0.1

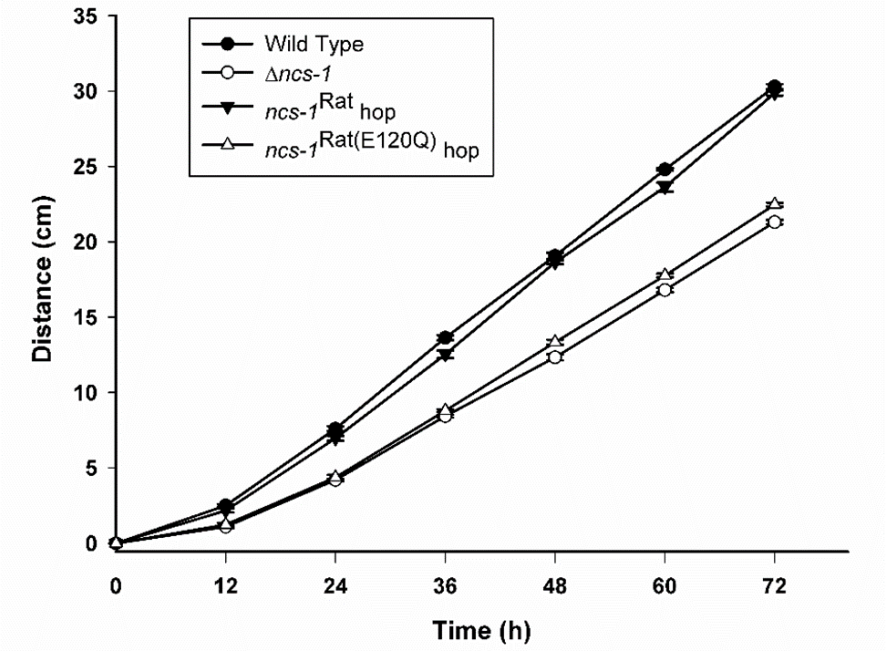

Fig. 5.15: Growth phenotype of the *ncs-1*$^{Rat\ (E120Q)}$ mutant. Agar plugs of the wild type, Δ*ncs-1*, homokaryotic *ncs-1*^{Rat}, and *ncs-1*$^{Rat\ (E120Q)}$ strains were inoculated at one end of the race tube containing 13 ml of VM agar and incubated at 30 °C for 72 h. The homokaryotic

ncs-1$^{Rat\ (E120Q)}$ mutant strains showed slow growth rate like the Δ*ncs-1* mutant. Error bars indicate the standard deviations calculated from the data for three independent experiments (n = 3).

5.2.7 The *ncs-1*$^{Rat\ (E120Q)}$ mutant was sensitive to the Ca^{2+} stress like the Δ*ncs-1* mutant

To test the effects of Ca^{2+} stress on the homokaryotic *ncs-1*$^{Rat\ (E120Q)}$ mutant strains, I studied growth of the *ncs-1*$^{Rat\ (E120Q)}$ hop (E5-3) and *ncs-1*$^{Rat\ (E120Q)}$ hop (E5-28) strains on VM agar medium supplemented with different concentrations of $CaCl_2$ (0, 0.2, 0.3, and 0.4 M) was performed. The wild type (FGSC 987, 988), Δ*ncs-1* (FGSC 11403, 11404), *ncs-1*^{Rat} hop (RB10-7) and *ncs-1*^{Rat} hop (RB10-14) were used as controls. The average colony growth rates for different $CaCl_2$ concentrations were expressed in percentage by dividing with the average colony growth rate at 0 M $CaCl_2$ and multiplying with 100. The homokaryotic *ncs-1*$^{Rat\ (E120Q)}$ strains displayed severe growth defect like the Δ*ncs-1* mutant in different $CaCl_2$ concentrations (Table 5.5; Fig. 5.16).

Table 5.5: Average colony growth rate (%) of the wild type, Δ*ncs-1* homokaryotic *ncs-1*^{Rat}, and *ncs-1*$^{Rat\ (E120Q)}$ strains at various concentrations of $CaCl_2$

Strains	Average colony growth rate (%) at various concentrations of $CaCl_2$ (M)			
	0	0.2	0.3	0.4
Wild type	100.0 ± 0.0	92.9 ± 2.5	84.4 ± 2.5	70.5 ± 1.5
Δ*ncs-1*	100.0 ± 0.0	72.7 ± 1.8	57.0 ± 1.0	32.1 ± 0.5
ncs-1^{Rat} hop	100.0 ± 0.0	91.0 ± 1.7	79.1 ± 1.9	65.0 ± 1.7
ncs-1$^{Rat(E120Q)}$ hop	100.0 ± 0.0	75.8 ± 2.3	58.0 ± 0.8	34.0 ± 0.3

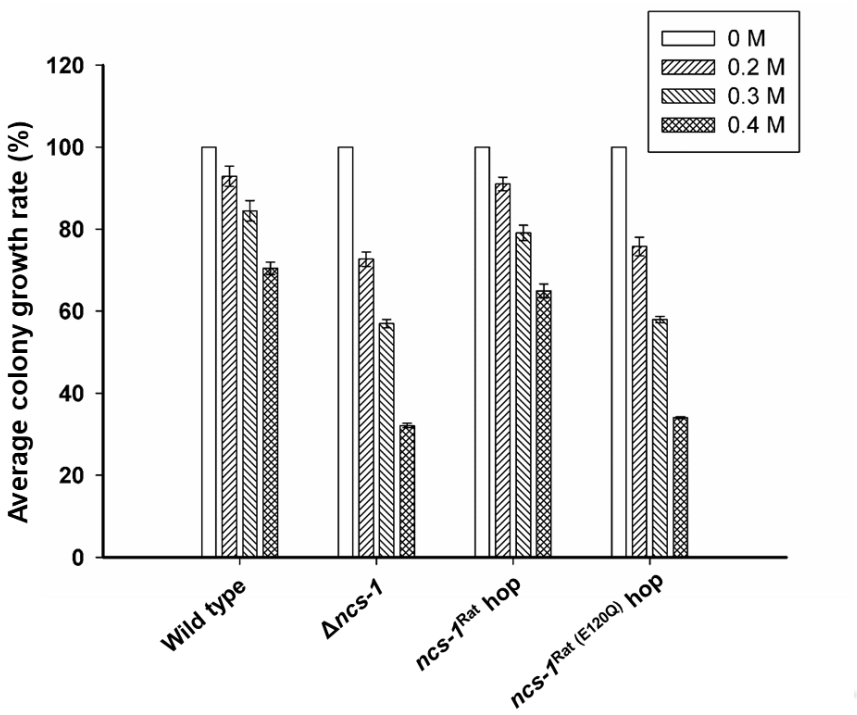

Fig. 5.16: Effect of Ca^{2+} stress on the growth of the *ncs-1*$^{Rat(E120Q)}$ mutant. The *N. crassa* strains were grown in VM supplemented with various amounts of $CaCl_2$ and incubated at 30 °C with shaking at 180 rpm for 18 h. Error bars indicate the standard deviation calculated from the data of three individual experiments (n = 3).

5.2.8 The *ncs-1*$^{rat\ (E120Q)}$ mutant was sensitive to UV stress like the Δ*ncs-1* mutant

The sensitivity of the homokaryotic *ncs-1*$^{Rat\ (E120Q)}$ strains to UV stress was tested both qualitatively and quantitatively as described above. The *upr-1* (34-97-3) mutant (Table 2.1) was used to compare relative UV sensitivity. The qualitative and quantitative UV survival assays (Table 5.6; Fig. 5.17) revealed that the *ncs-1*$^{Rat\ (E120Q)}$ homokaryotic strains were sensitive to UV exposure in a similar manner as the Δ*ncs-1* mutant strain.

Table 5.6: Relative UV-sensitivity of the wild type, Δ*ncs-1*, *upr*-1, homokaryotic *ncs-1*^{Rat}, and *ncs-1*$^{Rat\ (E120Q)}$ strains

Strains	% Survival in various doses of UV irradiation (J m^{-2})			
	0	100	200	300
Wild type	100.0 ± 0.0	64.6 ± 0.8	14.6 ± 0.2	0.8 ± 0.1
Δ*ncs-1*	100.0 ± 0.0	27.2 ± 1.4	0.9 ± 0.1	0.0 ± 0.0
ncs-1^{Rat} hop	100.0 ± 0.0	62.1 ± 0.8	14.6 ± 0.3	0.8 ± 0.1
ncs-1$^{Rat(E120Q)}$ hop	100.0 ± 0.0	30.6 ± 0.7	1.3 ± 0.2	0.0 ± 0.0
upr-1	100.0 ± 0.0	3.7 ± 0.5	0.0 ± 0.0	0.0 ± 0.0

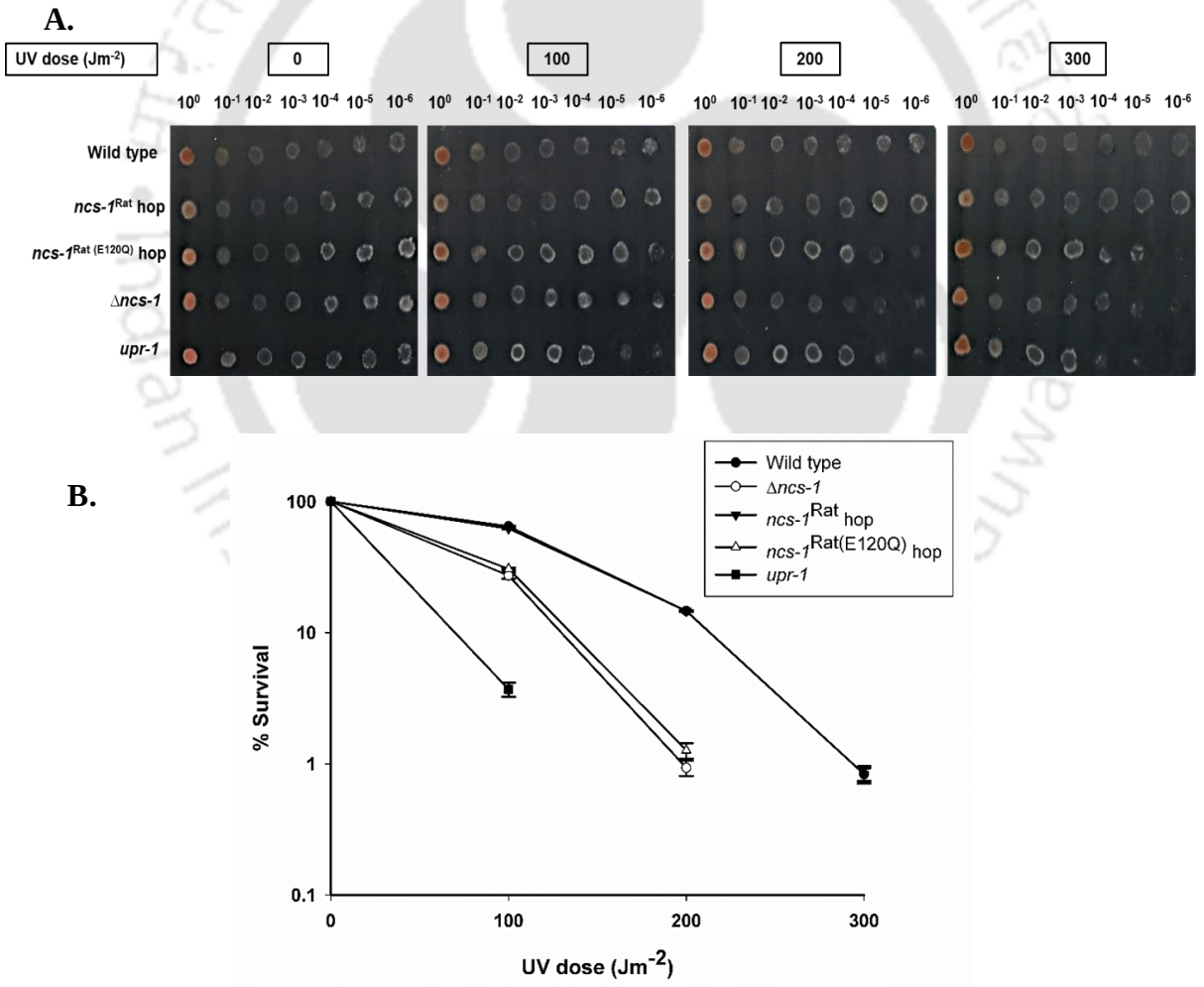

Fig. 5.17: The *ncs-1*$^{Rat\ (E120Q)}$ mutants were sensitive to UV irradiation like the Δ*ncs-1* mutant.

A. Qualitative UV sensitivity assay. An aliquot of 5 µl conidial suspensions of each dilution (10^0, 10^{-1}, 10^{-2}, 10^{-3}, 10^{-4}, 10^{-5}, and 10^{-6}) of the wild type, Δ*ncs-1*, *upr-1*, homokaryotic *ncs-1*^{Rat}, and *ncs-1*$^{Rat\ (E120Q)}$ strains were spotted on FGS agar plate and irradiated with UV doses of 0, 100, 200 and 300 J m^{-2} in a UV cross-linker (UVC 500, Hoefer, UK). The *ncs-1*$^{Rat\ (E120Q)}$ mutant displayed UV sensitivity similar to the Δ*ncs-1* mutant.

B. Quantitative UV sensitivity assay. Approximately 1000 conidia of the wild type, Δ*ncs-1*, *upr-1*, homokaryotic *ncs-1*^{Rat}, and *ncs-1*$^{Rat\ (E120Q)}$ strains were platted on FGS agar plates and irradiated with different UV doses of 0, 100, 200 and 300 J m^{-2}. A semi-logarithmic plot was obtained by plotting the survival percentage on logarithmic Y-axis against the UV doses on linear X-axis. The survival percentage of the *ncs-1*$^{Rat\ (E120Q)}$ mutant was reduced severely like the Δ*ncs-1* mutant. Percent survival was obtained by dividing the number of colonies from plates irradiated with different doses of UV by the number of colonies on control plates with no UV irradiation (0 J m^{-2}) and multiplying with 100. Error bars indicate the standard deviation calculated from the data of three individual experiments.

5.3 Discussion

NCS-1 is a highly conserved protein with an N-terminal myristoylation site and four EF-hand Ca^{2+}-binding domains. The human and rat NCS-1 are 100% identical and share a 66% identity with the *N. crassa* homolog (Fig. 5.1; Gohain *et al.*, 2016). In *S. cerevisiae*, the NCS-1 homologue Frq1 was found to be essential for cell growth and viability (Hendricks *et al.*, 1999). In *S. pombe*, Ncs1p, the NCS-1 ortholog is responsible for providing tolerance to Ca^{2+} stress (Hamasaki-Katagiri *et al.*, 2004; Hamasaki-Katagiri and Ames, 2010). In *N. crassa*, NCS-1 is associated with vegetative growth, Ca^{2+} and UV stress tolerance and germling fusion (Deka *et al.*, 2011; Palma-Guerrero *et al.*, 2013). In higher eukaryotic organisms including rat, NCS-1 is associated with learning and memory (Saab *et al.*, 2009). In human, NCS-1 has been reported

to be associated with neurological disorders like bipolar disorder, some forms of schizophrenia and also autism (Koh *et al.*, 2003; Handley *et al.*, 2010). To test if NCS-1 is also conserved functionally in *N. crassa* and human, an interspecific complementation study was performed by expressing the NCS-1^{Rat}, which is identical to its human ortholog, in *N. crassa*. The NCS-1^{Rat} tagged with GFP was expressed successfully in *N. crassa* and complemented the slow growth, Ca^{2+} and UV stress sensitive phenotypes of the Δ*ncs-1* mutant.

In NCS-1^{Rat}, the glutamic acid at position 120 was changed to glutamine (E120Q) using the site-directed mutational and the mutant construct was transformed in the *N. crassa* strain to study the effect of the mutation. The *N. crassa* strains expressing NCS-$1^{Rat(E120Q)}$ displayed the slow growth and sensitivity to Ca^{2+} and UV stress similar to the Δ*ncs-1* mutant. The glutamic acid at position 120 was conserved in all NCS-1 proteins and was also found to be critical for the NCS-1 functions in *N. crassa* (Gohain *et al.*, 2016). The glutamic acid at position 120 is located in the third EF-hand domain, which is an integral part of the 12 amino acid long Ca^{2+} binding loop present in EF-hand domains found in NCS-1 (Gifford *et al.*, 2007; Deka *et al.*, 2011; Tamuli *et al.*, 2011; Gohain *et al.*, 2016). In recoverin, another important protein of the NCS family, the E120Q mutation in the EF3 domain abolished its high Ca^{2+} affinity completely and affected the functionality of the protein (Permyakov *et al.*, 2000; Burgoyne and Weiss, 2001). The E120Q mutation affected the functions of both rat and *N. crassa* NCS-1, thus, establishing glutamic acid at position 120 to be critical for the functions of the NCS-1 from lower to higher eukaryotes.

Conclusions and future perspectives

6.1 Major conclusions of the study

In this work, I have studied the role of NCS-1 in Ca^{2+} stress tolerance in *N. crassa* and the molecular mechanism of NCS-1 mediated Ca^{2+} stress tolerance. In this study, a gradual increase in the *ncs-1* transcription in response to increasing $CaCl_2$ concentration was observed, suggesting that *ncs-1* transcription is induced by Ca^{2+} in *N. crassa*. In addition, I showed that NCS-1 overexpression, under the nitrogen-regulatable *nit-6* promoter (P_{nit-6}) had recovered the Δ*ncs-1* Ca^{2+} sensitive phenotype, revealing that NCS-1 is a key player in Ca^{2+} stress tolerance in *N. crassa*. A Ca^{2+} stress survival assay revealed that the Δ*crz-1* mutant was also sensitive to the Ca^{2+} stress like the Δ*ncs-1* mutant revealing the involvement of the transcription factor CRZ-1 in Ca^{2+} stress tolerance in *N. crassa*. The transcription level of the *ncs-1* was reduced drastically in the Δ*crz-1* mutant, and it remained reduced even under the Ca^{2+} stress suggesting the involvement of CRZ-1 in the transcription of *ncs-1* in *N. crassa*.

From the CHIP analysis, it became clear that the transcription factor CRZ-1 binds to the *ncs-1* promoter to upregulate its expression under the Ca^{2+} stress condition. The binding of CRZ-1 to the *ncs-1* promoter was Ca^{2+} induced as the binding intensity increased with increasing Ca^{2+} level. From the EMSA it was determined that CRZ-1 specifically binds to an 8 bp nucleotide sequence 5′-CCTTCACA-3′ in the *ncs-1* promoter, which is located 216 bp upstream of the start codon. In the confocal microscopy study, NCS-1 appeared to be plasma-membrane localized, which otherwise mostly remained cytosolic. Both in *vivo* and *in vitro* membrane pulldown assays and the Co-IP assay established the physical interaction between NCS-1 and MID-1 during Ca^{2+} stress which occurs only in the plasma membrane. In summary, under the Ca^{2+} stress, the transcription of *ncs-1* is induced by transcription factor CRZ-1 binding to its promoter and in turn, NCS-1 interacts with the Ca^{2+}-permeable channel MID-1. Therefore, from this study, it can be suggested that the *N. crassa* NCS-1 functions via the

calcineurin -CRZ-1 pathway for the closure of the Ca^{2+}-permeable channel MID-1 to prevent Ca^{2+} influx for survival under the Ca^{2+} stress condition.

Furthermore, an interspecific complementation study was performed by expressing the rat NCS-1, which is identical to its human homolog, in *N. crassa*. The rat NCS-1 tagged with GFP was successfully expressed in *N. crassa* and complemented the slow growth, Ca^{2+} and UV stress sensitive phenotypes of the Δ*ncs-1* mutant. In the rat NCS-1, the glutamic acid at position 120 was changed to glutamine (E120Q) using the site-directed mutation (SDM) and the *N. crassa* strains expressing rat NCS-1^{E120Q} displayed the slow growth, and sensitivity to Ca^{2+} and UV stress similar to the Δ*ncs-1* mutant. The glutamic acid at position 120 was conserved in all NCS-1 proteins and was also found to be critical for the NCS-1 functions in *N. crassa*. The E120Q mutation affected the functions of both rat NCS-1 and *N. crassa* NCS-1, thus, establishing glutamic acid at position 120 to be critical for the functions of the NCS-1 from lower to higher eukaryotes.

6.2 Future prospects of this research work:

Future directions will be: (i) to establish additional molecular details of the pathway involving calcineurin and the Ca^{2+} transporters for the mechanism of stress tolerance; (ii) to identify additional molecular targets of *N. crassa* NCS-1 for understanding its association with DNA damage repair pathway for its role in UV stress survival and (iii) to gain insight into the structure-function relationship of *N. crassa* NCS-1 using either Nuclear Magnetic Resonance (NMR) and X-ray crystallography studies.

Appendix

A1 Circadian rhythm in *N. crassa*: Circadian rhythms are universal biological oscillations with an approximately 24 h period, which controls diverse phenomena including cell division, immunity, physiology, homeostasis, and sleep-wake cycle in eukaryotes including fungi and mammals (Mehra *et al.*, 2009; O'Neill and Reddy, 2012). The daily clock or the internal timing mechanism having a frequency of one activity cycle in every 24 h was termed "circadian" in 1950s by Halberg, which came from the Latin words "*circa*" for "about" and "*dien*" for "day" to relate the biological activity (Halberg *et al.*, 2003). Circadian clock shows three characteristics including period (about 24 hr), sensitivity to light (reflecting the ability to adjust its phase to the phase of the environment), and the relative insensitivity of its period to the growth temperature which is known as temperature compensation (Mattern *et al*. 1982; Sargent *et al.* 1966). In *N. crassa*, conidia accumulate in discrete bands at an interval of about 22 h, showing a free-running, circadian rhythm (Pittendrigh, 1960). Similar to the circadian oscillator in *Drosophila melanogaster* and mammals, the core circadian oscillator in *N. crassa* consists of frequency (FRQ), FRQ-interacting RNA helicase (FRH), white collar-1 (WC-1), and white collar-2 (WC-2) proteins (Heintzen and Liu, 2007). In *N. crassa*, WC-1 and WC-2 play an indispensable role in maintaining the circadian feedback loop (Aronson *et al.*, 1994; Crosthwaite *et al.*, 1997; Garceau *et al.*, 1997). They interact with each other to form a white collar complex (WCC) via their conserved PAS (Per-Arnt-Sim) domains (Ballario *et al.*, 1998; He *et al.*, 2002) to maintain the circadian rhythm in constant darkness by regulating rhythmic expression of FRQ (Aronson *et al.*, 1994; Garceau *et al.*, 1997). In the negative feedback loop, FRQ inhibits its own transcription through FRQ-dependent phosphorylation of the WCC complex (Dunlap, 1999; Baker *et al.*, 2012). On the other hand, in the positive feedback loop FRQ acts positively on WC-1 and WC-2 by transcriptional upregulation of the *wc-2* mRNA level and post-transcriptional upregulation of the WC-1 protein level (Lee *et al.*, 2000; Cheng *et al.*, 2001; Merrow *et al.*, 2001).

In *N. crassa*, although the core clock mechanism had been identified, the role of Ca^{2+} signaling in circadian rhythm is yet to be understood. In mammals, extracellular signals mediated by the Ca^{2+} and cAMP signaling pathways affect circadian clock (Takahashi *et al.*, 2008). In mouse, a transmembrane Ca^{2+} flux is necessary for supporting molecular rhythmicity in the hypothalamic suprachiasmatic nucleus (SCN) that plays a critical role in controlling circadian rhythm in mammals (Lundkvist *et al.*, 2005). The role of NCS-1, CRZ-1 and MID-1 in *N. crassa* Ca^{2+} stress has been well established as described in the previous chapters. In this study, I investigated the role of *ncs-1*, *crz-1* and *mid-1* in the regulation of *N. crassa* circadian clock under different temperature conditions.

A2 Generation of strains: In the *N. crassa* wild type strain, rhythmic conidiation is suppressed due to the accumulation of CO_2, a respiratory by-product and therefore all strains used in this study (Table A1) carry the *ras-1*^{bd} allele, which allows clear visualization of conidial bands despite the CO_2 accumulation without affecting the clock mechanism (Sargent and Kaltenborn, 1972; Belden *et al.*, 2007). Crosses were performed between *ras-1*^{bd} strain (FGSC 1859) with the Δ*ncs-1 a*, Δ*crz-1 a*, and Δ*mid-1 a* strains (Table 2.1), respectively, using SCM agar. The strains with respective knockout mutant alleles and the *ras-1*^{bd} mutation were selected for the study (Table A1).

Table A1. List of *Neurospora crassa* strains used in circadian study

Sl. No.	Strains	Genotype	Source
1	1858	*ras-1*^{bd}; *mat a*	FGSC 1858
2	1859	*ras-1*^{bd}; *mat A*	FGSC 1859
3	Δ*ncs-1*; *ras-1*^{bd} (11)	Δ*ncs-1*::*hph*; *ras-1* ^{bd}; *mat a*	Our laboratory
4	Δ*crz-1*; *ras-1*^{bd} (9)	Δ*crz-1*::*hph*; *ras-1* ^{bd}; *mat A*	Our laboratory
5	Δ*mid-1*; *ras-1*^{bd} (5)	*ras-1*^{bd}; Δ*mid-1*::*hph*; *mat A*	Our laboratory

A3 Circadian regulated conidiation study: The *N. crassa* strains were inoculated at one end of the race tube containing ~13 ml of circadian agar media [1X Vogel's Medium N, 0.1% (w/v) glucose, 0.17% (w/v) arginine, 50 ng/ml biotin and 1.5% (w/v) agar]. The tubes were incubated at three different temperatures 20 °C, 25 °C and 30 °C in constant light for 24 h and the growth fronts were marked. The tubes were then shifted to constant darkness at 20 °C, 25 °C and 30 °C and the growth fronts were marked at regular interval of 24 h for 5 days under a red safe light. For calculating the period lengths distance between conidial bands were multiplied by the inverse of slope (http://www.fgsc.net/teaching/circad.htm). For the study of temperature compensation of the strains, the temperature coefficient (Q_{10}) was calculated by using the following formula (https://www.physiologyweb.com/calculators/q10_calculator.html)-

$$Q_{10} = \left(\frac{R_2}{R_1}\right)^{10/(T_2-T_1)}$$

R_1 and R_2 are rates of the reaction (period lengths) at T_1 and T_2 temperatures respectively.

A4 Quantitative real time assay for studying the expression of the *frq* and *wc-1* genes: For RNA isolation, *ras-1*^{bd} *A* (FGSC 1858), Δ*ncs-1*; *ras-1*^{bd} (11), Δ*crz-1*; *ras-1*^{bd} (9), and Δ*mid-1*; *ras-1*^{bd} (5) strains (Table A1) were first cultured in circadian agar medium under constant light for 48 h either at 20 °C or at 25 °C, as indicated. Approximately 1 x 10^7 conidia from 48 h old culture plate in 100 ml conical flask containing 25 ml of liquid circadian media. Flasks were incubated either at 20 °C or at 25 °C, as indicated and 125 rpm shaking under light for 2 h and then transferred to dark. Mycelia was harvested by filtration after 16 h incubation at dark and crushed in a mortar and pestle using liquid nitrogen (Aronson *et al.*, 1994). RNA was isolated from the crushed mycelial powder using Trizol reagent (Life Technologies, USA), and cDNA was synthesized from the total RNA using the Verso™ cDNA synthesis kit (Thermo Fisher Scientific, USA) according to the manufacture's protocol. The qRT-PCR was performed in an

an ABI 7500 Fast Real time PCR system (Applied Biosystems, USA) using the gene specific primers (Table A2), the SYBR Select Master Mix (Life technologies, USA), and cDNA according to the protocol provided by the manufacturer. The relative expression levels of the target genes were calculated by $2^{-\Delta\Delta C_T}$ method (Livak and Schmittgen, 2001), and *β*-tubulin expression level was used as the endogenous control.

Table A2. List of qRT-PCR primers used in this study

Primer	Sequence (5′→ 3′)	Source
RT-FRQ-F	GAATCGACATCGCAGAGGAG	Our laboratory
RT-FRQ-R	GCCCGTCGACATAGAGTTGT	Our laboratory
RT-WC-1-F	GCGGGAATCGAGATCTATGC	Our laboratory
RT-WC-1-R	TGAGTTCTTGGTAGCGGTGG	Our laboratory
Qtub-Fw	CCGTCCATCAGCTCGTTGA	Our laboratory
Qtub-Rv	ACGGTGACACCGGACATGA	Our laboratory

A5 Results:

A5.1 *N. crassa* Ca^{2+} stress responsive genes modulate the period lengths of circadian regulated conidiation in response to temperature variation: At 20 °C, the *ras-1*^{bd} strain had period length of 23.5 h, but both the Δ*ncs-1*; *ras-1*^{bd} (11) and Δ*crz-1*; *ras-1*^{bd} (9) strains (Table A1) had shown increased period lengths of 25.0 h and 25.2 h, respectively (Table A3, Fig. A1). But for 25 °C and 30 °C, their period lengths were decreased by at least 2 h than that of the *ras-1*^{bd} strain (Table A3, Fig. A1). Interestingly, the Δ*mid-1*; *ras-1*^{bd} (5) strain (Table A1) did not show any significant period length variation at any temperature compared to the *ras-1*^{bd} strain (Table A3, Fig. A1). The Q_{10} values (Table A4) were calculated to see the temperature compensation. The Q_{10} values of temperature compensated circadian rhythms normally range

between 0.8 and 1.2 (Saunders, 1977; Mattern *et al.*, 1982). The Δ*ncs-1*; *ras-1*^{bd} (11) and Δ*crz-1*; *ras-1*^{bd} (9) strains were unable to perform temperature compensation at 20 ºC as the Q_{10} value was 0.7 for both the strains (Table A4). On the other hand, the Δ*mid-1*; *ras-1*^{bd} (5) strain showed well temperature compensation like the *ras-1*^{bd} strain (Table A4).

Table A3. Period lengths of the *ras-1*^{bd}, Δ*ncs-1*; *ras-1*^{bd} (11), Δ*crz-1*; *ras-1*^{bd} (9), and Δ*mid-1*; *ras-1*^{bd} (5) strains in different temperatures

Strains	**[+]Period lengths ± SD (h)**		
	20 °C	25 °C	30 °C
ras-1^{bd}	23.5 ± 0.1	22.0 ± 0.2	20.4 ± 0.1
Δ*ncs-1*; *ras-1*^{bd} (11)	25.0 ± 0.2 (***)	20.2 ± 0.2 (***)	18.3 ± 0.1 (***)
Δ*crz-1*; *ras-1*^{bd} (9)	25.2 ± 0.5 (**)	20.6 ± 0.3 (**)	18.5 ± 0.1 (***)
Δ*mid-1*; *ras-1*^{bd} (5)	23.5 ± 0.1	21.5 ± 0.7	20.0 ± 0.2 (*)

[+]Results are shown as mean ± standard deviation (SD) for three independent experiments (n = 3) with *p-values* < 0.05(*), <0.01 (**), and <0.001 (***) compared with the *ras-1*^{bd} strain as measured by one-way ANOVA test.

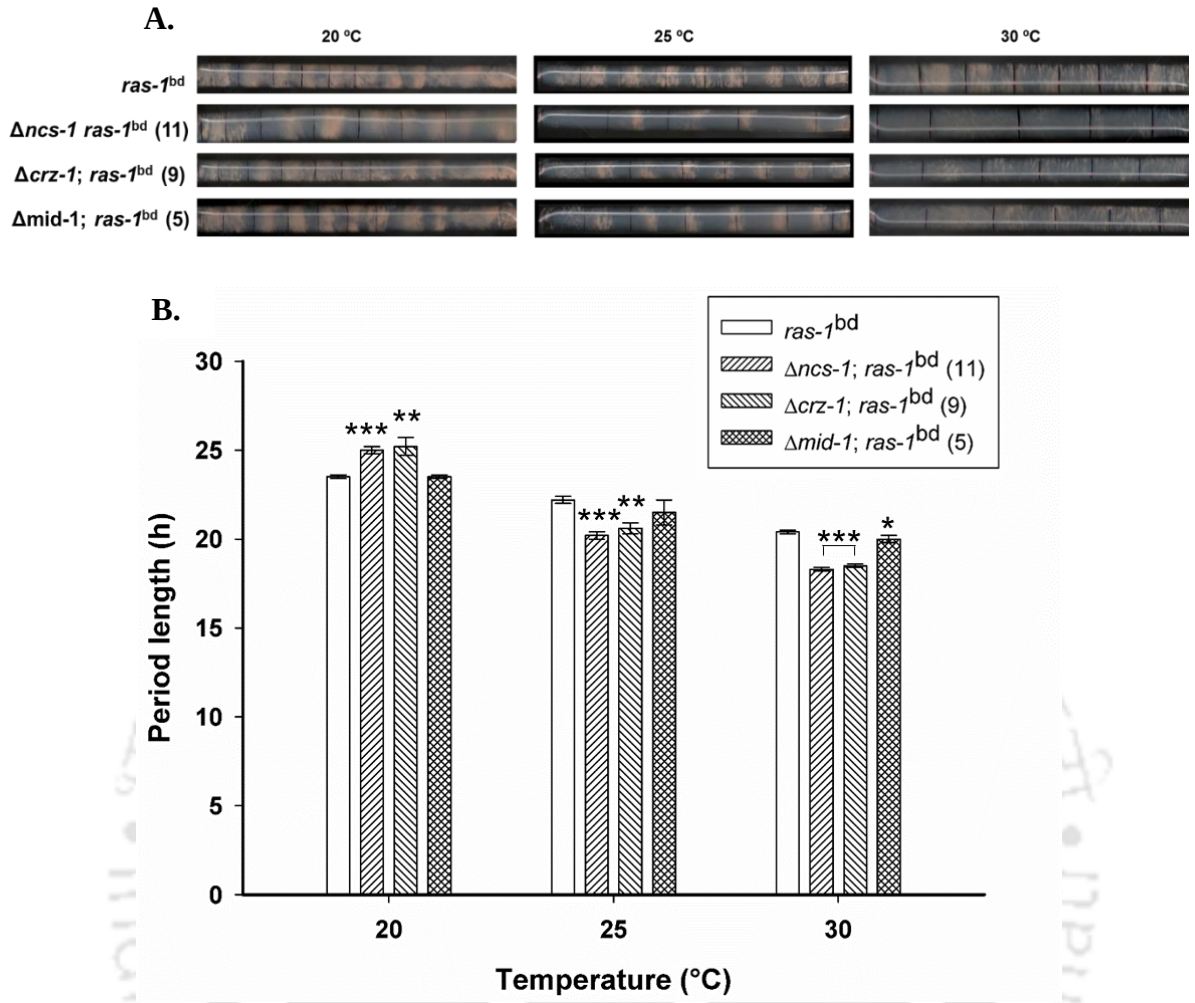

Fig. A1. Circadian regulated conidiation of *N. crassa* in different temperatures.

A. The Δ*ncs-1*; *ras-1*^{bd} (11), Δ*crz-1*; *ras-1*^{bd} (9), and Δ*mid-1*; *ras-1*^{bd} (5) strains showed distinct conidial bands at a regular interval in the race tube like the control *ras-1*^{bd} strain. The black mark indicates the growth front. Conidial bands were measured till 144 hours for all the strains.

B. Period lengths of the *ras-1*^{bd}, Δ*ncs-1*; *ras-1*^{bd} (11), Δ*crz-1*; *ras-1*^{bd} (9), and Δ*mid-1*; *ras-1*^{bd} (5) strains in different temperatures (20 °C, 25 °C and 30 °C). Error bars indicate the standard deviation calculated from the data of three individual experiments (n=3) with *p-values* < 0.05 (*), <0.01 (**), and <0.001 (***) compared with the *ras-1*^{bd} strain as measured by one-way ANOVA test.

Table A4. Q_{10} values from the period lengths of *ras-1*^{bd}, Δ*ncs-1; ras-1*^{bd} (11), Δ*crz-1; ras-1*^{bd} (9) and Δ*mid-1; ras-1*^{bd} (5) strains in different temperatures

Strains	Q_{10} values		
	T_1=20 ºC , T_2=25 ºC	T_1=25 ºC , T_2=30 ºC	T_1=20 ºC , T_2=30 ºC
ras-1^{bd}	0.9	0.9	0.9
Δ*ncs-1; ras-1*^{bd} (11)	0.7	0.8	0.7
Δ*crz-1; ras-1*^{bd} (9)	0.7	0.8	0.7
Δ*mid-1; ras-1*^{bd} (5)	0.8	0.9	0.9

A5.2 Variation in the period lengths is associated with the transcription of *frq* and *wc-1*: From the qRT-PCR analysis, it was observed that increasing period lengths in case of the Δ*ncs-1*; *ras-1*^{bd} (11) and Δ*crz-1*; *ras-1*^{bd} (9) strains (Table A1) at 20 °C corresponds to significant (~2-3 fold) increase (Table A5; Fig. A2) in the *frq* transcript level as compared to the *ras-1*^{bd} strain. Similarly, the decreased period lengths at 25 °C corresponds to the decreased *frq* transcript level (Table A5; Fig. A2). The increase in the *frq* transcript level for the Δ*mid-1*; *ras-1*^{bd} (5) strain (Table A1) was not significant at 20 °C and interestingly, *frq* transcript level similar to that of the *ras-1*^{bd} strain was observed at 25 °C (Table A5). The transcript levels of *wc-1* for all the three strains at both the temperatures did not vary significantly compared to the *ras-1*^{bd} strain (Table A5; Fig. A2).

Table A5. Relative expressions of *frq* and *wc-1* in the *ras-1*^{bd}, Δ*ncs-1; ras-1*^{bd} (11), Δ*crz-1; ras-1*^{bd} (9) and Δ*mid-1; ras-1*^{bd} (5) strains in different temperatures

Strains	[+]Relative expression ± SD (Fold)			
	frq		*wc-1*	
	20 °C	25 °C	20 °C	25 °C
ras-1^{bd}	1.0 ± 0.00	1.0 ± 0.00	1.0 ± 0.00	1.0 ± 0.00
Δ*ncs-1; ras-1*^{bd} (11)	2.7 ± 0.22 (**)	0.8 ± 0.07	1.1 ± 0.18	1.0 ± 0.13
Δ*crz-1; ras-1*^{bd} (9)	2.3 ± 0.24 (***)	0.9 ± 0.02	1.1 ± 0.12	1.1 ± 0.25
Δ*mid-1; ras-1*^{bd} (5)	1.5 ± 0.25	1.0 ± 0.06	1.1 ± 0.16	1.2 ± 0.25

[+]Results are shown as mean ± standard deviation (SD) for three independent experiments (n = 3) with *p-values* < 0.05 (*), <0.01 (**), and <0.001 (***) compared with the *ras-1*^{bd} strain as measured by one-way ANOVA test.

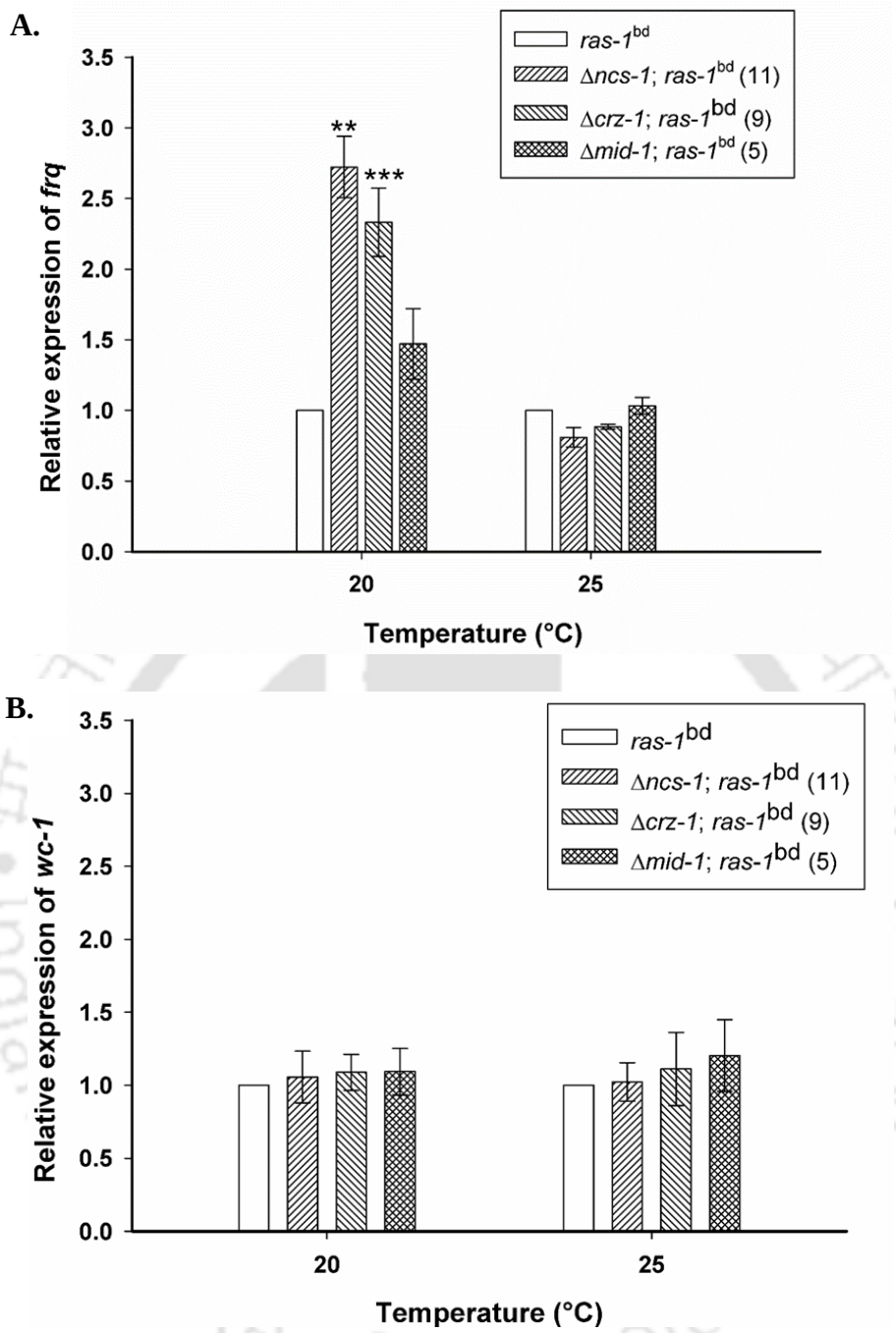

Fig. A2. Relative expression of *frq* and *wc-1* in the *ras-1*^{bd}, Δ*ncs-1*; *ras-1*^{bd} (11), Δ*crz-1*; *ras-1*^{bd} (9) and Δ*mid-1*; *ras-1*^{bd} (5) strains at different temperatures (20 °C and 25 °C).

A. The relative expression of *frq* was normalized to the *β*-tubulin expression, and compared with its relative expression in *ras-1*^{bd} strain for both the temperature.

B. The relative expression of *wc-1* was normalized to the *β*-tubulin expression, and compared with its relative expression in the *ras-1*^{bd} strain for both the temperature.

Error bars indicate the standard deviation calculated from the data of three individual experiments (n=3) with *p-values* < 0.05 (*), <0.01 (**), and <0.001 (***) compared with the *ras-1*^{bd} strain as measured by one-way ANOVA test.

A6 Discussion: In this study, I evaluated the role of *ncs-1*, *crz-1* and *mid-1* in the regulation of the *N. crassa* circadian clock at three different temperatures. It was observed that the Δ*ncs-1*; *ras-1*^{bd} (11) and Δ*crz-1*; *ras-1*^{bd} (9) strains had shown increased period lengths at 20 °C while decreased period lengths at 25 °C and 30 °C compared to the *ras-1*^{bd} strain. On the other hand, the Δ*mid-1*; *ras-1*^{bd} (5) strain did not show significant variation in period length in response to the temperature difference. Moreover, in the Δ*ncs-1*; *ras-1*^{bd} (11) and Δ*crz-1*; *ras-1*^{bd} (9) strains, the *frq* transcript level was also increased ~2-3 fold at 20 °C and decreased marginally at 25 °C in comparison to the *ras-1*^{bd} strain, while no significant variation was observed for the Δ*mid-1*; *ras-1*^{bd} (5) strain. Therefore, changes in the *frq* expression in the Δ*ncs-1*and Δ*crz-1* mutants could be associated with the change in period length in these mutants even there was no significant variation in the expression of *wc-1*. The role of *mid-1* in *N. crassa* circadian rhythm could not be established as no variation in the period length as well as the *frq* expression was observed. This preliminary finding establishes the role of *ncs-1* and *crz-1* in regulation of the circadian clock. Further studies will establish the complete molecular pathway.

References

Altschul, S.F., Gish, W., Miller, W., Myers, E.W., and Lipman, D.J. (1990) Basic local alignment search tool. *J Mol Biol* 215: 403–410.

Altschul, S.F., Madden, T.L., Schäffer, A.A., Zhang, J., Zhang, Z., Miller, W., and Lipman, D.J. (1997) Gapped BLAST and PSI-BLAST: a new generation of protein database search programs. *Nucleic Acids Res* 25: 3389–3402.

Altschul, S.F., Wootton, J.C., Gertz, E.M., Agarwala, R., Morgulis, A., Schäffer, A.A., and Yu, Y. (2005) Protein database searches using compositionally adjusted substitution matrices. *FEBS J* 272: 5101–5109.

Ames, J.B., Ishima, R., Tanaka, T., Gordon, J.I., Stryer, L., and Ikura, M. (1997) Molecular mechanics of calcium–myristoyl switches. *Nature* 389: 198–202.

Aronson, B.D., Johnson, K.A., Loros, J.J., and Dunlap, J.C. (1994) Negative feedback defining a circadian clock: autoregulation of the clock gene frequency. Science 263: 1578–1584.

Baker, C.L., Loros, J.J., and Dunlap, J.C. (2012) The circadian clock of *Neurospora crassa*. FEMS *Microbiol Rev* 36: 95–110.

Ballario, P., Talora, C., Galli, D., Linden, H., and Macino, G. (1998) Roles in dimerization and blue light photoresponse of the PAS and LOV domains of *Neurospora crassa* white collar proteins. *Mol Microbiol* 29: 719–729.

Barman, A., and Tamuli, R. (2017) The pleiotropic vegetative and sexual development phenotypes of *Neurospora crassa* arise from double mutants of the calcium signaling genes *plc-1*, *splA2*, and *cpe-1*. *Curr Genet* 63: 861–875.

Beadle, G.W., and Tatum, E.L. (1941) Genetic control of biochemical reactions in Neurospora. *Proc Natl Acad Sci* 27: 499–506.

Belden, W.J., Larrondo, L.F., Froehlich, A.C., Shi, M., Chen, C.-H., Loros, J.J., and Dunlap, J.C. (2007) The band mutation in *Neurospora crassa* is a dominant allele of *ras-1* implicating RAS signaling in circadian output. *Genes Dev* 21: 1494–1505.

Benito, B., Garciadeblás, B., and Rodríguez-Navarro, A. (2000) Molecular cloning of the calcium and sodium ATPases in *Neurospora crassa*. *Mol Microbiol* 35: 1079–1088.

Bergson, C., Levenson, R., Goldman-Rakic, P.S., and Lidow, M.S. (2003) Dopamine receptor-interacting proteins: the Ca^{2+} connection in dopamine signaling. *Trends Pharmacol Sci* 24: 486–492.

Berridge, M.J. (1987) Inositol trisphosphate and diacylglycerol: two interacting second messengers. *Annu Rev Biochem* 56: 159–193.

Berridge, M.J. (1993) Inositol trisphosphate and calcium signalling. *Nature* 361: 315–325.

Berridge, M.J., Bootman, M.D., and Lipp, P. (1998) Calcium-a life and death signal. *Nature* 395: 645–648.

Berridge, M.J., Bootman, M.D., and Roderick, H.L. (2003) Calcium: calcium signalling: dynamics, homeostasis and remodelling. *Nat Rev Mol cell Biol* 4: 517–529.

Berridge, M.J., Lipp, P., and Bootman, M.D. (2000) The versatility and universality of calcium signalling. *Nat Rev Mol Cell Biol* 1: 11–21.

Bhat, A., Tamuli, R., and Kasbekar, D.P. (2004) Genetic transformation of *Neurospora tetrasperma*, demonstration of repeat-induced point mutation (RIP) in self-crosses and a screen for recessive RIP-defective mutants. *Genetics* 167: 1155–1164.

Blasiole, B., Kabbani, N., Boehmler, W., Thisse, B., Thisse, C., Canfield, V., and Levenson, R. (2005) Neuronal calcium sensor-1 gene *ncs-1a* is essential for semicircular canal formation in zebrafish inner ear. *J Neurobiol* 64: 285–297.

Bootman, M.D., Collins, T.J., Peppiatt, C.M., Prothero, L.S., MacKenzie, L., De Smet, P., Travers, M., Tovey, S.C., Seo, J.T., Berridge, M.J., and Ciccolini, F. (2001) Calcium signalling–an overview. *Semin Cell Dev Biol* 12: 3–10.

Borkovich, K.A., Alex, L.A., Yarden, O., Freitag, M., Turner, G.E., Read, N.D., Seiler, S., Bell-Pedersen, D., Paietta, J., Plesofsky, N., Plamann, M., Goodrich-Tanrikulu, M., Schulte, U., Mannhaupt, G., Nargang, F.E., Radford, A., Selitrennikoff, C., Galagan, J.E., Dunlap, J.C., Loros, J.J., Catcheside, D., Inoue, H., Aramayo, R., Polymenis, M., Selker, E.U., Sachs, M.S., Marzluf, G.A., Paulsen, I., Davis, R., Ebbole, D.J., Zelter, A., Kalkman, E.R., O'Rourke, R., Bowring, F., Yeadon, J., Ishii, C., Suzuki, K., Sakai, W,, Pratt, R. (2004) Lessons from the genome sequence of *Neurospora crassa*: tracing the path from genomic blueprint to multicellular organism. *Microbiol Mol Biol Rev* 68:1–108.

Bourne, Y., Dannenberg, J., Pollmann, V., Marchot, P., and Pongs, O. (2001) Immunocytochemical localization and crystal structure of human frequenin (neuronal calcium sensor 1). *J Biol Chem* 276: 11949–11955.

Bowman, B.J., Draskovic, M., Freitag, M., and Bowman, E.J. (2009) Structure and distribution of organelles and cellular location of calcium transporters in *Neurospora crassa*. *Eukaryot Cell* 8: 1845–1855.

Bowman, B.J., Abreu, S., Margolles-Clark, E., Draskovic, M., and Bowman, E.J. (2011) Role of four calcium transport proteins, encoded by *nca-1*, *nca-2*, *nca-3*, and *cax*, in maintaining intracellular calcium levels in *Neurospora crassa*. *Eukaryot Cell* 10: 654–661.

Brock, T.D. (1973) Lower pH limit for the existence of blue-green algae: evolutionary and ecological implications. *Science* 179: 480–483.

Brown, E.M., Gamba, G., Riccardi, D., Lombardi, M., Butters, R., Kifor, O., et al. (1993) Cloning and characterization of an extracellular Ca^{2+}-sensing receptor from bovine parathyroid. *Nature* 366: 575–580.

Burgoyne, R.D. (2007) Neuronal calcium sensor proteins: generating diversity in neuronal Ca^{2+} signalling. *Nat Rev Neurosci* 8: 182–193.

Burgoyne, R.D., O'Callaghan, D.W., Hasdemir, B., Haynes, L.P., and Tepikin, A.V. (2004) Neuronal Ca^{2+}-sensor proteins: multitalented regulators of neuronal function. *Trends Neurosci* 27: 203–209.

Burgoyne, R.D., and Weiss, J.L. (2001) The neuronal calcium sensor family of Ca^{2+}-binding proteins. *Biochem J* 353: 1–12.

Burnett, J.H. (1975) *Mycogenetics*. London: John Wiley & Sons.

Cambareri, E.B., Jensen, B.C., Schabtach, E., and Selker, E.U. (1989) Repeat-induced GC to AT mutations in *Neurospora. Science* 244: 1571–1575.

Campbell, A.K. (1983) *Intracellular calcium, its universal role as regulator*. London: John Wiley & Sons.

Capelli, N., Tuinen, D. van, Perez, R.O., Arrighi, J.-F., and Turian, G. (1993) Molecular cloning of a cDNA encoding calmodulin from *Neurospora crassa*. *FEBS Lett* 321: 63–68.

Carafoli, E. (1987) Intracellular calcium homeostasis. *Annu Rev Biochem* 56: 395–433.

Carneiro, P., Duarte, M., and Videira, A. (2007) The external alternative NAD(P)H dehydrogenase NDE3 is localized both in the mitochondria and in the cytoplasm of *Neurospora crassa*. *J Mol Biol* 368: 1114–1121.

Carrié, A., Jun, L., Bienvenu, T., Vinet, M.-C., McDonell, N., Couvert, P., et al. (1999) A new member of the IL-1 receptor family highly expressed in hippocampus and involved in X-linked mental retardation. *Nat Genet* 23: 25–31.

Carugo, O., Djinović, K., and Rizzi, M. (1993) Comparison of the co-ordinative behaviour of calcium (II) and magnesium (II) from crystallographic data. *J Chem Soc Dalt Trans* 2127–2135.

Case, R.M., Eisner, D., Gurney, A., Jones, O., Muallem, S., and Verkhratsky, A. (2007) Evolution of calcium homeostasis: from birth of the first cell to an omnipresent signalling system. *Cell Calcium* 42: 345–350.

Cerella, C., Diederich, M., and Ghibelli, L. (2010) The dual role of calcium as messenger and stressor in cell damage, death, and survival. *Int J Cell Biol* 2010.

Chafouleas, J.G., Bolton, W.E., and Means, A.R. (1984) Potentiation of bleomycin lethality by anticalmodulin drugs: a role for calmodulin in DNA repair. *Science* 224: 1346–1348.

Chard, P.A. (1987) DNA repair in human cells: Methods for the determination of calmodulin involvement. *Methods Enzymol* 139: 715–730.

Chen, C.-K., Inglese, J., Lefkowitz, R.J., and Hurley, J.B. (1995) Ca^{2+}-dependent interaction of recoverin with rhodopsin kinase. *J Biol Chem* 270: 18060–18066.

Chen, Y.-L., Kozubowski, L., Cardenas, M.E., and Heitman, J. (2010) On the roles of calcineurin in fungal growth and pathogenesis. *Curr Fungal Infect Rep* 4: 244–255.

Cheng, P., Yang, Y., Heintzen, C., and Liu, Y. (2001) Coiled-coil domain-mediated FRQ–FRQ interaction is essential for its circadian clock function in *Neurospora*. *EMBO J* 20: 101–108.

Chin, D., and Means, A.R. (2000) Calmodulin: a prototypical calcium sensor. *Trends Cell Biol* 10: 322–328.

Clapham, D.E. (2007) Calcium Signaling. Cell 131: 1047–1058.

Colot, H. V, Park, G., Turner, G.E., Ringelberg, C., Crew, C.M., Litvinkova, L., et al. (2006) A high-throughput gene knockout procedure for *Neurospora* reveals functions for multiple transcription factors. *Proc Natl Acad Sci* 103: 10352–10357.

Cornelius, G., Gebauer, G., and Techel, D. (1989) Inositol trisphosphate induces calcium release from *Neurospora crassa* vacuoles. *Biochem Biophys Res Commun* 162: 852–856.

Cortat, M., and Turian, G. (1974) Conidiation of *Neurospora crassa* in submerged culture without mycelial phase. *Arch Microbiol* 95: 305–309.

Crabtree, G.R., and Olson, E.N. (2002) NFAT signaling: choreographing the social lives of cells. *Cell* 109: S67–S79.

Crosthwaite, S.K., Dunlap, J.C., and Loros, J.J. (1997) *Neurospora wc-1* and *wc-2*: transcription, photoresponses, and the origins of circadian rhythmicity. *Science* 276: 763–769.

Cunningham, K.W., and Fink, G.R. (1996) Calcineurin inhibits VCX1-dependent H^+/Ca^{2+} exchange and induces Ca^{2+} ATPases in *Saccharomyces cerevisiae*. *Mol Cell Biol* 16: 2226–2237.

Dason, J.S., Romero-Pozuelo, J., Marin, L., Iyengar, B.G., Klose, M.K., Ferrús, A., and Atwood, H.L. (2009) Frequenin/NCS-1 and the Ca^{2+}-channel α1-subunit co-regulate synaptic transmission and nerve-terminal growth. *J Cell Sci* 122: 4109–4121.

Davis, R.H. (2000) Neurospora: contributions of a model organism. Oxford University Press.

Davis, R.H., and Perkins, D.D. (2002) *Neurospora*: a model of model microbes. Nat Rev Genet 3: 397–403.

Davis, R.H., and de Serres, F.J. (1970) Genetic and microbiological research techniques for *Neurospora crassa*. *Methods Enzymol* 13: 79–143.

Deka, R., Kumar, R., and Tamuli, R. (2011) *Neurospora crassa* homologue of Neuronal Calcium Sensor-1 has a role in growth, calcium stress tolerance, and ultraviolet survival. *Genetica* 139: 885–894.

Deka, R., and Tamuli, R. (2013) *Neurospora crassa ncs-1*, *mid-1* and *nca-2* double-mutant phenotypes suggest diverse interaction among three Ca^{2+}-regulating gene products. *J Genet* 92: 559–563.

Dizhoor, A.M., Ray, S., Kumar, S., Niemi, G., Spencer, M., Brolley, D., Walsh, K.A., Philipov, P.P., Hurley, J.B., and Stryer, L. (1991) Recoverin: a calcium sensitive activator of retinal rod guanylate cyclase. *Science* 251: 915–918.

Dodge, B.O. (1939) Some problems in the genetics of the fungi. *Science* 90: 379–385.

Dunlap, J.C. (1999) Molecular bases for circadian clocks. *Cell* 96: 271–290.

Erickson, M.A., Lagnado, L., Zozulya, S., Neubert, T.A., Stryer, L., and Baylor, D.A. (1998) The effect of recombinant recoverin on the photoresponse of truncated rod photoreceptors. *Proc Natl Acad Sci* 95: 6474–6479.

Exley, G.E., Colandene, J.D., and Garrett, R.H. (1993) Molecular cloning, characterization, and nucleotide sequence of nit-6, the structural gene for nitrite reductase in *Neurospora crassa*. *J Bacteriol* 175: 2379–2392.

Fang, L., Huang, S., and Lin, K. (1997) High temperature induces the synthesis of heat-shock proteins and the elevation of intracellular calcium in the coral *Acropora grandis*. *Coral Reefs* 16: 127–131.

Felsenstein, J. (1985) Confidence limits on phylogenies: an approach using the bootstrap. *Evolution* 39: 783–791.

Freitag, M., Hickey, P.C., Raju, N.B., Selker, E.U., and Read, N.D. (2004) GFP as a tool to analyze the organization, dynamics and function of nuclei and microtubules in *Neurospora crassa*. *Fungal Genet Biol* 41: 897–910.

Galagan, J.E., Calvo, S.E., Borkovich, K.A., Selker, E.U., Read, N.D., Jaffe, D., FitzHugh, W., Ma, L.J., Smirnov, S., Purcell, S., Rehman, B., Elkins, T., Engels, R., Wang, S., Nielsen, C.B., Butler, J., Endrizzi, M., Qui, D., Ianakiev, P., Bell-Pedersen, D., Nelson, M.A., Werner-Washburne, M., Selitrennikoff, C.P., Kinsey, J.A., Braun, E.L., Zelter, A., Schulte, U., Kothe, G.O., Jedd, G., Mewes, W., Staben, C., Marcotte, E., Greenberg, D., Roy, A., Foley, K., Naylor, J., Stange-Thomann, N., Barrett, R., Gnerre, S., Kamal, M., Kamvysselis, M., Mauceli, E., Bielke, C., Rudd, S., Frishman, D., Krystofova, S., Rasmussen, C., Metzenberg, R.L., Perkins, D.D., Kroken, S., Cogoni, C., Macino, G., Catcheside, D., Li, W., Pratt, R.J., Osmani, S.A., DeSouza, C.P., Glass, L., Orbach, M.J., Berglund, J.A., Voelker, R., Yarden, O., Plamann, M., Seiler, S., Dunlap, J., Radford, A., Aramayo, R., Natvig, D.O., Alex, L.A., Mannhaupt, G., Ebbole, D.J., Freitag, M., Paulsen, I., Sachs, M.S., Lander, E.S., Nusbaum, C., Birren, B. (2003) The genome sequence of the filamentous fungus *Neurospora crassa*. *Nature* 422:859–868.

Gambino, F., Pavlowsky, A., Béglé, A., Dupont, J.L., Bahi, N., Courjaret, R., Gardette, R., Hadjkacem, H., Skala, H., Poulain, B., and Chelly, J. (2007) IL1-receptor accessory

protein-like 1 (IL1RAPL1), a protein involved in cognitive functions, regulates N-type Ca^{2+}-channel and neurite elongation. *Proc Natl Acad Sci* 104: 9063–9068.

Garceau, N.Y., Liu, Y., Loros, J.J., and Dunlap, J.C. (1997) Alternative initiation of translation and time-specific phosphorylation yield multiple forms of the essential clock protein *FREQUENCY*. Cell 89: 469–476.

Garcia-Bustos, J.F., Marini, F., Stevenson, I., Frei, C., and Hall, M.N. (1994) PIK1, an essential phosphatidylinositol 4-kinase associated with the yeast nucleus. *EMBO J* 13: 2352–2361.

Garnjobst, L., and Tatum, E.L. (1967) A survey of new morphological mutants in *Neurospora crassa*. Genetics 57: 579.

Gavric, O., dos Santos, D.B., and Griffiths, A. (2007) Mutation and divergence of the phospholipase C gene in *Neurospora crassa*. *Fungal Genet Biol* 44: 242–249.

Gerloff, G.C., and Fishbeck, K.A. (1969) Quantitative cation requirements of several green and blue-green algae. *J Phycol* 5: 109–114.

Gifford, J.L., Walsh, M.P., and Vogel, H.J. (2007) Structures and metal-ion-binding properties of the Ca^{2+}-binding helix–loop–helix EF-hand motifs. *Biochem J* 405: 199–221.

Gilroy, S., Blowers, D.P., and Trewavas, A. (1987) Calcium: a regulation system emerges in plant cells. *Development* 100: 181–184.

Gohain, D., Deka, R., and Tamuli, R. (2016) Identification of critical amino acid residues and functional conservation of the *Neurospora crassa* and *Rattus norvegicus* orthologues of neuronal calcium sensor-1. *Genetica* 144: 665–674.

Gomez, M., De Castro, E., Guarin, E., Sasakura, H., Kuhara, A., Mori, I., Bartfai, T., Bargmann, C.I., and Nef, P. (2001) Ca^{2+} signaling via the neuronal calcium sensor-1 regulates associative learning and memory in *C. elegans. Neuron* 30: 241–248.

Gromada, J., Bark, C., Smidt, K., Efanov, A.M., Janson, J., Mandic, S.A., Webb, D.L., Zhang, W., Meister, B., Jeromin, A., and Berggren, P.O. (2005) Neuronal calcium sensor-1 potentiates glucose-dependent exocytosis in pancreatic β cells through activation of phosphatidylinositol 4-kinase β. *Proc Natl Acad Sci* 102: 10303–10308.

Guignard, R., Grange, F., and Turian, G.T. (1984) Microcycle conidiation induced by partial nitrogen deprivation in *Neurospora crassa*. *Can J Microbiol* 30: 1210–1215.

Halachmi, D., and Eilam, Y. (1989) Cytosolic and vacuolar Ca^{2+} concentrations in yeast cells measured with the Ca^{2+}-sensitive fluorescence dye indo-1. *FEBS Lett* 256: 55–61.

Halberg, F., Cornélissen, G., Katinas, G., Syutkina, E.V., Sothern, R.B., Zaslavskaya, R., Halberg, F., Watanabe, Y., Schwartzkopff, O., Otsuka, K., and Tarquini, R. (2003) Transdisciplinary unifying implications of circadian findings in the 1950s. *J Circadian Rhythms* 1: 2.

Hama, H., Schnieders, E.A., Thorner, J., Takemoto, J.Y., and DeWald, D.B. (1999) Direct involvement of phosphatidylinositol 4-phosphate in secretion in the yeast *Saccharomyces cerevisiae*. *J Biol Chem* 274: 34294–34300.

Hamasaki-Katagiri, N., and Ames, J.B. (2010) Neuronal calcium sensor-1 (Ncs1p) is up-regulated by calcineurin to promote Ca^{2+} tolerance in fission yeast. *J Biol Chem* 285: 4405–4414.

Hamasaki-Katagiri, N., Molchanova, T., Takeda, K., and Ames, J.B. (2004) Fission yeast homolog of neuronal calcium sensor-1 (Ncs1p) regulates sporulation and confers calcium tolerance. J Biol Chem 279: 12744–12754.

Handley, M.T.W., Lian, L.-Y., Haynes, L.P., and Burgoyne, R.D. (2010) Structural and functional deficits in a neuronal calcium sensor-1 mutant identified in a case of autistic spectrum disorder. *PLoS One* 5: e10534.

Hao, L., Rigaud, J.L., and Inesi, G. (1994) Ca^{2+}/H^{+} countertransport and electrogenicity in proteoliposomes containing erythrocyte plasma membrane Ca-ATPase and exogenous lipids. *J Biol Chem* 269: 14268–14275.

Haynes, L.P., Sherwood, M.W., Dolman, N.J., and Burgoyne, R.D. (2007) Specificity, Promiscuity and Localization of ARF Protein Interactions with NCS-1 and Phosphatidylinositol-4 Kinase-IIIβ. *Traffic* 8: 1080–1092.

Haynes, L.P., Thomas, G.M.H., and Burgoyne, R.D. (2005) Interaction of neuronal calcium sensor-1 and ADP-ribosylation factor 1 allows bidirectional control of phosphatidylinositol 4-kinase β and trans-Golgi network-plasma membrane traffic. *J Biol Chem* 280: 6047–6054.

He, Q., Cheng, P., Yang, Y., Wang, L., Gardner, K.H., and Liu, Y. (2002) White collar-1, a DNA binding transcription factor and a light sensor. *Science* 297: 840–843.

Heintzen, C., and Liu, Y. (2007) The *Neurospora crassa* circadian clock. *Adv Genet* 58: 25–66.

Hendricks, K.B., Qing Wang, B., Schnieders, E.A., and Thorner, J. (1999) Yeast homologue of neuronal frequenin is a regulator of phosphatidylinositol-4-OH kinase. *Nat Cell Biol* 1: 234–241.

Hidaka, H., and Okazaki, K. (1993) Neurocalcin family: a novel calcium-binding protein abundant in bovine central nervous system. *Neurosci Res* 16: 73–77.

Hirayama, S., Sugiura, R., Lu, Y., Maeda, T., Kawagishi, K., Yokoyama, M., Tohda, H., Giga-Hama, Y., Shuntoh, H., and Kuno, T. (2003) Zinc finger protein Prz1 regulates Ca^{2+} but not Cl^- homeostasis in fission yeast. Identification of distinct branches of calcineurin signaling pathway in fission yeast. *J Biol Chem* 278: 18078–18084.

Hoffman, C.S. (2001) Preparation of yeast DNA. *Curr Protoc Mol Biol* 39: 13.11.1–13.11.4.

Hogan, P.G., Chen, L., Nardone, J., and Rao, A. (2003) Transcriptional regulation by calcium, calcineurin, and NFAT. *Genes Dev* 17: 2205–2232.

Hui, H., McHugh, D., Hannan, M., Zeng, F., Xu, S., Khan, S., U.H., Levenson, R., Beech, D.J., and Weiss, J.L. (2006) Calcium-sensing mechanism in TRPC5 channels contributing to retardation of neurite outgrowth. *J Physiol* 572: 165–172.

Hui, K., Fei, G.-H., Saab, B.J., Su, J., Roder, J.C., and Feng, Z.-P. (2007) Neuronal calcium sensor-1 modulation of optimal calcium level for neurite outgrowth. *Development* 134: 4479–4489.

Huttner, I.G., Strahl, T., Osawa, M., King, D.S., Ames, J.B., and Thorner, J. (2003) Molecular interactions of yeast frequenin (Frq1) with the phosphatidylinositol 4-kinase isoform, Pik1. *J Biol Chem* 278: 4862–4874.

Iida, H., Nakamura, H., Ono, T., Okumura, M.S., and Anraku, Y. (1994) MID1, a novel *Saccharomyces cerevisiae* gene encoding a plasma membrane protein, is required for Ca^{2+} influx and mating. *Mol Cell Biol* 14: 8259–8271.

Iida, H., Yagawa, Y., and Anraku, Y. (1990) Essential role for induced Ca^{2+} influx followed by $[Ca^{2+}]_i$ rise in maintaining viability of yeast cells late in the mating pheromone

response pathway. A study of $[Ca^{2+}]_i$ in single *Saccharomyces cerevisiae* cells with imaging of fura-2. *J Biol Chem* 265: 13391–13399.

Ikura, M. (1996) Calcium binding and conformational response in EF-hand proteins. *Trends Biochem Sci* 21: 14–17.

Inoue, H., Nojima, H., and Okayama, H. (1990) High efficiency transformation of *Escherichia coli* with plasmids. *Gene* 96: 23–28.

Jaiswal, J.K. (2001) Calcium –how and why? *J Biosci* 26: 357–363.

Johannes, E., Brosnan, J.M., and Sanders, D. (1991) Calcium channels and signal transduction in plant cells. *BioEssays* 13: 331–336.

Júnior, A.O.M., Malavazi, I., Soriani, F.M., Heinekamp, T., Jacobsen, I., Brakhage, A.A., Savoldi, M., Goldman, M.H.S., da Silva Ferreira, M.E., and Goldman, G.H. (2008) Molecular characterization of the *Aspergillus fumigatus* NCS-1 homologue, NcsA. *Mol Genet genomics* 280: 483.

Kabbani, N., Negyessy, L., Lin, R., Goldman-Rakic, P., and Levenson, R. (2002) Interaction with neuronal calcium sensor NCS-1 mediates desensitization of the D2 dopamine receptor. *J Neurosci* 22: 8476–8486.

Kader, M.A., and Lindberg, S. (2010) Cytosolic calcium and pH signaling in plants under salinity stress. *Plant Signal Behav* 5: 233–238.

Kapp-Barnea, Y., Melnikov, S., Shefler, I., Jeromin, A., and Sagi-Eisenberg, R. (2003) Neuronal calcium sensor-1 and phosphatidylinositol 4-kinase β regulate IgE receptor-triggered exocytosis in cultured mast cells. *J Immunol* 171: 5320–5327.

Kawamura, S. (1993) Rhodopsin phosphorylation as a mechanism of cyclic GMP phosphodiesterase regulation by S-modulin. Nature 362: 855–857

Kazmierczak, J., Kempe, S., and Kremer, B. (2013) Calcium in the early evolution of living systems: a biohistorical approach. *Curr Org Chem* 17: 1738–1750.

Kim, H., Wright, S.J., Park, G., Ouyang, S., Krystofova, S., and Borkovich, K.A. (2012) Roles for receptors, pheromones, G proteins and mating type genes during sexual reproduction in *Neurospora crassa*. *Genetics* 190: 1389–1404.

Klee, C.B., Crouch, T.H., and Krinks, M.H. (1979) Calcineurin: a calcium-and calmodulin-binding protein of the nervous system. *Proc Natl Acad Sci* 76: 6270–6273.

Klee, C.B., Ren, H., and Wang, X. (1998) Regulation of the calmodulin-stimulated protein phosphatase, calcineurin. *J Biol Chem* 273: 13367–13370.

Knight, H. (1999) Calcium signaling during abiotic stress in plants. *Int Rev Cytol* 195: 269–324.

Koh, P.O., Undie, A.S., Kabbani, N., Levenson, R., Goldman-Rakic, P.S., and Lidow, M.S. (2003) Up-regulation of neuronal calcium sensor-1 (NCS-1) in the prefrontal cortex of schizophrenic and bipolar patients. *Proc Natl Acad Sci* 100: 313–317.

Kothe, G.O., and Free, S.J. (1998) Calcineurin subunit B is required for normal vegetative growth in *Neurospora crassa*. *Fungal Genet Biol* 23: 248–258.

Kretsinger, R.H., and Wasserman, R.H. (1980) Structure and evolution of calcium-modulated protein. *Crit Rev Biochem Mol Biol* 8:119–174.

Krystofova, S., Borkovich, K.A. (2005) The heterotrimeric G-protein subunits GNG-1 and GNB-1 form a Gβγ dimer required for normal female fertility, asexual development, and Gα protein levels in *Neurospora crassa*. *Eukaryot Cell* 4: 365–378.

Kudla, J., Batistič, O., and Hashimoto, K. (2010) Calcium signals: the lead currency of plant information processing. *Plant Cell* 22: 541–563.

Kumar, K.S., Kumar, B.R., Siddavattam, D., and Subramanyam, C. (2006) Characterization of calcineurin-dependent response element binding protein and its involvement in copper-metallothionein gene expression in *Neurospora*. *Biochem Biophys Res Commun* 345: 1010–1013.

Kumar, R., and Tamuli, R. (2014) Calcium/calmodulin-dependent kinases are involved in growth, thermotolerance, oxidative stress survival, and fertility in *Neurospora crassa*. *Arch Microbiol* 196: 295–305.

Lamb, T.M., Vickery, J., and Bell-Pedersen, D. (2013) Regulation of gene expression in *Neurospora crassa* with a copper responsive promoter. *G3 (Bethesda)* 3: 2273–2280.

Larkin, M.A., Blackshields, G., Brown, N.P., Chenna, R., McGettigan, P.A., McWilliam, H., Valentin, F., Wallace, I.M., Wilm, A., Lopez, R,. and Thompson, J.D. (2007) Clustal W and Clustal X version 2.0. *Bioinformatics* 23: 2947–2948.

Laxmi, V., and Tamuli, R. (2015) The *Neurospora crassa cmd, trm-9*, and *nca-2* genes play a role in growth, development, and survival in stress conditions. *Genomics App Biol* 6: 1–8.

Laxmi, V., and Tamuli, R. (2017) The calmodulin gene in *Neurospora crassa* is required for normal vegetative growth, ultraviolet survival, and sexual development. *Arch Microbiol* 199: 531–542.

Lee, K., Loros, J.J., and Dunlap, J.C. (2000) Interconnected feedback loops in the *Neurospora* circadian system. *Science* 289: 107–110.

Lew, R.R., Abbas, Z., Anderca, M.I., and Free, S.J. (2008) Phenotype of a mechanosensitive channel mutant, mid-1, in a filamentous fungus, *Neurospora crassa*. *Eukaryot Cell* 7:

647–655.

Livak, K.J., and Schmittgen, T.D. (2001) Analysis of relative gene expression data using real-time quantitative PCR and the $2^{-\Delta\Delta C_T}$ method. *Methods* 25: 402–408.

Lundkvist, G.B., Kwak, Y., Davis, E.K., Tei, H., and Block, G.D. (2005) A calcium flux is required for circadian rhythm generation in mammalian pacemaker neurons. *J Neurosci* 25: 7682–7686.

Lytton, J. (2007) Na^+/Ca^{2+} exchangers: three mammalian gene families control Ca^{2+} transport. *Biochem J* 406: 365–382.

Marchler-Bauer, A., Anderson, J.B., Chitsaz, F., Derbyshire, M.K., DeWeese-Scott, C., Fong, J.H., Geer, L.Y., Geer, R.C., Gonzales, N.R., Gwadz, M., and He, S. (2008) CDD: specific functional annotation with the Conserved Domain Database. *Nucleic Acids Res* 37: D205–D210.

Marchler-Bauer, A., and Bryant, S.H. (2004) CD-Search: protein domain annotations on the fly. *Nucleic Acids Res* 32: W327–W331.

Margolin, B.S., Freitag, M., and Selker, E.U. (1997) Improved plasmids for gene targeting at the *his-3* locus of *Neurospora crassa* by electroporation. *Fungal Genet Rep* 44: 34–36.

Mattern, D.L., Forman, L.R., and Brody, S. (1982) Circadian rhythms in *Neurospora crassa*: a mutation affecting temperature compensation. *Proc Natl Acad Sci* 79: 825–829.

McCluskey, K. (2003) The fungal genetics stock center: from molds to molecules. *Adv. Appl. Microbiol* 5: 245–262.

McCluskey, K., Wiest, A., and Plamann, M. (2010) The Fungal Genetics Stock Center: a repository for 50 years of fungal genetics research. *J Biosci* 35: 119–126.

McFerran, B.W., Weiss, J.L., and Burgoyne, R.D. (1999) Neuronal Ca^{2+} Sensor 1 characterization of the myristoylated protein, its cellular effects in permeablized adrenal chromaffin cells Ca^{2+}-independent membrane association, and interaction with

binding proteins, suggesting a role in rapid Ca^{2+} signal transduction. *J Biol Chem* 274: 30258–30265.

McNally, M.T., and Free, S.J. (1988) Isolation and characterization of a *Neurospora* glucose-repressible gene. *Curr Genet* 14: 545–551.

Mehra, A., Shi, M., Baker, C.L., Colot, H. V, Loros, J.J., and Dunlap, J.C. (2009) A role for casein kinase 2 in the mechanism underlying circadian temperature compensation. *Cell* 137: 749–760.

Melo, A.M., Duarte, M., Møller, I.M., Prokisch, H., Dolan, P.L., Pinto, L., Nelson, M.A., and Videira, A. (2001) The external calcium-dependent NADPH dehydrogenase from *Neurospora crassa* mitochondria. *J Biol Chem* 276: 3947–3951.

Melo, A.M.P., Duarte, M., and Videira, A. (1999) Primary structure and characterisation of a 64 kDa NADH dehydrogenase from the inner membrane of *Neurospora crassa* mitochondria1. *Biochim Biophys Acta Bioenerg* 1412: 282–287.

Merrow, M., Franchi, L., Dragovic, Z., Görl, M., Johnson, J., Brunner, M., Macino, G., and Roenneberg, T. (2001) Circadian regulation of the light input pathway in *Neurospora crassa*. *EMBO J* 20: 307–315.

Miller, A.J., Vogg, G., and Sanders, D. (1990) Cytosolic calcium homeostasis in fungi: roles of plasma membrane transport and intracellular sequestration of calcium. *Proc Natl Acad Sci* 87: 9348–9352.

Mirzayans, R., Famulski, K.S., Enns, L., Fraser, M., and Paterson, M.C. (1995) Characterization of the signal transduction pathway mediating gamma ray-induced inhibition of DNA synthesis in human cells: indirect evidence for involvement of calmodulin but not protein kinase C nor p53. *Oncogene* 11: 1597–1605.

Møller, J. V, Juul, B., and le Maire, M. (1996) Structural organization, ion transport, and energy transduction of P-type ATPases. *Biochim Biophys Acta Rev Biomembr* 1286: 1–51.

Montagne, C. (1843) Quatrieme centurie plantes cellulaires exotiques nouvelles. Decades VIII, IX, X. *Ann Sci Nat Bot*, 20: 339–352.

Murray, N.E., and Perkins, D.D. (1963) Stanford *Neurospora* methods. *Neurospora News* l4: 21–25.

Nakayama, S., and Kretsinger, R.H. (1994) Evolution of the EF-hand family of proteins. *Annu Rev Biophys Biomol Struct* 23: 473–507.

Nef, P. (1996) Neuron-specific calcium sensors (the NCS subfamily). In: Celio, M.R. (ed.) *Guidebook to Calcium-Binding Proteins* (pp 94–98). New York: Oxford University Press.

Nicholas, K.B. (1997) GeneDoc: analysis and visualization of genetic variation. *Embnet.news* 4: 1–4.

Norris, V., Grant, S., Freestone, P., Canvin, J., Sheikh, F.N., Toth, I., et al. (1996) Calcium signalling in bacteria. *J Bacteriol* 178: 3677–3682.

O'Neill, J.S., and Reddy, A.B. (2012) The essential role of cAMP/Ca^{2+} signalling in mammalian circadian timekeeping. *Biochem Soc Trans* 40: 44–50.

Ochiai, E.-I. (1991) Why calcium? Principles and applications in bioorganic chemistry-IV. *J Chem Educ* 68: 10–12.

Olafsson, P., Wang, T., and Lu, B. (1995) Molecular cloning and functional characterization of the Xenopus Ca (2+)-binding protein frequenin. *Proc Natl Acad Sci* 92: 8001–8005.

Ouyang, S., Beecher, C.N., Wang, K., Larive, C.K., and Borkovich, K.A. (2015) Metabolic impacts of using nitrogen and copper-regulated promoters to regulate gene expression in *Neurospora crassa*. *G3 (Bethesda)* 5: 1899–1908.

Palma-Guerrero, J., Hall, C.R., Kowbel, D., Welch, J., Taylor, J.W., Brem, R.B., and Glass, N.L. (2013) Genome wide association identifies novel loci involved in fungal communication. *PLoS Genet* 9: e1003669.

Pall, M.L. (1993) The use of Ignite (Basta; glufosinate; phosphinothricin) to select transformants of bar containing plasmids in *Neurospora crassa*. *Fungal Genet Newslett* 40:58.

Pavelić, K. (1987) Calmodulin antagonist W 13 prevents DNA repair after bleomycin treatment of human urological tumor cells growing on extracellular matrix. *Int J Biochem* 19: 1091–1095.

Payen, A. (1843) Extrait d'un rapport adressé aM. Le Maréchal Duc de Dalmatie, Ministre de la Guerre, Président du Conseil, sur une altération extraordinaire du pain de munition. *Ann Chim Phys* 3: 5–21.

Perkins, D.D. (1992) *Neurospora*: the organism behind the molecular revolution. *Genetics* 130: 687–701.

Perkins, D.D., and Davis, R.H. (2000) *Neurospora* at the millennium. *Fungal Genet Biol* 31: 153–167.

Permyakov, S.E., Cherskaya, A.M., Senin, I.I., Zargarov, A.A., Shulga-Morskoy, S.V., Alekseev, A.M., Zinchenko, D.V., Lipkin, V.M., Philippov, P.P., Uversky, V.N., and Permyakov, E.A. (2000) Effects of mutations in the calcium-binding sites of recoverin on its calcium affinity: evidence for successive filling of the calcium binding sites. *Protein Eng* 13: 783–790.

Persikov, A. V, Osada, R., and Singh, M. (2008) Predicting DNA recognition by Cys_2His_2 zinc finger proteins. *Bioinformatics* 25: 22–29.

Persikov, A. V, and Singh, M. (2013) De novo prediction of DNA-binding specificities for Cys_2His_2 zinc finger proteins. *Nucleic Acids Res* 42: 97–108.

Pittendrigh, C.S. (1960) Circadian rhythms and the circadian organization of living systems. *Cold Spring Harb Symp Quant Biol* 25: 159–184.

Plesofsky-Vig, N., Light, D., and Brambl, R. (1983) Paedogenetic conidiation in *Neurospora*

crassa. *Exp Mycol* 7: 283–286.

Polisensky, D.H., and Braam, J. (1996) Cold-shock regulation of the *Arabidopsis* TCH genes and the effects of modulating intracellular calcium levels. *Plant Physiol* 111: 1271–1279.

Pongs, O., Lindemeier, J., Zhu, X.R., Theil, T., Engelkamp, D., Krah-Jentgens, I., Koch, K.W., Schwemer, J., Rivosecchi, R., Mallart, A., and Galceran, J. (1993) Frequenin–a novel calcium-binding protein that modulates synaptic efficacy in the *Drosophila* nervous system. *Neuron* 11: 15–28.

Prokisch, H., Yarden, O., Dieminger, M., Tropschug, M., and Barthelmess, I.B. (1997) Impairment of calcineurin function in *Neurospora crassa* reveals its essential role in hyphal growth, morphology and maintenance of the apical Ca^{2+} gradient. Mol Genet Genomics 256: 104–114.

Raju, N.B. (1980) Meiosis and ascospore genesis in *Neurospora*. *Eur J Cell Biol* 23: 208–223.

Raju, N.B. (1992) Genetic control of the sexual cycle in *Neurospora*. *Mycol Res* 96: 241–262.

Romano, N., and Macino, G. (1992) Quelling: transient inactivation of gene expression in *Neurospora crassa* by transformation with homologous sequences. *Mol Microbiol* 6: 3343–3353.

Romero-Pozuelo, J., Dason, J.S., Mansilla, A., Baños-Mateos, S., Sardina, J.L., Chaves-Sanjuán, A., Jurado-Gómez, J., Santana, E., Atwood, H.L., Hernández-Hernández, Á., and Sánchez-Barrena, M.J. (2014) The guanine-exchange factor Ric8a binds the calcium sensor NCS-1 to regulate synapse number and probability of release. *J Cell Sci* 127: 4246–4259.

Romero-Pozuelo, J., Dason, J.S., Atwood, H.L., and Ferrús, A. (2007) Chronic and acute alterations in the functional levels of Frequenins 1 and 2 reveal their roles in synaptic transmission and axon terminal morphology. *Eur J Neurosci* 26: 2428–2443.

RStudio Team (2015) RStudio: *Integrated Development for R.* RStudio, Inc., Boston, MA URL http://www. rstudio com/.

Rumi-Masante, J., Rusinga, F.I., Lester, T.E., Dunlap, T.B., Williams, T.D., Dunker, A.K., Weis, D.D., and Creamer, T.P. (2012) Structural basis for activation of calcineurin by calmodulin. *J Mol Biol* 415: 307–317.

Rusnak, F., and Mertz, P. (2000) Calcineurin: form and function. *Physiol Rev* 80: 1483–1521.

Ryan, F.J. (1950) Selected methods of *Neurospora* genetics. *Methods Med Res* 3: 51–75.

Ryan, F.J., Beadle, G.W., and Tatum, E.L. (1943) The tube method of measuring the growth rate of *Neurospora*. *Am J Bot* 30: 784–799.

Rzhetsky A, Nei M (1992) Statistical properties of the ordinary least-squares, generalized least-squares, and minimum-evolution methods of phylogenetic inference. *J Mol Evol* 35:367–375.

Saab, B.J., Georgiou, J., Nath, A., Lee, F.J., Wang, M., Michalon, A., Liu, F., Mansuy, I.M., and Roder, J.C. (2009) NCS-1 in the dentate gyrus promotes exploration, synaptic plasticity, and rapid acquisition of spatial memory. *Neuron* 63: 643–656.

Sadakane, Y., and Nakashima, H. (1996) Light-induced phase shifting of the circadian conidiation rhythm is inhibited by calmodulin antagonists in *Neurospora crassa*. *J Biol Rhythms* 11: 234–240.

Saitoh, K., Arie, T., Teraoka, T., Yamaguchi, I., and Kamakura, T. (2003) Targeted gene disruption of the neuronal calcium sensor 1 homologue in rice blast fungus, *Magnaporthe grisea*. *Biosci Biotechnol Biochem* 67: 651–653.

Sambrook, J., and Russel, D.W. (2001) *Molecular cloning: A laboratory Manual*. (3rd ed.) New York: Cold spring harbor laboratory press.

Sanders, D., Pelloux, J., Brownlee, C., and Harper, J.F. (2002) Calcium at the crossroads of signaling. *Plant Cell* 14: S401–S417.

Sargent, M.L., Briggs, W.R., and Woodward, D.O., 1966. Circadian nature of a rhythm expressed by an invertaseless strain of *Neurospora crassa*. *Plant Physiol* 41: 1343–1349.

Sargent, M.L., and Kaltenborn, S.H. (1972) Effects of medium composition and carbon dioxide on circadian conidiation in *Neurospora*. *Plant Physiol* 50: 171–175.

Saunders, D.S. (1977) *An introduction to biological rhythms*. London: Blackie.

Schaad, N.C., De Castro, E., Nef, S., Hegi, S., Hinrichsen, R., Martone, M.E., Ellisman, M.H., Sikkink, R., Rusnak, F., Sygush, J., and Nef, P. (1996) Direct modulation of calmodulin targets by the neuronal calcium sensor NCS-1. *Proc Natl Acad Sci* 93: 9253–9258.

Schlecker, C., Boehmerle, W., Jeromin, A., DeGray, B., Varshney, A., Sharma, Y., Szigeti-Buck, K., and Ehrlich, B.E. (2006) Neuronal calcium sensor-1 enhancement of $InsP_3$ receptor activity is inhibited by therapeutic levels of lithium. *J Clin Invest* 116: 1668–1674.

Schmitz, H.-P., and Heinisch, J.J. (2003) Evolution, biochemistry and genetics of protein kinase C in fungi. *Curr Genet* 43: 245–254.

Shapiro, R., Jordan, M.L., Scantlebury, V.P., Vivas, C., Gritsch, H.A., Corry, R., Egidi, F., McCauley, J., Ellis, D., Gilboa, N., and Lombardozzi-Lane, S. (1995) The superiority of tacrolimus in renal transplant recipients–The Pittsburgh experience. *Clin Transpl* 1995: 199–205.

Shear, C.L., and Dodge, B.O. (1927) Life histories and heterothallism of the red bread-mold fungi of the *Monilia sitophila* group. J Agric Res 34: 1019–1042.

Shiu, P.K.T., Raju, N.B., Zickler, D., and Metzenberg, R.L. (2001) Meiotic silencing by unpaired DNA. *Cell* 107: 905–916.

Soriani, F.M., Malavazi, I., da Silva Ferreira, M.E., Savoldi, M., Von Zeska Kress, M.R., de Souza Goldman, M.H., Loss, O., Bignell, E., and Goldman, G.H. (2008) Functional

characterization of the *Aspergillus fumigatus* CRZ1 homologue, CrzA. *Mol Microbiol* 67: 1274–1291.

Springer, M.L. (1993) Genetic control of fungal differentiation: the three sporulation pathways of *Neurospora crassa*. *Bioessays* 15: 365–374.

Stathopoulos-Gerontides, A., Guo, J.J., and Cyert, M.S. (1999) Yeast calcineurin regulates nuclear localization of the Crz1p transcription factor through dephosphorylation. *Genes Dev* 13: 798–803.

Stathopoulos, A.M., and Cyert, M.S. (1997) Calcineurin acts through the *CRZ1*/*TCN1*-encoded transcription factor to regulate gene expression in yeast. *Genes Dev* 11: 3432–3444.

Strahl, T., Hama, H., DeWald, D.B., and Thorner, J. (2005) Yeast phosphatidylinositol 4-kinase, Pik1, has essential roles at the Golgi and in the nucleus. *J Cell Biol* 171: 967–979.

Strahl, T., Huttner, I.G., Lusin, J.D., Osawa, M., King, D., Thorner, J., and Ames, J.B. (2007) Structural insights into activation of phosphatidylinositol 4-kinase (Pik1) by yeast frequenin (Frq1). *J Biol Chem* 282: 30949–30959.

Suresh, K., and Subramanyam, C. (1997) A putative role for calmodulin in the activation of *Neurospora crassa* chitin synthase. *FEMS Microbiol Lett* 150: 95–100.

Swain, A.L., Kretsinger, R.H., and Amma, E.L. (1989) Restrained least squares refinement of native (calcium) and cadmium-substituted carp parvalbumin using X-ray crystallographic data at 1.6-A resolution. *J Biol Chem* 264: 16620–16628.

Takahashi, J.S., Hong, H.-K., Ko, C.H., and McDearmon, E.L. (2008) The genetics of mammalian circadian order and disorder: implications for physiology and disease. *Nat Rev Genet* 9: 764–775.

Tamuli, R., Deka, R., and Borkovich, K.A. (2016) Calcineurin subunits A and B interact to regulate growth and asexual and sexual development in *Neurospora crassa*. *PLoS One*

11: e0151867.

Tamuli, R., Kumar, R., and Deka, R. (2011) Cellular roles of neuronal calcium sensor-1 and calcium/calmodulin-dependent kinases in fungi. *J Basic Microbiol* 51: 120–128.

Tamuli, R., Kumar, R., Srivastava, D.A., and Deka, R. (2013) Calcium signaling. In: D.P. Kasbekar, and McCluskey, K. (eds.), *Neurospora Genomics and Molecular Biology* (pp 35–57). Norfolk: Caister Academic Press.

Tamuli, R., Ravindran, C., and Kasbekar, D.P. (2006) Translesion DNA polymerases Pol ζ, Pol η, Pol ι, Pol κ and Rev1 are not essential for repeat-induced point mutation in *Neurospora crassa*. *J Biosci* 31: 557–564.

Tamura, K., Stecher, G., Peterson, D., Filipski, A., and Kumar, S. (2013) MEGA6: molecular evolutionary genetics analysis version 6.0. *Mol Biol Evol* 30: 2725–2729.

Testa, G., and Klintmalm, G.B. (1997) Cyclosporine and tacrolimus: the mainstay of immunosuppressive therapy for solid organ transplantation. *Clin Liver Dis* 1: 417–437.

That, T.C.T., and Turian, G. (1978) Ultrastructural study of microcyclic macroconidiation in *Neurospora crassa*. *Arch Microbiol* 116: 279–288.

Thompson, J.D., Gibson, T.J., Plewniak, F., Jeanmougin, F., and Higgins, D.G. (1997) The CLUSTAL_X windows interface: flexible strategies for multiple sequence alignment aided by quality analysis tools. *Nucleic Acids Res* 25: 4876–4882.

Tsujimoto, T., Jeromin, A., Saitoh, N., Roder, J.C., and Takahashi, T. (2002) Neuronal calcium sensor 1 and activity-dependent facilitation of P/Q-type calcium currents at presynaptic nerve terminals. *Science* 295: 2276–2279.

Tzingounis, A. V, Kobayashi, M., Takamatsu, K., and Nicoll, R.A. (2007) Hippocalcin gates the calcium activation of the slow after hyperpolarization in hippocampal pyramidal cells. *Neuron* 53: 487–493.

Verkhratsky, A., and Parpura, V. (2014) Calcium signalling and calcium channels: evolution and general principles. *Eur J Pharmacol* 739: 1–3.

Virgilio, S., Cupertino, F.B., Ambrosio, D.L., and Bertolini, M.C. (2017) Regulation of the reserve carbohydrate metabolism by alkaline pH and calcium in *Neurospora crassa* reveals a possible cross-regulation of both signaling pathways. *BMC Genomics* 18: 457.

Vogel, H.J. (1956) A convenient growth medium for *Neurospora crassa* (N medium). *Microb Genet Bull* 13: 42–43.

Vogel, H.J. (1964) Distribution of lysine pathways among fungi: evolutionary implications. *Am Nat* 98: 435–446.

Walch-Solimena, C., and Novick, P. (1999) The yeast phosphatidylinositol-4-OH kinase Pik1 regulates secretion at the Golgi. *Nat Cell Biol* 1: 523–525.

Weiss, J.L., Archer, D.A., and Burgoyne, R.D. (2000) Neuronal Ca^{2+} sensor-1/frequenin functions in an autocrine pathway regulating Ca^{2+} channels in bovine adrenal chromaffin cells. *J Biol Chem* 275: 40082–40087.

Westergaard, M., and Mitchell, H.K. (1947) *Neurospora* V. A synthetic medium favoring sexual reproduction. *Am J Bot* 34: 573–577.

Wickham, H. (2016) *ggplot2-Elegant graphics for data analysis* (2^{nd} ed.). USA: Springer.

Williams, R.J.P. (2007) The evolution of the biochemistry of calcium. *New Compr Biochem* 41: 23–48.

Winkler, M.A., Merat, D.L., Tallant, E.A., Hawkins, S., and Cheung, W.Y. (1984) Catalytic site of calmodulin-dependent protein phosphatase from bovine brain resides in subunit *A. Proc Natl Acad Sci* 81: 3054–3058.

Yang, Y., Cheng, P., Zhi, G., and Liu, Y. (2001) Identification of a calcium/calmodulin-dependent protein kinase that phosphorylates the *Neurospora* circadian clock protein Frequency. J Biol Chem 276: 41064–41072.

Yoshimoto, H., Saltsman, K., Gasch, A.P., Li, H.X., Ogawa, N., Botstein, D., Brown, P.O., and Cyert, M.S. (2002) Genome-wide analysis of gene expression regulated by the calcineurin/Crz1p signaling pathway in *Saccharomyces cerevisiae*. *J Biol Chem* 277: 31079–31088.

Zelter, A., Bencina, M., Bowman, B.J., Yarden, O., and Read, N.D. (2004) A comparative genomic analysis of the calcium signaling machinery in *Neurospora crassa*, *Magnaporthe grisea*, and *Saccharomyces cerevisiae*. *Fungal Genet Biol* 41: 827–841.

Publications

Publications:

1. Gohain, D., and Tamuli R. (2019) The calcineurin responsive zinc-finger-1 binds to a unique promoter sequence to induce expression of the neuronal calcium sensor-1 that interacts with the MID-1 ion channel for calcium stress tolerance in *Neurospora crassa*. *Mol Microbiol* 111:1510–1528.

2. Barman, A., Gohain, D., Bora, U., and Tamuli, R. (2018) Phospholipases play multiple cellular roles including growth, stress tolerance, sexual development, and virulence in fungi. *Microbiol Res* 209: 55–69.

3. Gohain, D., Roy, A. and Tamuli, R. (2017) Calcium signalling proteins in human diseases and their potential as drug targets. *Ann Pharmacol Pharm* 2: 1–3.

4. Gohain, D., Deka, R., Tamuli, R. (2016) Identification of critical amino acid residues and functional conservation of the *Neurospora crassa* and *Rattus norvegicus* orthologues of neuronal calcium sensor-1. *Genetica* 144: 665–674.

Poster presentation:

1. Gohain, D., and Tamuli, R. (2017) The transcription factor CRZ-1 upregulates the expression of NCS-1 that closes MID-1 channel for calcium stress tolerance in *Neurospora crassa*. National conference on Fungal Biology: Recent trends and future prospects and 44th annual meeting of the Mycological Society of India (MSI), Jammu University, Jammu, India.

2. Kumar, A., Roy, A., Gohain, D., and Tamuli, R. (2017) Calcineurin – a serine/threonine protein phosphatase and its role in calcium signalling. Research Conclave'17, IIT Guwahati, Guwahati, India.

3. Gohain, D., and Tamuli, R. (2016) Understanding the functions of neuronal calcium sensor1 (NCS-1) of *Neurospora crassa* and its rat orthologue. XL All India Cell Biology Conference & International Symposium on Functional Genomics and Epigenomics, Jiwaji University, Gwalior, India.
4. Gohain, D., and Tamuli, R. (2015) Involvement of rat NCS-1 in ultraviolet light induced DNA damage repair process. 9th International Conference on Yeast Biology, IACS, Kolkata, India.
5. Barman, A., Gohain, D., and Tamuli, R. (2015) Functional analysis of calcium signalling genes and a novel approach to study direct protein-protein interaction in *Neurospora crassa.* Research Conclave'15, IIT Guwahati, Guwahati, India.
6. Barman A, Gohain D, Laxmi V, Deka R, Kumar R, Tamuli R (2014) Cellular functions of calcium signalling machinery in the model filamentous fungus *Neurospora crassa*. MIPPM, Tezpur University, Assam, India.
7. Gohain, D., Deka, R., and Tamuli, R. (2013) Studies on the effect of the post-translational modifications of *Neurospora crassa* homologue of neuronal calcium sensor-1 in various cell functions. 8th International Conference on Yeast Biology, IMTECH, Chandigarh, India.

Oral presentation:

- Gohain, D., and Tamuli, R. (2014) Calcineurin and its role in drug resistance in pathogenic fungi. International Conference on Disease Biology and Therapeutics, IASST, Guwahati, Assam, India.

Molecular Microbiology (2019) 0(0), 1–19 doi:10.1111/mmi.14234

Calcineurin responsive zinc-finger-1 binds to a unique promoter sequence to upregulate neuronal calcium sensor-1, whose interaction with MID-1 increases tolerance to calcium stress in *Neurospora crassa*

Dibakar Gohain and Ranjan Tamuli *
Department of Biosciences and Bioengineering, Indian Institute of Technology Guwahati, Guwahati, 781 039, Assam, India.

Summary

We studied the molecular mechanism of neuronal calcium sensor-1 (NCS-1) signaling pathway for tolerance to Ca^{2+} stress in *Neurospora crassa*. Increasing concentration of Ca^{2+} increased the expression of *ncs-1*; however, the calcineurin inhibitor FK506 severely reduced ncs-*1* mRNA transcript levels. Chromatin immunoprecipitation (ChIP) studies revealed that the transcription factor calcineurin responsive zinc finger-1 (CRZ-1) binds to the *ncs-1* promoter, and CRZ-1 binding upregulated *ncs-1* expression under high Ca^{2+} concentrations. These results suggested the regulation of NCS-1 function through calcineurin- CRZ-1 signaling pathway. Furthermore, the electrophoretic mobility shift assay (EMSA) revealed that the CRZ-1 binds specifically to an 8 bp sequence 5′-CCTTCACA-3′ in the *ncs-1* promoter 216 bp upstream of the ATG start codon. We also showed that NCS-1 binds to the Ca^{2+} permeable channel MID-1 for tolerance to Ca^{2+} stress. Therefore, CRZ-1 binds to a unique sequence in the *ncs-1* promoter, causing upregulation of NCS-1 that binds to MID-1 for tolerance to Ca^{2+} stress.

Introduction

Calcium ion (Ca^{2+}) is a ubiquitous intracellular second messenger signaling molecule having a versatile role in regulating a wide variety of cellular processes and adaptive responses in eukaryotic organisms (Berridge *et al.*, 1998; Sanders *et al.*, 2002; Davies and Terhzaz, 2009). Ca^{2+}-signaling is triggered when the resting level of cytosolic free Ca^{2+} concentration ($[Ca^{2+}]_c$), which is maintained around 100 nM, transiently rises to 1 μM or more (Chin and Means, 2000; Bootman *et al.*, 2001). In eukaryotic organisms, including the filamentous fungus *Neurospora crassa*, resting level of $[Ca^{2+}]_c$ is maintained via Ca^{2+} transport mechanisms across the plasma membrane and buffering processes in the organelles (Bowman *et al.*, 2011; Barman and Tamuli, 2015). Ca^{2+} signaling pathway is involved in several biological processes, such as circadian regulated conidiation, growth, hyphal tip branching, ion transport, sexual development, stress tolerance, thermotolerance and ultraviolet (UV) survival in *N. crassa* (Deka *et al.*, 2011; Tamuli *et al.*, 2011; 2016; Kumar and Tamuli, 2014; Barman and Tamuli, 2015; 2017; Laxmi and Tamuli, 2015; 2017).

Transient increase in the $[Ca^{2+}]_c$ causes activation of various Ca^{2+} sensors, including neuronal calcium sensor-1 (NCS-1), a member of the NCS protein family (Pongs *et al.*, 1993; Bourne *et al.*, 2001). The NCS family members are Ca^{2+}-myristoyl switch proteins, containing an N-terminal myristoylation domain and four Ca^{2+} binding EF-hand domains (Burgoyne *et al.*, 2004; Burgoyne, 2007). NCS-1 protein is evolutionarily conserved across the species, and its homologues have been identified in yeast, filamentous fungi, *Drosophila*, nematodes, fish, birds, rodents and humans (Nef, 1996; Sánchez-Gracia *et al.*, 2010; Tamuli *et al.*, 2011). The N-terminal myristoylation motif in NCS-1 is required for its association with lipid membranes; however, N-terminal myristoylation is non-essential for the function of Frq1, the *Saccharomyces cerevisiae* homologue of NCS-1 (Hendricks *et al.*, 1999; Strahl *et al.*, 2003). In addition, only three out of four EF hands are functional in NCS-1, the first EF-hand of the N-terminal domain contains cysteine and proline residues in the putative Ca^{2+}-binding loop that make it incapable of Ca^{2+} binding (Burgoyne *et al.*, 2004; Tamuli *et al.*, 2011).

Accepted 26 February, 2019. *For correspondence. E-mails ranjan-tamuli@iitg.ac.in, ranjan.tam@gmail.com; Tel. (+91) 361 258 2220; Fax (+91) 361 258 2249/269 0762.

Microbiological Research 209 (2018) 55–69

Contents lists available at ScienceDirect

Microbiological Research

journal homepage: www.elsevier.com/locate/micres

Phospholipases play multiple cellular roles including growth, stress tolerance, sexual development, and virulence in fungi

Ananya Barman, Dibakar Gohain, Utpal Bora, Ranjan Tamuli*

Department of Biosciences and Bioengineering, Indian Institute of Technology Guwahati, Guwahati 781 039, Assam, India

ARTICLE INFO

Keywords:
Calcium signaling
Fungi
Phospholipids
Second messenger
Stress tolerance
Virulence

ABSTRACT

Phospholipases are ubiquitous enzymes that hydrolyze phospholipids. Based on the cleavage site of the ester linkage in the substrate phospholipids, phospholipases are classified into four major types, phospholipase A (PLA), phospholipase B (PLB), phospholipase C (PLC), and phospholipase D (PLD), which are further classified into various subtypes. Phospholipases hydrolyze phospholipids into various signaling products including phosphatidic acid (PA), diacylglycerol (DAG), free fatty acids (FFAs), and lyso-phospholipids (LPLs). These signaling products regulate numerous processes such as cytoskeletal dynamics, growth, homeostasis, membrane remodeling, nutrient acquisition, secretion, signal transduction, stress tolerance, sexual development, and virulence in various organisms including fungi. Due to these key cellular roles, phospholipases are also promising targets in diagnostic and therapeutic applications. In this review, we discuss current knowledge about the cellular roles of different classes of phospholipases in fungi.

1. Introduction

Lipids are essential constituents of living cells, and a class of complex lipids called phospholipids serves as the building blocks of almost all cellular membranes by forming the lipid bilayer and maintains cell shape and integrity (Bollag, 2016). Phospholipids are also important cellular intermediates that play multiple roles in cell development, metabolism, and signaling (Hong et al., 2016). The composition and content of phospholipids vary among different membranes, and typically changes during development and due to different stress cues (Hong et al., 2016). Similar to most eukaryotes, fungi also possess phospholipid based plasma membrane and intracellular organelles. The most abundant classes of phospholipids found in fungi includes phosphatidylcholine (PC) and phosphatidylethanolamine (PE), while phosphatidylglycerol (PG), phosphatidylinositol (PI), phosphatidylserine (PS), diphosphatidylglycerol (cardiolipin), and lyso-derivatives of PC and PE are found only in minor amounts (Dembitskii and Pechenkina, 1991). The hydrolysis of the phospholipids by the enzyme phospholipase yields fatty acids and a number of lipophilic molecules such as diacylglycerol (DAG), free fatty acids (FFAs), phosphatidic acid (PA), and lyso-phospholipids (LPLs) that are involved in signaling (Köhler et al., 2006; Hong et al., 2016). Phospholipases are classified into four major types phospholipase A (PLA_1 and PLA_2), phospholipase B (PLB), phospholipase C (PLC), and phospholipase D (PLD) on the basis of cleavage of ester linkage within a phospholipid molecule (Fig. 1). The PLA and PLB belongs to acyl hydrolase class of phospholipids, while PLC and PLD are members of the phosphodiesterase class of phospholipids (Richmond and Smith, 2011). In this review, we discuss about various cellular roles of the phospholipase superfamily members in fungi.

2. Phospholipase A (PLA)

The PLA superfamily of enzymes catalyze the hydrolysis of membrane phospholipids into FFAs and other lipid soluble molecules. The majority of the eukaryotic PLAs consists of the Gly-Xaa-Ser-Xaa-Gly (Xaa represents any amino acid) motif in its active site with catalytic Ser at the center, a catalytic triad of Ser-Asp-His residues, and a number of disulfide bonded Cys residues necessary for the stability of these enzymes. Based on their site of cleavage, PLA enzyme family can be classified into two types, phospholipase A_1 (PLA_1) cleaves the ester bond of glycerophospholipids at the *sn-1* position and produces FFAs and 2-acyl-LPL, while phospholipase A_2 (PLA_2) cleaves at the *sn-2* ester linkage and liberates FFAs and 1-acyl-LPL (Fig. 2 a, b; Ghannoum, 2000; Arioka et al., 2005; Köhler et al., 2006). FFAs and LPLs in turn regulate various biological functions in different organisms (Cavazzini et al., 2013).

2.1. Phospholipase A_1 (PLA_1)

PLA_1 activity has been studied in a wide range of tissues and cells of

* Corresponding author.
E-mail address: ranjantamuli@iitg.ernet.in (R. Tamuli).

https://doi.org/10.1016/j.micres.2017.12.012
Received 1 August 2017; Received in revised form 21 December 2017; Accepted 31 December 2017
Available online 03 January 2018
0944-5013/

Annals of Pharmacology and Pharmaceutics

Review Article
Published: 10 Nov, 2017

Calcium Signaling Proteins in Human Diseases and their Potential as Drug Targets

*Gohain D, Avishek Roy and Ranjan Tamuli**

Department of Biosciences and Bioengineering, Indian Institute of Technology Guwahati, India

Abstract

The calcium (Ca^{2+}) signaling proteins are activated by a transient increase in free resting intracellular free Ca^{2+} concentration and regulate numerous cell process including disease conditions. The neuronal Ca^{2+} sensor-1, calmodulin, Ca^{2+}/calmodulin dependent protein kinases, and calcineurin are some of the important Ca^{2+} signaling proteins known to play an important role various organisms and in human diseases, and have the potential as drug targets.

Introduction

Cell signaling is essential for all living organisms to communicate with both intracellular and extracellular environments. Cell signaling is mediated by several pathways including G-protein coupled receptors (GPCRs), and calcium (Ca^{2+}) signaling pathway that affects almost all cell process ranging from fertilization to death, and therefore, Ca^{2+} is also called as molecule of "life and death"[1].A typical human cell maintains about 2 mM of Ca^{2+} in blood and extracellular fluid, whereas, the resting intracellular free Ca^{2+} concentration ($[Ca^{2+}]_i$) is about 100 nM that transiently increases to about 100 M during the Ca^{2+} signaling process [2-3]. In the signaling process, many Ca^{2+} binding proteins binds to the increased $[Ca^{2+}]_i$ to regulated downstream effectors and also act as buffers to maintain the Ca^{2+} homeostasis in the cell [3-5].The Ca^{2+} signaling proteins have emerged as potential biomarkers for several disorders and also as drug targets for the treatment of infectious diseases in human. In this mini-review, cell functions of Ca^{2+}- signaling proteins neuronal calcium sensor-1, calmodulin, Ca^{2+}/calmodulin dependent protein kinases, and calcineurin, their roles in human diseases and potential as drug targets have been discussed.

Neuronal Calcium Sensor-1

One of the Ca^{2+}-binding proteins, neuronal calcium sensor-1 (NCS-1) is highly conserved from fungi to human containing four-EF hand Ca^{2+} binding domains, although, only three of the EF binds to Ca^{2+}[6-9]. NCS-1 has a critical physiological role in various organisms[7-10], such as neuronal growth, secretion, and regulation of Ca^{2+} channels in *Lymnaea stagnalis*, *Xenopus*, *Drosophila*, and mammals [11],memory and learningin *Caenorhabditis elegan*[12] and mice [13], neurotransmitter release in *Drosophila* [14], activity dependent synaptic facilitation of voltage-gated Ca^{2+} channels in rat calyceal nerve terminal [15], and in short-term synaptic plasticity in rat hippocampal neurons[16], long-term depression (LTD) via activation of metabotropic glutamate receptors (mGluRs) in rat cortical neurons[17], exploratory behavior and in the acquisition of spatial memory in mouse [18], and in neurite sprouting and spinal cord regeneration in rat [19]. In human, NCS-1 level was found up regulated in the prefrontal cortex of schizophrenic and bipolar patients [20], but, its level was decreased in leukocytes of schizophrenia and bipolar disorder patients [21], suggesting that NCS-1 may be associated with these abnormalities. In addition, NCS-1 is also a novel binding partner of paclitaxel (taxol), one of the most effective anticancer drugs, and protection of NCS-1 from paclitaxel-induced degradation by inhibiting calpain, a Ca^{2+}-dependent enzyme, might be useful for protection from peripheral neuropathy, a major side effect caused by paclitaxel treatment [22-24].

Calmodulin

The Ca^{2+} binding protein calmodulin (CaM) interacts with various target kinases, and phosphatases including calcineurin [4, 25, 26] The increased CaM level in peripheral blood cells is a distinct feature Alzheimer's disease (AD), although, the changes in CaM level was not correlated with the severity of AD, suggesting that the increased CaM level may be an early manifestation of AD [27]. Moreover, the increased level of CaM level in peripheral blood cells was not detected

OPEN ACCESS

Correspondence:

Ranjan Tamuli, Department of Biosciences and Bioengineering, Indian Institute of Technology Guwahati, India, Tel: +91 361 258 2220, Fax: +91 361 258 2249/269 0762; E-mail: ranjan.tam@gmail.com

Received Date: *01 Aug 2017*

Accepted Date: *20 Oct 2017*

Published Date: *10 Nov 2017*

Citation:

Gohain D, Roy A, Tamuli R. Calcium Signaling Proteins in Human Diseases and their Potential as Drug Targets. Ann Pharmacol Pharm. 2017; 2(22): 1117.

Genetica (2016) 144:665–674
DOI 10.1007/s10709-016-9933-y

Identification of critical amino acid residues and functional conservation of the *Neurospora crassa* and *Rattus norvegicus* orthologues of neuronal calcium sensor-1

Dibakar Gohain[1] · Rekha Deka[1] · Ranjan Tamuli[1]

Received: 24 June 2016 / Accepted: 11 October 2016 / Published online: 31 October 2016

Abstract Neuronal calcium sensor-1 (NCS-1) is a member of neuronal calcium sensor family of proteins consisting of an amino terminal myristoylation domain and four conserved calcium (Ca^{2+}) binding EF-hand domains. We performed site-directed mutational analysis of three key amino acid residues that are glycine in the conserved site for the N-terminal myristoylation, a conserved glutamic acid residue responsible for Ca^{2+} binding in the third EF-hand (EF3), and an unusual non-conserved amino acid arginine at position 175 in the *Neurospora crassa* NCS-1. The *N. crassa* strains possessing the *ncs-1* mutant allele of these three amino acid residues showed impairment in functions ranging from growth, Ca^{2+} stress tolerance, and ultraviolet survival. In addition, heterologous expression of the NCS-1 from *Rattus norvegicus* in *N. crassa* confirmed its interspecies functional conservation. Moreover, functions of glutamic acid at position 120, the first Ca^{2+} binding residue among all the EF-hands of the *R. norvegicus* NCS-1 was found conserved. Thus, we identified three critical amino acid residues of *N. crassa* NCS-1, and demonstrated its functional conservation across species using the orthologue from *R. norvegicus*.

Keywords Calcium binding · EF-hand domain · Heterologous expression · N-terminal myristoylation · Neuronal calcium sensor-1 · *Neurospora crassa* · *Rattus norvegicus* · Site- directed mutagenesis · Ultraviolet survival

Dibakar Gohain and Rekha Deka have contributed equally to this work.

Electronic supplementary material The online version of this article (doi:10.1007/s10709-016-9933-y) contains supplementary material, which is available to authorized users.

✉ Ranjan Tamuli
ranjantamuli@iitg.ernet.in; ranjan.tam@gmail.com

[1] Department of Biosciences and Bioengineering, Indian Institute of Technology Guwahati, Guwahati 781 039, India

Introduction

The neuronal calcium sensor-1 (NCS-1), a member of the neuronal calcium sensor (NCS) family of proteins, was first discovered in *Drosophila melanogaster* as frequenin, a calcium (Ca^{2+}) binding protein associated with frequency-dependent increase in neurotransmission (Pongs et al. 1993). NCS-1 is a highly conserved protein, its orthologues have been identified in yeast, fungi, Drosophila, nematodes, birds, rodents, and humans (Nef 1996; Tamuli et al. 2011). Members of the NCS protein family are Ca^{2+}-myristoyl-switch proteins with four Ca^{2+}binding EF-hand domains (Burgoyne 2007; Burgoyne et al. 2004). The myristoylation motif at the N-terminus presumably allows NCS-1 to associate with lipid membranes (Burgoyne et al. 2004). Protein N-myristoylation is found in viruses, fungi, and higher eukaryotes that involve the covalent attachment of myristoyl group via an amide bond to the α-amino group of an N-terminal glycine residue exposed during co-translational N-terminal methionine removal (Podell and Gribskov 2004). Attachment of the myristoyl group to the target N-terminal glycine residue alters the lipophilicity of the target protein and facilitates its interaction with membranes, and affects its subcellular localization or the hydrophobic domains of other proteins for transducing signal downstream (Batistič et al. 2008; Benetka et al. 2008; Olsen and Kaarsholm 2000; Resh 1999). The glycine at second position is the site for N-terminal myristoylation, which is an irreversible co-translational protein modification catalyzed by enzyme